Faculty of Medicine
University of Crete

PhD Thesis

Study of the mechanism underlying premature suture closure in the animal model of ERF-related craniosynostosis

Διδακτορική Διατριβή

Μελέτη του μηχανισμού που οδηγεί στην πρόωρη σύντηξη των ραφών στο ζωικό μοντέλο της σχετιζόμενης με τον ERF κρανιοσυνοστέωσης

Angeliki C. Vogiatzi

Under the supervision of
Prof. George Mavrothalassitis

Heraklion, 2021

To my parents, Maria & Christopher,

My lovely sister Helen,

To auntie Georgia & granny Helen,

For their endless support and patience during hard times.

Acknowledgements

Reaching to the end of this long journey, I would like to express my gratitude to my supervisor, Professor George Mavrothalassitis, not only because he kindly let me join his group and gave me the opportunity to complete this thesis, but also because he taught me things that I would never have learnt otherwise and made me familiar with a different way of thinking and an urge to overcome any obstacles arise. Before coming to his laboratory, I was a biologist. Yet now he has taught me how to be a researcher too. I will never forget that.

I would also like to thank my committee members, Professor George Chalepakis and Professor Dimitris Kardassis, for all their helpful comments and suggestions and for providing me with fascinating ideas and a completely different and sometimes unexpected point of view. I really thank them for all the support and inspiration they provided me. The same holds true for Professor Andrew Wilkie and Dr. Stephen Twigg in England. Their contribution to this project was really invaluable.

A special thank to all the members of this laboratory too, Ioanna Peraki, Elena Vorgia, Andreas Zaragkoulias and of course to my collaborators, Konstantinos Makris, Angelos Gkikas, Maria Kokkori and Sofia Archontidi for their great work in the challenging project of craniosynostosis. I also want to express my appreciation to all IMBB-FORTH members that participated in the completion and publication of this work and especially to Elena Deligianni, Vasiliki Theodorou and Emmanuel Dialynas. A special thank to Ismini Baltsavia and Ioannis Iliopoulos from the Medical School of the University of Crete. Their contribution was absolutely significant and invaluable.

Furthermore, I would like to express my gratitude to the Onassis Foundation, the State Scholarships Foundation (IKY) and the Maria Michail Manasaki Foundation for their invaluable support during difficult times. I wish they continue to give strength and support to young students and researchers, helping them to achieve their goal.

Finally, my family has my deepest thanks. I 'm grateful for all the affection, the support and the encouragement they lavishly gave to me. I hope that I will be closer to them from now on, as I 'm now sure that nothing in the world can be more invaluable than the people we have around us.

As you set out for Ithaka
hope your road is a long one,
full of adventure, full of discovery.
Laistrygonians, Cyclops,
angry Poseidon – don't be afraid of them:
you'll never find things like that on your way
as long as you keep your thoughts raised high,
as long as a rare excitement
stirs your spirit and your body.

"Ithaca" by C. P. Cavafy

Contents

Περίληψη……..7

Summary……...9

1. Introduction……11

1.1 Anatomy of the Cranium…….....12

1.2 Craniofacial Development……14

1.3 From MSCs to Osteocytes and Bone: exploring the route……..17

1.4 Craniosynostosis…….20

1.5 Craniosynostosis syndromes and associated mechanisms……22

1.6 ERF-related craniosynostosis……25

1.7 ERF: the gene, the protein and the reported roles……27

1.8 Aim of the study……..30

2. Materials & Methods…….....31

2.1 Materials, mouse lines & cell lines……..32

2.1.1 Mouse lines……32

2.1.2 Cell lines……32

2.1.3 Cell culture media……32

2.1.4 Solutions & Buffers……...35

2.1.5 Antibodies, reagents & fluorescent dyes……...37

2.1.6 Primers for qPCR……..37

2.2 Methods……40

2.2.1 Cranial suture cell isolation and cultivation……40

2.2.2 Selective expansion of suture-derived mesenchymal stem/ progenitor cells……..41

2.2.3 Freezing and thawing cells……..41

2.2.4 Estimation of the population doubling level (PDL)……42

2.2.5 Osteogenic differentiation……...42

2.2.6 Adipogenic differentiation……..43

2.2.7 Chondrogenic differentiation……43

2.2.8 Alizarin Red S: preparation, staining & quantification……44

2.2.9 Oil Red O: preparation, staining & quantification……45

2.2.10 Alcian blue: preparation & staining……46

2.2.11 Transfection of Cos7 cells & LIF production……...46

2.2.12 Cell cycle phase study with propidium iodide……...47

2.2.13 MTT assay……48

2.2.14 BrdU incorporation assay……..48

2.2.15 Flow cytometry staining……50

2.2.16 RNA isolation from cultured cells for qPCR……...51

2.2.17 cDNA synthesis & real-time PCR……51

2.2.18 RNA isolation from cultured cells for sequencing……53

2.2.19 Protein isolation from cultured eukaryotic cells……54

2.2.20 SDS-PAGE (Polyacrylamide gel electrophoresis) & blots……54

2.2.21 Cranial suture tissue processing & immunofluorescence staining……..55

2.2.22 Preparation of gelatin-coated dishes for cell culture……..56

2.2.23 Preparation of gelatinized slides for cryosections……..56

2.2.24 DNA isolation from mouse tails……...57

2.2.25 PCR for the detection of *Erf*^{LoxP} allele……...57

2.2.26 PCR for the detection of *Erf*^{del} allele……..57

2.2.27 PCR for the detection of Nestin-cre……..58

2.2.28 PCR for the detection of Rosa-mTmG……..59

2.2.29 Viral infection of primary cells……..59

2.2.30 RNA sequencing……60

3. Results……..61

3.1 Freshly derived suture cells from *Erf*$^{LoxP/-}$ craniosynostosis mice display decreased capacity to mineralize *in vitro*……...62

3.2 LIF-selected long-term expanded suture derived cells possess *in vitro* characteristics of mesenchymal stem/ progenitor cells……...65

3.3 Efforts to eliminate *Erf* by adenoviral infection of suture-derived MSCs using a vector containing the sequence of Cre-recombinase gene……..68

3.4 Efforts to eliminate *Erf* in mesenchymal lineages using the B6.Cg-Tg(Nes-cre)1Kln/J mouse line……...71

3.5 Erf insufficiency does not affect the cycling of suture mesenchymal stem/ progenitor cells but compromises their differentiation towards the osteogenic lineage……75

3.6 Erf seems to be required for the initial commitment of suture mesenchymal stem/ progenitor cells towards the osteogenic lineage……78

3.7 Erf insufficiency is associated with altered cell proliferation rates in cranial sutures and in cultures undergoing osteogenic differentiation …..……82

3.8 Erf insufficiency is associated with retinoic acid (RA) signalling alterations and exogenous supplementation with retinoic acid seems to restore the differentiation defect of *Erf*$^{LoxP/-}$ cells *in vitro*……..86

4. Discussion……89

4.1 LIF-selected long-term expanded cranial suture cells possess *in vitro* characteristics of mesenchymal stem/ progenitor cells……...90

4.2 Erf, a downstream target of Erks, affects the commitment and maintenance of osteoprogenitor cells in cranial sutures ……91

4.3 Erf regulates the osteogenic commitment of cranial suture mesenchymal stem/progenitor cells via the retinoic acid (RA) pathway……...92

4.4 Therapeutic outlook for Erf-associated craniosynostosis ...……...94

4.5 Conclusion & Future directions……95

5. References……97

6. Publications……...107

Περίληψη

Η ανάπτυξη της κεφαλής του ανθρώπου αποτελεί μία πολύπλοκη διαδικασία που εμπλέκει την αλληλεπίδραση ιστών προερχόμενων από διαφορετικές βλαστικές στιβάδες του εμβρύου καθώς και την ενεργοποίηση ποικίλων μοριακών σηματοδοτικών μονοπατιών σε διαφορετικά χρονικά διαστήματα και τοπολογίες. Οι κρανιακές ραφές αποτελούν το συνδετικό ιστό που υπάρχει μεταξύ των οστών του κρανίου και κατέχουν κύριο ρόλο στην αύξησή τους κατά την ανάπτυξη. Μεσεγχυματικά βλαστικά κύτταρα που εντοπίζονται στην κεντρική περιοχή της ραφής ακολουθούν την οδό της ενδομεμβρανώδους (ή υμενογενούς) οστεοποίησης και διαφοροποιούνται σε οστεοπρογονικά και προ-οστεοβλαστικά κύτταρα με ικανότητα αυτοανανέωσης, τα οποία στη συνέχεια με τη σειρά τους διαφοροποιούνται σε οστεοβλάστες που εναποθέτουν εξωκυττάρια ύλη στις άκρες των οστών προς αύξηση (οστεογονικά μέτωπα). Αργότερα κατά την ανάπτυξη, οστική απορρόφηση από τους οστεοκλάστες και αναδόμηση λαμβάνουν επίσης χώρα στις κρανιακές ραφές. Η ισορροπία μεταξύ όλων αυτών των διαφορετικών κυτταρικών πληθυσμών –από τα πρόδρομα μεσεγχυματικά κύτταρα μέχρι τους οστεοβλάστες και τους οστεοκλάστες- είναι κρίσιμη για το εάν η ραφή θα παραμείνει ανοιχτή, χωρίς να οστεοποιηθεί πρόωρα, και συνεπώς είναι καθοριστική για την συντονισμένη αύξηση κρανίου και εγκεφάλου. Η αλλοίωση αυτής της ισορροπίας δύναται να οδηγήσει στο πρόωρο κλείσιμο της ραφής, μία πάθηση που καλείται κρανιοσυνοστέωση και εμφανίζεται με συχνότητα μία στις 2500 γεννήσεις. Αποτέλεσμα είναι συχνά η παραμόρφωση του σχήματος της κεφαλής, καθώς επίσης και προβλήματα στην όραση, την ακοή και την νοητική λειτουργία αν δεν υπάρξει άμεση χειρουργική παρέμβαση. Κατά τη διάρκεια των τελευταίων δεκαετιών σημαντικές προσπάθειες καταβάλλονται στη διερεύνηση των μηχανισμών που οδηγούν στην εμφάνιση του φαινοτύπου της κρανιοσυνοστέωσης. Όμως η ύπαρξη πολλαπλών κυτταρικών πληθυσμών στις ραφές, η απουσία χαρακτηριστικών κυτταρικών μαρτύρων, καθώς και οι δυσκολίες στην απομόνωση και ταυτοποίηση των μεσεγχυματικών βλαστικών κυττάρων έχουν αποτελέσει τροχοπέδη στην πλήρη κατανόηση της παθοφυσιολογίας.

Η απλοανεπάρκεια του μεταγραφικού καταστολέα ERF (ETS2 Repressor Factor) προκαλεί κρανιοσυνοστέωση στον άνθρωπο, αλλά και στα ποντίκια $Erf^{LoxP/-}$ τα οποία εκφράζουν μόνο το 29% των φυσιολογικών επιπέδων της πρωτεΐνης αυτής. Όπως οι άνθρωποι, έτσι και τα ποντίκια $Erf^{LoxP/-}$ εμφανίζουν δυσμορφία προσώπου, χωρίς όμως άλλες εμφανείς σκελετικές ανωμαλίες πέραν της συνοστέωσης και μια ελάττωση στην συνολική οστεοποίηση του κρανίου στις αρχές της μετεμβρυϊκής ζωής. Προηγούμενες μελέτες έχουν αναδείξει την εμπλοκή του ERF στη ρύθμιση του κυτταρικού πολλαπλασιασμού καθοδικά του σηματοδοτικού μονοματιού των ERK1/2 κινασών, καθώς επίσης και στη ρύθμιση της κυτταρικής διαφοροποίησης με χαρακτηριστικότερα παραδείγματα τη διαφοροποίηση των τροφοβλαστικών κυττάρων και των αιμοποιητικών κυττάρων της ερυθρής σειράς. Καμία όμως αναφορά δεν υπήρχε σχετικά με τον πιθανό ρόλο του ERF στο σχηματισμό των οστών

ή στην ανάπτυξη του κρανιοπροσωπικού συμπλέγματος. Στόχος λοιπόν της παρούσας μελέτης είναι να συμβάλλει στην κατανόηση του μηχανισμού που οδηγεί στην εκδήλωση του φαινοτύπου της σχετιζόμενης με τον ERF κρανιοσυνοστέωσης, φαινότυπος ο οποίος έχει χαρακτηρισθεί και ως «ύπουλος» λόγω της ετερογένειας που εμφανίζει στο χρόνο αλλά και την ένταση των συμπτωμάτων.

Στην παρούσα μελέτη καθιερώσαμε *in vitro* πρωτογενείς καλλιέργειες κυττάρων κρανιακών ραφών και αναπτύξαμε μια μέθοδο επιλεκτικής επιβίωσης και επέκτασης των μεσεγχυματικών βλαστικών κυττάρων ώστε να μελετηθεί ο ρόλος του παράγοντα ERF στις κρανιακές ραφές και την ενδομεμβρανώδη οστεογένεση του κρανίου. Μέσω *ex vivo* κυτταρικών δοκιμασιών και ανάλυσης του μεταγραφώματος, παρέχουμε στοιχεία που υποστηρίζουν ότι ο ERF είναι απαραίτητος για την αρχική δέσμευση των μεσεγχυματικών βλαστικών κυττάρων προς την οστεογονική γενεαλογία, ενώ επιπλέον σε μετέπειτα στάδιο είναι σημαντικός για τη διατήρηση των πολλαπλασιαζόμενων οστεοπρογονικών κυττάρων που βρίσκονται καθ' οδόν της πορείας διαφοροποίησης τους στις ραφές. Τα δεδομένα της μελέτης μας υποστηρίζουν ότι ο Erf ρυθμίζει τη δέσμευση και τη διαφοροποίηση των μεσεγχυματικών βλαστικών κυττάρων προς οστεοπρογονικά κύτταρα μέσω του σηματοδοτικού μονοπατιού του ρετινοϊκού οξέος (RA). Συγκεκριμένα η ανεπάρκεια του Erf οδηγεί σε αύξηση των επιπέδων του *Cyp26b1*, γονιδίου που κωδικοποιεί τον παράγοντα αποικοδόμησης του ρετινοϊκού οξέος, γεγονός που οδηγεί στη διατήρηση της αυτό-ανανέωσης των μεσεγχυματικών κυττάρων και της μείωσης του ρυθμού διαφοροποίησής τους. Η εξωγενής προσθήκη ρετινοϊκού οξέος επαναφέρει το φυσιολογικό πρότυπο *in vitro* διαφοροποίησης των $Erf^{LoxP/-}$ κυττάρων με βάση τα δεδομένα της μελέτης μας. Η παθολογική ασβεστιοποίηση των κρανιακών οστών δύναται να αποδοθεί στη διαταραχή της βαθμίδωσης συγκέντρωσης ρετινοϊκού οξέος. Περαιτέρω μελέτες απαιτούνται όμως για τον καθορισμό του ρόλου του Erf και του RA σηματοδοτικού μονοπατιού στα επιμέρους στάδια της οστεογένεσης. Η φαρμακολογική ενίσχυση της πυρηνικής δράσης του ERF στα κύτταρα καθώς και η ρύθμιση των επιπέδων ρετινοϊκού οξέος θα μπορούσαν δυνητικά να αποτελέσουν μια υποσχόμενη προοπτική στην αντιμετώπιση της κρανιοσυνοστέωσης και αναδεικνύουν ότι η συνεχής παρουσία του παράγοντα αυτού είναι αναγκαία για τη φυσιολογική ανάπτυξη του κρανιοπροσωπικού συμπλέγματος.

Summary

The formation of the human head is a complex process involving sequences of crosstalk events between different germ layers and tissues and spatiotemporal activation of a variety of molecular signaling cascades. Cranial sutures comprise the connective tissues between the bony elements of skull and have a critical role in the development and growth of the calvarial bones. Non committed mesenchymal stem cells are found to reside in the suture mesenchyme that once enter the intramembranous ossification pathway give rise to proliferating populations of osteoprogenitor and preosteoblast cells that eventually appose osteoblasts at the edges of the developing bones. Resorption and bone reshaping takes place by osteoclasts later too. The balance between all these populations of cells seems to be crucial for the suture patency and consequently for the coordination of skull and brain development. Distortion of this balance can lead to the premature closure of one or more of the cranial sutures, a condition termed craniosynostosis, with an occurrence rate of approximately one in 2500 births, that results in abnormal head shapes along with vision, hearing and mental impairment unless treated. During the last decades, considerable amount of effort has been put into the identification of the mechanisms that lead to the appearance of the phenotype. However, the presence of multiple cell populations in sutures, the lack of specific cellular markers and the difficulties in the isolation of suture stem cells, hinder such efforts.

Haploinsufficiency of the ETS-DNA binding transcriptional repressor factor ERF causes premature suture closure in humans and in $Erf^{LoxP/-}$ mice expressing only 29% of the normal Erf protein levels. Like humans, $Erf^{LoxP/-}$ mice display facial dysmorphism with no other obvious skeletal defects beyond synostosis which is preceded by a reduction in the ossification of calvarial bones at the onset of postnatal life. In previous studies ERF has been shown to regulate cellular proliferation downstream of ERK1/2 signalling along with differentiation processes with particular respect to trophoblast stem cell and erythroid differentiation. There were no reports however, about its role in either bone formation or craniofacial development. The aim of the current study was to provide an understanding of the mechanisms underlying the emergence of ERF-associated craniosynostosis phenotype, often characterised as insidious due to its high complexity.

In the present study, we established *in vitro* cultures of primary suture-derived cells and developed selective conditions for the expansion of a mesenchymal stem/ progenitor cell population from suture explants to study the role of Erf in cranial suture fate and intramembranous skull ossification. By performing *ex vivo* cellular assays and transcriptomic analysis we provide evidence that Erf is required for the initial commitment of suture mesenchymal stem/ progenitor cells towards the osteogenic lineage, while at a later stage seems to be also essential for the maintenance of committed proliferating progenitor cells undergoing differentiation. Our data indicate that Erf affects the commitment and differentiation of cranial suture

mesenchymal stem/ progenitor cells via the retinoic acid (RA) pathway. Decreased levels of Erf lead to increased expression of *Cyp26b1* gene, encoding the RA-catabolizing enzyme, resulting in sustained proliferation and decreased mesenchymal stem cell differentiation. Exogenous addition of retinoic acid rescues the osteogenesis defect of Erf-insufficient ($Erf^{LoxP/-}$) cells. The abnormal mineralization of the calvarial bones may be attributed to the distortion in retinoic acid concentration gradient during skull development. Further studies would be necessary to explore the spatiotemporal function of Erf and its effect on RA concentration gradients in cranial bone and suture development. Pharmacological enhancement of nuclear Erf action as well as retinoic acid level modulation hold promise for the treatment of craniosynostosis and reassert that continuous ERF presence is required for normal craniofacial development.

1. Introduction

1. Introduction

1.1 Anatomy of the Cranium

The skull is a structure of high complexity that protects the brain and supports the organs of the face. This bony structure is composed of the neurocranium that covers the brain and the viscerocranium that includes the bones of the face. The neurocranium is the focus of this thesis. In humans it consists of 8 bones: the frontal one, two parietal bones, two temporal bones, the sphenoid bone, the ethmoid and the occipital one. Analogous bones are observed in mice in which the occipital bone is composed of different parts with the interparietal one often being separated from the rest throughout adulthood (Fig. 1) [1, 2]. Bone is generally composed of inorganic mineral material (~70%), organic material (~20%) and water (~10%). Type I collagen constitutes approximately 90% of the organic component and is synthesized and secreted by osteoblasts along with non-collagenous proteins such as the osteocalcin, the osteopontin, the bone sialoprotein, proteoglycans and many cytokines.

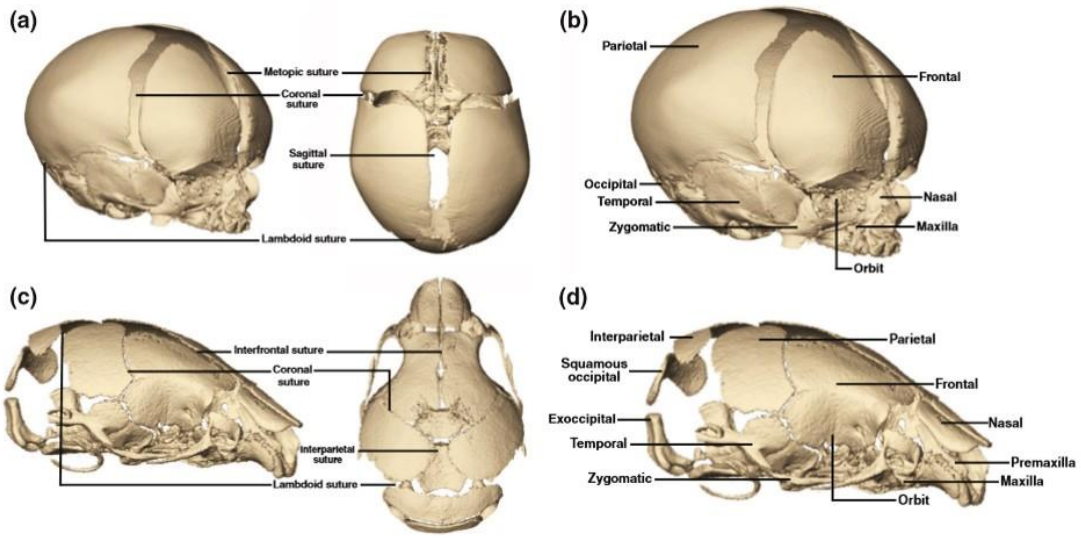

Figure 1: Three-dimensional (3D) reconstructions of computed tomography (CT) images of a neonatal human skull (a and b) and a newborn mouse skull (c and d) illustrating corresponding cranial bones and sutures of the two species. In panels a and c, an oblique lateral view is shown at left and a superior view at right with face towards the top and occiput towards the bottom of page. The human sagittal and metopic sutures (a) correspond to the murine interparietal and interfrontal sutures (c), respectively. Selected corresponding cranial bones in the neonatal human (b) and mouse (d) skull are shown. The interparietal bone in mice is analogous to the most superior segment of the squamosal portion of the occipital bone in humans. The premaxilla is a separate bone in mice but is fused with the maxilla prior to birth in humans. Flaherty K., Singh N., Richtsmeier J. (2016), Understanding craniosynostosis as a growth disorder. *WIREs Dev Biol* 5:429–459.

Ossification may occur through either the intramembranous pathway or the endochondral one. In the intramembranous ossification pathway, mesenchymal stem cells differentiate towards bone-forming osteoblasts through intermediate steps of

proliferating populations of osteoprogenitor and preosteoblast cells. During endochondral ossification, however, mesenchymal stem cells differentiate towards chondrocytes that form cartilage which is later replaced by bone. In mammals the majority of the facial bones along with the cranial vault bones (frontal, parietal, squamous temporal and interparietal bone) are formed through the intramembranous osteogenesis, while the bones of the cranial base (e.g. ethmoid, basi-occipital, basi-sphenoid) are mainly formed through the endochondral pathway (Fig. 3) [1]. Sutures comprise the fibrous connective tissues that exists between the bones of the skull and have crucial role in the coordination of brain and skull development. Although they are also found between facial bones in the viscerocranium, the sutures existing between calvarial bones are of particular interest to this study. The metopic suture (or interfrontal suture as is called in mice) is located between the frontal bones, the coronal sutures are found between the frontal and parietal bones, the sagittal suture between the two parietal bones while the lambdoid sutures are the ones between the parietal bones and the occipital one (interparietal bone in mice), as shown in Figure 1. Non-committed mesenchymal stem cells (MSCs) are found to be located in the middle of the sutures [3], while more differentiated cells are found to populate the regions surrounding the osteogenic fronts (Fig. 2). Since the majority of the facial bones and the flat bones of the cranial vault are formed through the intramembranous ossification pathway, cranial sutures have generally been characterized as intramembranous bone growth sites [4]. Yet studies in rodents reveal that the posterior part of the interfrontal suture fuses through a cartilaginous template, thereby displaying endochondral ossification ability [5, 6].

Although the facial skeleton springs primarily from neural crest mesenchymal stem cells, the bones of the cranial vault originate from two sources: both neural crest- and mesoderm-derived mesenchymal cells. More specifically, the frontal bones and the squamous temporal bones come from the cranial neural crest cells, while the parietal bones and the occipital one come primarily from mesoderm-derived mesenchymal stem cells (Fig. 3) [1, 7]. The interfrontal suture and the sagittal suture are mainly populated by neural crest-derived mesenchymal cells, yet the coronal sutures have been shown to contain mesoderm-derived mesenchymal cells [8]. Analogous origin is displayed by the dura mater underlying the cranial vault bones, as presented in the next section.

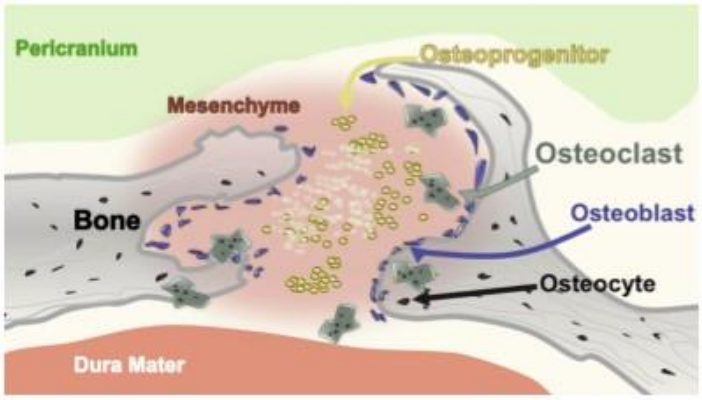

Figure 2: A schematic representation of the cranial suture complex. Two osteogenic bone fronts are bridged by mesenchymal tissue with the associated osteoclasts, the osteoblasts, and osteoprogenitor cells. The underlying dura mater and overlying pericranium also contribute to this functional complex. Beederman M., et al. (2014), *Genes & Diseases* 1, 120-125.

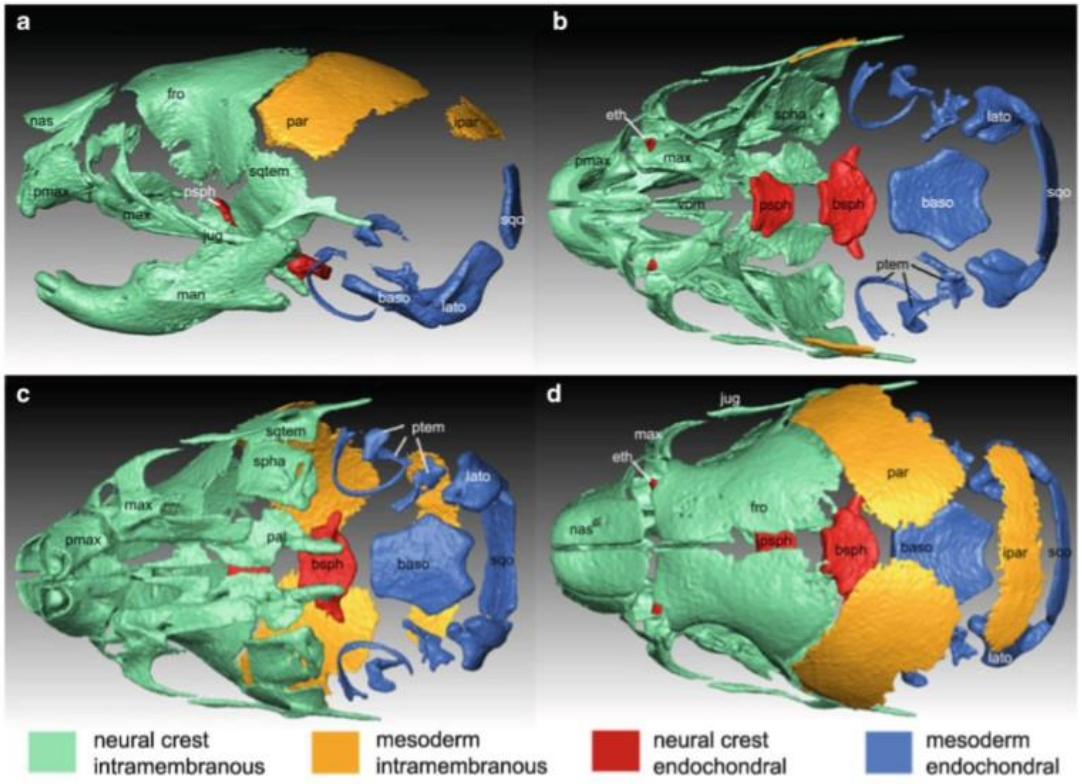

Figure 3: Cell origin and ossification type of the skull bones. 3D reconstruction of high-resolution micro-computed tomography images of a newborn mouse head segmented to visualize mineralized bone. Individual cranial elements are colour-coded to represent the contribution of neural crest or mesoderm and whether the bone forms intramembranously or endochondrally. In all views rostral is to left and caudal is to right. Views are lateral (a), superior with cranial vault removed (b), inferior with mandible removed (c), superior (d). Abbreviations of individual bones are as follows: facial skeleton: max maxillae, jug jugal, nas nasal, pmax premaxillae, vom vomer, pal palatine (includes pterygoid), man mandible; cranial vault: fro frontal, par parietal, ipar interparietal, sqtem squamous temporal; cranial base: lato lateral occipital, sqo squamous occipital, baso basi occipital, psph presphenoid, spha sphenoid alae, bsph basi sphenoid, ptem petrous temporal, eth ethmoid. Abbreviations for bones that occur bilaterally are given only on one side. Though primarily of mesoderm origin, the center of the interparietal (ipar) bone receives small numbers of neural crest cells and the presphenoid (psph) receives small numbers of neural crest cells between the sphenoid alae and base. At P0 the petrous temporal (ptem) and the ethmoid (eth) are mostly cartilaginous. Richtsmeier J.T., and Flaherty K. (2013), Hand in glove: brain and skull in development and dysmorphogenesis. *Acta Neuropathol* 125, 469-489.

1.2 Craniofacial Development

Three germ layers are formed during the early embryonic development of vertebrates: ectoderm, mesoderm and endoderm, while neural crest cells that are sometimes considered as the fourth germ layer, are derived from ectodermal cells that undergo epithelial-to-mesenchymal transition during the formation of the neural tube. The bony skull is composed of the neurocranium and the viscerocranium. The neurocranium, which surrounds the brain, is formed from mesoderm and neural crest cells, while the viscerocranium that refers to the facial skeleton, is primarily derived

from neural crest cells [9]. During mouse development, by embryonic day 10 (E10) mesenchymal cells originating from the neural crest and the mesoderm complete their migration towards the first and second branchial arches and the positions of the future skull bones [10]. Especially for the frontal and parietal bones, the flat bones of the skull, groups of neural crest- and mesoderm-derived cells accumulate in a location above the developing eye called the supraorbital regulatory centre at around E10.5 (Fig. 4), from which they migrate to the sites of the future frontal and parietal bones respectively, between E11.5 and E13.5 [11-13]. Cellular proliferation and mesenchymal condensation precede the expression of osteogenic markers which starts from E13.5 and on. The appearance of mineralized extracellular matrix as an indication of the first bony element, takes place between E15.5 and E17.5. At the same time, cranial sutures form. The interfrontal suture and the sagittal suture of the skull are mainly populated by neural crest-derived mesenchymal cells, while the coronal sutures contain primarily mesoderm-derived mesenchymal cells [8]. The cranial sutures in mice remain patent throughout life with the exception of the interfrontal suture which fuses in a biphasic manner, with the first phase including the formation of cartilage from postnatal day 10 (P10) to P20 and the second phase including the mineral deposition from P21 to P45 [14]. The interfrontal suture closure occurs in an anterior to posterior direction [15].

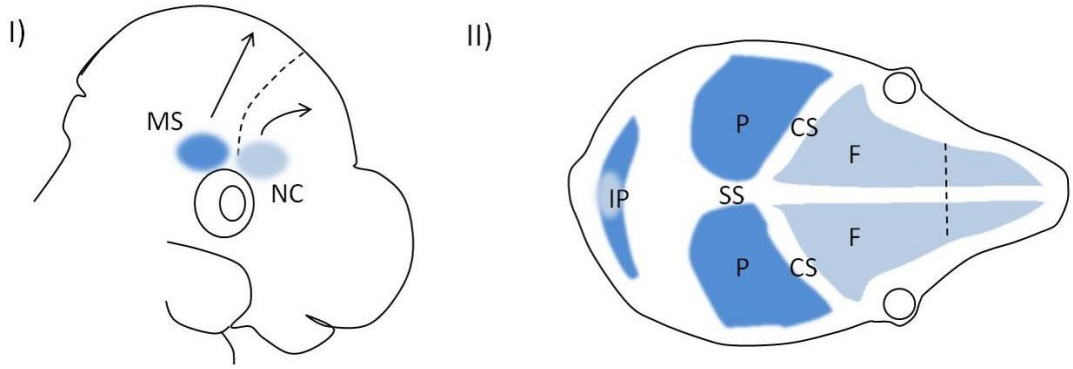

Figure 4: Mouse embryonic craniofacial development. (I) Populations of mesoderm-derived mesenchymal cells (shown in dark blue) and neural crest-derived mesenchymal cells (shown in light blue) accumulate at the supraorbital regulatory centre at E10.5, from which they migrate to the sites of the future parietal and frontal bones, respectively, shown in (II). MS, mesoderm-derived mesenchymal cells; NC, neural crest-derived mesenchymal cells; F, frontal bone; P, parietal bone; IP, interparietal bone; CS, coronal suture; SS, sagittal suture. Vogiatzi A. and Mavrothalassitis G. (2019), Craniofacial, orofacial and dental disorders: the role of the RAS/ERK pathway. *Expert Rev Mol Med* 21, e2

In humans mesenchymal condensations lead to the formation of a membrane-like structure around the developing brain called meninx primitiva during the 5th week post conception [16, 17]. This is the first indication of the cranial vault. The meninx primitiva gradually gives rise to two distinct cell layers: the endomeninx, which develops into the arachnoid and pia mater later at around the 8th week post conception, and the ectomeninx, which develops into the dura mater and a superficial layer with

osteogenic and chondrogenic capacity that contributes to the formation of calvarial bones (Fig. 5).

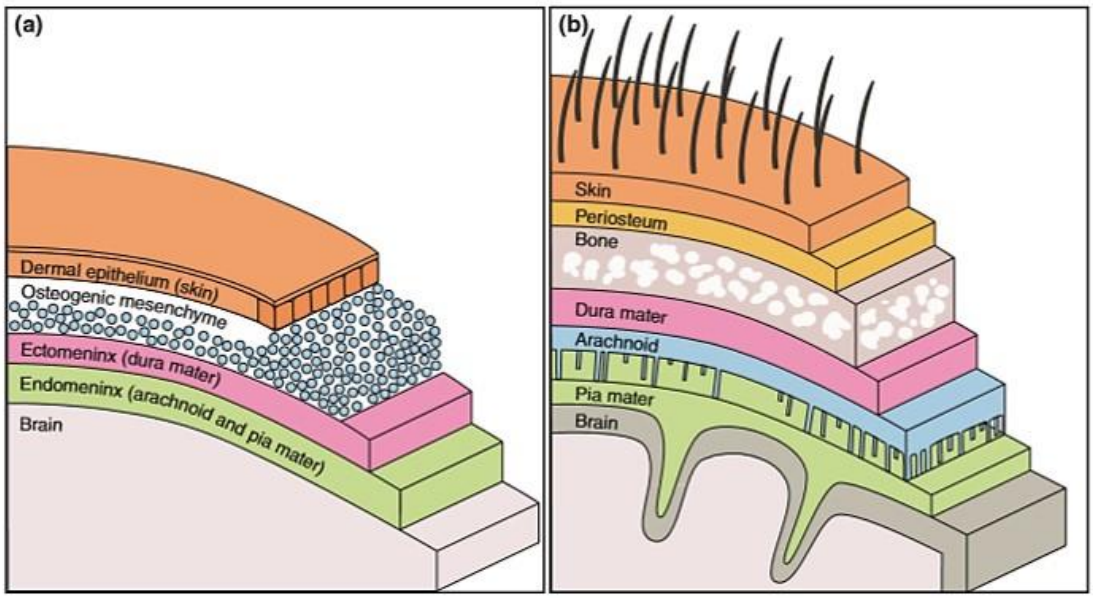

Figure 5: Coronal section showing layers from dermal epithelium to brain during osteogenesis (a) before bone formation and (b) after bone formation. Flaherty K., Singh N., Richtsmeier J. (2016), Understanding craniosynostosis as a growth disorder. *WIREs Dev Biol* 5:429–459.

The first ossification centres can be detected between the 7th and 8th week post conception and by the 14th week considerable formation of the frontal and parietal bones can be seen (Fig. 6). By the 16th week the opposing bones have developed and cranial sutures begin to form. Woven bone is the first type of bone formed in the embryo displaying an immature structure with randomly organised collagen fibers. However, at around birth time this woven bone is replaced by the lamellar bone which presents a regular parallel alignment of collagen fibers and is stronger. As opposed to mice in which the majority of cranial sutures remain unossified throughout life, sutures in humans close gradually. The metopic suture is the one that fuses first starting from the 2nd postnatal year until around the 7th year of life. The majority of the other cranial sutures close by the 12th year, but the process of suture closure may last until the 3rd decade of human life and beyond [18]. During the first year calvarial bones grow fast following the growth of the brain which is rapid as well. The bone growth is performed by the differentiation of osteogenic cells and the deposition of osteoblasts/ osteocytes at the sutural margins.

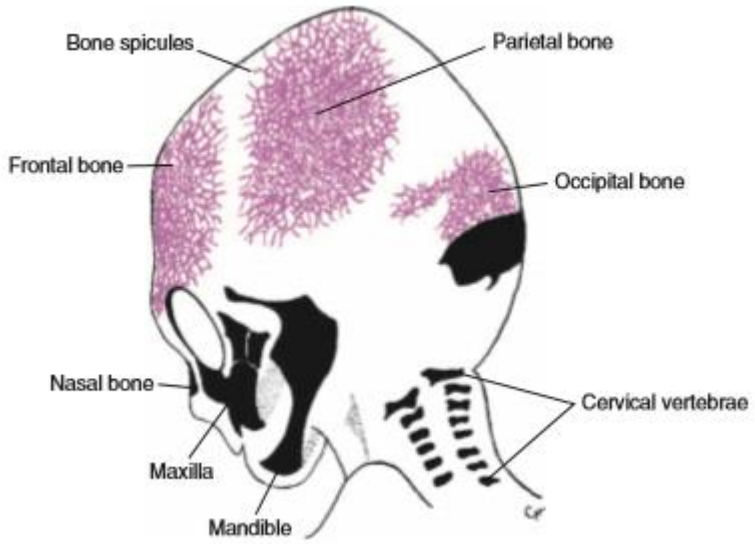

Figure 6: Skull bones of a 3-month-old fetus show the spread of bone spicules from the primary ossification centres in the flat bones of the human skull. Sadler T.W. and Langman J. (2012), Langman's medical embryology, 12th edition.

1.3 From MSCs to Osteocytes and Bone: exploring the route

During the intramembranous ossification process, non-committed mesenchymal stem cells once induced, give rise to populations of proliferating osteoprogenitor and preosteoblast cells, that finally differentiate towards bone-forming osteoblasts and osteocytes. Although well-studied through the years, no specific unique markers have been found to characterize the particular populations of cells. However, *Runt-related transcription factor-2* (*Runx2*) and *Osterix* are the main factors that are up-regulated during the transition from MSCs to osteoprogenitor and preosteoblast cells. This proliferating phase is characterized also by the expression of cell cycle-associated genes such as the *c-Myc* and *c-Fos*, while the downregulation of proliferation and the initiation of extracellular matrix synthesis, deposition and mineralization performed particularly by osteoblasts, correlates with the expression of collagenous and non-collagenous proteins such as the osteopontin (OPN), bone sialoprotein (BSP), alkaline phosphatase (ALP or TNSALP) and osteocalcin (OCN) and matrix modifying enzymes such as matrix metalloproteinases (MMPs) [19]. An overview of the process including the sequence of cell types and markers expressed during the intramembranous osteogenesis pathway is shown in Figure 7.

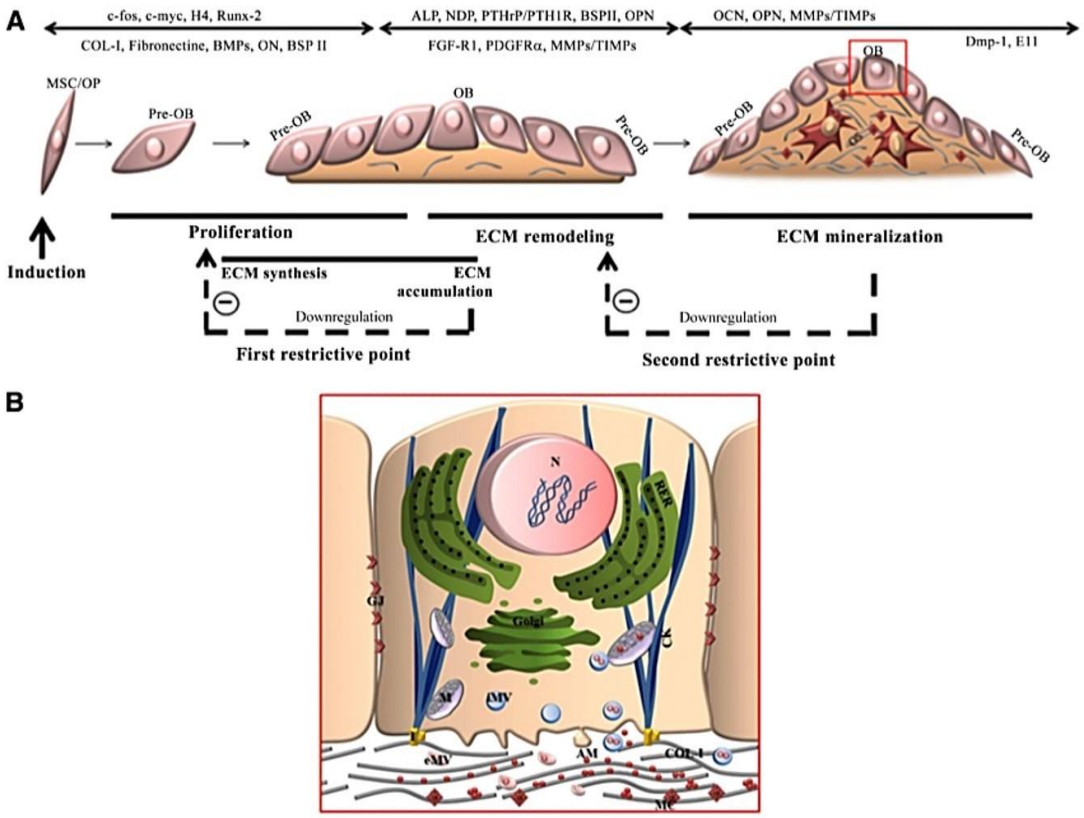

Figure 7: Bone-like nodule formation. (A): Schematic overview of developmental sequences involving morphologic progressions and selective expression of genes that regulate cell proliferation and promote osteoprogenitor commitment and bone-like nodule formation. These processes were schematically illustrated by three major stages divided by two restrictive points. Downregulation of proliferation/ ECM accumulation and ECM remodeling/ mineral deposition corresponds, respectively, to the first and second restrictive points. Details about OB-mediated ECM mineralization (red square) are provided in (B). (B): The proposed OB-dependent mechanism of calcium phosphate nucleation includes both extracellular and intracellular matrix vesicles. Abbreviations: AM, amorphous mineral; CK, cytoskeleton; COL-I, type-1 collagen; ECM, extracellular matrix; eMV, extracellular matrix vesicle; GJ, gap junction; I, integrin; iMV, intracellular matrix vesicle; M, mitochondria; MC, mineral crystal; MSC, mesenchymal stem cell; N, nucleus; OB, osteoblast; OP, osteoprogenitor cell; RER, rough endoplasmic reticulum. Mechiche Alami S. et al. (2016), Concise Review: In Vitro Formation of Bone-Like Nodules Sheds Light on the Application of Stem Cells for Bone Regeneration. *STEM CELLS TRANSLATIONAL MEDICINE* 5:1587–1593

In vitro the proliferation of osteoprogenitor and preosteoblast cells and the secretion and mineralization of the extracellular matrix (ECM) by osteoblasts results in the formation of three-dimensional structures called bone-like nodules. In vivo, calcifying nodules are also detected in the osteoid beneath mature osteoblasts in bone regions (Fig. 8) [20].

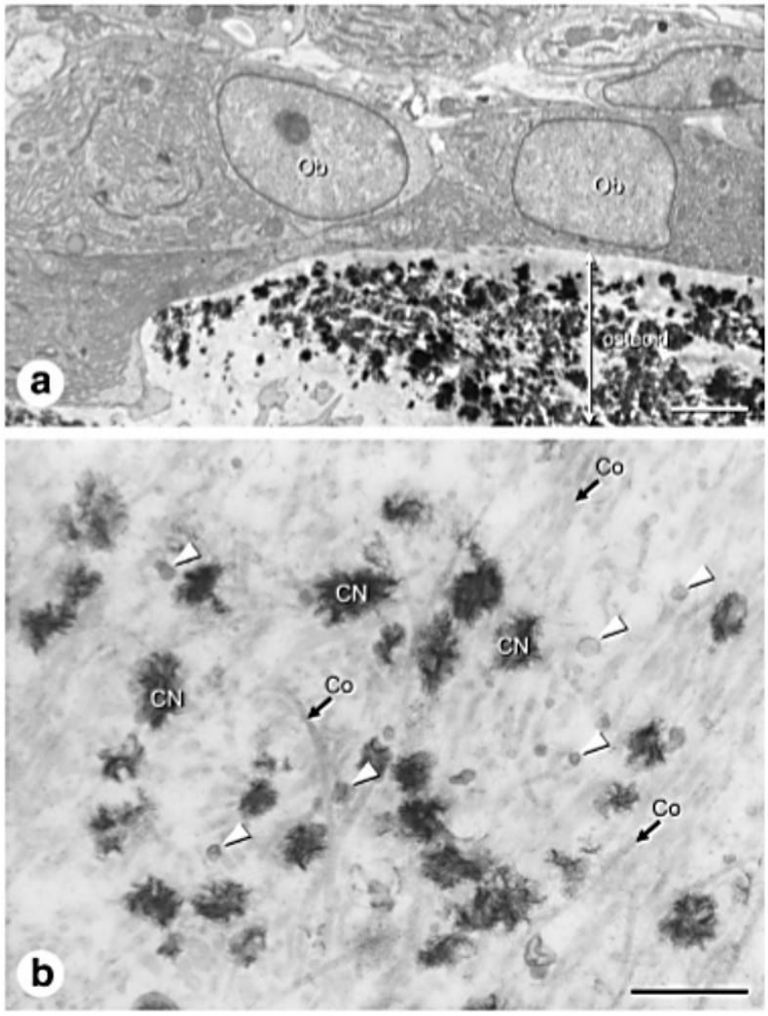

Figure 8: TEM observation of matrix vesicles and calcifying nodules in osteoid. Panel a demonstrates many calcifying nodules shown in black in the osteoid beneath mature osteoblasts (Ob). At a higher magnification of the osteoid, many matrix vesicles indicated by white arrowheads, calcifying nodules (CN) and collagen fibrils (Co) can be seen (panel b). Bars, a) 2 µm, b) 1 µm. Hasegawa T. (2018), Ultrastructure and biological function of matrix vesicles in bone mineralization. *Histochemistry and Cell Biology* 149:289–304.

It is believed that the mineralization of the ECM is mediated by matrix vesicles that constitute small extracellular vesicles of approximately 100-300nm in diameter secreted by mature osteoblasts containing ions and enzymes promoting the growth of calcium phosphate crystals inside [20, 21]. Particularly, although calcium (Ca^{+2}) is considered to be more abundant throughout the tissues, the entry of phosphate (PO_4^{-3}) ions into the matrix vesicles is shown to be mediated by enzymes and transporter proteins such as the ectonucleotide pyrophosphatase/phosphodiesterase 1 (ENPP1), ankylosis (ANK), tissue nonspecific alkaline phosphatase (TNSALP), and phosphoethanolamine/ phosphocholine phosphatase (PHOSPHO1). ENPP1 is expressed by osteoblasts and generates extracellular and intracellular pyrophosphate (PPi) by hydrolyzing molecules such as the ATP. ANK has a role in PPi transport from the intracellular to the extracellular space and into the matrix vesicles, while ALP (or

TNSALP) hydrolyzes PPi to Pi monomers that are finally supplied and accumulated in the vesicles, thus promoting crystalline nucleation and growth (Fig. 9). Finally, the crystal is thought to penetrate the membrane of the matrix vesicle and grow out forming the calcifying nodule. Although the exact biogenesis of matrix vesicles remains elusive, in vitro and in vivo data indicate the binding of these vesicles to deposited collagen fibers and a defined role in the calcification of ECM.

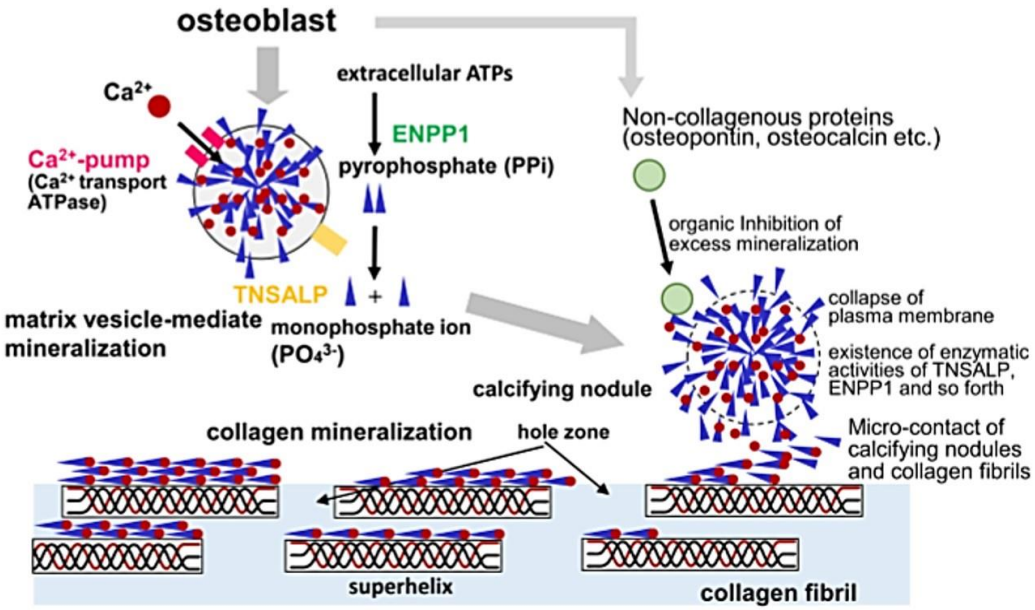

Figure 9: A schematic design of collagen mineralization. Many mineral crystals penetrate the vesicles' membranes to form a globular assembly of numerous mineral crystals, i.e., a calcifying nodule. Even though the plasma membrane of matrix vesicles collapse, the enzymatic activities still remain to deposit Ca^{2+} and PO_4^{3-} onto calcifying nodules. When calcifying nodules make contact with surrounding collagen fibrils, mineral crystals from the calcifying nodule extend along the superhelix of collagen fibrils. Hasegawa T. (2018), Ultrastructure and biological function of matrix vesicles in bone mineralization. *Histochemistry and Cell Biology* 149:289–304.

1.4 Craniosynostosis

The formation of the human head is a complex process involving sequences of crosstalk events between different germ layers and tissues and spatiotemporal activation of a variety of molecular signaling cascades [13]. Deviations from this well-orchestrated programme can lead to craniofacial malformations, some of which reaching the point of life-threatening unless treated. Focusing our study to the cranial suture biology and the formation of the cranial vault, it is worth mentioning that Hippocrates was the first to describe the abnormalities in head shape caused by the premature closure of specific cranial sutures [22]. Today, craniosynostosis is the term used to describe the condition in which one or more of the sutures of the skull close prematurely, resulting in abnormal head shapes often including vision, hearing and mental impairment as well. Craniosynostosis has an occurrence rate of about one in

2250 births and consists the second most common human craniofacial disorder after orofacial clefts [12, 22]. It is classified as isolated or complex craniosynostosis depending on the number of prematurely fused sutures. It can be also divided into non-syndromic and syndromic according to the presence of additional phenotypic traits beyond the fused sutures. The phenotype of synostosis usually becomes evident between the last months of prenatal period and the end of the first year of postnatal life [12]. The growth of the skull is strongly inhibited in the plane perpendicular to the fused suture and is allowed to proceed in the direction parallel to that, thus causing a distortion in the head shape. Different types of synostosis displaying characteristic clinical features arise from the premature fusion of particular sutures (Fig. 10) [23].

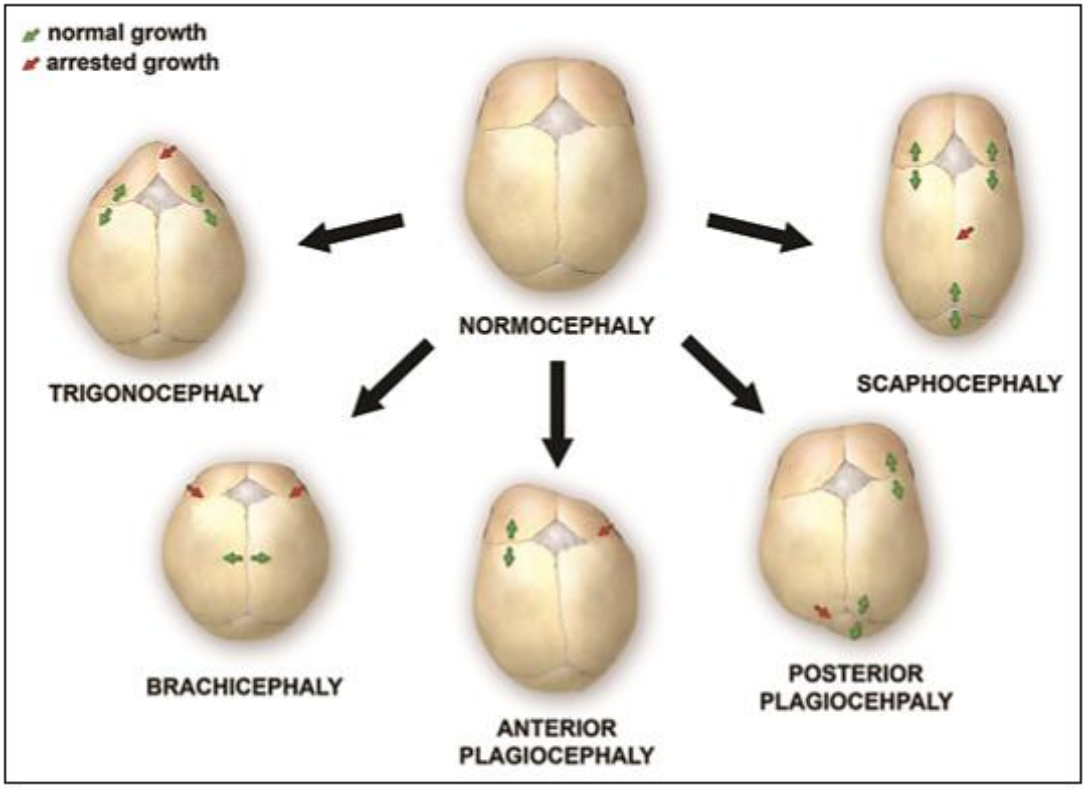

Figure 10: Various deformations of the skull, associated with single-suture synostoses. Kajdic N. et al. (2018), Craniosynostosis- Recognition, clinical characteristics and treatment. *Bosn J Basic Med Sci* 18(2):110-116.

Surgical intervention is the only therapeutic approach currently available for craniosynostosis. It is required both for the correction of craniofacial morphology that unless treated may lead to psychosocial instability for the child, and for creating the appropriate skull volume to accommodate the expanding brain thus ensuring normal cognitive functions. Surgical management can be divided into open cranial vault reconstruction procedures and minimally invasive surgical approaches including endoscopic strip craniectomies, spring-assisted cranioplasty and distraction osteogenesis [24, 25]. However, complications often occur and include intraoperative

bleeding, wound infections and hyperthermia among others [23]. In the late 1800s surgery for craniosynostosis had a mortality rate of approximately 50% [26]. Until 2010 this rate dropped to 0.1% [27].

1.5 Craniosynostosis syndromes and associated mechanisms

Although the aetiology is still unknown for many cases of craniosynostosis, specific gene mutations have been linked to the pathogenesis of the disease and are shown to lead to particular phenotypes that comprise the associated craniosynostosis syndromes. Especially gain-of-function mutations in *FGFRs* account for the majority of syndromic incidences displaying usually an autosomal dominant pattern of inheritance. Some of the most known craniosynostosis syndromes along with potential molecular and cellular mechanisms that are reported so far are presented in this section.

Apert Syndrome

Mutations in *FGFR2* resulting in protein gain-of-function lead to Apert syndrome in humans characterised by premature fusion of cranial sutures, syndactyly in hands and/or feet along with developmental retardation among other features. Ser252Trp, Pro253Arg [28] and Glu731Lys [29] substitutions on FGFR2 are found to be the causative mutations in patients with Apert syndrome. Mice carrying the $Fgfr2^{S252W}$ allele ($Fgfr2^{S252W/+}$ mice) display craniosynostosis [30], while a decrease in the overall bone mass and mineral density is also reported by another study [31]. Increased p38 Mapk and Erk1/2 signalling were shown to mediate the appearance of the abnormal phenotypes [31, 32]. Furthermore, in an independent study calvarial cells isolated from Apert infants and fetuses with S252W mutation displayed enhanced osteogenic differentiation and in vitro bone matrix production suggesting that craniosynostosis could spring from an increase in the number of precursor cells that enter the osteogenic pathway [33]. However, another study proposes that the presence of increased apoptosis detected in human Apert S252W primary calvarial cells could be implicated in the pathophysiology of the disorder [34]. Considering the second mutation, mice carrying the $Fgfr2^{P253R}$ allele display craniosynostosis, growth retardation, syndactyly and defects in the cranial base and the growth plates of the long bones [35]. Increased levels of phosphorylated p38 and Erk1/2 Mapks were detected in neurocranial tissues of E17.5 embryos [36] while the administration of PD98059 (a MEK inhibitor) was shown to alleviate the premature suture fusion in calvaria organ cultures isolated from $Fgfr2^{P253R/+}$ mice [35]. Finally, MC3T3–E1 calvarial preosteoblasts expressing the $Fgfr2^{E731K}$ allele exhibit accelerated proliferation, elevated Runx2 transcriptional activity and increased expression of the alkaline phosphatase gene (*Alp*) which is a marker of osteogenic differentiation [29]. Enhanced Erk1/2 pathway activation was reported in this case too. Collectively, increased osteogenic differentiation of calvarial cells, altered cellular proliferation and elevated apoptosis have been suggested to

participate in the pathophysiological mechanisms of the disease while ERK1/2 and p38 molecular pathways seem to have central roles in mediating the effects.

Pfeiffer Syndrome

Pfeiffer syndrome is caused by more than 30 possible mutations in *FGFR2* gene while the Pro252Arg substitution in FGFR1 accounts for some cases too [37-40]. Craniosynostosis, facial deformities, brachydactyly and syndactyly are some of the features of patients with Pfeiffer syndrome. Mice carrying the Pro250Arg mutation in FGFR1 (*Fgfr1*$^{P250R/+}$ mice) corresponding to the Pfeiffer syndrome mutation in humans, exhibit premature fusion of calvarial sutures and craniofacial deformities [41]. Elevated cellular proliferation along with increased expression of osteogenic differentiation markers were detected in the sutures of mutant mice. In an independent study, *Fgfr1*$^{P250R/+}$ mice were also shown to have synostosis of multiple facial sutures leading to midfacial hypoplasia in the absence of a prematurely ossified cranial base [42]. Since identical mutations in *FGFR2* can cause either Pfeiffer or Crouzon syndrome in humans [43], further evidence on potential molecular and cellular mechanisms from mouse studies are presented in the following part addressing Crouzon syndrome cases.

Crouzon Syndrome

A group of mutations in *FGFR2* gene has been identified to have a causative role in the appearance of Crouzon syndrome in humans, with Cys342Arg, Cys342Tyr, Cys342Ser, Tyr340His and Ser354Cys protein substitutions being reported among others [44]. Characteristic craniofacial deformities along with premature cranial suture fusion result in Crouzonoid facies, however abnormalities in limbs are not usually detected in patients with this syndrome [40]. Mice carrying the Crouzon and Pfeiffer gain-of-function mutation Cys342Tyr (*Fgfr2c*$^{C342Y/+}$ mice) display severe coronal synostosis along with increased Erk1/2 phosphorylation in coronal sutures from E18.5 to postnatal day 1 (P1) [45]. Interestingly, although *Fgfr2c*$^{-/-}$ mice exhibit decreased mineralisation of the calvarial bones and lower levels of phosphorylated Erk1/2, they also develop the craniosynostosis phenotype [45], indicating the complexity of the role of the ERK pathway in cranial suture formation and maintenance [13]. In bone marrow mesenchymal cells derived from the Crouzon mouse model *Fgfr2*$^{C342Y/+}$, increased early-stage osteogenic differentiation was reported upon in vitro induction conditions, followed however by decreased late-stage mineralisation in comparison to that of wild type cells [46]. Furthermore, in an independent study, OB1 osteoblastic cell lines modified to express the Crouzon-related C342Y-FGFR2 mutant or the Apert-related S252W-FGFR2 mutant displayed diminished calcification upon in vitro osteogenic differentiation conditions [47]. These data indicate that altered FGFR signalling may affect the cranial suture maintenance and skull ossification in a time- and stage-dependent manner.

Saethre-Chotzen Syndrome

This syndrome is reported to be caused by nonsense and missense mutations, as well as insertions and deletions in the *TWIST1* locus coding for a basic helix-loop-helix transcription factor [48, 49]. Facial dysmorphism, craniosynostosis, brachydactyly and partial cutaneous syndactyly are listed among the features displayed by patients with this syndrome. Mice heterozygous for Twist1 (*Twist1*$^{+/-}$ mice) present mandibular hypoplasia, incomplete ossification of the temporal bone and zygomatic arch [50], while other studies mention the existence of premature coronal suture closure and facial and digit dysmorphology with variable severity [48, 51]. Of course, it should be mentioned that all those phenotypic traits described in various mouse models of craniosynostosis syndromes depend sometimes upon the genetic background of the animals, hence there is a lot of variation in the appearance of particular phenotypes in some cases. In a study on human adipose-derived mesenchymal stem cells (hASCs), suppression of TWIST1 was shown to activate both BMP and FGF/ ERK pathways which led to an increase in the osteogenic differentiation of the cells mediated by TAZ (transcriptional coactivator with PDZ-binding motif) upregulation [52]. Furthermore, in an independent study, *Twist1*$^{+/-}$ mice displayed reduced percentage of Gli1^{+} mesenchymal stem cells in cranial sutures, suggesting that the phenotype of craniosynostosis could result in time from a depletion of skeletal stem cells residing in sutures [53]. Last but not least, it was shown that in *Twist1*$^{+/-}$ mice the coronal suture closes between postnatal day 9 (P9) and P14 through a cartilaginous intermediate, thereby displaying endochondral ossification ability [54]. This suggests that the synostosis mechanism could also involve a shift from the intramembranous ossification to the endochondral one.

Beyond the well-known craniosynostosis syndromes described above, there are also many others [12, 39, 40] not mentioned in the present thesis due to space limitations, while the list of the mutated causative genes becomes even more extended through the years. Continuous research also provides insight into the potential molecular and cellular mechanisms underlying the appearance of the phenotype. Figure 11 is a collective representation of genes and associated mechanisms reported so far for a variety of craniosynostosis cases [12]. Further experimental work is however required to understand the interplay of the implicated factors.

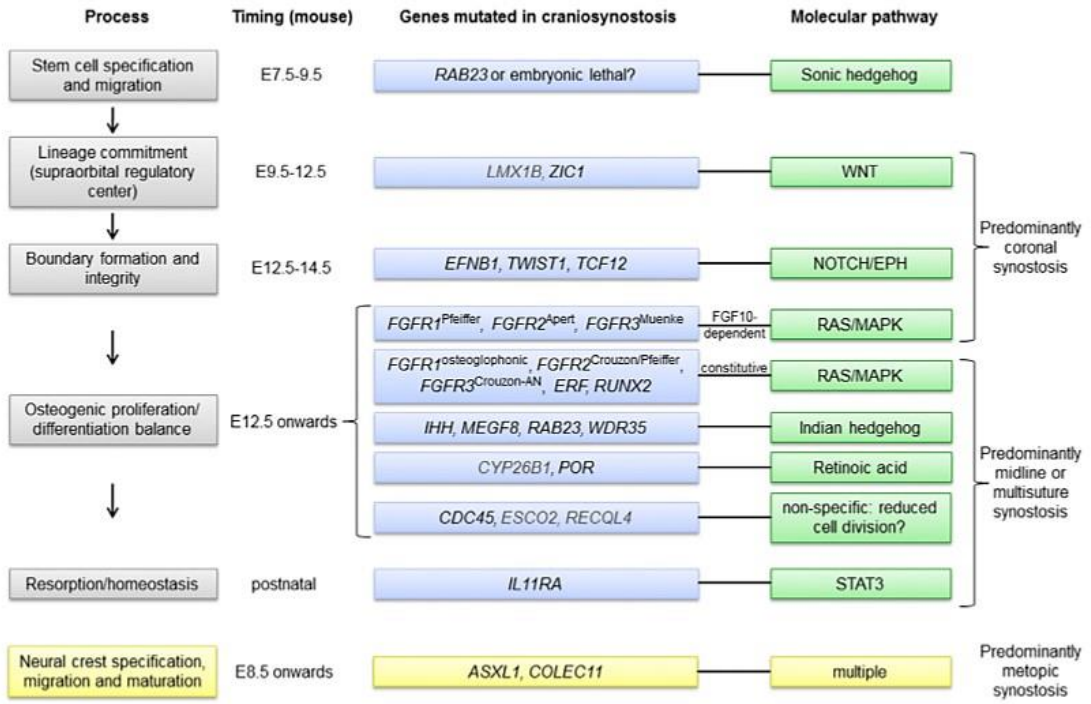

Figure 11: A Genetic-Pathophysiological Framework for Craniosynostosis. Processes in suture formation are displayed on the left (gray boxes). Other panels show relative timing of events in mouse, genes mutated (blue boxes; black type for core genes and gray type for additional genes), and pathways proposed to be affected (green boxes). Patterning of the supraorbital regulatory center and boundary formation are events particular to coronal suture development; correspondingly, mutations disrupting these processes lead predominantly to coronal craniosynostosis. Later developmental processes (proliferation-differentiation balance, homeostasis) apply to all sutures and correspondingly, pathological suture involvement tends to be more generalized. Twigg S. and Wilkie A. (2015), A genetic-pathophysiological framework for craniosynostosis. *Am J Hum Genet*., 97, 359-377.

1.6 ERF-related craniosynostosis

Heterozygous loss-of-function mutations in *ERF* (*ETS2 Repressor Factor*) locus coding for an ETS-DNA binding transcriptional repressor protein, cause complex craniosynostosis (CRS4) in humans along with facial dysmorphism, Chiari-1 malformation, language delay and behavioral problems in some cases [55-57]. Non-sense and missense mutations such as Arg183*, Arg86Cys, Arg65Gln as well as frameshift mutations such as Phe504Leufs*27, Gly299Argfs*9 and Lys401Glufs*10 have all been reported among others in patients with CRS4 (Fig. 12).

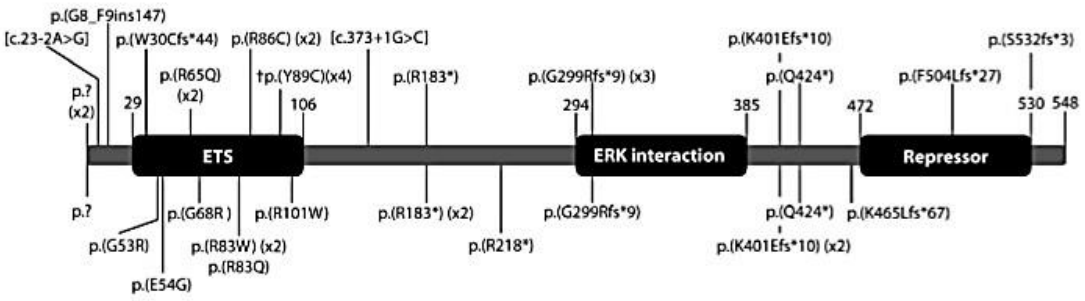

Figure 12: Domain structure of the ERF protein and the mutations identified. Mutations identified in different cohorts are shown underneath and above. †Refers to the heterozygous ERF missense substitution found to cause Chitayat syndrome. Glass G. et al (2018), ERF-related craniosynostosis: the phenotypic and developmental profile of a new craniosynostosis syndrome. *Am J Med Genet.* 179A:615–627.

Among syndromic craniosynostosis cases, the overall prevalence of *ERF* mutations is estimated to be around 2%, while this number drops to 0.7% for non-syndromic cases [58]. Premature closure is most commonly observed in the sagittal and lambdoid sutures, however pansynostosis is also reported [55, 56]. Interestingly, in contrast to other syndromic forms, ERF-associated craniosynostosis displays a late disease onset often accompanied by an insidious progression [56]. Concerning the phenotypic traits of the affected individuals, there is not an exact phenotype-genotype correlation and the features are reported to vary in severity [55, 56]. Recently, another missense mutation on ERF sequence (Tyr89Cys, located in the DNA-binding domain of the protein) was found to be the cause of Chitayat syndrome, characterised by hyperphalangism, facial dysmorphism and respiratory defects [59]. Craniosynostosis was not reported among the individuals carrying the corresponding mutation, however further studies are needed in order to elucidate the phenotypes and the associated mechanisms. Mice expressing approximately 30% of the wild-type ERF protein levels ($Erf^{LoxP/-}$ mice) –due to the presence of the hypomorphic Erf^{LoxP} allele- display domed heads and craniosynostosis affecting multiple cranial sutures, yet no other skeletal abnormalities are observed (Fig. 13) [55].

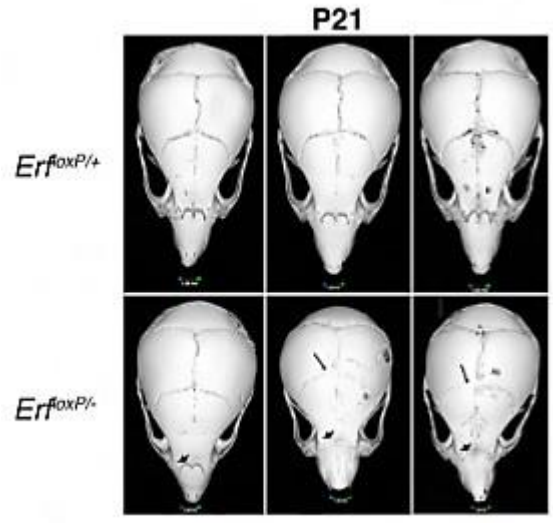

Figure 13: ERF-related craniosynostosis in mice. Micro-CT scans of postnatal day 21 (P21) skulls from $Erf^{LoxP/+}$ (top) and $Erf^{LoxP/-}$ (bottom) littermates. Coronal synostosis is beginning to be apparent in 2 of 3 $Erf^{LoxP/-}$ animals (arrows). The nasal bones (arrowheads) are already abnormal in all three $Erf^{LoxP/-}$ animals. Twigg S., Vorgia E. et al. (2013), Reduced dosage of ERF causes complex craniosynostosis in humans and mice and links ERK1/2 signalling to regulation of osteogenesis. *Nat Genet.* 45, 308-313.

$Erf^{+/-}$, $Erf^{LoxP/+}$ and $Erf^{LoxP/LoxP}$ mice exhibit a normal phenotype, while $Erf^{-/-}$ die by E10.5 due to severe placental defects [60]. Of note premature suture fusion in $Erf^{LoxP/-}$ mice becomes apparent during the first 3-6 weeks of postnatal life and is preceded by a mild reduction in the ossification of calvarial bones [55]. Also, a reduction in the expression levels of particular osteogenic markers was evident in E16.5 calvarial tissue from

Erf$^{LoxP/-}$ mutants in comparison to healthy littermates. These data indicate possibly a complex role for Erf in calvarial bone development. However, no reports existed about the potential involvement of this factor in either osteogenesis or cranial suture biology mechanisms so far.

1.7 ERF: the gene, the protein and the reported roles

ERF (ETS2 repressor factor) is an ~75kDa protein present in almost all cell types and tissues. It is encoded by the *ERF* gene located on human chromosome 19 which produces a 2.7 kb mRNA carrying the information for the synthesis of a 548 amino acid polypeptide chain [61]. The gene in both humans and mice consists of 4 exons over a region of 10kb and the human and mouse proteins are estimated to have 98% identity with all basic motifs conserved between the two species [62]. *ERF* belongs to the family of ETS genes (E26 transformation specific) whose products recognize and bind DNA on the ets-binding-site (EBS) lying in the regulatory regions of a variety of genes. The ETS transcription factor family today is reported to contain 28 members in humans that are clustered into 12 subfamilies based on their sequence alignment data (Fig. 14) [63, 64]. Although the majority of the members act as transcriptional activators, ERF is shown to possess suppressor activity [61]. Its DNA-binding domain is located at the N-terminus of the protein, while its repressor domain lies at the C-terminus between residues 472-548 (Fig. 12). In the intermediate part of the polypeptide chain there is a region carrying FXF motif sequences that participate in the interaction of ERF with active and inactive ERKs [65].

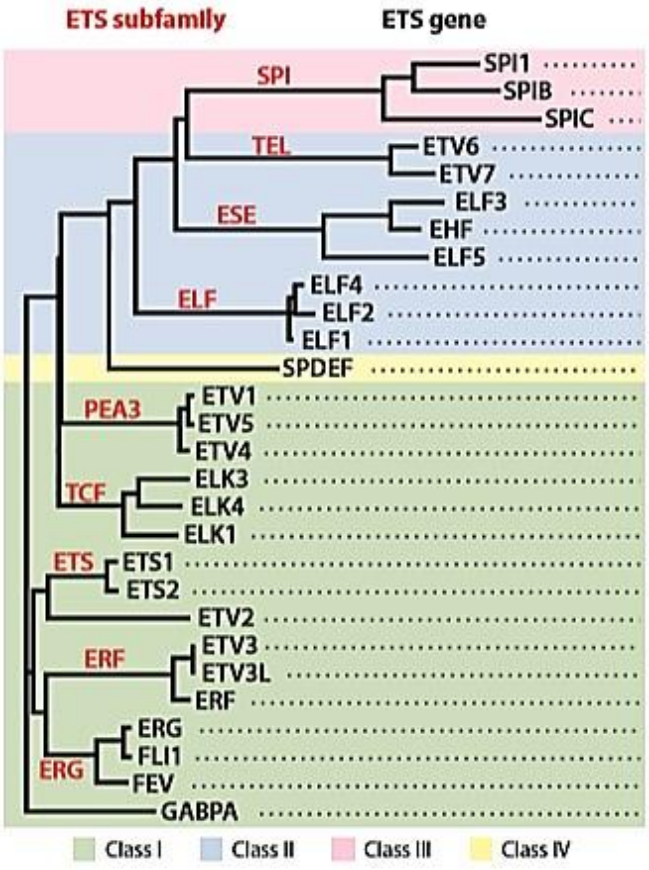

Figure 14: Members of the ETS transcription factor family. A dendrogram shows the degree of relatedness of 28 human ETS domain sequences built by ClustalW using the neighbor-joining method. The length of each horizontal line indicates estimated evolutionary distance. Branches that separate an individual subfamily are labeled in red. Classes defined by differences in the in vitro derived binding site are indicated by background colors. Hollenhorst P., et al. (2011), Genomic and biochemical insights into the specificity of ETS transcription factors. *Annu. Rev. Biochem*. 2011. 80:437–71

Activated ERKs are shown to phosphorylate ERF on residues Ser161, Ser246, Ser251 and Thr526 and these phosphorylation events lead to the nuclear export of ERF in a CRM1-dependent manner and the derepression of its target genes [66, 67]. This nucleocytoplasmic shuttling that depends on the phosphorylation status of the protein is the main regulator of ERF function in the cell (Fig. 15). Phosphorylation-defective ERF mutants exhibit constitutive nuclear localization, arrest normal cells at G1 phase of the cell cycle and have the ability to block the oncogenic transformation of NIH3T3 cells by the *Ras* oncogene [66, 67]. These effects were shown to be mediated by ERF regulation of *c-Myc* transcription [68]. In fact, *c-Myc* was the first gene identified to be transcriptionally controlled by ERF. In another study, overexpression of ERF in mammary epithelial cells carrying the oncogenic *Ras* inhibited the TGF-β-induced EMT (epithelial-to-mesenchymal transition) via suppression of *Semaphorin-7a* expression [69]. Furthermore, beyond its potential oncosuppressive activity, ERF was also shown to induce erythroid differentiation of human pluripotent cell lines [70], indicating a role for this factor in cellular differentiation processes in addition to the one in cell cycle control. Concerning its own regulation, little is known beyond the ERK1/2-mediated phosphorylation that determines its subcellular localization. miR-7 is shown to directly suppress the expression of ERF in a study on lung cancer [71]. Also, looking at the transcriptomic level, the promoter of *ERF* is reported to contain binding sites for putative transcription factors like SP1, CREB/ATF as well as ETS factors [62], however further studies are needed in order to understand the

mechanisms that potentially regulate the expression of ERF in various cell types and tissues.

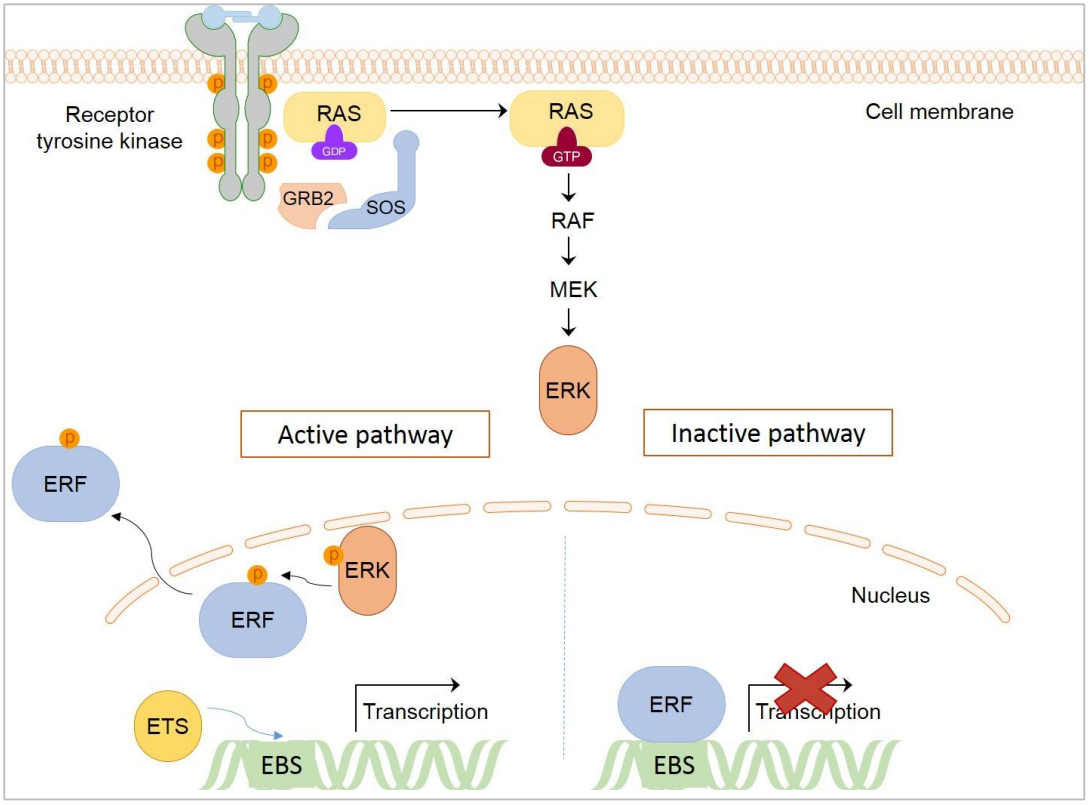

Figure 15: Schematic representation of the regulation of ERF by ERK1/2 signalling. In the absence of ERK activity, ERF is in the nucleus and represses the transcription of genes (right). Upon pathway activation, phosphorylated ERK translocates into the nucleus and phosphorylates ERF (left). This event results in the nuclear export of ERF and the activation of transcription by another ETS factor. For abbreviations, see please in the text.

Additional roles of ERF are constantly being revealed from studies on mouse models. *Erf* knock-out mice die on embryonic day 10.5 (E10.5) due to a block in chorionic cell differentiation [60]. This effect was shown to be mediated in part by the elevated expression of *Fgf2* in *Erf*$^{-/-}$ cells. In fact, Erf was shown to directly bind and suppress *Fgf2* thus promoting proper chorionic trophoblast stem cell differentiation during development [72]. Elimination of *Erf* in the embryo proper using the conditional Meox2-cre animals results in embryonic death at around E14.5 due to severe anemia [73]. This study demonstrates that Erf is required for both the primitive and the definitive wave of hematopoiesis in mice and probably has a role in hematopoietic stem cell maintenance or differentiation processes too. Efficient differentiation of erythroid precursors into mature erythrocytes seems to be also dependent on Erf levels [73]. Finally, *Erf*$^{LoxP/-}$ mice expressing approximately 30% of the wild-type Erf protein levels, display craniosynostosis affecting multiple cranial sutures, facial dysmorphia but no other obvious skeletal defects [55]. This is the first time however that ERF seems to be linked with craniofacial development and

osteogenesis implicating additional emerging roles for this factor that remain to be further examined.

1.8 Aim of the Study

Haploinsufficiency of the transcriptional repressor ERF (ETS2 repressor factor) leads to late-onset complex craniosynostosis in humans and mice preceded by a mild reduction in the ossification of calvarial bones [55]. This newly described type of craniosynostosis (craniosynostosis-4, CRS4) is characterized as insidious due to its late onset and the appearance of subtle phenotypic traits that gradually can lead to detrimental effects [56]. ERF is a member of the ETS transcription factor family that is regulated by nucleocytoplasmic shuttling depended on ERK1/2 activation [66, 67]. It is shown to be involved in cell cycle control via *c-Myc* regulation [68], epithelial-to-mesenchymal transition (EMT) processes via *Semaphorin-7a* suppression [69] and is required for chorionic trophoblast stem cell differentiation during mouse embryonic development mainly through *Fgf2* regulation [60]. Recently, it was demonstrated that Erf has a crucial role in hematopoiesis too [73]. However, no reports existed so far about a potential involvement of ERF in either craniofacial development or osteogenesis procedures. The aim of this study is to explore the role of Erf in intramembranous skull ossification and understand the mechanisms underlying the premature suture fusion phenotype using the mouse model of ERF-related craniosynostosis. The achievement of this goal along with the well-defined pattern of ERF subcellular localization modulation can possibly hold promise for a future therapeutic intervention for craniosynostosis besides the conventional surgical management.

2. Materials & Methods

2. *Materials & Methods*

2.1 Materials, mouse lines & cell lines

2.1.1 Mouse lines

All experiments were performed with $Erf^{LoxP/+}$ and $Erf^{LoxP/-}$ littermates and in agreement with the General Directorate of Veterinary Services. In order to obtain $Erf^{LoxP/+}$ and $Erf^{LoxP/-}$ littermates we crossed $Erf^{+/-}$ mice with $Erf^{LoxP/LoxP}$ mice, both of which previously analyzed in the literature [55]. Furthermore, to eliminate *Erf* in mesenchymal stem/ progenitor cells, we utilized the conditional Nestin-cre/+ mice that express Cre recombinase under the control of the promoter of *Nestin* gene, previously reported to be active in neuroectodermal and mesodermal lineages [74-76]. By crossing Nestin-cre/+ with $Erf^{LoxP/LoxP}$ mice, we finally obtained *Nestin-cre/+;*$Erf^{LoxP/LoxP}$ mice, in which the extent of recombination was evaluated by employing the Gt(ROSA)26Sor$^{tm4(ACTB-tdTomato,-EGFP)Luo}$ mouse line by Jackson [77]. All animals used in our experiments were of a mixed 129/SV × C57BL/6 background.

2.1.2 Cell lines

Cos7 cells: *Cercopithecus aethiops* (African green monkey) kidney cells, SV40 transformed, utilized in our study for the production of Leukemia Inhibitory Factor (LIF).

2.1.3 Cell culture media

Maintenance medium for freshly derived mouse cranial suture cells:

DMEM-F12 Gibco (by Thermo Scientific 31330038)
10% FBS Gibco (by Thermo Scientific 10270106)
100 U/ml penicillin/ streptomycin (by Thermo Scientific 15140122)

Maintenance medium for long-term expanded suture mesenchymal stem/ progenitor cells:

Knock-OUT DMEM Gibco (by Thermo Scientific 10829018)
12% FBS HyClone (by GE Healthcare SV30160.03)
2mM L-glutamine Gibco (by Thermo Scientific 25030024)
1% non-essential amino acids (by Thermo Scientific 11140050)
0.1 mM β-mercaptoethanol (by Fluka)
0.3% v/v leukemia inhibitory factor- LIF (produced in our laboratory)
100 U/ml penicillin/ streptomycin (by Thermo Scientific 15140122)

Maintenance medium for Cos7 cells:

High-glucose DMEM (4,5 g/l) Gibco (by Thermo Scientific 11995-065)
10% FBS Gibco (by Thermo Scientific 10270106)
100 U/ml penicillin/ streptomycin (by Thermo Scientific 15140122)

Maintenance medium for human primary bone marrow mesenchymal stem cells:

A-MEM HyClone (by GE Healthcare SH30265.01)
10% FBS Gibco (by Thermo Scientific 10270106)
100 U/ml penicillin/ streptomycin (by Thermo Scientific 15140122)

Osteogenesis medium for mouse suture-derived cells (both freshly derived & stem cells):

Low-glucose DMEM (1 g/l) Gibco (by Thermo Scientific 21885025)
10% FBS Gibco (by Thermo Scientific 10270106)
100 U/ml penicillin/ streptomycin (by Thermo Scientific 15140122)
0.1 µM dexamethasone
50 µM ascorbate-2-phosphate (by SIGMA A8960)
10 mM β-glycerophosphate (by SIGMA G5422)

Osteogenesis medium for human bone marrow mesenchymal stem cells:

A-MEM HyClone (by GE Healthcare SH30265.01)
2% FBS Gibco (by Thermo Scientific 10270106)
100 U/ml penicillin/ streptomycin (by Thermo Scientific 15140122)
0.1 µM dexamethasone
85 µM ascorbate-2-phosphate (by SIGMA A8960)
3 mM NaH_2PO_4

Adipogenesis medium for mouse suture-derived cells (both freshly derived & stem cells):

High-glucose DMEM (4,5 g/l) Gibco (by Thermo Scientific 11995-065)
10% FBS Gibco (by Thermo Scientific 10270106)
100 U/ml penicillin/ streptomycin (by Thermo Scientific 15140122)
Supplemented with: 1 µM dexamethasone
0.5 mM IBMX (by SIGMA I5879)
0.1 mM indomethacine (by Santa Cruz sc-200503)
10 µg/ml insulin for induction mode

Supplemented with: 10 µg/ml insulin for maintenance mode

Adipogenesis medium for human bone marrow mesenchymal stem cells:

Low-glucose DMEM (1 g/l) Gibco (by Thermo Scientific 21885025)
10% FBS Gibco (by Thermo Scientific 10270106)
100 U/ml penicillin/ streptomycin (by Thermo Scientific 15140122)
1 µM dexamethasone
0.5 mM IBMX (by SIGMA I5879)
60 µM indomethacine (by Santa Cruz sc-200503)

Chondrogenesis medium for both human and mouse primary cells:

High-glucose DMEM (4,5 g/l) Gibco (by Thermo Scientific 11995-065)
100 U/ml penicillin/ streptomycin (by Thermo Scientific 15140122)

Supplemented with: 0.1 µM dexamethasone
170 µM ascorbate-2-phosphate (by SIGMA A8960)
10 ng/ml TGF-β1 (by PEPROTECH 100-21)
0.35 mM l-proline (by SIGMA 81709)
1 mM sodium pyruvate (by Thermo Scientific 11360)
6.25 µg/ml insulin (Humulin Regular)
6.25 µg/ml transferrin (by SIGMA T0665)
6.25 ng/ml selenous acid
1.25 mg/ml BSA
5.35 µg/ml linoleic acid

Freezing medium for primary cells:

95% FBS (serum)
5% DMSO (by AppliChem A3672)

Freezing medium for cell lines:

60% DMEM
30% FBS (serum)
10% DMSO (by AppliChem A3672)

2.1.4 Solutions & Buffers

PBS (10X):
1.37 M NaCl
27 mM KCl
100 mM Na_2HPO_4
18 mM KH_2PO_4 pH=7.4

DNA extraction from mouse tails (solution A):
25 mM NaOH
0.2 mM EDTA pH=12

DNA extraction from mouse tails (solution B):
40 mM Tris-HCl pH=3.5

TBE (5X):
446 mM Tris-HCl
445 mM boric acid
10 mM EDTA pH=8.3

DNA loading buffer (10X):
50% v/v glycerol
100 mM EDTA
0.1% w/v Orange G dye

Protein extraction- RIPA buffer:
50 mM Tris-HCl pH=8
150 mM NaCl
1% v/v NP40
0.5% w/v DOC
0.1% w/v SDS

Protease inhibitors:
1 µM pepstatin
1 µM bestatin
0.1 mM AEBSF (Pefabloc)
10 µg/ml aprotinin
10 µg/ml leupeptin

Protein- SDS gel loading buffer (4X):

200 mM Tris-HCl, pH=6.8
8% w/v SDS
40% v/v glycerol
4% v/v mercaptoethanol
0.04% w/v bromophenol blue

SDS-PAGE Tris- Glycine Running buffer (10X):

250 mM Tris
2 M glycine
1% w/v SDS pH=8.3

Protein transfer buffer (1X):

20 mM Tris
160 mM glycine
0.08% w/v SDS
20% v/v methanol

TBS (10X):

0.5 M Tris-HCl pH=8.0
1.38 M NaCl
27 mM KCl

TBS-T (1X):

50 mM Tris-HCl pH=8.0
138 mM NaCl
2.7 mM KCl
0.05% v/v Tween20

Denaturation solution for BrdU detection:

2 N HCl
0.5% Tritox-X-100
in PBS

Neutralization solution for BrdU detection:

0.1 M sodium tetraborate pH=8.5

2.1.5 Antibodies, reagents and fluorescent dyes

A list of the antibodies and reagents used in this study is provided below. The respective dilutions are also indicated on the right.

Primary antibodies

FITC-conjugated anti-mouse/human CD44 (Biolegend 103006)	1:100
APC-conjugated anti-mouse Sca1 (Biolegend 108111)	1:100
PE-conjugated anti-mouse CD105 (Biolegend 120407)	1:200
PE/Cy5-conjugated anti-mouse/rat CD29 (Biolegend 102219)	1:200
PE/Cy7-conjugated anti-mouse CD90.2 (Biolegend 105325)	1:600
PerCP/Cy5.5-conjugated anti-mouse CD45 (Biolegend 103131)	1:400
PE-conjugated anti-mouse CD31 (BD Pharmingen 553373)	1:200
APC-conjugated anti-mouse CD34 (Biolegend 119309)	1:100
PE-conjugated anti-mouse CD265/ RANK (Biolegend 119805)	1:50
PerCP/Cy5.5-conjugated anti-mouse CD146 (Biolegend 134709)	1:50
Rat monoclonal anti-BrdU (AbD Serotec MCA2060GA)	1:800
Rabbit polyclonal anti-mouse/human ERF S17S	1:1000
Rabbit anti-p44/42 MAPK [Erk1/2] (Cell Signaling 4695)	1:2000
Rabbit anti-phosphop44/42 MAPK [Erk1/2] (Cell Signaling 9101)	1:1000

Secondary antibodies, reagents & fluorescent dyes

Biotin-conjugated anti-Rat IgG (Sigma B7139)	1:100
Peroxidase-conjugated anti-Rabbit IgG (Jackson 111035144)	1:5000
FITC-conjugated anti-Mouse IgG (Jackson 715095150)	1:200
FITC-conjugated Streptavidin (Biolegend 405201)	1:1000
TO-PRO-3 nuclear stain (Invitrogen T3605)	1:1000
Hoechst 33342 nuclear stain (Invitrogen H1399)	1:1000

2.1.6 Primers for qPCR

The following primer pairs were used for real-time qPCR analysis of gene expression in mouse suture-derived cells. The annealing temperature is indicated in the right list.

Gene	Sequence	Temperature
Runx2:	FW: 5′-GAACCAAGAAGGCACAGACA RV: 5′-AACTGCCTGGGGTCTGAAAA	60 oC

Gene	Sequence	Temperature
Osterix:	FW: 5′- TCTGCTTGAGGAAGAAGCTC RV: 5′- TCCATTGGTGCTTGAGAAGG	56 oC
Col1a2:	FW: 5′- TGAAGTGGGTCTTCCAGGTC RV: 5′- GACCAGGCTCACCAACAAGT	58 oC
Col2a1:	FW: 5′- TCCAGATGACTTTCCTCCGTCTA RV: 5′-CAGGTAGGCGATGCTGTTCTTAC	62 oC
Col10a1:	FW: 5′-TTCTGCTGCTAATGTTCTTGACC RV: 5′-GGGATGAAGTATTGTGTCTTGGG	56 oC
Alp:	FW: 5′- AATGCCCTGAAACTCCAAAAGC RV: 5′- CCTCTGGTGGCATCTCGTTATC	58 oC
Ocn:	FW: 5′- CTCTGTCTCTCTGACCTCACAG RV: 5′- CAGGTCCTAAATAGTGATACCG	60 oC
Axin2:	FW: 5′-AGCCTAAAGGTCTTATGTGG RV: 5′-ATGGAATCGTCGGTCAGT	56 oC
Gli1:	FW: 5′-TTATGGAGCAGCCAGAGAGA RV: 5′-GAGCCCGCTTCTTTGTTAAT	60 oC
Prrx1:	FW: 5′-GCGGAGAAACAGGACAACAT RV: 5′-ACTTGGCTCTTCGGTTCTGA	60 oC
Twist1:	FW: 5′-CATGGCTAACGTGCGGGA RV: 5′-CGCCAGTTTGAGGGTCTGAA	60 oC
Nestin:	FW: 5′-GGCTGAGACAGGTGAGATCC RV: 5′-GAGCAGTCTCGTGGGAAAGC	58 oC
Erf:	FW: 5′-CCTGATGAAGTGGCTCGC RV: 5′-GTTTCCCCTTGGTCTTGTGTAG	56 oC

Gapdh:	FW: 5′-CCAGTATGACTCCACTCACG	56 oC
	RV: 5′-GACTCCACGACATACTCAGC	

2. *Materials & Methods*

2.2 Methods

2.2.1 Cranial suture cell isolation and cultivation

Sagittal and coronal sutures of the cranial vault are used in this protocol since these sutures are most frequently observed to undergo premature fusion in the animal model of ERF-related craniosynostosis ($Erf^{LoxP/-}$ mice). The isolation is performed from 5-day-old (P5) $Erf^{LoxP/+}$ (healthy) and $Erf^{LoxP/-}$ mice that have not yet developed the phenotype of synostosis. Based on our observations, craniosynostosis becomes evident in mice older than P10 and at variable age and level of severity. The procedure that is followed is mainly adopted by previous studies [78-80], slightly modified and is described below:

1. Mice are sacrificed by decapitation and the skin is removed from the skull. The cranial base and the mandible are excised so that the removal of the brain becomes more feasible. The brain is discarded. When released, the cranial vault including the region of interest (sagittal & coronal sutures along with parietal and frontal bones) is placed in PBS (phosphate buffer saline) supplemented with 1% penicillin/ streptomycin (pen/strep).
2. In this step, the tissue in PBS is transferred under a stereomicroscope so that any traces of blood, along with part of the dura mater underneath and the periosteum from above can be removed with care. Attention should be paid not to injure the bones and the regions of sutures. Extensive cleaning may result in cell loss since efforts to remove the dura mater may also lead to suture mesenchymal cell damage.
3. The sagittal suture and the coronal sutures containing approximately 0.5 mm bony margins are excised from the tissue and placed into a 100mm-cell culture dish in presence of 5 ml suture cell maintenance medium (DMEM-F12, 10% FBS, 1% pen/strep). In this step the sutures are placed with the endocranial surface flush to the dish, cut into small pieces and transferred at 37 ^{o}C for culture. Approximately 9-12 explants are placed per 100mm-dish.
4. The suture cells are allowed to migrate from explants over 8 days in culture. For the first 3 days, avoid moving the dish so as not to disturb the onset of migration. Medium is changed every third day.
5. After a total of 8 days in culture, cells are harvested by trypsinization: following an initial wash with PBS, a solution of 0.25% Trypsin-EDTA (Gibco 25200-072) is added to the cells for 2-3 min at 37 ^{o}C. Equal or higher volume of FBS-containing maintenance medium is then added in order to inhibit the trypsin action on cells. Cells devoid of any explant pieces are transferred into a 15ml-tube and counted for further experimentation, subsequent cultivation or freezing.

2.2.2 Selective expansion of suture-derived mesenchymal stem/ progenitor cells

To obtain a population of suture-derived mesenchymal stem/ progenitor cells, cranial sutures are isolated from P5 mice and processed exactly as described in the previous section. However, in this protocol suture explants are placed into gelatinized dishes and cultured in presence of leukemia inhibitory factor (LIF), already known for its role in sustaining the stem cell state while inhibiting the differentiation [81, 82]. The complete medium is described below:

Knock-OUT DMEM, 12% FBS, 1% pen/strep, 2 mM L-glutamine, 1% non-essential amino acids, 0.1 mM β-mercaptoethanol and 0.3% v/v LIF

Cells are harvested and further cultured (passaged) without the explants under the same conditions in gelatinized dishes for a total of at least 8 population doublings (PDs) during a period of approximately 50-60 days. During this long-term culture in the presence of LIF, the majority of the differentiated cells are either left behind or subjected to death so that the population is gradually becoming enriched with cells possessing self-renewal ability like mesenchymal stem and progenitor cells. The seeding density can be as low as 2000 cells/cm^2 however lower densities have not been tested in this study. The suture-derived cells can be generally subjected to freezing at any time/ passage and this is strongly recommended since the contaminating hematopoietic cell populations cannot survive the freezing procedure.

2.2.3 Freezing and thawing cells

Once the cells are confluent, trypsinized from the dish and counted, they are placed into a 15ml-tube and centrifuged for 5 min at 200 x g at room temperature. The supernatant is discarded carefully and the cell pellet is then resuspended into freshly prepared freezing medium for primary cells: 95% FBS (serum), 5% DMSO. Approximately 1 ml freezing medium is used for 600,000-1,000,000 cells. For fewer cells e.g. 300,000-500,000, a volume of ~0.6 ml was used in this study. After complete resuspension, the cells are transferred into a cryogenic vial, placed into a container filled with isopropanol and stored at -80 ^{o}C overnight. The isopropanol container allows the cells to freeze gradually so as to reduce the risk of crystal formation and preserve cell viability upon recovery. On the next day, the vial is removed from -80 ^{o}C freezer and transferred at -145 ^{o}C for long-term storage. The same procedure is followed for cell lines, however the freezing medium used in this case is: 60% DMEM medium, 30% FBS, 10% DMSO.

In order to thaw and culture primary cells, the corresponding cryogenic vial is removed from -145 ^{o}C and rapidly thawed. The vial is agitated and once the cells have acquired the liquid state completely, they are transferred into either a 100mm-dish or a T25-cell-culture flask in presence of pre-warmed maintenance/ growth medium. For cells ≥ 300,000 a 100mm-dish is used here (10 ml medium). For cells ‹ 300,000 a T25-

flask can be used (6 ml medium). After the cells have become attached to the surface of the dish (usually ~ 4 hours for suture cells), the medium is changed so as to remove the residual DMSO that may interfere with growth and cell viability. For cell lines this step of medium change after certain hours can be omitted when a centrifugation step (200 x g for 3min) is performed right before the beginning of the culture that enables the removal of DMSO. ! Attention, the seeding cell density and the centrifugation conditions are mainly referred to cranial suture cells and may differ for other cell types.

2.2.4 Estimation of the population doubling level (PDL)

The following equation was used to estimate the population doubling level at the end of each passage:

$$PD = \frac{LogN1 - LogN0}{Log2}$$

where, N_1 is the number of cells harvested from the dish and N_0 is the number of cells that were seeded initially. PD stands for population doublings. The population doublings of the current passage are then added to the previous population doubling level (PDL), to yield the cumulative population doubling level of the culture (CPD).

2.2.5 Osteogenic differentiation

Cells are seeded in wells of a 48-well-plate at a density of ~20,000 /cm^2 in presence of maintenance/ growth medium. This starting density ensures that the cells will be quite confluent after 1-2 days to begin osteogenesis. The cells are suggested to be at least 60% confluent for osteogenic induction. Once the cells display the desired confluency, the maintenance medium is removed and is replaced by 0.5 ml of the osteogenesis medium per well of the 48-well-plate. The osteogenesis medium for mouse suture-derived cells is always freshly prepared in our experiments and consists of DMEM low-glucose, 10% FBS, 1% pen/strep, 0.1 µM dexamethasone, 50 µM ascorbate-2-phosphate and 10 mM β-glycerophosphate. The cells are cultured under these conditions without passaging for 28 days. The medium is changed every third day. In the experiments with inhibitors, the freshly prepared osteogenic differentiation medium was supplemented with either 2 µM U0126 (Cell guidance systems SM106) or 10 nM KPT330 before every medium change. In the experiment with retinoic acid, the osteogenic medium was supplemented with 0.5 µM all-*trans* RA. At certain time-points (i.e. day 7, 14, 21, 28) the differentiation state is evaluated by Alizarin Red S staining of the cultures. Same procedure was followed for human bone marrow mesenchymal stem cells in which only the medium for osteogenesis differs (please see section of materials).

2.2.6 Adipogenic differentiation

Cells are seeded in wells of a 48-well-plate at a density of 35,000 /cm^2 in presence of maintenance/ growth medium. For successful adipogenic differentiation it is important to start the induction in post-confluent cultures. Almost one week after the cell seeding, the maintenance medium is removed and freshly prepared adipogenic induction medium is added to the cells (DMEM high-glucose, 10%FBS, 1% pen/strep, 1 μM dexamethasone, 0.5 mM IBMX, 0.1 mM indomethacine, 10 μg/ml insulin). The cells are incubated with 0.5 ml adipogenic induction medium for 4 days. Then this medium is replaced by the adipogenic maintenance medium (DMEM high-glucose, 10%FBS, 1% pen/strep, 10 μg/ml insulin) and the cells are further cultured for 3 days. This is one cycle of induction-maintenance and is sufficient to induce adipogenesis in freshly derived suture cells. More cycles are detrimental to cell viability based on our observations on these cells. Of note, 2-3 cycles of adipogenic induction-maintenance are performed for long-term expanded suture mesenchymal stem/ progenitor cells in our study. The protocol for the adipogenic differentiation of human bone marrow mesenchymal stem cells used in this study is kindly provided by the Hematology lab of Prof. Papadaki and involves culture of post-confluent cells in presence of DMEM low-glucose, 10%FBS, 1% pen/strep, 1 μM dexamethasone, 0.5 mM IBMX and 60 μM indomethacine for 3 weeks. At the end of each week, the differentiation state is evaluated by Oil Red O staining of the cultures.

2.2.7 Chondrogenic differentiation

The differentiation of mesenchymal progenitor cells towards the chondrogenic lineage can be generally performed by various ways: 1) micromass cultures involving droplets of cells at high density [83], 2) conventional monolayer cultures and 3) pellet cultures [84, 85], are all reported to be employed for the efficient formation of cartilage in vitro. In this study, pellet cultures are chosen to be performed since the 3D growth of cells is reported to enhance the chondrogenic induction.

1. Approximately 500,000 cells are placed into a 15ml-polypropylene tube and centrifuged for 5 min at 200 x g at room temperature.
2. Supernatant is discarded and the cell pellet is resuspended in the chondrogenic differentiation medium (w/o TGF-β, please see the recipe of the complete medium in the section of materials). Attention should be paid so that the resuspension is good enough to wash all cells. The aim of these steps is to finally create a cell pellet devoid of any residual FBS. FBS is reported to inhibit the efficient chondrogenic differentiation in vitro.
3. The cells are again centrifuged for 5 min at 200 x g at room temperature.
4. Supernatant is again discarded and the cell pellet is resuspended in complete chondrogenic differentiation medium + TGF-β.
5. The cells are centrifuged for 2 min at 200 x g at room temperature.

6. Incubate the cells as a pellet in the 15ml-polypropylene tube at 37 ^{o}C. Leave the cap of the tube slightly open. Avoid moving the tube for the first 2 days.
7. On the third day, flick the bottom of the tube after changing the medium, so that the chondropellet becomes free-floating (important).

The medium is replaced by freshly prepared one every third day. The differentiation takes place for 21 days. Finally, the chondropellet is harvested and evaluated for cartilage formation by Alcian Blue staining.

2.2.8 Alizarin Red S: preparation, staining & quantification

Alizarin Red S is a dye that binds Ca^{+2} ions hence it is used for the detection of calcium deposits in mineralizing tissues and cells undergoing in vitro osteogenic differentiation. To prepare a solution of 2% w/v Alizarin Red S in water, 1 gr of Alizarin Red S powder is dissolved into 50 ml of dH_2O. The pH should be adjusted at 4.1-4.3 by the addition of ammonium hydroxide solution 5% (NH_4OH). Then the Alizarin Red S solution is filtered and stored at room temperature protected from light.

Staining procedure

Cells in wells of a 48-well-plate are subjected to osteogenic differentiation and at certain time-points (i.e. on day 7, 14, 21, 28) calcium deposits are detected by Alizarin Red S staining according to the following protocol:

1. The medium is removed from the wells and the cells are washed with PBS.
2. The cells are fixed with 4% PFA solution in PBS at room temperature for 10min.
3. Then they are washed twice with dH_2O.
4. Alizarin Red S 2% w/v solution is added to the wells for 5min (0.2 ml per well)
5. Then the cells are washed extensively with dH_2O (at least 3 washes).
6. Finally, 0.5 ml fresh dH_2O is added per well and the cells are observed in an inverted microscope.

Extraction & quantification procedure

At this point the dye can be extracted from the wells using acetic acid and quantified [86]. The procedure is described below:

1. 100 μl of acetic acid solution 10% are added to each well of a 48-well-plate previously stained with Alizarin Red S. Any remaining water in the well should be removed prior to the addition of acetic acid. The cells are incubated with the acetic acid solution at room temperature for 30 min.
2. The content of each well (the solution along with any remaining cell layer) is transferred into a 1.5ml-tube and subjected to vortexing for 30 sec.
3. The samples are heated at 85 ^{o}C for 10 min. Then they are placed in ice for 5 min.
4. The samples are centrifuged at 16,000 x g for 15 min at room temperature and the supernatant (~90 μl) is transferred into a new 1.5ml-tube.

5. To elevate the pH, 9 μl of ammonium hydroxide solution 10% are added to each sample and mixed. For a correct absorbance measurement, the pH of the sample finally should be within the range of 4.1-4.4.
6. 50 μl from each sample are transferred into a well of a 96-well-plate and the absorbance is measured at 405 nm.

2.2.9 Oil Red O: preparation, staining & quantification

Oil Red O stains lipid droplets and vacuoles in tissues and cultures. In this study it is used for the detection of intracellular lipid droplets after in vitro adipogenic differentiation that would indicate the presence of adipocytes. To prepare a solution of 0.5% w/v Oil Red O, 0.25 gr of Oil Red O powder are dissolved into 50 ml of 99% isopropanol. The solution is mixed very well and slightly heated at ~38 ^{o}C for several hours throughout the day. Finally, it is filtered and stored at room temperature protected from light.

Staining procedure

Cells in wells of a 48-well-plate are differentiating towards adipocytes and at certain time-points, the appearance of lipid droplets is evaluated by Oil Red O staining following the protocol described below:

1. A working solution of Oil Red O is freshly prepared: 6 ml of Oil Red O stock solution 0.5% w/v are mixed with 4 ml of dH_2O. Mix well and let stand for approximately 10 min. Then the working solution is filtered through a 0.45μm-pore size filter right before use.
2. The medium is now removed from the culture wells and the cells are washed with PBS.
3. The cells are fixed with 4% PFA solution in PBS for 10 min at room temperature.
4. Then they are washed twice with PBS.
5. Oil Red O working solution (0.2 ml) is added to each well for 15-20 min at room temperature.
6. Then the cells are washed with dH_2O at least 2 times.
7. To be able to count the cells, the nuclei can be stained with Hoechst dye (1:1000 dilution in PBS) for 10 min at room temperature. ! Attention should be paid not to add any detergents hence we use the Hoechst dye that passes through intact membranes.
8. Finally, the cells are washed and 0.5 ml of either PBS or water is added per well and the plate is observed in the inverted microscope. The adipocytes are presented as % of the total cells in the well.

2.2.10 Alcian Blue: preparation & staining

Alcian Blue is a cationic dye that binds to acidic polysaccharides like glycosaminoglycans of cartilage. Although its targets are not restricted to cartilage matrix, the presence of blue colour in the cells of our study is used as an indication of chondrogenic differentiation. To prepare a solution of 1.5% w/v Alcian blue, 0.75 gr of Alcian blue powder are dissolved into 50 ml of 1.5% acetic acid solution and the pH is adjusted at 2.2. Finally, the solution is filtered and stored at room temperature protected from light.

Staining procedure

Cells previously induced to differentiate along the chondrogenic lineage in form of a pellet culture, are stained with Alcian blue according to the following protocol:

1. The medium is carefully removed and the chondropellet is washed twice with PBS.
2. The chondropellet is fixed with 4% PFA solution in PBS for 1-2 hours at 4 ^{o}C (for small pellets, use the reduced time).
3. The chondropellet is then washed with PBS three times and dehydrated overnight in 30% sucrose solution in PBS at 4 ^{o}C.
4. Next day, once dehydrated the chondropellet is transferred to 60% sucrose/ PBS solution at 4 ^{o}C for further dehydration.
5. At this point, the chondropellet can be frozen using OCT compound (Sakura Tissue-Tek 4583) and 2-methylbutane/ dry ice chamber at -35 ^{o}C. The frozen pellet can now be stored at -80 ^{o}C and is ready for cryosectioning.
6. Slides with cryosections of the chondropellet (7 μm section thickness used here) are stained with Hematoxylin Harris for 2 min at room temperature.
7. The slides are then extensively washed with water.
8. Differentiation takes place with 0.38% HCl in 70% EtOH solution for 3 sec.
9. The slides are rinsed with water (perform at least 3 changes).
10. Then the chondropellets are placed into the 1.5% Alcian blue, 1.5% acetic acid solution for 10-20 min.
11. The pellets are then washed with dH_2O 3 times and the slides are rinsed in 95% EtOH. Then the slides are placed into 100% EtOH twice for 3 min and finally cleared in xylene.
12. The mounting is performed with Entellan and the slides are ready for observation.

2.2.11 Transfection of Cos7 cells & LIF production

A vector containing leukemia inhibitory factor (LIF) sequence is introduced into Cos7 cells for the production of the protein that is secreted and collected finally from the cell culture medium. The protocol that is followed is described below and is kindly provided by Eirini Nomikou from Prof. Kardasis Laboratory:

1. One day before the transfection, 300,000 Cos7 cells are seeded into a 100mm-dish.
2. On the next day, the medium of the cells is removed and replaced by 10 ml of fresh one.
3. Transfection: 4 µg of the plasmid LIF DNA are diluted into 300 µl of DMEM medium without antibiotics, FBS or any supplement. 15 µl of Attractene transfection reagent (Qiagen Cat No./ID: 301005) are added to the mix and pipetted up and down in the 1.5ml-tube.
4. The transfection mix is incubated for 15 min at room temperature.
5. The mix is finally added to the cells drop-wise. The cell culture dish is placed back in the incubator.
6. On the next day, the medium of the cells is changed and replaced by 5 ml of fresh one. The cells are incubated in this medium without any change for the next 5 days.
7. In the end, the cell culture medium is collected from the 100mm-dish, placed into a 15ml-tube and centrifuged.
8. The supernatant is now transferred into a new 15ml-tube and filtered through a 0.2µm-filter.
9. The LIF containing medium is finally dispensed into aliquots of approximately 300 µl and stored at -80 ^{o}C.

2.2.12 Cell cycle phase study with propidium iodide

To study the distribution profile of cells in the different phases of the cell cycle, we utilize the propidium iodide (PI) agent that binds to double-stranded DNA and perform the following protocol in which PI is added to isolated nuclei in hypotonic solution [87]:

1. Cells that have reached a confluency of approximately 60-70% (not more) are harvested from the culture dish by trypsinization and washed with PBS. Then they are transferred into a 1.5ml-tube.
2. The cells are centrifuged at 200 x g for 5 min at room temperature, the PBS is discarded and the cell pellet is resuspended into the following hypotonic solution: 0.01% w/v sodium citrate tribasic dihydrate, 0.03% v/v Triton-X-100, 2 µg/ml RNase A and 50 µg/ml PI. Usually 300,000 cells are resuspended into approximately 300 µl of this hypotonic staining solution.
3. The cells are mixed well, probably also vortexed for a while and kept at 4 ^{o}C protected from light for 30 min up to maximum 1 hour in total before the analysis by flow cytometry. The fluorescence of PI is detected at the PE channel of the FACSCalibur flow cytometer (Becton Dickinson). The data in our study are analyzed using Modfit software.

2.2.13 MTT assay

MTT [3-(4,5-dimethylthiazol-2-yl)-2,5-diphenyltetrazolium bromide] is a yellow salt that is commonly used for the evaluation of cell metabolic activity which is often indicative of cellular viability. Inside the viable cells this yellow salt is reduced to purple formazan crystals that are finally dissolved and the absorbance of the resulting colored solution is measured and used as an estimation of the number of active cells [88].

1. The cells are preferentially cultured into wells of a 96-well-plate. On the day of the MTT assay, the medium is removed from the cells and 100 μl of DMEM maintenance medium + 11 μl of MTT salt solution (5 mg/ml stock) are mixed and added to each well.
2. The cells are incubated with the MTT mix at 37 ^{o}C for a total of 4 hours. (Different cells types may require different incubation times.) During this time, the formation of purple crystals may be sporadically monitored.
3. Next, the supernatant is discarded and 100 μl of isopropanol/ HCl solution (250:1) are added to each well. This step serves the solubilization of the crystals.
4. The cells are incubated with this solution at room temperature for 30 min and the content of each well is pipetted up and down to facilitate homogenization. This pipetting is necessary particularly for osteogenic differentiated cells that are covered from the calcified extracellular matrix.
5. Finally, the absorbance is measured at 600 nm.

2.2.14 BrdU incorporation assay

BrdU (5-bromo-2'-deoxyuridine) is a thymidine analog that is used to detect the proliferating cells in cultures and tissues in vivo. It is incorporated into newly synthesized DNA and can be later detected by an anti-BrdU antibody.

For cultured cells

The cells are previously seeded into wells of a 24-well-plate on round coverslips. On the day of BrdU assay:

1. The cell culture medium is supplemented with BrdU at a final concentration of 10 μM. The cells are further incubated for 8 hours at 37 ^{o}C. The time of BrdU incubation depends on the cell doubling times. In rapidly proliferating cells, it can be as low as 2 hours.
2. Then, the cell culture medium is removed, the cells are washed with PBS and fixed with 4% PFA for 10 min at room temperature.
3. The wells are washed with PBS 3 times and the staining procedure begins.
4. Denaturation solution (2 N HCl, 0.5% Triton-X-100 in PBS) is added to the wells for 20 min at room temperature. This step facilitates the cell permeabilization and the DNA denaturation.

5. The denaturation solution is removed and the neutralization one is now added to the wells. Neutralization solution: 0.1 M sodium tetraborate pH=8.5. The samples are washed at least three times with the neutralization solution. Finally, PBS is added to the wells.
6. The cells are incubated overnight with rat anti-BrdU antibody (AbD Serotec MCA2060GA) at a dilution of 1:800 in PBS, 10% FBS, 0.1% Triton-X-100 solution at 4 ^{o}C.
7. On the next day, the primary antibody is removed and the samples are washed with PBS 3 times.
8. The secondary antibody, biotin-conjugated anti-rat antibody (Sigma B7139), is added to the samples at a dilution of 1:100 in PBS, 1% FBS, 0.1% BSA solution for 1 hour at room temperature.
9. The cells are washed with PBS and incubated with FITC-conjugated streptavidin (Biolegend 405201) at 1:1000 for 30 min at room temperature.
10. Finally, the samples are washed with PBS and the nuclei are stained with TOPRO-3 (1:1000) in PBS for 10 min.
11. The coverslips are air-dried and mounted with mowiol mounting medium.

For living tissues

1. 100 μg of BrdU per gr of body mass are injected into the peritoneum of either P5 or P15 mice.
2. 4 hours later the mice are sacrificed and the tissue of interest (i.e. the skull) is removed and cleaned with PBS. The time of BrdU incorporation is dependent on the proliferation rate of cells of a particular tissue.
3. The region of interest (i.e. the coronal and sagittal suture area) is cleaned from any remaining blood, excised from the skull and placed into 4% PFA solution in PBS for 30 min at room temperature. To achieve better tissue preservation, the dura mater and the periosteum are not removed but remain intact onto the tissue.
4. The tissue is then washed 3 times with PBS and decalcified into 0.5 M EDTA pH=8.0 for 3 days. Decalcification is required for bony tissues so that the cryosectioning becomes easier.
5. After the three days, the tissue is washed with PBS and dehydrated into 30% sucrose/ PBS solution overnight at 4 ^{o}C. Next day, it is placed into 60% sucrose/ PBS solution for further dehydration.
6. Finally, the tissue is embedded in OCT compound (Sakura Tissue-Tek 4583), particular sutures along with their bony margins are excised, placed in OCT molds and frozen into 2-methylbutane/ dry ice chamber at -35 ^{o}C. The blocks can be stored at -80 ^{o}C.
7. Cryosections are performed at 7 μm thickness.
8. The slides are now ready for the staining procedure and the detection of BrdU.
9. The slides are initially placed into PBS so as to be hydrated.

10. Then they are placed into a glass container filled with the denaturation solution for 30 min at 37 °C. Denaturation solution: 2 N HCl, 0.5% Triton-X-100 in PBS.
11. The slides are then placed into the neutralization solution and washed at least 3 times (3 changes). Neutralization solution: 0.1 M sodium tetraborate, pH=8.5. Finally, they are rinsed in PBS.
12. The sections are incubated overnight with rat anti-BrdU antibody (AbD Serotec MCA2060GA) at a dilution of 1:800 in PBS, 10% FBS, 0.1% Triton-X-100 solution at 4 °C.
13. On the next day, the primary antibody is removed and the samples are washed with PBS 3 times. The secondary antibody, biotin-conjugated anti-rat antibody (Sigma B7139), is added to the sections at a dilution of 1:100 in PBS, 1% FBS, 0.1% BSA solution for 1 hour at room temperature.
14. The slides are washed with PBS and incubated with FITC-conjugated streptavidin (Biolegend 405201) at 1:1000 for 30 min at room temperature.
15. Finally, the slides are washed with PBS and the nuclei are stained with TOPRO-3 (1:1000) in PBS for 10 min. Rinse the slides once in PBS.
16. The slides are air-dried and covered with mowiol mounting medium.

2.2.15 Flow cytometry staining

The following protocol is used when the epitope of interest is a membrane-bound receptor/ protein and not an intracellular one.

1. The cells are harvested from the culture dish by trypsinization and washed with PBS. Then they are centrifuged at 200 x g for 5 min at room temperature.
2. The supernatant is discarded and the cell pellet in now resuspended into the following solution containing the antibody for the epitope of interest: PBS, 1% FBS. For up to 500,000 cells, a volume of approximately 50 μl of this solution was added to the cells. The cells are pipetted up and down and incubated in this antibody solution for 30 min at 4 °C in the dark. For antibody suggested dilutions, please see the 2.1.5 section of materials. The antibodies used in this study are already conjugated with fluorescent dyes (e.g. PE, FITC) and there is no need for secondary antibodies for flow cytometry.
3. Next the cells are washed with 1 ml PBS and centrifuged at 200 x g for 5 min at 4 °C.
4. The supernatant is discarded and the cell pellet is resuspended into approximately 300 μl of PBS, 1% FBS solution and placed on ice protected from light until transferred to the Becton Dickinson FACSCalibur flow cytometer. The analysis in our experiments was performed using Flowing Software 2.5.1 version.

2.2.16 RNA isolation from cultured cells for qPCR

In the following protocol, TRI reagent (SIGMA T9424) is utilized to extract the RNA from the primary cells under investigation. TRI reagent is a mixture of guanidine thiocyanate and phenol in a single-phase solution and is used in our study to isolate RNA for quantitative PCR (real-time PCR) after cDNA synthesis. The steps that are followed are described below:

1. The cells are harvested from the culture dish by trypsinization and washed with PBS. Then they are centrifuged at 200 x g for 5 min.
2. The supernatant is removed except for the last ~10-15 µl in which the cell pellet should be now resuspended.
3. Once the cell pellet is resuspended into this small volume, TRI reagent is added to the cells. Approximately 500 µl of TRI reagent are added for 500,000 cells. The tube is inverted up and down for proper mixing and is incubated for 5 min at room temperature.
4. Then 200 µl chloroform (per ml of TRI-reagent) are added to the tube. The tube is shaken vigorously by hand for 15 sec. Incubate for 5 min at room temperature.
5. The samples are now centrifuged at 12,000 x g for 15 min at 4 ^{o}C.
6. The supernatant is transferred into a new 1.5ml-tube and 0.5 ml isopropanol (per ml of TRI-reagent) are added to the samples.
7. After isopropanol addition, the samples are mixed well and incubated for at least 10 min at room temperature.
8. Next, they are centrifuged at 12,000 x g for 15 min at 4 ^{o}C to precipitate the RNA.
9. The supernatant is discarded and the pellet is washed with 1 ml of 70% EtOH (per ml of TRI-reagent). Centrifuge the samples at 7,500 x g for 5 min at 4 ^{o}C.
10. Finally, the supernatant is discarded, the nucleic acid pellet is air-dried and nano-pure H_2O is added to dissolve the RNA. For a very small pellet that is almost invisible, add only 10-15 µl of H_2O. Avoid pipetting. The RNA samples should be stored at -80 ^{o}C.

2.2.17 cDNA synthesis & real-time PCR

The procedure described above results in the isolation of RNA that is often contaminated with DNA molecules. Therefore, before the cDNA synthesis it is necessary to remove the remaining DNA:

DNase treatment

In a reaction tube, the following components are added and mixed:
2,500 ng RNA
1 µl 10 x DNase buffer (Invitrogen 8167G)
0.5 µl TURBO DNase I 2U/µl (Invitrogen 2238G)
nano-pure H_2O [up to V_f = 10 µl]

The reaction takes place at 37 ^{o}C for 45 min-1 hour.

Then the enzyme is inactivated by the addition of 1 μl of DNase inactivation resin (Invitrogen 8174G) per sample. The resin is incubated with the sample for 2 min at room temperature and the sample is finally centrifuged for 1 min. The supernatant containing the RNA is transferred into a new tube.

cDNA synthesis

In a reaction tube (tube A), the following components are added:

1000 ng RNA (4 μl from DNase reaction)

0.5 μl dNTPs (from 10 mM stock)

0.5 μl oligodT primers (from 0.5 μg/μl stock)

For 5 min at 65 ^{o}C incubation. Then the mix is immediately placed on ice for at least 1 min.

In a separate tube (tube B), the following components are added:

2 μl of 5X RT Buffer

0.5 μl DTT (from 0.1 M stock)

0.5 μl RNaseOUT (40 U/μl)

0.5 μl Minotech RT (200 U/μl)

1.5 μl H_2O , V_f = 5 μl

Now the components of tube B are mixed with the components of tube A.

The reaction takes place at 50-55 ^{o}C for 1 hour. Temperature and time depend on the RT enzyme and may differ among companies/ manufacturers. Finally, the reaction is terminated by heating the samples at 70 ^{o}C for 15 min. The samples are placed on ice for 5 min. Collect by centrifugation and store cDNAs at -80 ^{o}C.

Real-time PCR

Initially, standard samples are prepared by serial dilutions of cDNAs so that by pipetting 2.5 μl in a final reaction-well, the following quantities of cDNA are totally added:

25 ng cDNA (Standard sample A conc: 10 ng/μl)

5 ng cDNA (Standard sample B conc: 2 ng/μl)

1 ng cDNA (Standard sample C conc: 0.4 ng/μl)

0.2 ng cDNA (Standard sample D conc: 0.08 ng/μl)

Next, each of the cDNA samples to be tested is diluted at 2 ng/μl final concentration.

The following mix is prepared:

5 μl of 2X BrilliantIII SYBRGREEN QPCR mastermix (STRATAGENE 600882-51)

2.5 μl of primers (from a combined stock of 1 μM each)

Finally, 7.5 μl from the above mix are pipetted into each well of a 96-well-plate. Then 2.5 μl of the cDNA sample is added per well (5 ng cDNA totally).

The plate is placed into the machine (STEP ONE Plus Real-time PCR system, Applied Biosystems) and the temperatures and times of reaction are determined. Different sets of primers recognizing various target genes display different conditions for optimum function and efficiency.

2.2.18 RNA isolation from cultured cells for sequencing

An RNeasy Mini kit (74104) is used for the isolation of total RNA from our cultured primary cells. This technology combines the selective binding properties of a silica-gel-based membrane with the speed of microspin technology. All RNAs longer than 200 nucleotides can be isolated with this procedure. The protocol is described below:

1. The cells are harvested from the culture dish by trypsinization and washed with PBS. Then they are centrifuged at 200 x g for 5 min.
2. The supernatant is removed except for the last ~10-15 μl in which the cell pellet should be now resuspended.
3. Once the cell pellet is resuspended into this small volume, RLT Lysis buffer is added to the cells. Approximately 300 μl of RLT buffer are added for < 5,000,000 cells. The tube is inverted up and down for proper mixing and is incubated for 3-5 min at room temperature. At this step, the samples can be frozen.
4. The samples are centrifuged at max speed for 5 min at 4 ^{o}C.
5. The supernatant is now transferred into a new tube and 1 volume of 70% EtOH is added to the lysate. Mix well by pipetting but do not spin.
6. The whole lysate (up to approximately 700 μl) is loaded onto the RNeasy spin column, the lid is closed gently and the column with the sample is centrifuged for 15sec at > 8,000 g at room temperature. The flow-through is discarded.
7. The column is washed with 500 μl of RPE buffer. The lid is closed gently and the column is centrifuged for 15sec at > 8,000 g at room temperature. The flow-through is again discarded.
8. 500 μl of 70% EtOH are added to the spin column. The lid is closed and the samples are centrifuged for 2 min at > 8,000 g at room temperature. The flow-through is discarded.

9. Now the column is placed into a new 2ml-tube, the lid is opened and the samples are centrifuged for 5 min at max speed at room temperature to dry membrane.
10. Finally, the column is placed into a new 1.5ml-tube and nano-pure H_2O is added to the centre of the column to elute RNA. Approximately 20 µl of H_2O are added. Spin for 1 min at max speed. Approximately 16-17 µl is the total final yield of RNA sample in the tube.

2.2.19 Protein isolation from cultured eukaryotic cells

The following protocol is used in this study for the isolation of proteins from primary cultured cells for SDS-PAGE and Western blot.

1. The cells are harvested for the culture dish by trypsinization and washed with PBS.
2. They are centrifuged at 200 x g for 5 min at room temperature.
3. The supernatant is removed except for the last ~10-15 µl in which the cell pellet should be now resuspended.
4. RIPA buffer is now added to the cells for lysis. Approximately 100 µl of RIPA buffer are added for 300,000 cells. Shake well. [RIPA buffer should be generally stored at 4 ^{o}C and any protease/ phosphatase inhibitors should be added prior to cell lysis on the day of experiment- freshly prepared mix of inhibitors was used in this study.]
5. The sample is centrifuged at max speed for 15 min at 4 ^{o}C. The supernatant containing the soluble proteins is transferred into a new 1.5ml-tube. At this step, the protein sample can be frozen.
6. Finally, the protein concentration is estimated by Bradford assay: 5-10 µl of protein sample are added into 800 µl of dH_2O and then mixed with 200 µl of 5X Protein Assay Dye Reagent (Bio-Rad). Absorbance at 595 nm is measured using a spectrophotometer and finally protein concentration is estimated by a standard curve of BSA solutions of known concentration. Each measurement is performed in duplicates.
7. Usually 10- 15 µg of total protein extract are mixed with protein loading buffer (for recipe see please material section) and loaded onto a polyacrylamide gel.

2.2.20 SDS-PAGE (Polyacrylamide gel electrophoresis) and blots

Protein samples with SDS-loading buffer are heated for 5 min at 100 ^{o}C. Then they are loaded onto an acrylamide gel consisting of a 4% upper part (stacking gel) and a 10 or 12% separating gel and subjected to electrophoresis. The gel is finally used for protein transfer into a nitrocellulose membrane (western blot). The transfer of proteins is performed using the semi-dry method in a SEMI-PHOR transfer apparatus for 90 min at 40 mA. Finally, the membrane is removed, air-dried and ready for

blocking and antibody incubation. The membrane is incubated for 30 min into blocking solution containing 5% nonfat milk dissolved into TBS-T. The following antibodies are used in this study for the detection of Erf and Erk1/2 proteins: anti-ERF S17S rabbit polyclonal antibody at a dilution of 1:1000 in TBS buffer containing 1% w/v dry milk and 0.05% Tween20 overnight at 4 oC, anti-p44/p42 MAPK (ERK1/2) rabbit monoclonal antibody (Cell Signaling 4695) and anti-phospho p44/p42 MAPK (ERK1/2) Thr202/Tyr204 rabbit polyclonal antibody (Cell Signaling 9101) according to company's recommendations. A goat anti-rabbit antibody conjugated to horseradish peroxidase (Jackson Immunoresearch 111035144) at a dilution of 1:5000 is used for the detection and visualization of protein bands.

2.2.21 Cranial suture tissue processing and immunofluorescence staining

Bony tissues like femurs, tibia and calvarial bones usually require an additional step during their processing, the step of decalcification. The decalcification is performed in this study by the addition of EDTA that binds Ca^{+2} ions, thus softening the tissue and facilitating the cryosectioning. The protocol described below was used in this study for the isolation and processing of mouse cranial sutures:

1. The mice are sacrificed and the skull is removed and cleaned with PBS.
2. The region of interest (i.e. the one containing the sagittal and coronal sutures) is cleaned from any remaining blood, excised from the skull and placed into 4% PFA solution in PBS for 30 min at room temperature. To achieve better tissue preservation, the dura mater and the periosteum are not removed but remain intact onto the tissue.
3. The tissue is then washed 3 times with PBS and decalcified into 0.5 M EDTA pH=8.0 for 3 days. The decalcification step requires 3 days for tissues of P5 mice, but may require additional days for tissues of older mice.
4. After that, the tissue is washed with PBS and dehydrated into 30% sucrose/ PBS solution overnight at 4 ^{o}C. Next day, it is placed into 60% sucrose/ PBS solution for further dehydration.
5. Finally, the tissue is embedded in OCT compound (Sakura Tissue-Tek 4583). Particular sutures along with their bony margins are excised, placed in OCT molds and frozen into 2-methylbutane/ dry ice chamber at -35 ^{o}C. The blocks can be stored at -80 ^{o}C. A stereomicroscope is used for the excision of sutures during this step.
6. Cryosections are performed at 7 μm thickness on gelatinized slides. The slides can be stored at -80 ^{o}C.
7. On the day of immunofluorescence staining, the slides are removed from -80 ^{o}C and left dry (~45 min).
8. A hydrophobic barrier is created around the tissue sections using Pap pen. Let it become dry.
9. The slides are now placed into PBS to become hydrated. The sections are fixed with 4% PFA solution for 5 min at room temperature.

10. The slides are now washed with PBS 3 times for 5 min each time.
11. For the detection of an intracellular antigen, the slides are placed into the blocking solution: 10% FBS, 1% BSA, 0.5% Triton-X-100 in PBS for 45min- 1h at room temperature.
12. Rinse in PBS once.
13. The primary antibody is applied in sections in the following solution: 1% FBS, 0.1% BSA in PBS overnight at 4 ^{o}C.
14. On the next day, the slides are washed with PBS 3 times for 5 min each time. Then they are incubated with the secondary antibody into 1% FBS, 0.1% BSA in PBS for 1h at room temperature.
15. The samples are washed with PBS and stained with TOPRO-3 at a 1:1000 dilution in PBS for 10 min.
16. Rinse slides in PBS, dry and mount with mowiol mounting medium.

2.2.22 Preparation of gelatin-coated dishes for cell culture

Gelatinized dishes are used in this study for the culture and maintenance of LIF-selected long-term expanded suture mesenchymal cells. The following protocol is performed:

1. Prepare 1% gelatin solution in nano-pure H_2O and autoclave. This solution can be later stored at 4 ^{o}C.
2. Prepare a 0.1% gelatin solution with nano-pure H_2O and add 6 ml per 100mm-dish.
3. Incubate for 20 min at room temperature.
4. Aspirate the gelatin solution and let the dishes become completely dry (~20 min) at room temperature. The dishes can be also stored at 4 ^{o}C.

2.2.23 Preparation of gelatinized slides for cryosections

The following protocol is used for the preparation of gelatinized slides for cryosections.

1. The slides are washed with dH_2O for 5 min.
2. Then they are placed into 100% EtOH for 5 min. Let them dry.
3. In the meantime, 1 lt of dH_2O is warmed at ~50 ^{o}C and 5 gr of gelatin are gradually added and dissolved into this water.
4. Once the gelatin is dissolved completely, allow the solution to cool.
5. Now 0.5 gr of chrome alum is added to the gelatin solution. Mix well.
6. The slides are finally incubated into this gelatin- chrome alum solution for 3 min at room temperature. Be careful not to make any bubbles.
7. Let them dry overnight. Store them at room temperature.

2.2.24 DNA isolation from mouse tails

The following method is used for the extraction of DNA from mouse tails for PCR and genotyping. This method does not provide purified DNA.

1. The tails are incubated into 300 µl of DNA extraction solution A: 25 mM NaOH, 0.2 mM EDTA pH=12, for 15 min at 95 ^{o}C.
2. Equal volume of DNA extraction solution B: 40 mM Tris-HCl pH=3.5 is added to each sample. Mix well.
3. The samples are finally centrifuged for 2 min at max speed.
4. DNA is counted and ready for PCR.

2.2.25 PCR for the detection of *Erf^{LoxP}* allele

The following PCR conditions and reagents are used for the detection of *Erf^{LoxP}* allele in the mouse genome isolated from tails.

1 µl DNA (~30 ng/µl)
2.5 µl 10X buffer E Invitrogen*
0.5 µl dNTPs (from stock 40 mM/ 10 mM each)
0.5 µl 11671 F primer (from stock 25 µM)
0.5 µl 11771 R primer (from stock 25 µM)
0.5 µl DMSO
0.5 µl Taq pol (5 U/µl)
19 µl H_2O
V_f= 25 µl

Primer Sequences 5′-3′	Annealing	Elongation
11671F: ACGCCACAGCCCAACTCTCC	56 ^{o}C, 20′′	72 ^{o}C, 30′′
11771R: CAGCAAAAGCTCAGGGAGTG		

PCR products:
LoxP band: ~170 bp
Wt band: ~101 bp

* Invitrogen E buffer 10X: 600 mM Tris-HCl pH=9, 150 mM ammonium sulfate, 15 mM $MgCl_2$.

2.2.26 PCR for the detection of *Erf^{fdel}* allele

The following PCR conditions and reagents are used for the detection of *Erf^{fdel}* allele in the mouse genome isolated from tails.

1 µl DNA (~30 ng/µl)
2.5 µl 10X buffer F Invitrogen*
0.5 µl dNTPs (from stock 40 mM/ 10 mM each)
0.5 µl 4021 F primer (from stock 25 µM)
0.5 µl 11771 R primer (from stock 25 µM)
0.5 µl Taq pol (5 U/µl)
19.5 µl H_2O
V_f= 25 µl

Primer Sequences 5′-3′	Annealing	Elongation
4021F: GCACTGCTAGCTCTGAATGG	58 °C, 10′′	72 °C, 20′′
11771R: CAGCAAAAGCTCAGGGAGTG		

PCR products:
Deletion band: 178 bp

* Invitrogen F buffer 10X: 600 mM Tris-HCl pH=9, 150 mM ammonium sulfate, 20 mM $MgCl_2$.

2.2.27 PCR for the detection of Nestin-cre

The following PCR conditions and reagents are used for the detection of Nestin-cre in the mouse genome isolated from tails.

1 µl DNA (~50 ng/µl)
2.5 µl 10X buffer Minotech w/o $MgCl_2$*
2 µl $MgCl_2$ (from stock 25 mM)
0.5 µl dNTPs (from stock 40 mM/ 10 mM each)
0.5 µl Nestin-Cre F primer (from stock 25 µM)
0.5 µl Nestin-Cre R primer (from stock 25 µM)
0.5 µl MEH F primer (from stock 25 µM)
0.5 µl MEH R primer (from stock 25 µM)
0.5 µl DMSO
0.5 µl Taq pol (5 U/µl)
16 µl H_2O
V_f= 25 µl

Primer Sequences 5′-3′	Annealing	Elongation
NestinCreF: AGGTGTAGAGAAGGCACTCAGC	64 °C, 30′′	72 °C, 30′′
NestinCreR: CTAATCGCCATCTTCCAGCAGG		
MEH F: AAGTGAGTTTGCATGGCGCAGC		
MEH R: CCCTTTAGCCCCTTCCCTCTG		

PCR products:
Cre band: 411 bp Internal control band: 341 bp

* Minotech buffer 10X w/o $MgCl_2$: 100 mM Tris-HCl pH=8.5, 500 mM KCl, 1% Triton-X-100.

2.2.28 PCR for the detection of Rosa-mTmG

The following PCR conditions and reagents are used for the detection of RosamTmG in the genome from tails of newborn mice upon crossing with the Gt(ROSA)26Sor$^{tm4(ACTB-tdTomato,-EGFP)Luo}$ mouse line.

1 µl DNA (~50 ng/µl)
2.5 µl 10X buffer Minotech w/o $MgCl_2$*
2 µl $MgCl_2$ (from stock 25 mM)
0.5 µl dNTPs (from stock 40 mM/ 10 mM each)
0.5 µl oIMR7318 common primer (from stock 25 µM)
0.5 µl oIMR7319 wt primer (from stock 25 µM)
0.5 µl oIMR7320 mut primer (from stock 25 µM)
0.5 µl Taq pol (5 U/µl)
17 µl H_2O
V_f= 25 µl

Primer Sequences 5'-3'	Annealing	Elongation
oIMR7318: CTCTGCTGCCTCCTGGCTTCT	61 °C, 10''	72 °C, 20''
oIMR7319: GGCGGATCACAAGCAATA		
oIMR7320: TCAATGGGCGGGGGTCGTT		
PCR products: Wt band: 320 bp	RosamTmG band: 250 bp	

* Minotech buffer 10X w/o $MgCl_2$: 100 mM Tris-HCl pH=8.5, 500 mM KCl, 1% Triton-X-100.

2.2.29 Viral infection of primary cells

In this study to eliminate Erf in suture-derived mesenchymal cells from *Erf*$^{LoxP/LoxP}$ mice, we performed adenoviral infections using a vector containing the sequence of Cre-recombinase gene and the fluorescent protein GFP, as a marker of successful infection. The virus is stated below as AdCreGFP virus.

1. Two days before the infection, 20,000 cells are seeded into each well of a 48-well-plate (20,000 cells/cm^2 for suture-derived cells).
2. On the day of the infection, prepare DMEM medium without FBS, without antibiotics or any culture supplement. The final volume of medium per well will be approximately 125 µl. In this study to improve the efficiency of the infection we tested the addition of supplements: PLL (poly-l-lysine) and

Polybrene, a cationic polymer. PLL is added at a final concentration of 0.5 μg/ml and Polybrene is added at the final concentration of 8 μg/ml. So, DMEM medium is added into 1.5ml-tubes and the supplements (either PLL or Polybrene) are added into this medium and mixed well. Incubate for 5-10 min at room temperature.

3. Now, the AdCreGFP virus is added into the mix at the appropriate MOI (multiplicity of infection). MOI=1 means that 1 pfu of virus is added per cell. In these experiments we used AdCreGFP virus stock with titer 10^{10} pfu/ml prepared on 25.02.2017. We diluted this viral stock so as MOI 250, 50 and 10 were finally added into each mix (for each well). It is important to know the number of cells per well so as to calculate the quantity of virus (pfus) to add according to the MOI wanted. Incubate for 5-10 min at room temperature.
4. Now, the old medium is removed from cells. The wells are washed with DMEM medium w/o FBS, w/o antibiotics.
5. The viral media (~125 μl mix/ well) are added to the cells for 2 hours at 37 ^{o}C.
6. Now remove the viral media and add finally fresh complete maintenance medium. On the following days you can observe the cells under a fluorescence microscope for GFP presence.

2.2.30 RNA Sequencing

NGS libraries were generated from 500 ng input total RNA with the Lexogen-QuantSeq 3′ mRNA-Seq Library Prep Kit FWD for Illumina, according to the manufacturer's protocol. Libraries were run on Illumina 500 on 1x150 Flowcells. Fastq files from Illumina-BaseSpace were mapped to mm10 genes (iGenomes UCSC/mm10) using hisat2 version 2.1.0 (--score-min L 0,-0.5). Gene counts were computed with htseq-count (-s yes, version 0.11.2). Differential analysis was performed with edgeR (3.24.3). Genes with cpm>2 in at least 3 samples were included in the analysis. Samples were normalized by TMM. Sample grouping for the Design matrix was performed by one combined factor, which took into account ERF status, (plus =wt cells, minus=ERF KD cells) coupled to differentiation status (fresh=freshly harvested, LIF=long-term expanded or osteo=osteogenic induced), including also batch effect correction (model.matrix(~0+ERFstatus.DIFFstatus+batch)). Differential analyses were performed by likelihood ratio tests using the estimated negative binomial common dispersion.

3. Results

3. Results

3.1 Freshly derived suture cells from *Erf*$^{LoxP/-}$ craniosynostosis mice display decreased capacity to mineralize in vitro

Our previous work has reported the presence of a mildly delayed ossification pattern in calvarial bones of *Erf*$^{LoxP/-}$ mice that develop premature suture fusion [55]. To explore the role of Erf in the differentiation of cells during intramembranous skull ossification, we isolated cells from cranial sutures of *Erf*$^{LoxP/+}$ and *Erf*$^{LoxP/-}$ mice of postnatal day 5 (P5) and tested their ability to differentiate towards bone-forming osteoblasts in our *ex vivo* culture system. This population represents cells of a mixed differentiation state found naturally in sutures. Following 28 days of osteogenic differentiation *Erf*$^{LoxP/-}$ cells displayed decreased capacity to mineralize *in vitro* in comparison to cells isolated from healthy littermates as evidenced by Alizarin Red S staining of calcium deposits and quantification of the extracted dye (Fig. 1a, b). Although on day 21, *Erf*$^{LoxP/-}$ cells showed a slight increase in their mineralization levels, this observation did not reach the point of statistical significance.

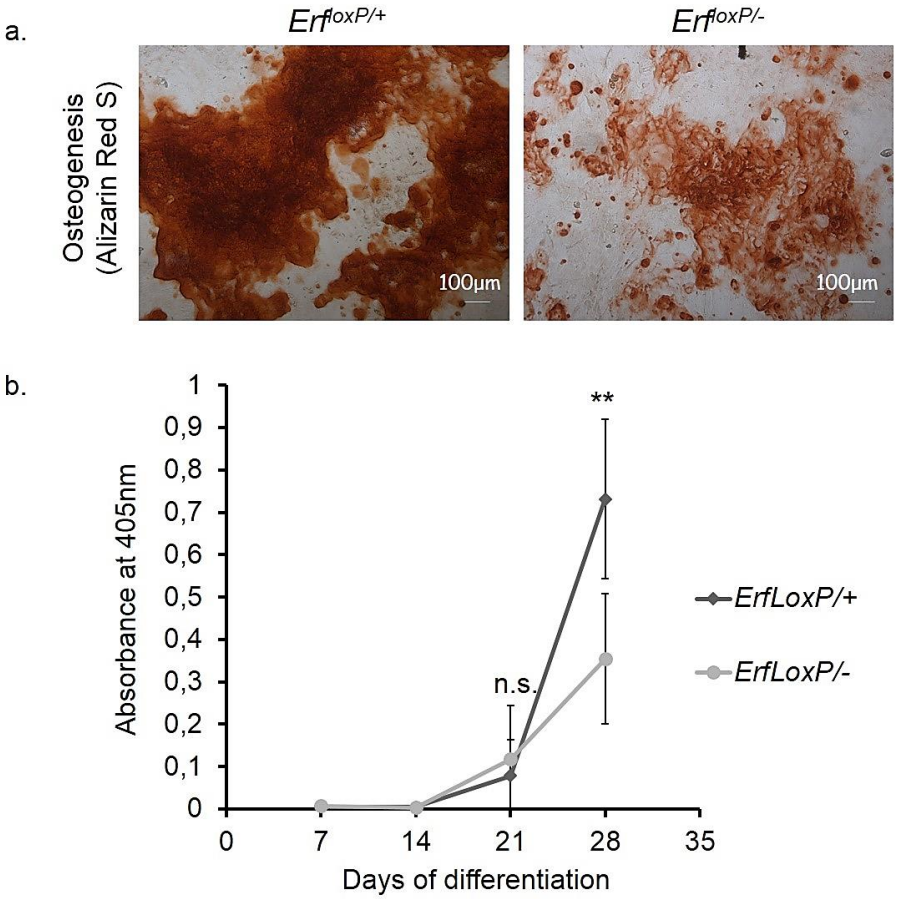

Figure 1: Cranial suture cells from Erf craniosynostosis mice display decreased capacity to mineralize in vitro. a) Freshly derived suture cells were induced to differentiate along the osteogenic lineage for 28 days and stained with Alizarin Red S for calcium deposits. b) Quantification of Alizarin Red S levels after extraction from culture wells at the indicated time-points of differentiation. Statistical analysis was performed using a paired t-test with two-tailed distribution. * $p < 0.05$, ** $p < 0.01$, *** $p < 0.001$

As mentioned above, freshly isolated suture cells constitute a highly heterogeneous population [80] that encompasses a few non-committed mesenchymal cells in a multitude of committed ones. Consequently we hypothesized that the decreased mineralization outcome of $Erf^{LoxP/-}$ cells could possibly implicate either a decline in the abundance of mesenchymal stem cells (MSCs) that eventually give rise to bone or a defect in the MSC osteogenic differentiation pathway per se. Interestingly, looking at the other two cell lineages that originate from MSCs, namely chondrocytes and adipocytes, we observed that $Erf^{LoxP/-}$ cells appeared to have slightly higher potential for *in vitro* adipogenic commitment in comparison to control cells that showed only minor differentiation efficiency (Fig. 2), indicating possibly the existence of a greater proportion of stem or precursor populations among $Erf^{LoxP/-}$ suture cells.

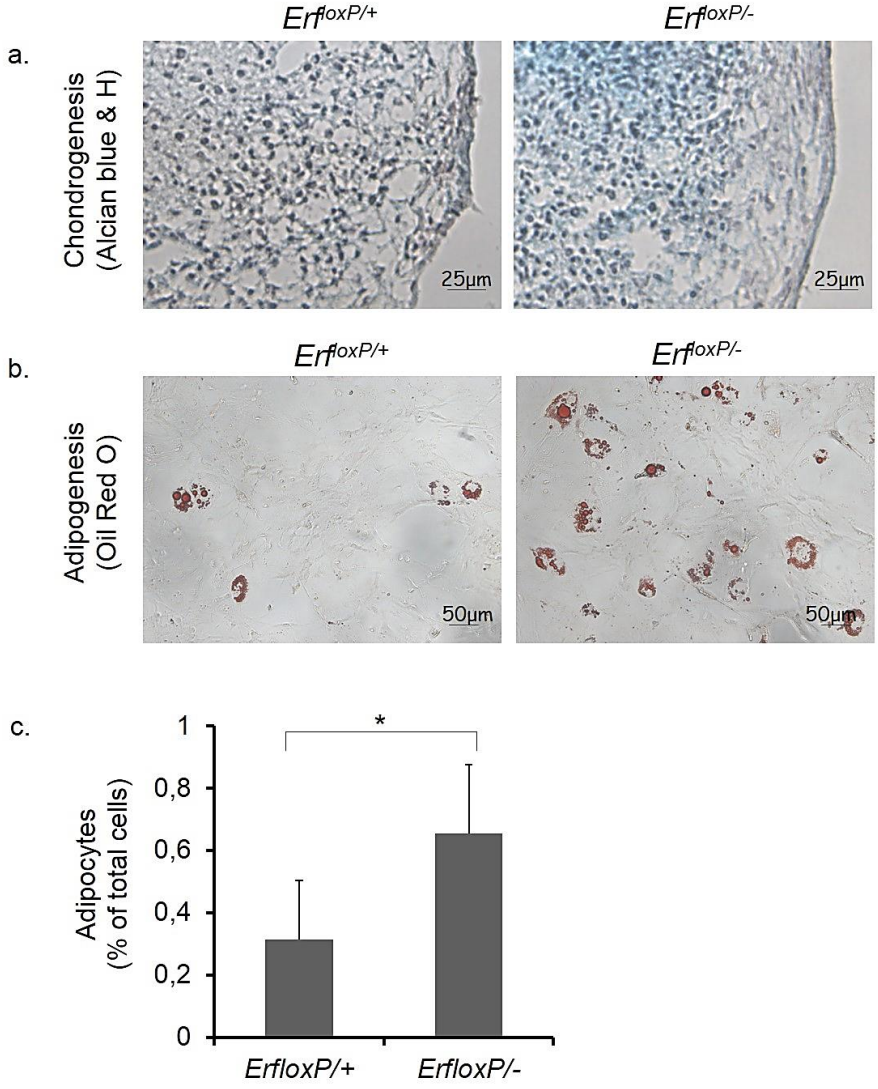

Figure 2: Cranial suture cells from Erf craniosynostosis mice exhibit slightly higher potential for *in vitro* adipogenic commitment. Freshly derived suture cells were induced to differentiate towards a) chondrocytes and b, c) adipocytes and stained with Alcian blue/ Hematoxylin and Oil Red O, respectively. In c) the total number of cells was defined by Hoechst staining of the nuclei. Statistical analysis was performed using a t-test with two-tailed distribution. * $p < 0.05$, ** $p < 0.01$, *** $p < 0.001$

Erf is a transcriptional repressor and its subcellular localization and function is known to be regulated by Erk1/2-mediated phosphorylation [61, 66, 67]. Given that the $Erf^{LoxP/-}$ cells still express approximately 30% of wild-type Erf protein levels, we hypothesized that pharmacological compounds that could increase the amount of nuclear non-phosphorylated form of Erf, could also potentially restore the differentiation defect of these cells. We tested two molecules: U0126, a specific inhibitor of MEK-ERK signalling [89] that was also previously reported in the treatment of craniosynostosis in an Apert syndrome mouse model [32], and the KPT330-compound, a selective inhibitor of the nuclear exportin XPO1/CRM1 that is widely being tested as potential antitumor drug [90, 91]. Experiments performed with HeLa cells transfected with the GFP-ERF fusion plasmid DNA and tested in presence of different inhibitor quantities showed that 10 μM of U0126 was the minimum concentration able to significantly increase the nuclear GFP-ERF localization signal, while KPT330 was shown to lead to nuclear ERF accumulation from 50 nM on (data from A. Gkikas & K. Makris thesis). Next we tested the effect of U0126 and KPT330 at the suboptimal concentrations of 2 μM and 10 nM respectively, on the osteogenic differentiation of freshly isolated suture-derived cells. The addition of U0126 in suture cells that were induced to differentiate along the osteogenic lineage resulted in significantly increased per cell mineralization in the case of $Erf^{LoxP/+}$ cells (Fig. 3a). Although not statistical significant, KPT330-compound also provoked an increase in the mineralization of $Erf^{LoxP/+}$ cells. However, the inhibitors did not seem to have an effect on differentiating $Erf^{LoxP/-}$ cells, indicating the necessity of sufficient Erf levels in the osteogenic differentiation process followed by these cells. Higher concentration of inhibitors resulted in attenuation of cell cycle, survival and differentiation of cells (Fig. 3b), hence they were not further included in the experimental design.

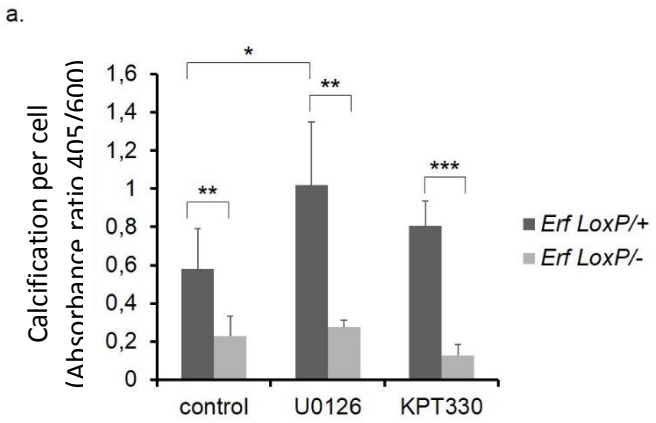

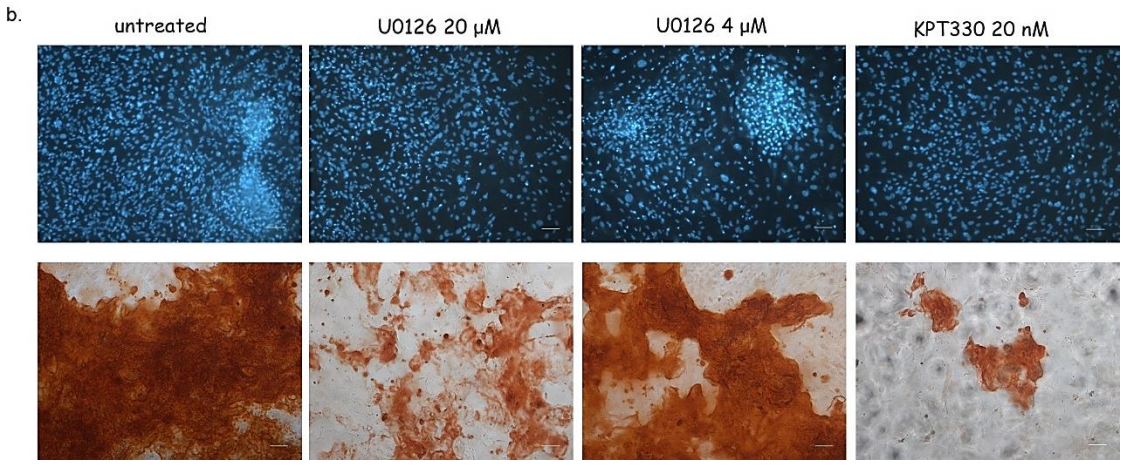

Figure 3: The effect of U0126 and KPT330-compound on the osteogenic differentiation of freshly isolated cranial suture cells. a) Calcium deposition per cell of $Erf^{LoxP/+}$ and $Erf^{LoxP/-}$ cells growing for 28 days in presence of osteogenic media supplemented with 2 μM U0126 or 10 nM KPT330. Cell numbers were estimated with MTT assay by the absorbance at 600 nm and calcium deposits by the absorbance of Alizarin Red S at 405 nm. Data were analyzed with one-way ANOVA followed by Dunnett's (two-sided) test to compare all groups (treatments) against control group. Unpaired (two-sided) t-test was used for comparisons between the two genotypes in each group. The experiment was performed in triplicate * $p < 0.05$, ** $p < 0.01$, *** $p < 0.001$. b) Microphotographs of cells growing for 28 days in osteogenic medium in presence of the indicated concentrations of the Mek1/2 and Xpo1 inhibitors. Upper: Hoechst staining of the nuclei, Lower: Alizarin Red S staining of calcium deposits. Scale bars: 100μm

3.2 LIF-selected long-term expanded suture derived cells possess *in vitro* characteristics of mesenchymal stem/ progenitor cells

To investigate the role of Erf in mesenchymal stem/ progenitor cell maintenance and differentiation, we established a protocol for the selective expansion of these cells from cranial suture cultures using leukemia inhibitory factor (LIF) already known for its role in sustaining the stem cell state while inhibiting differentiation [81, 82]. Suture explants maintained in LIF for 7 days yielded twice as many cells as those in the standard culture protocol (Fig. 4a). The cultivation of suture-derived cells in presence of LIF for a total of 8 population doublings (PDs) during a period of approximately 50-60 days resulted in a population of cells that were plastic-adherent, fibroblast-like in shape (Fig. 4b, c) and expressed high levels of CD44, CD29, Sca1 and CD90 antigens typically found in MSCs [53, 92-94], as shown by flow cytometric analysis (Fig. 5a). Neither hematopoietic (CD45, CD34) nor endothelial markers (CD31) were significantly expressed. A reduction in the mRNA levels of *Osterix*, marking differentiated cells along the osteogenic lineage, and an increase in *Axin2* mRNA levels, previously reported to characterize suture mesenchymal stem cells [95], were evident in cultures of 8 PDs in comparison to the initial population (Fig. 5b).

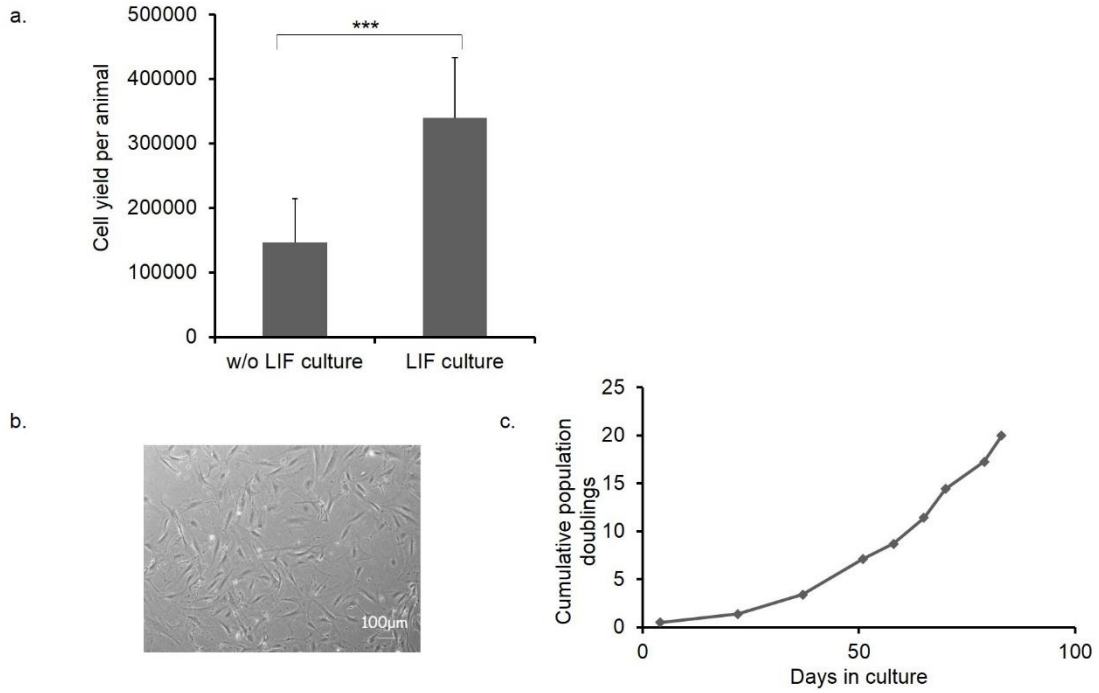

Figure 4: ***In vitro*** **morphology and growth properties of LIF-expanded suture mesenchymal cells.** a) Comparison of total cell numbers derived from cranial sutures of wild-type mice cultured in the presence or absence of LIF for 7 days. b) Phase-contrast image of suture-derived cells expanded in presence of LIF for 8 population doublings (PDs). c) Graph showing the population doublings over time in culture for LIF-expanded suture mesenchymal cells. Each measurement (point in graph) has been performed at the end of each passage. Statistical analysis was conducted using an unpaired t-test with two-tailed distribution. * $p < 0.05$, ** $p < 0.01$, *** $p < 0.001$

Furthermore, these cells were shown to have the ability to undergo *in vitro* chondrogenic, osteogenic and adipogenic differentiation (Fig. 6a), although with respect to adipogenesis, mainly immature adipocytes with small lipid droplets were observed to form. For comparison, human bone marrow mesenchymal stem cells were also induced to differentiate along the three lineages (Fig. 6b). Under the conditions we established, suture mesenchymal cells were maintained in culture for longer than 80 days giving more than 20 PDs (Fig. 4c). Collectively, these data indicate that suture-derived cells long-term expanded in presence of LIF possess *in vitro* characteristics of mesenchymal stem/ progenitor cells.

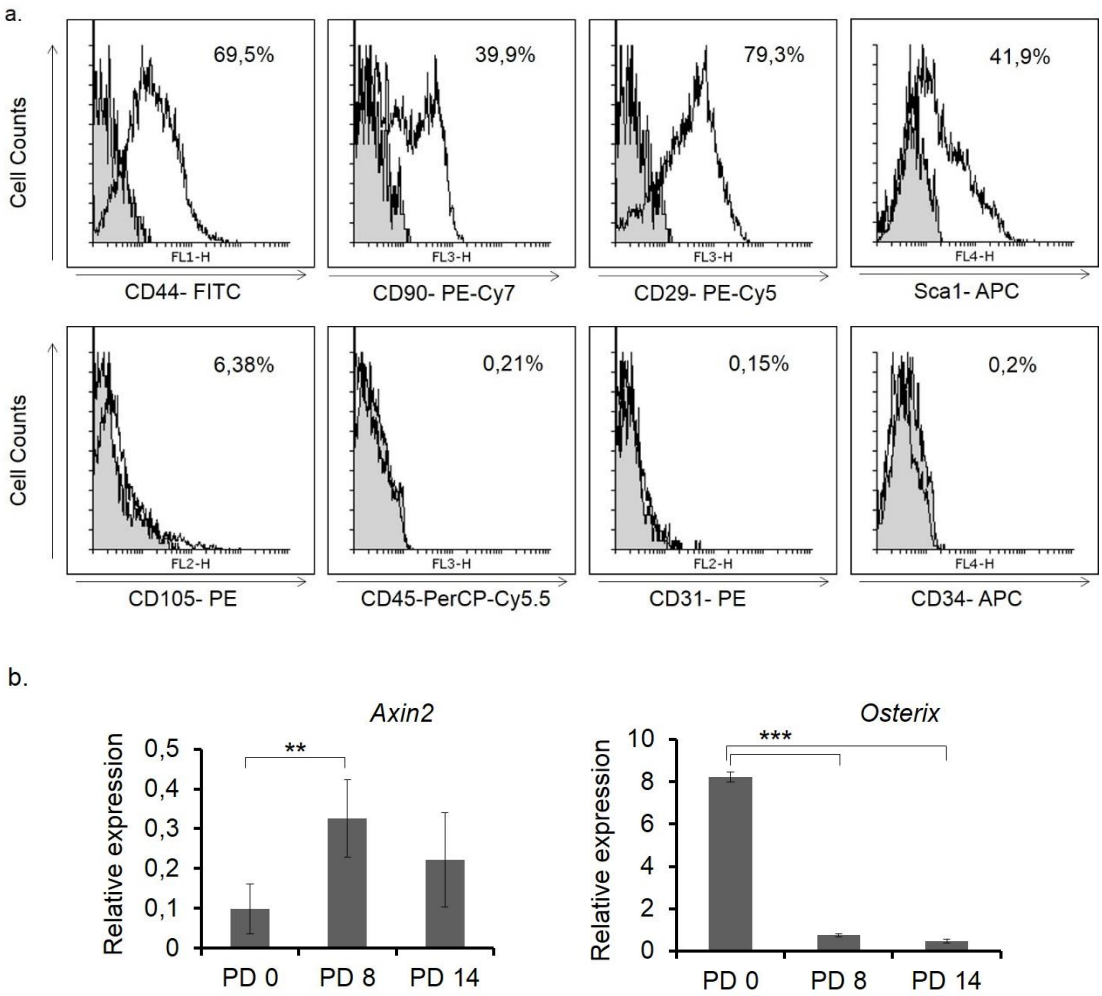

Figure 5: Characterization of LIF-expanded suture mesenchymal cells based on extracellular antigens and intracellular markers. a) Flow-cytometric analysis of cells for mesenchymal stem cell (MSC) markers (CD44, CD90, CD29, Sca1, CD105) and hematopoietic/ endothelial markers (CD45, CD34, CD31) after expansion for 8 population doublings (PDs). Filled histograms indicate the unlabelled cells used as negative controls. b) *Axin2* and *Osterix* mRNA levels normalized to *Gapdh* as determined by qPCR in suture cells of the indicated population doubling level (PD). Statistical analysis was conducted using ANOVA followed by Dunnett's (two-sided) test to compare all groups against control group (PD 0) * $p < 0.05$, ** $p < 0.01$, *** $p < 0.001$

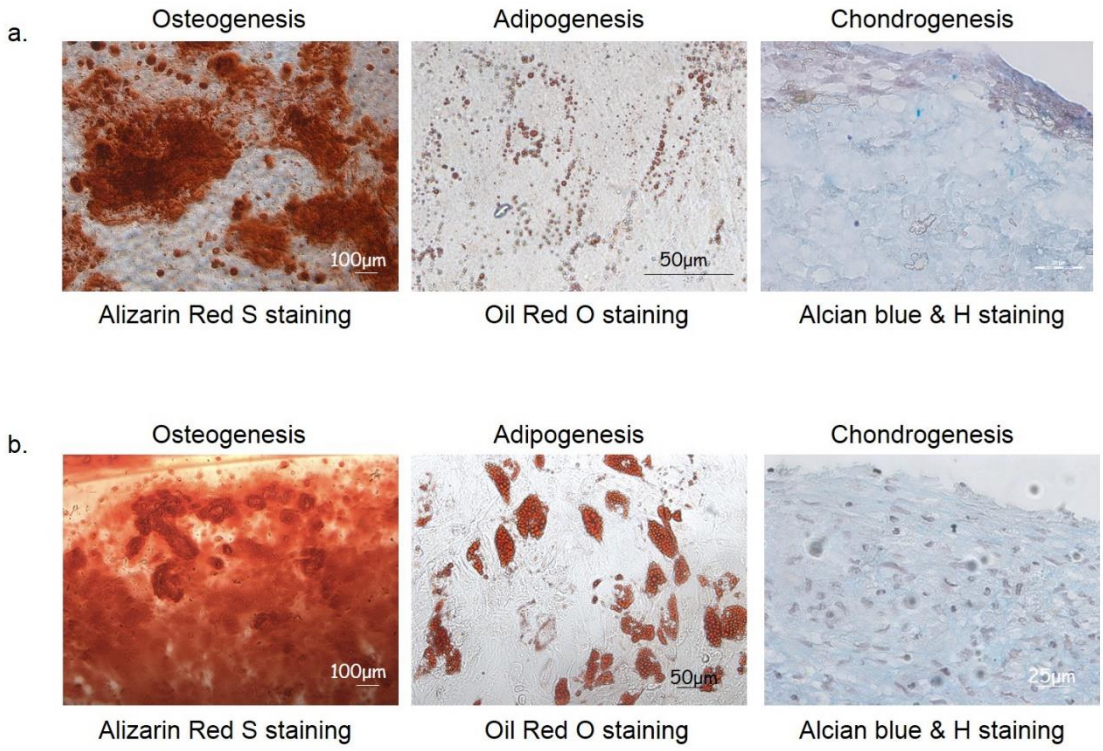

Figure 6: Trilineage differentiation of LIF-expanded suture mesenchymal cells and human bone marrow MSCs. LIF-selected mouse suture derived cells expanded for 10 PDs in a) and human bone marrow mesenchymal stem cells in b) were induced to differentiate towards osteocytes, adipocytes and chondrocytes, and stained respectively with Alizarin Red S, Oil Red O and Alcian blue/ Hematoxylin.

3.3 Efforts to eliminate *Erf* by adenoviral infection of suture derived MSCs using a vector containing the sequence of Cre-recombinase gene

In an effort to eliminate *Erf* from suture derived mesenchymal stem/ progenitor cells (sdMSCs) isolated from $Erf^{LoxP/LoxP}$ mice and monitor their differentiation along the osteogenic lineage, we initially tested the optimal conditions for a successful infection that would maintain cell viability in wild type (wt) sdMSCs. AdCreGFP virus was used at various MOIs (Multiplicity of Infection), and different supplements along with different times of viral incubation were also tested. Although the number of GFP^+ (infected) cells increased with increasing MOIs of virus, no difference was observed between 2 h and 24 h incubation of cells with the viral medium as evaluated on day 3 post-infection (Fig. 7a, b). The addition of Polybrene which is a cationic polymer used to enhance the efficiency of viral infection, resulted in slightly more GFP^+ cells. However, on day 12 post-infection the percentage of GFP^+ cells was generally decreased, and the condition of MOI 50 in presence of PLL (poly-l-lysine) seemed to better preserve the infected cells (Fig. 7c, d).

a.

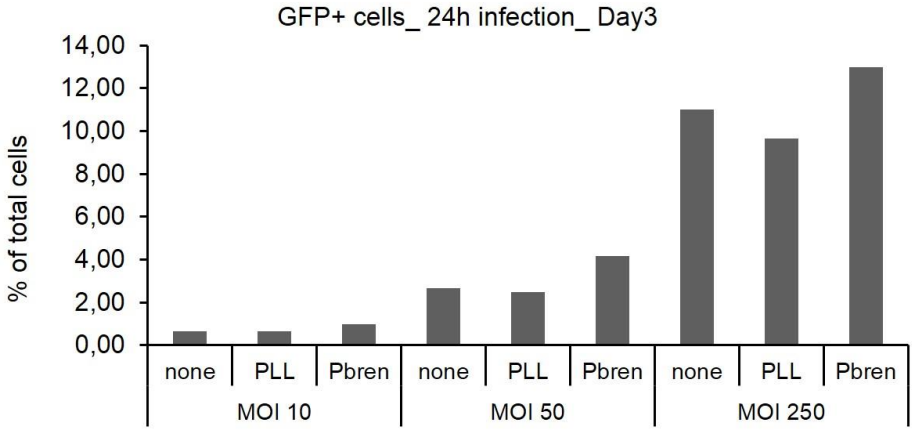
GFP+ cells_ 24h infection_ Day3
% of total cells
14,00
12,00
10,00
8,00
6,00
4,00
2,00
0,00
none
PLL
Pbren
MOI 10
MOI 50
MOI 250

b.

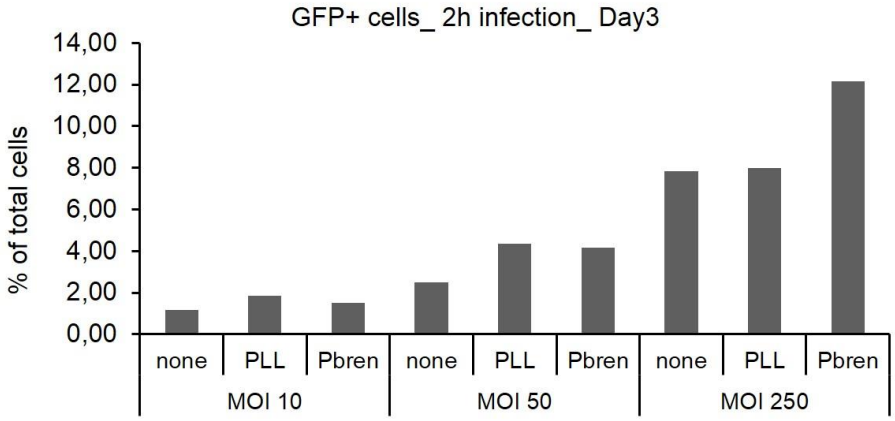
GFP+ cells_ 2h infection_ Day3
% of total cells
14,00
12,00
10,00
8,00
6,00
4,00
2,00
0,00
none
PLL
Pbren
MOI 10
MOI 50
MOI 250

c.

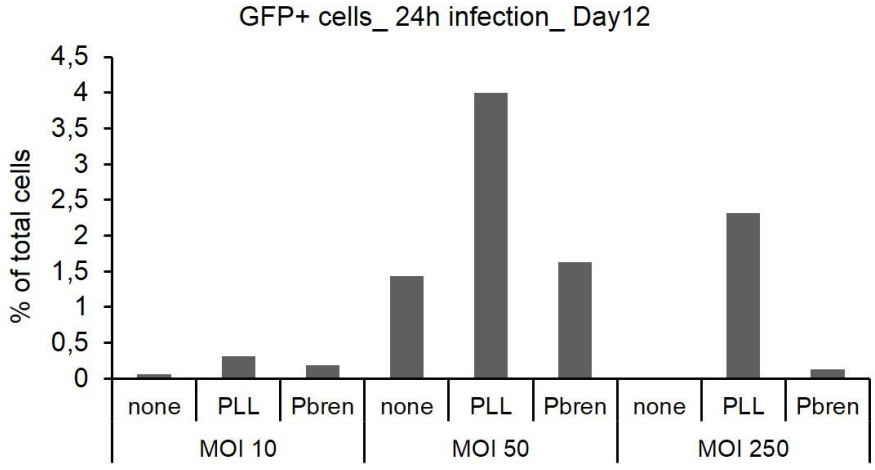
GFP+ cells_ 24h infection_ Day12
% of total cells
4,5
4
3,5
3
2,5
2
1,5
1
0,5
0
none
PLL
Pbren
MOI 10
MOI 50
MOI 250

d.

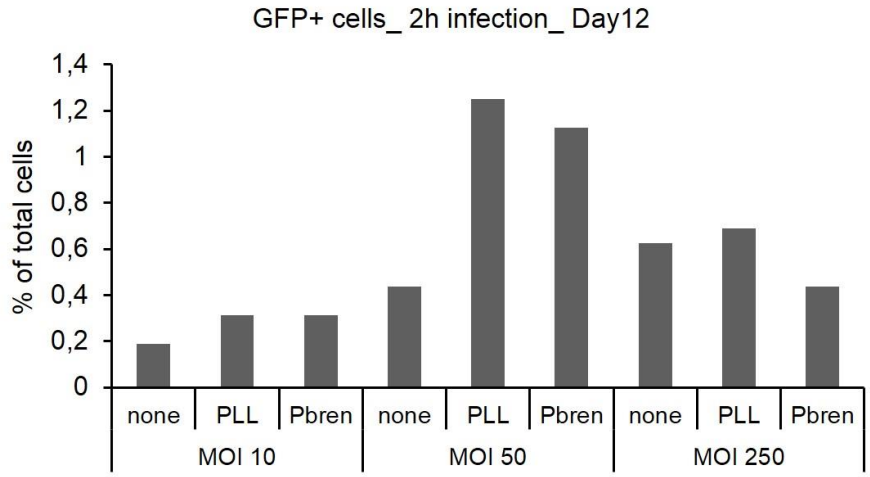

Figure 7: Efficiency of adenoviral infection of sdMSCs. Wild type sdMSCs were infected with AdenoCreGFP virus at the indicated conditions (presence or absence of supplements, time of viral incubation and MOI) and the percentage of GFP positive cells was evaluated 3 days post-infection a, b) and 12 days post-infection c, d) in presence of osteogenic differentiation medium. MOI: Multiplicity of Infection, none: no supplement, PLL: poly-l-lysine, Pbren: Polybren.

Interestingly though, increasing MOIs seemed to seriously affect the overall mineralization of both wild type sdMSCs and freshly isolated wild type suture cells during the osteogenic differentiation (Fig. 8). This phenomenon could probably be attributed to cell stress or change in cell behavior upon the addition of the medium containing the viral particles.

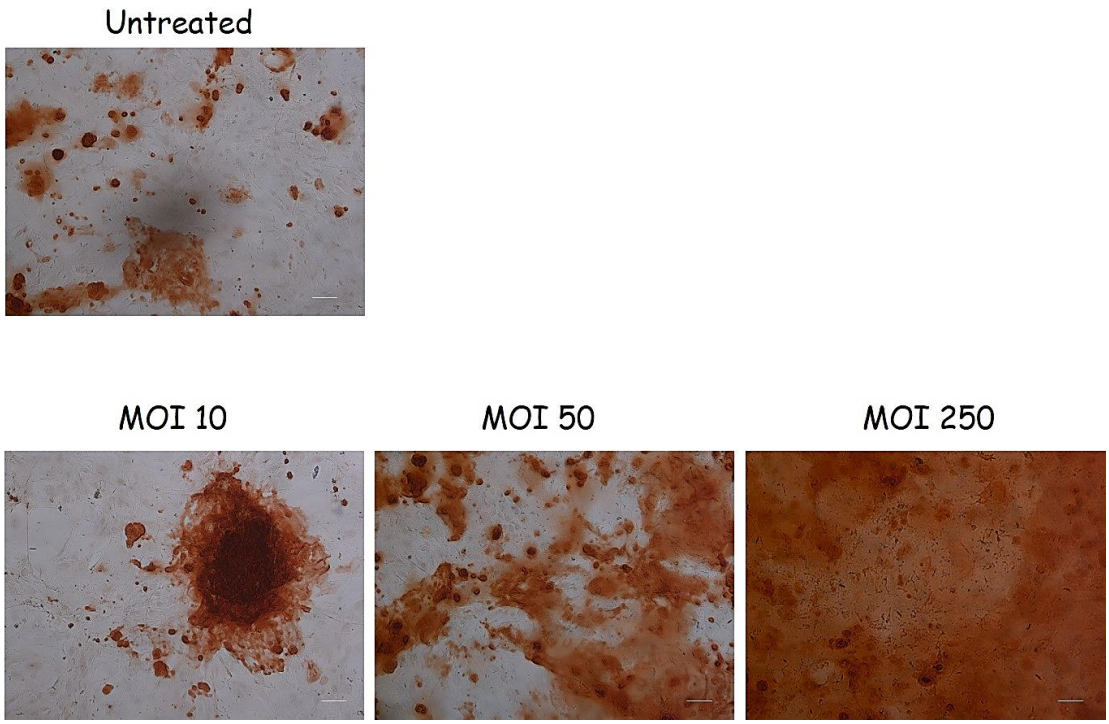

Figure 8: The effect of adenoviral infection on the differentiation of cranial suture cells towards the osteogenic lineage. Wild type freshly isolated suture cells were infected with AdCreGFP virus at the indicated MOIs for 2 hrs and then induced to differentiate towards matrix-producing osteoblasts for 21 days. Representative images are shown from Alizarin Red S staining on day 21. Scale bar: 100μm.

Our data collectively indicate that both freshly isolated cranial suture cells and sdMSCs can be infected with the adenovirus type 5 (Ad5) at efficiency that depends primarily on the MOIs and secondarily on the presence of cationic polymers and time of viral incubation. However, since the percentage of infected (GFP^+) cells drops over time in culture and the procedure of viral infection itself seriously affects the osteogenic differentiation of cranial suture cells, the adenoviral-mediated elimination of *Erf* is not a suitable approach to follow for a long-term study as osteogenesis.

3.4 Efforts to eliminate *Erf* in mesenchymal lineages using the B6.Cg-Tg(Nes-cre)1Kln/J mouse line

$Erf^{LoxP/-}$ mice that display the craniosynostosis phenotype, still express approximately 30% of the wild-type Erf protein levels in each cell. To study the effect of the complete Erf elimination in mesenchymal lineages, we utilized the B6.Cg-Tg(Nes-cre)1Kln/J mouse line, in which the Cre recombinase is expressed under the control of the promoter of *Nestin* gene, previously reported to be active in neuroectodermal and mesodermal lineages. By crossing Nestin-cre/+ with $Erf^{LoxP/LoxP}$ mice, we finally obtained *Nestin-cre*/+;$Erf^{LoxP/LoxP}$ mice, that although displaying a smaller body size (data not shown) and a slightly altered craniofacial morphology, they did not present synostosis of the calvarial bones (Fig. 9). The experiment was performed in collaboration with M. Kokkori and additional images can be found in the respective thesis.

Figure 9: MicroCT images of skulls from *Erf*$^{LoxP/+}$ and *Nestin-cre/+;Erf*$^{LoxP/LoxP}$ mice at P65. At least three mice from the indicated genotypes were sacrificed at the age of P65 and skulls were analyzed by microCT imaging. Left: dorsal views, right: lateral views of skulls. The yellow arrows indicate the presence of the open sagittal and coronal sutures in *Nestin-cre/+;Erf*$^{LoxP/LoxP}$ mice, while the red asterisk is used to mark the mandibular defect.

To evaluate the extent of Cre recombination in *Nestin-cre/+;Erf*$^{LoxP/LoxP}$ mice, we utilized the Gt(ROSA)26Sor$^{tm4(ACTB-tdTomato,-EGFP)Luo}$ mouse line by Jackson, from now on stated as Rosa-mTmG in this manuscript. Upon Cre recombination, the red fluorescence is substituted by the green one, thus marking cells that are positive for Cre activity. Analysis of cranial sutures from *Nestin-cre/+;Rosa-mTmG/+;Erf*$^{LoxP/LoxP}$ mice showed that only a small fraction of total suture cells (approximately 2-6% depending on the suture involved) express the green fluorescent protein (GFP) indicative of Cre-mediated *Erf* elimination (Fig. 10).

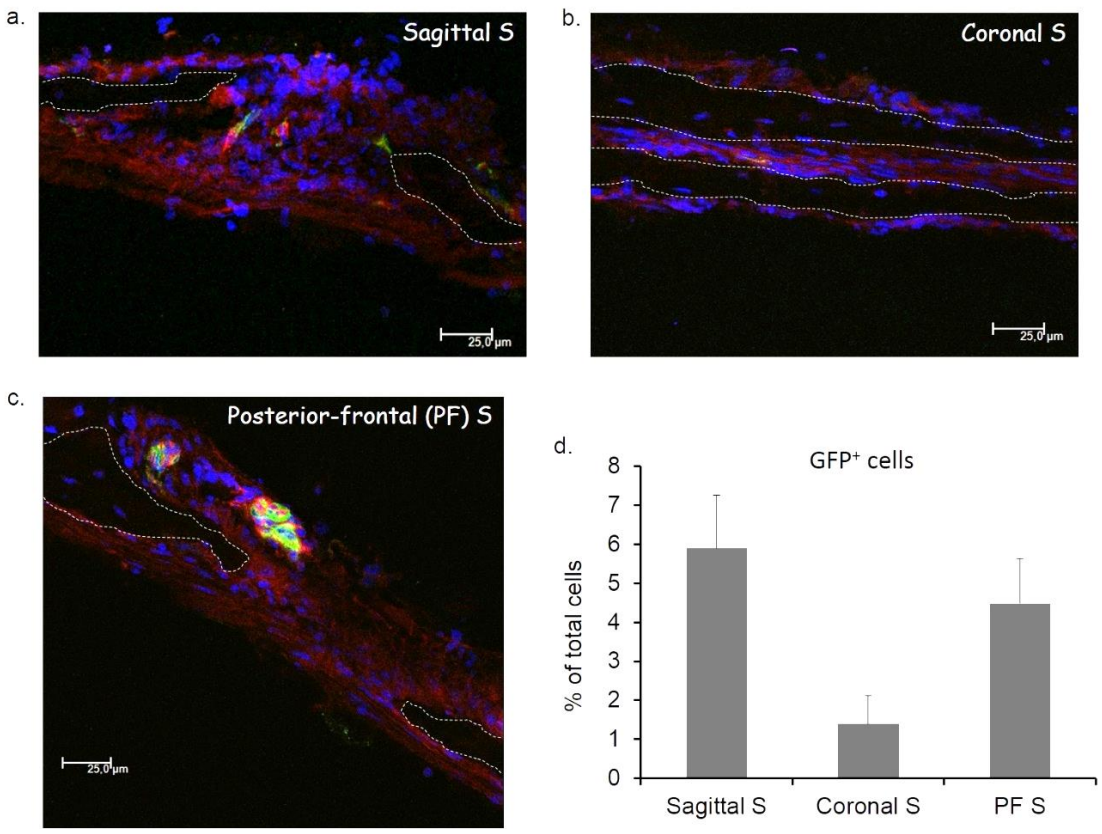

Figure 10: The extent of Cre recombination activity in cranial sutures of *Nestin-cre/+;Rosa-mTmG/+;Erf*$^{LoxP/LoxP}$ mice. Mice of postnatal day 5 (P5) were sacrificed and representative confocal microscopy images of sections of the sagittal suture in a), the coronal suture in b) and the posterior frontal (PF) suture in c) are shown. Red: Tomato fluorescence, Green: GFP fluorescence, Blue: nuclei stained with TOPRO-3. Dotted lines indicate the developing bones. The quantification of GFP$^+$ cells in the respective sutures as an estimate of Cre recombination activity is shown in d.

Furthermore, we isolated cells from coronal and sagittal sutures of *Nestin-cre/+;Rosa-mTmG/+;Erf*$^{LoxP/LoxP}$ mice of postnatal day 5 (P5) using the LIF-culture condition protocol and monitored the number of GFP$^+$ cells for at least 5 consecutive passages. We observed a decline in the percentage of GFP$^+$ cells over time in culture as evidenced by fluorescence microscopy on coverslip-grown cells (Fig. 11a) and was also confirmed later by flow cytometric analysis (Fig. 11b).

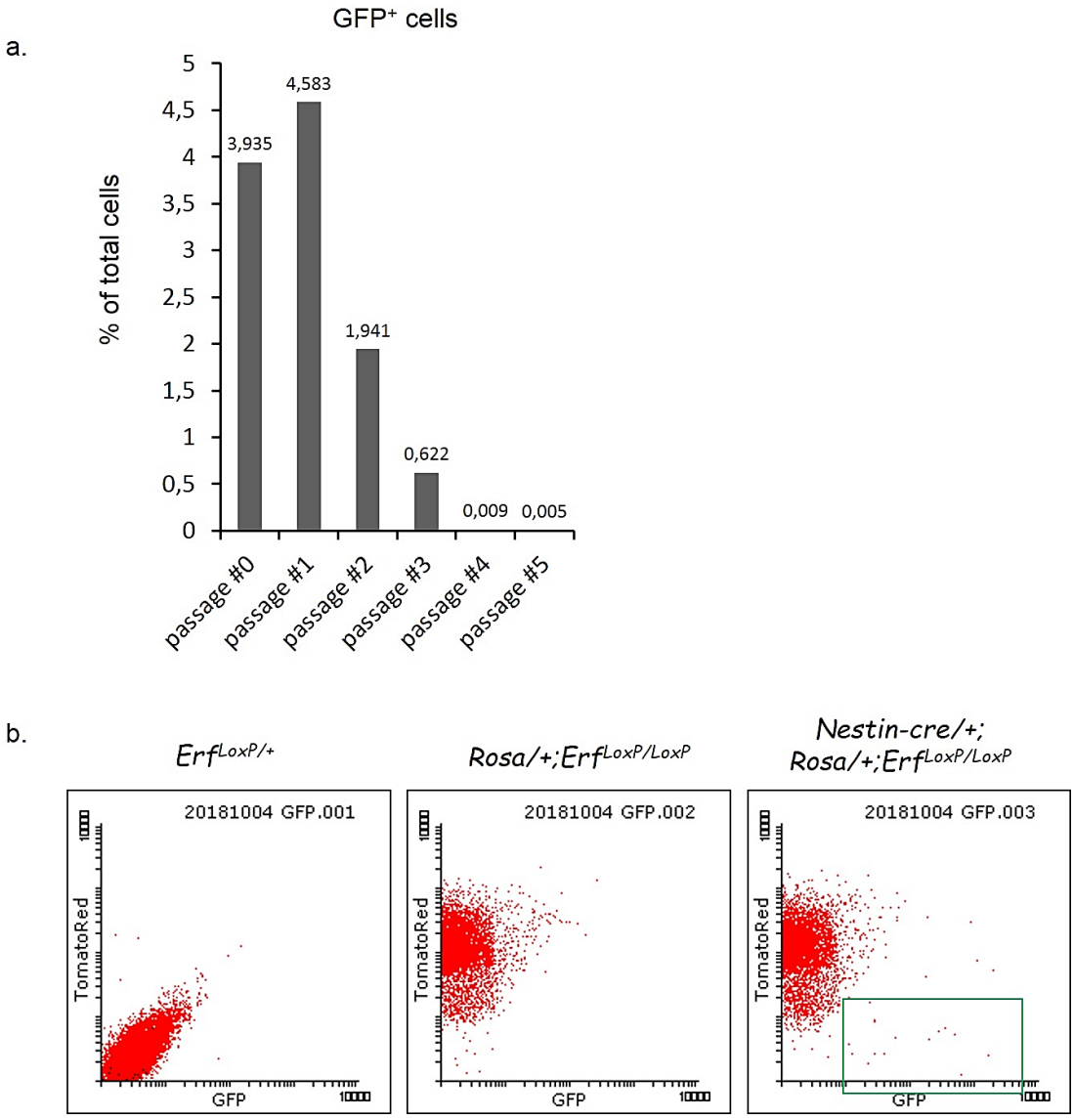

Figure 11: Monitoring the percentage of GFP⁺ cells in cultures of sutures from *Nestin-cre/+;Rosa-mTmG/+;Erf$^{LoxP/LoxP}$* mice. Cells from sagittal and coronal sutures of P5 mice were isolated and cultured in presence of LIF for 5 consecutive passages and the percentage of GFP⁺ cells is depicted in the graph in a) as estimated by fluorescence microscopy at the end of each passage. b) Flow cytometric analysis of cells from the indicated genotypes at the end of passage #3. The boxed area marks the GFP single positive cells that reach only 0.34% of total cells.

These results indicate that only a small fraction of cells in cranial sutures of P5 *Nestin-cre/+;Erf$^{LoxP/LoxP}$* mice express the Cre recombinase gene and consequently may display *Erf* elimination. This small number of GFP/Cre⁺ cells cannot be either maintained or propagated in vitro under the conditions optimized for cranial suture derived MSCs that we have established. This is true for suture cells derived from both *Nestin-cre/+;Rosa-mTmG/+;Erf$^{LoxP/LoxP}$* and *Nestin-cre/+;Rosa-mTmG/+;Erf$^{LoxP/+}$* mice (data not shown), indicating possibly that the elimination of *Erf* is not the crucial point for the in vitro survival of these cells.

The absence of the craniosynostosis phenotype in the majority of *Nestin-cre/+;Erf*$^{LoxP/LoxP}$ mice, along with the apparent limited number of cranial suture cells positive for Cre recombinase activity make this mouse model unsuitable for further experimentation on the potential effect of total *Erf* elimination in calvarial bone development.

3.5 Erf insufficiency does not affect the cycling of suture mesenchymal stem/ progenitor cells but compromises their differentiation towards the osteogenic lineage

Cell cycle phase analysis of mesenchymal stem/ progenitor cells (sdMSCs) from *Erf*$^{LoxP/+}$ and *Erf*$^{LoxP/-}$ mice showed no significant difference in the distribution profiles of cells (Fig. 12a). Furthermore, the cell doubling time was studied at various population doubling levels (PDs) of the culture and although changes were observed among specific PDs, no difference was detected between *Erf*$^{LoxP/+}$ and *Erf*$^{LoxP/-}$ cells of each particular doubling level (Fig. 12b). These findings suggest that MSC self-renewal and growth kinetics are not significantly affected by the insufficiency of Erf.

a.

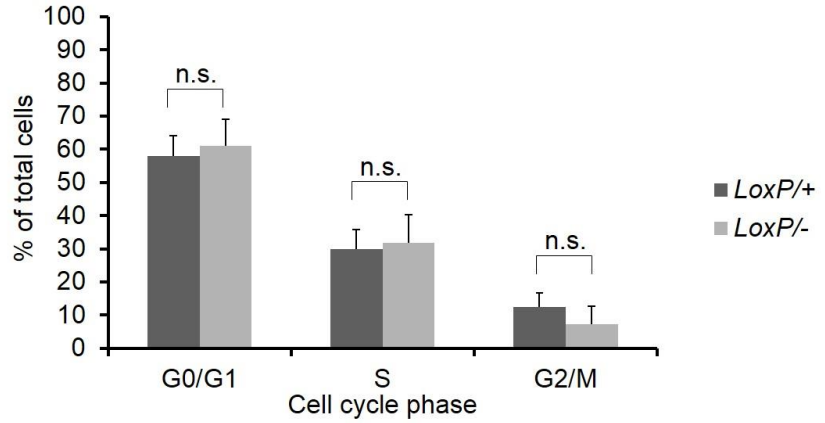

b.

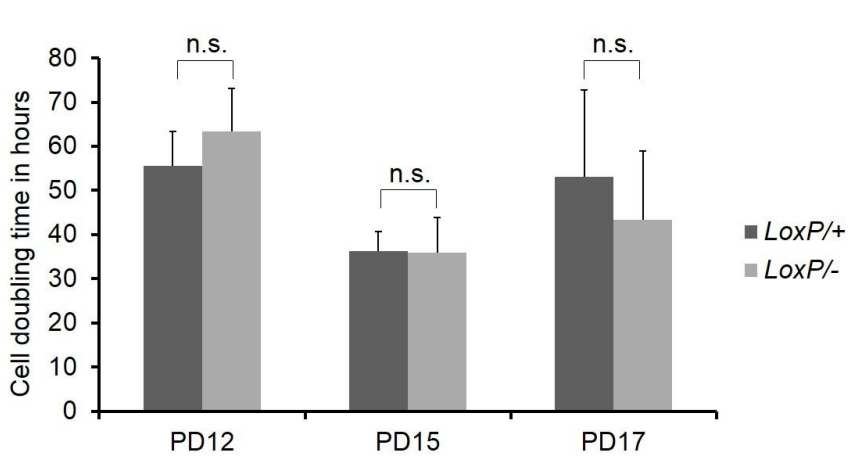

Figure 12: Erf insufficiency does not seem to affect the cycling of LIF-selected suture mesenchymal stem/ progenitor cells under maintenance conditions in culture. a) Frequency of cells in each of the cell cycle phases as determined by propidium iodide staining and flow cytometry. b) Doubling time in hours of $Erf^{LoxP/+}$ and $Erf^{LoxP/-}$ mesenchymal stem/ progenitor cells at the indicated population doubling levels (PDs). Three independent biological experiments were conducted and the statistical analysis was performed using two-tailed t-test for comparisons between the two genotypes (n.s. stands for no significance).

Next, we examined whether the decreased Erf levels could have an impact on the differentiation of these cells along the osteogenic, chondrogenic and adipogenic lineages. $Erf^{LoxP/+}$ and $Erf^{LoxP/-}$ mesenchymal stem/ progenitor cells showed comparable efficiency for *in vitro* chondrogenic and adipogenic commitment (Fig. 13a, b). However, $Erf^{LoxP/-}$ cells displayed decreased ability to mineralize as defined by Alizarin Red S staining of calcium deposits and quantification of the extracted dye (Fig. 13c, d), implying an impairment in the osteogenic differentiation of these cells. This finding is consistent with the one obtained from the freshly derived suture cell cultures upon osteogenic induction.

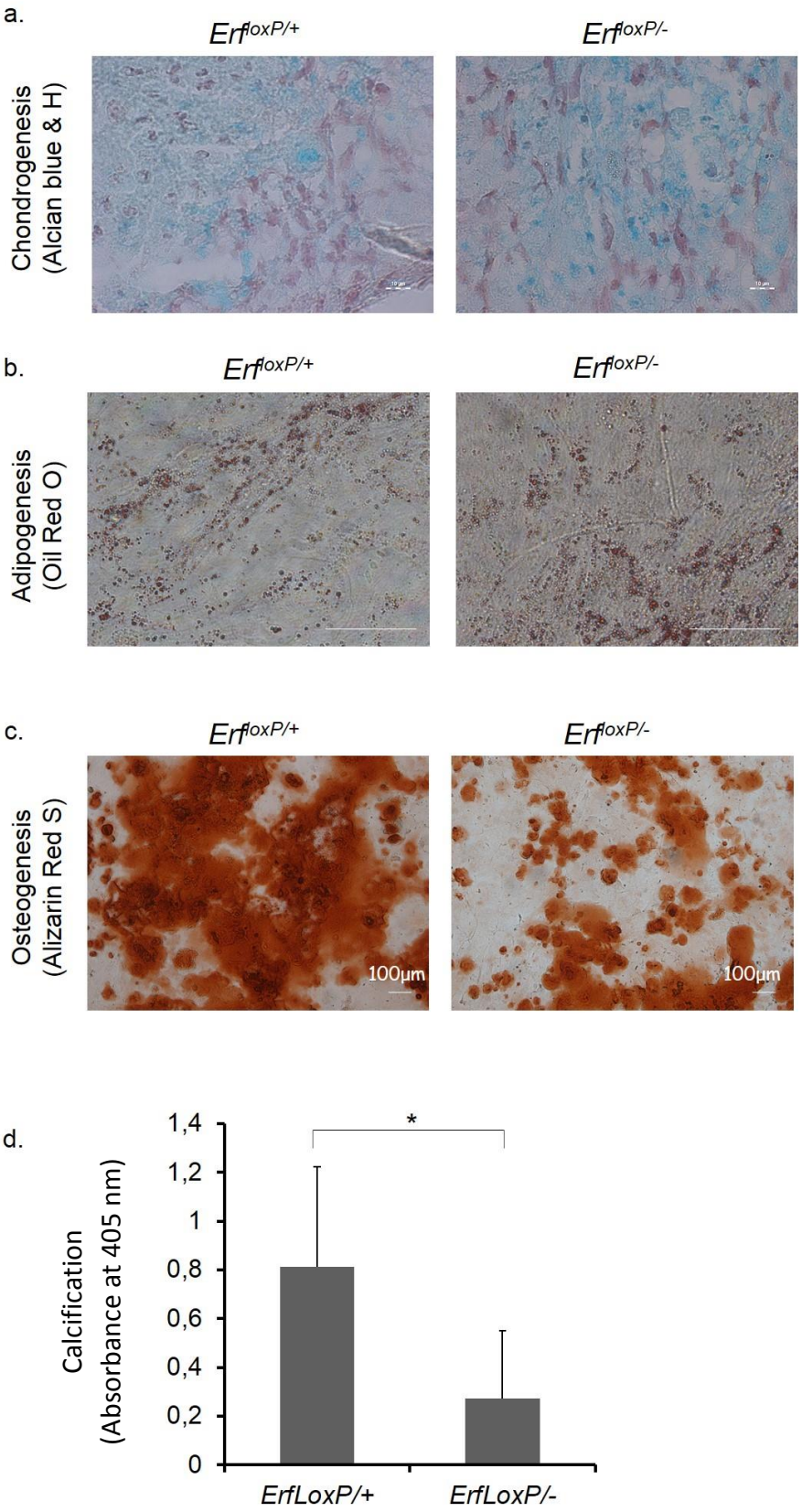

Figure 13: Erf insufficiency, although not affecting chondrogenesis and adipogenesis, seems to compromise the differentiation of mesenchymal stem/ progenitor cells along the osteogenic lineage. Suture mesenchymal stem/ progenitor cells were induced to differentiate along the chondrogenic for 21 days in a), the adipogenic for 21 days in b) and the osteogenic

lineage for 28 days in c) and stained respectively with Alcian blue & Hematoxylin, Oil Red O and Alizarin Red S. Measurements of the extracted Alizarin Red S dye are depicted in d. Statistical analysis was conducted using an unpaired t-test with two-tailed distribution. * $p < 0.05$, ** $p < 0.01$, *** $p < 0.001$

Taken together, these results indicate that Erf insufficiency does not affect MSC self-renewal/ maintenance but rather causes a defect in the MSC osteogenic differentiation pathway per se.

3.6 Erf seems to be required for the initial commitment of suture mesenchymal stem/ progenitor cells towards the osteogenic lineage

Erf is a transcriptional repressor and its subcellular localization and function is known to be regulated by Erk1/2-mediated phosphorylation [61, 66, 67]. Western blot analysis of protein extracts isolated from wild type suture mesenchymal stem/ progenitor cells showed an increase in the amount of the active, non-phosphorylated form of Erf one hour after osteogenic induction (Fig. 14a). Consistently, the levels of phosphorylated Erk1/2 were found to be decreased. The presence of the active, non-phosphorylated Erf protein was detected for at least 8 hours post induction (Fig. 14b).

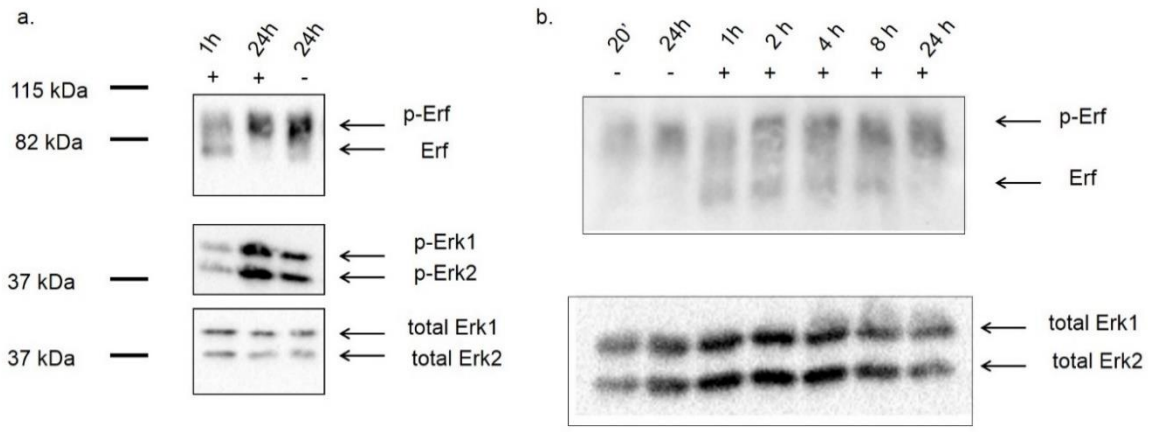

Figure 14: Erf phosphorylation status upon *in vitro* osteogenic induction of suture mesenchymal stem/ progenitor cells. Suture mesenchymal stem/ progenitor cells were induced to differentiate along the osteogenic lineage (+ marks the addition of differentiation medium) and protein extracts were collected at the indicated time points post induction and analyzed by SDS-PAGE and antibodies against a) Erf and phosphorylated Erk1/2 and b) Erf. Levels of total Erk1/2 were used as loading control.

To further understand the role of Erf in the osteogenic commitment and differentiation of suture mesenchymal stem/ progenitor cells, we proceeded to RNA-Seq analysis of cell samples collected from $Erf^{LoxP/+}$ and $Erf^{LoxP/-}$ mice. RNA was isolated from both freshly derived suture cells ("fresh-F") and long-term expanded LIF-selection subjected mesenchymal stem/ progenitor cells ("LIF-L") as well (Fig. 15a). Besides, to uncover potential molecular changes associated with Erf insufficiency upon osteogenic commitment, we isolated RNA from suture mesenchymal stem/ progenitor cells that were previously induced to differentiate along the osteogenic lineage for 24 hours ("osteo-O"). The analysis showed that although no major differences are observed between $Erf^{LoxP/+}$ and $Erf^{LoxP/-}$ mesenchymal stem/ progenitor cells under maintenance conditions, upon osteogenic induction (comparison L-O plus vs L-O minus), $Erf^{LoxP/-}$ cells fail to significantly elevate the expression of genes associated with the ossification process and the extracellular matrix synthesis (Fig. 15b & Table 1). These data suggest that Erf seems to be required for the efficient commitment of suture-derived stem/ progenitor cells towards the osteogenic lineage.

a.

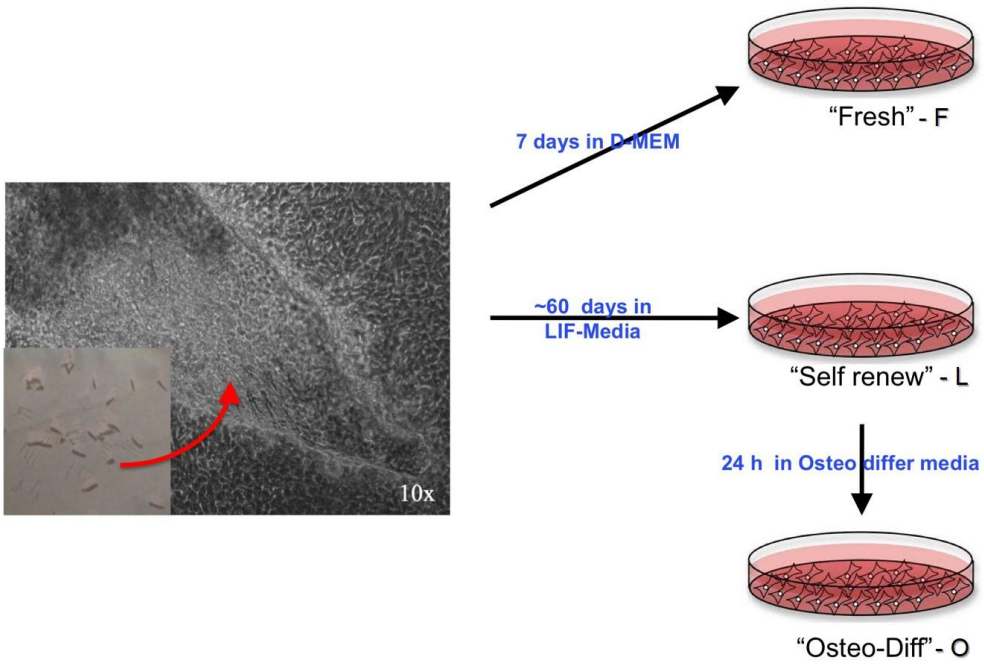

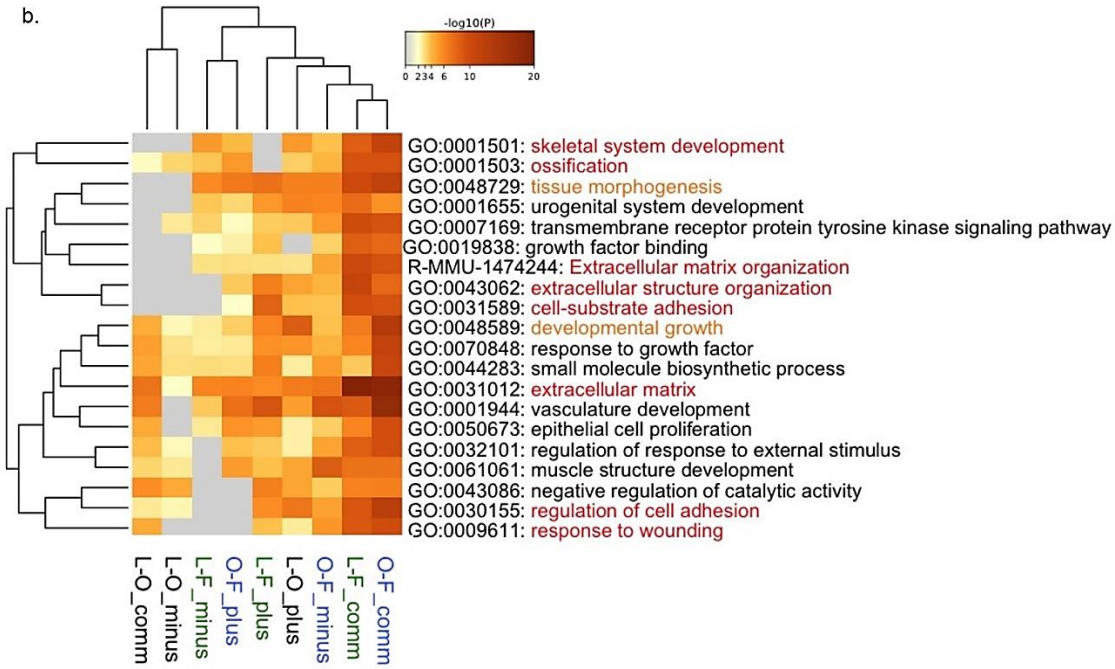

Figure 15: Transcriptome analysis indicates a deficit of extracellular matrix- and ossification-related genes in Erf-insufficient cells. a) Workflow for the collection of samples for RNA sequencing. RNA was collected from freshly derived suture cells cultured for 7 days in maintenance medium ("fresh [F]" - upper right), suture-derived mesenchymal stem cells (sdMSCs) cultured for 8 PDs in maintenance medium ("self-renew [L]" - middle right) and sdMSCs of 8 PDs induced with osteogenic differentiation medium for 24h ("osteo-diff [O]" - lower right). At least 3-4 mice were used per genotype for each of the above conditions tested per experiment and at least 4 independent experiments were conducted. b) Differentially expressed genes identified by transcriptome analysis of sdMSCs (L), sdMSCs growing in osteogenic differentiation media for 24 h (O) and freshly isolated suture cells (F), from Erf-competent (plus) and Erf-insufficient (minus) animals, were clustered based on their ontology with the Metascape program. L-O comm.: genes found differentially expressed during the 24h differentiation of sdMSCs of both Erf-competent and Erf-insufficient cells. L-O plus: genes found differentially expressed during the 24h differentiation only in the Erf-competent sdMSCs. L-O minus: genes found differentially expressed during the 24h differentiation only in the Erf- insufficient sdMSCs. Respectively "L-F" indicates genes found different between sdMSCs and freshly isolated cells and "O-F" between sdMSCs differentiating for 24h and freshly isolated cells. Red lettering indicates ossification-related ontologies and orange lettering indicates differentiation-related ontologies. Only the top 20 categories are shown.

sdMSC in Self renewal	sdMSC in Osteo differentiation	suture-derived cells in DMEM-FBS
Increased in P/+	Increased in P/+	Increased in P/+
Add3	Epb4.1l4a	Arf1
Amph	Btbd2	AW551984
Epb4,1l4a	Cd34	*Clec11a*
Erf	*Col14a1*	Dkk2
Nell1	*Cthrc1*	*Edil3*
Nts	Cygb	Erf
Ostn	Cyp2c29	*Gpc1*
Slitrk6	Cyp2c54	*Igfbp5*
Tmod2	Cyp2d26	*Lum*
Zfp729a	*Emilin2*	Lyz1
	Erf	Med12l
	Esm1	Myof
	F5	*Ptn*
	Gfra1	*Sema3a*
	Gpx3	*Sema3e*
	H2afv	*Serpinb1a*
	Lrg1	Slc1a7
	Mgst1	*Tgfbi*
	Nav1	Zcchc5
	Rnpepl1	
	Saa2	
	Slc25a47	
	Tmod2	
	Ttpa	
	Zfp738	

Increased in P/-	Increased in P/-	Increased in P/-
4930511M06Rik	Acta1	Ackr3
Fst	Actg2	Ccl2
Styk1	Asb2	Ccl7
	Atp2b4	Cyp26b1
	Cnn1	Dynap
	Cyp26b1	F3
	Dmpk	Fbxl19
	Eng	Gsto1
	F2r	Id4
	Fst	Irx1
	Ldb3	Lrrc32
	Lmod1	Lrrk2
	Lrrc58	Ltbp2
	Mbp	Lurap1l
	Myh11	Mfap5
	Pip4k2a	Ppap2b
	Plac8	Rgs16
	Pnck	Saal1
	Sh3bgr	Serpinb2
	Tagln	Sfrp1
	Tbx18	Siglecg
	Tnfaip2	Stc1
	Vwce	Tm4sf1
		Twist2

Table 1: Differentially expressed genes between $Erf^{LoxP/+}$ and $Erf^{LoxP/-}$ cells in each one of the indicated culture conditions. Genes different at least 1.5 fold with less than 0.05 FDR are shown. Those associated with Matrisome are displayed in italics.

3.7 Erf insufficiency is associated with altered cell proliferation rates in cranial sutures and in cultures undergoing osteogenic differentiation

In an effort to further explore the effect of Erf insufficiency on the intramembranous osteogenesis pathway and the cranial suture fate, we induced $Erf^{LoxP/+}$ and $Erf^{LoxP/-}$ mesenchymal stem/ progenitor cells and monitored the percentage of proliferating osteogenic cells for three weeks of differentiation. While on day 2 of differentiation $Erf^{LoxP/-}$ cells displayed significantly higher proportion of proliferating cells in comparison to control cells, consistent with their decreased capacity to exit self-renewal and commit, later on day 5 a reduced percentage of proliferating populations was observed in differentiating $Erf^{LoxP/-}$ cells in comparison to $Erf^{LoxP/+}$ cells (Fig. 16a). Given the variation of the primary cell culture the observed difference is 94% accurate instead of the generally accepted 95%, yet it may indicate that the intermediate progenitor cells may be exhausted faster in the presence of lower Erf levels. In agreement with this *in vitro* finding, reduced proportion of proliferating cells was detected in comparably open (Fig. 17a, b) coronal sutures of $Erf^{LoxP/-}$ mice on postnatal day 15 (P15) as shown by in vivo BrdU incorporation assay (Fig. 16b, c) albeit again with 93% certainty. This decreased coronal suture cell proliferation is a late onset event, as sutures from P5 mice exhibited no difference in the proliferation rate between the two genotypes (Fig. 18a, b). Collectively, these results indicate that Erf insufficiency apart from impairing efficient osteogenic commitment of mesenchymal stem/ progenitor cells, leads also to a reduction in the number of proliferating populations among suture cells later during differentiation. The limiting number of committed proliferating progenitor cells may drive the premature suture closure, depleting the suture from an expanding cell population.

a.

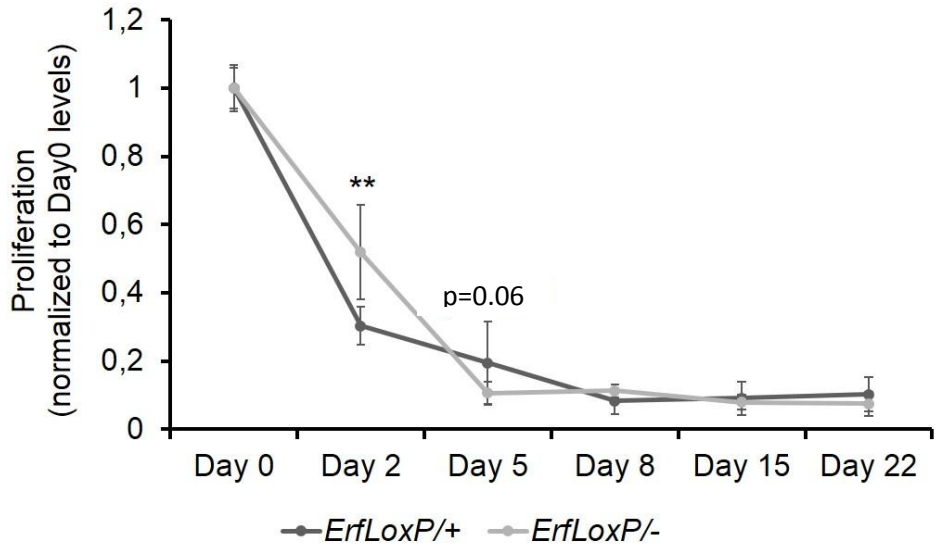

b.

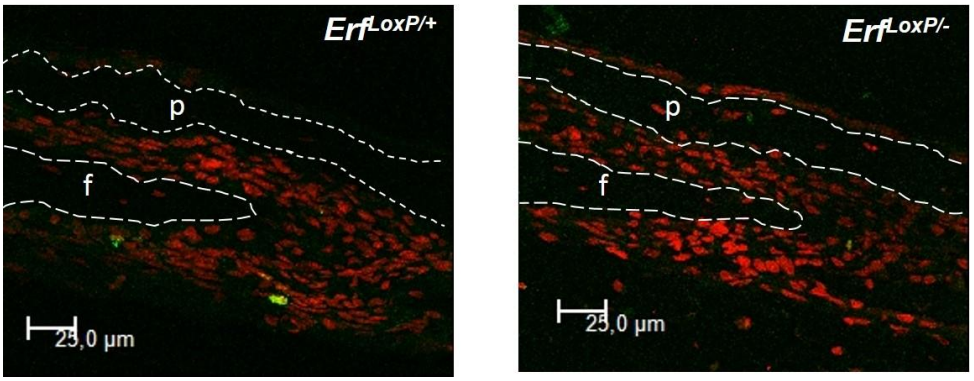

c.

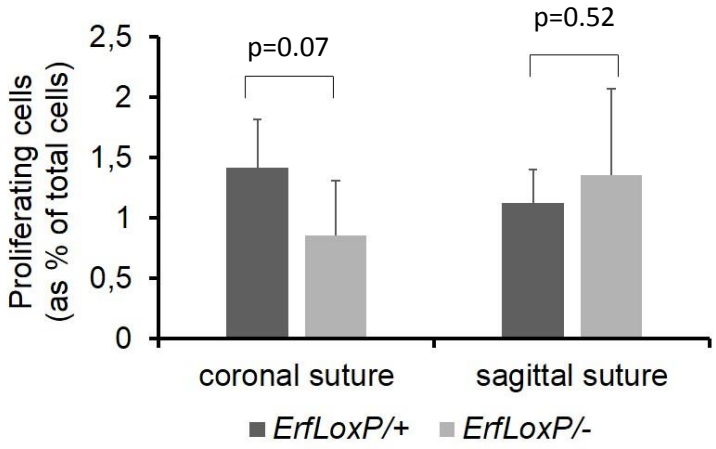

Figure 16: Erf insufficiency leads to altered proliferation rate of differentiating suture cells. a) Suture-derived mesenchymal stem cells (sdMSCs) were induced to differentiate along the osteogenic lineage and the percentage of proliferating BrdU+ cells normalized to day 0 levels is depicted in the graph for the indicated time-points of differentiation. Four independent biological experiments were conducted and each experiment included cells of at least three mice. b) Representative images of coronal suture sections of P15 mice. BrdU+ cells are identified by the green fluorescence of FITC-conjugated streptavidin. Dotted lines indicate the developing bones. p: parietal bone, f: frontal bone. c) Quantification of BrdU+ cells in $Erf^{LoxP/+}$ and $Erf^{LoxP/-}$ P15 suture sections following *in vivo* BrdU administration. At least five animals per genotype were included in the study. The statistical analysis was performed in all cases using an unpaired t-test with two-tailed distribution. * $p < 0.05$, ** $p < 0.01$, *** $p < 0.001$.

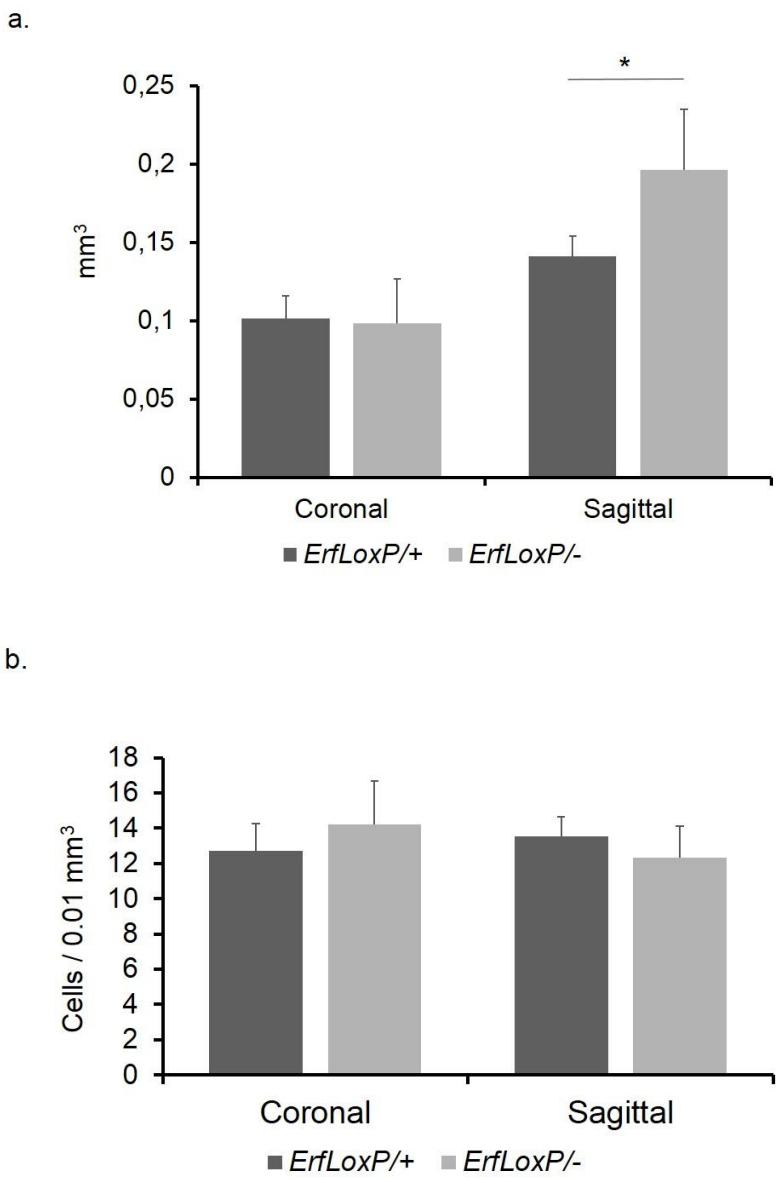

Figure 17: Suture size and number of cells are comparable between healthy and craniosynostosis P15 mice used for the assessment of *in vivo* proliferation. a) The overall volume and b) number of cells in cranial suture cryosections from Erf-competent ($Erf^{loxp/+}$) and Erf-insufficient ($Erf^{loxp/-}$) P15 mice that were used to evaluate suture proliferation rates in Figure 16.

a.

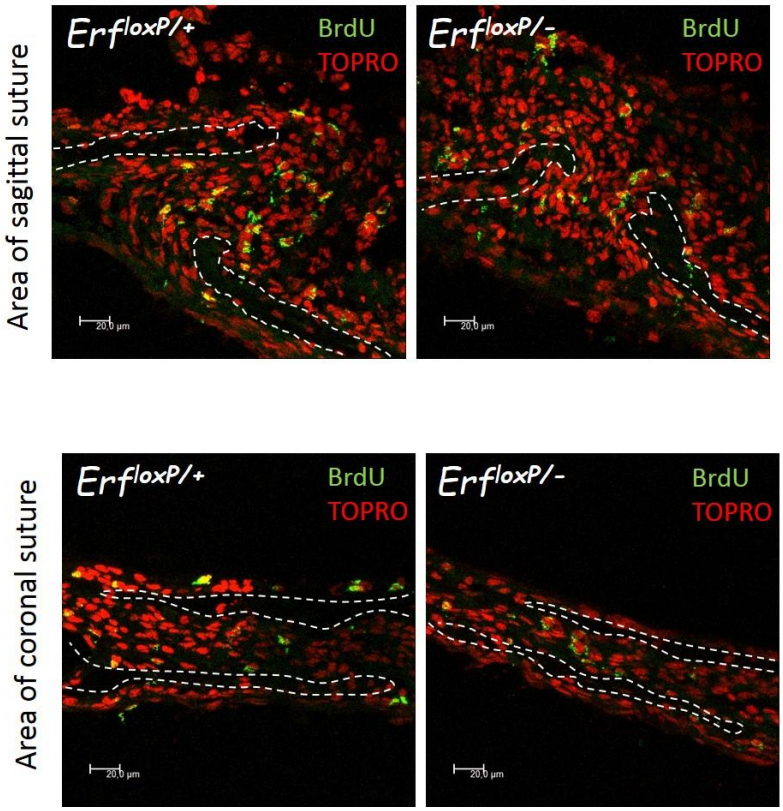

b.

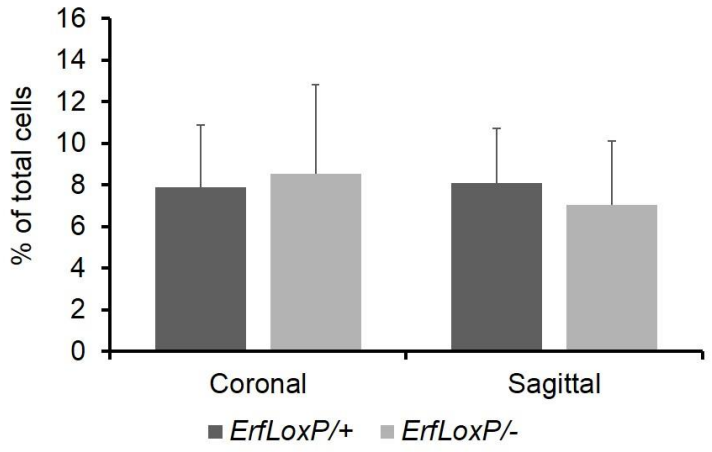

Figure 18: No difference in cellular proliferation at cranial sutures between healthy and craniosynostosis mice of postnatal day 5. a) Representative images of suture sections of P5 mice. BrdU+ cells are identified by the green fluorescence of FITC-conjugated streptavidin. Dotted lines indicate the developing bones. b) Quantification of BrdU+ cells in $Erf^{LoxP/+}$ and $Erf^{LoxP/-}$ P5 suture sections following *in vivo* BrdU administration. At least seven animals per genotype were included in the study.

Consequently, it appears that Erf may have a dual role in the differentiation of suture cells towards the osteogenic lineage promoting the commitment of sdMSCs and maintaining the numbers of differentiating cells that would keep the suture open. These presumably opposing roles would be consistent with the late onset craniosynostosis phenotype preceded by the mildly delayed ossification pattern in the skull at the early postnatal life.

3.8 Erf insufficiency is associated with retinoic acid (RA) signalling alterations and exogenous supplementation with retinoic acid seems to restore the differentiation defect of *Erf*$^{LoxP/-}$ cells *in vitro*

Focusing again on the sdMSC transcriptomic data, we observed that the cytochrome P450 superfamily member *Cyp26b1*, a gene encoding a retinoic acid catabolizing enzyme, was elevated upon Erf insufficiency in both differentiating sdMSC cells and in the initial freshly isolated heterogeneous suture cell population (Table 1 and Fig. 19a). Retinoic acid (RA) signalling is known to affect craniofacial development and interestingly, null mutations in *CYP26B1* have been shown to lead to cranial bone hypoplasia and craniosynostosis in humans. In *Erf*$^{LoxP/-}$ cells, increased levels of *Cyp26b1* indicate possibly decreased retinoic acid levels and a downregulation in RA pathway that could affect cranial bone and suture development.

We hypothesized that supplementation of osteogenic medium with retinoic acid could potentially rescue the differentiation defect of *Erf*$^{LoxP/-}$ cells. First we tested the effect of different RA concentrations on sdMSC survival and verified that exogenous addition of RA at concentrations below 1 μM did not affect cell growth and viability (Fig. 19b). Then we induced *Erf*$^{LoxP/+}$ and *Erf*$^{LoxP/-}$ cells to differentiate along the osteogenic lineage for 30 days in presence of 0.5 μM RA. Retinoic acid although not affecting Erf-sufficient cells, reduced the elevated cell numbers of *Erf*$^{LoxP/-}$ cells and rescued their mineralization defect (Fig. 19c, d).

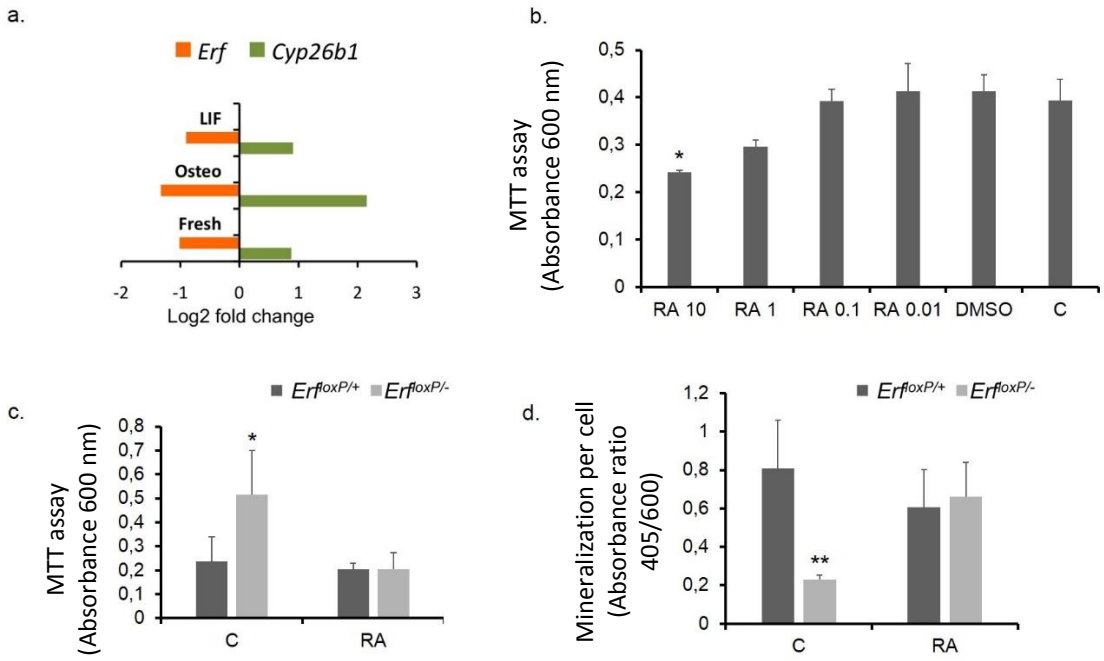

Figure 19: Retinoic acid reverts the osteogenic deficiency of *Erf*$^{LoxP/-}$ cells. a) Fold change in the expression level of *Erf* and *Cyp26b1* between Erf-competent (*Erf*$^{LoxP/+}$) and Erf-deficient (*Erf*$^{LoxP/-}$) cells in self-renewing sdMSCs (LIF), differentiating sdMSCs (Osteo) and freshly derived suture cells (Fresh). Values are derived from RNA sequencing dataset. b) Formazan absorbance after MTT assay indicative of cell numbers of sdMSCs after 4 days in self-renewal LIF-containing medium in the presence of the indicated µM concentration of all-*trans* retinoic acid (RA) or 0.1% DMSO. Statistically significant difference compared to the untreated cells (C) is indicated. c) Cell numbers, as evaluated by formazan absorbance after 30 days in osteogenic differentiation medium in the presence or absence (C) of 0.5 µM all-*trans* retinoic acid (RA). d) Calcification potential per cell as evaluated by the alizarin red s to formazan absorbance after 30 days of osteogenic differentiation in the presence or absence (C) of 0.5 µM all-*trans* retinoic acid (RA). Data are derived from four experiments and the statistical analysis was performed using an unpaired t-test with two-tailed distribution. * $p < 0.05$, ** $p < 0.01$, *** $p < 0.001$.

These data suggest that Erf insufficiency is associated with an increase in retinoic acid catabolism through Cyp26b1 leading to increased cell proliferation and decreased osteogenic differentiation of suture-derived cells. Thus Erf may affect cranial bone and suture development through retinoic acid gradient regulation.

4. Discussion

4. Discussion

Haploinsufficiency of the ETS2 repressor factor (ERF) causes craniosynostosis (CRS-4) in humans and mice, preceded by a mild reduction in the ossification of calvarial bones in the early postnatal life [55]. A potential link between ERF and osteogenesis or calvarium morphogenesis had never been explored before. The aim of the current study was to provide an understanding of the mechanisms underlying the emergence of ERF-associated craniosynostosis phenotype, often characterised as insidious due to its complexity [56]. By establishing a method for the in vitro expansion of a suture-derived mesenchymal stem/ progenitor cell population, we provide evidence that Erf is required for the initial commitment of suture MSCs towards the osteogenic lineage, while at a later stage seems to be also essential for the maintenance of committed proliferating progenitor cells undergoing differentiation. Transcriptome analysis indicates that reduced retinoic acid (RA) signalling due to elevated expression of the RA-catabolizing enzyme *Cyp26b1* may underlie the phenotype of Erf-insufficient ($Erf^{LoxP/-}$) cells. Exogenous addition of retinoic acid rescued the osteogenic differentiation defect in $Erf^{LoxP/-}$ cells, suggesting that Erf may affect intramembranous skull ossification through retinoic acid gradient regulation.

4.1 LIF-selected long-term expanded cranial suture cells possess *in vitro* characteristics of mesenchymal stem/ progenitor cells

The isolation and identification of mesenchymal stem cells from cranial sutures has long been in the centre of research interest associated with craniofacial development and malformations. In this study we developed a method for the *in vitro* expansion of a suture-derived population displaying characteristics of mesenchymal stem/ progenitor cells. Independent studies have indicated *in vivo* the presence of postnatal suture populations with stem-cell properties designated by the expression of specific markers, such as the Gli1-expressing cells [53], the Axin2-positive cells [95], and the Prx1-positive ones [96]. The population of *in vitro* long-term self-renewing cells that we have obtained based on LIF selection, although not characterized *in vivo*, displays expression of the Gli1, Axin2 and Prx1 genes as shown by our transcriptomic and qPCR data (Fig. 5b), indicating that we cannot exclude the possibility of an overlap between these cells and the ones already described *in vivo* according to the literature. Further characterization of the LIF-selected long-term expanded suture mesenchymal cells showed that they express a set of surface antigens reported as MSC markers [92, 93] such as CD44, CD90, Sca1 and CD29, while they are negative for established endothelial and hematopoietic markers (Fig. 5a). Interestingly, although usually included among the MSC markers, CD105 is not significantly expressed in our cells as shown by the flow-cytometric data. However, populations of CD105-negative MSCs

have already been identified among murine adipose tissue mesenchymal cells [97]. In general, the combination of expressed antigens is reported to be highly heterogeneous and often connected with the MSC source [98, 99]. The ability of MSCs to differentiate towards various lineages is also associated with their source. The suture-derived mesenchymal stem/ progenitor cells we obtained upon LIF culture conditions, show comparable efficiency in osteogenic and chondrogenic differentiation with human bone marrow derived MSCs (Fig. 6) when tested *in vitro*. However, the adipogenic differentiation seems to be less efficient for suture-derived MSCs, since only immature adipocytes with small lipid droplets are observed to form. A similar result was obtained also for the $Gli1^{+}$ MSC population of sutures when compared with mouse bone marrow MSCs in an independent study [53], indicating possibly that suture MSCs have a natural tendency to commit more easily towards the osteochondrogenic lineages.

4.2 Erf, a downstream target of Erks, affects the commitment and maintenance of osteoprogenitor cells in cranial sutures

Stem cell depletion [53] and osteogenic differentiation-proliferation imbalance [33, 100, 101] have been previously proposed as potential mechanisms able to lead to premature suture fusion. In this study, the insufficiency of Erf does not seem to affect the maintenance of suture mesenchymal stem cells as evidenced from the cell cycle phase and *in vitro* doubling time experiments in $Erf^{LoxP/-}$ cells (Fig. 12). Given that the transcriptional function of ERF is inhibited by activated ERKs, this result is consistent with a previously reported role of Erk1/2 signalling in sustaining the undifferentiated self-renewing state of bone marrow derived mesenchymal stem cells [102]. The decreased levels of Erf, however, seem to compromise the commitment of suture mesenchymal stem/ progenitor cells towards the osteogenic lineage (Fig. 13). $Erf^{LoxP/-}$ cells upon osteogenic induction fail to significantly increase the expression of genes associated with ossification as shown by the transcriptomic analysis (Fig. 15), display sustained *in vitro* proliferation and produce decreased amounts of mineralized extracellular matrix in comparison to $Erf^{LoxP/+}$ cells as assessed by Alizarin Red S staining of cultures (Fig. 13, 16). All these observations are consistent with the delayed ossification pattern displayed by $Erf^{LoxP/-}$ mice in the early postnatal life [55]. Later, however, during *in vitro* osteogenic differentiation reduced proportion of proliferating cells is evident in $Erf^{LoxP/-}$ cells while *in vivo*, decreased proliferation is also observed in coronal sutures of $Erf^{LoxP/-}$ mice that have not developed synostosis yet (Fig. 16). These data indicate that beyond the apparent initial delay in the ossification of calvarial bones, the insufficiency of Erf causes a disruption in the maintenance of proliferating cells undergoing differentiation later in development accounting possibly for the synostosis phenotype. This fact suggests that Erf may have an additional role either in reinforcing the proliferation of committed osteogenic cells or in impeding their subsequent differentiation towards mature osteoblasts.

Erk1/2 signalling has been reported to have stage-specific effects on the osteogenic differentiation process, and a lot of controversy existing in the literature about the final outcome of its action could be attributed to such a multistep role. In a study on human bone marrow mesenchymal stem cells, once activated by FGFs, ERK1/2 signalling was shown to suppress the commitment of cells towards the osteogenic lineage and entrap them in a pre-committed state [103]. Although Erks have a plethora of downstream targets beyond Erf, that could possibly mediate such events, this effect is consistent with the decreased osteogenic commitment of suture mesenchymal stem/ progenitor cells observed upon Erf insufficiency. Furthermore, a series of different studies have revealed the positive contribution of ERK pathway in later stages of osteogenesis such as the transition of immature pre-osteoblastic cells towards mature osteoblasts [104] and the differentiation to osteocytes [105]. In an independent study on human adipose-derived stem cell populations, the levels of the active, phosphorylated ERK1/2 were shown to correlate with mineralizing populations and increase at the later stages of osteogenic induction [106]. In our study Erf is shown to be required for the maintenance of the population of committed proliferating immature cells at later stages *in vivo* and *in vitro*. Consistent with the above-mentioned positive contribution of Erk pathway at these stages of osteogenesis, Erf could potentially act by inhibiting the differentiation of proliferating committed cells towards a more mature phenotype. Given the established role of Runx2 in the osteogenic differentiation and the cooperative regulation of transcription by the two genes [55], it is likely that decreased amounts of Erf could accelerate the differentiation of committed precursor cells leading to their depletion and synostosis (Figure 20).

4.3 Erf regulates the osteogenic commitment of cranial suture mesenchymal stem/ progenitor cells via the retinoic acid (RA) pathway

ERF belongs to the family of ETS transcription factors that regulate a variety of different target genes. One of its targets, *Ets2*, once overexpressed in mice, was shown to lead to skeletal defects and craniofacial abnormalities [107]. *Fgf2*, previously also shown to be transcriptionally regulated by Erf, is reported to participate in cranial suture fate regulation [108-110]. Based on the transcriptomic analysis we performed, limited genes were found to significantly differ between Erf-competent and Erf-insufficient cells, which may be partially due to the presence of high MAPK activity in the cultured cells and the fact that the 50% reduction in *Erf* may not be sufficient to induce extensive quantitative changes that would evade the detection cutoff limits. Another reason for the absence of striking molecular changes could also be that Erf acts in synergy or in competition with other factors to affect cellular homeostasis. Genes affected during MSC differentiation for example, have ChIP-seq-identified Erf binding sites almost exclusively in putative regulatory regions and away from the transcription start site. Interestingly, *Cyp26b1* gene, coding for a member of the cytochrome P450 family that is involved in the degradation of retinoic acid (RA), was

elevated in all biological samples upon Erf insufficiency suggesting a decrease in RA response for $Erf^{LoxP/-}$ cells. Hypomorphic and null mutations in *Cyp26b1* have been reported to lead to cranial bone hypoplasia and craniosynostosis in humans [111], while its loss has been associated with craniofacial abnormalities in both zebrafish and mice [111, 112]. In our study, exogenous addition of retinoic acid (RA) during differentiation of sdMSCs fully alleviated the osteogenesis defect in $Erf^{LoxP/-}$ cells, with no apparent effect to Erf competent cells (Fig. 19), suggesting that *Erf* through *Cyp26b1* regulation affects retinoic acid levels thus controlling the differentiation outcome (Figure 20). This role for Erf is consistent with the one of Fgf as activator of Cyp26b1 [113, 114]. However, whether Erf regulates *Cyp26b1* directly or indirectly, remains to be further explored.

Retinoic acid (RA) acting as a morphogen regulates developmental processes through concentration gradients in multiple systems. Calvarial bone formation seems to be sensitive to retinoic acid concentration and action. Excessive amounts of RA have been shown to have teratogenic effects during pregnancy causing multiple craniofacial abnormalities to embryos [115-117]. In zebrafish, *cyp26b1* is shown to be expressed at the osteogenic fronts after suture formation and its partial loss results in craniosynostosis [111]. Interestingly, *Cyp26b1(-/-)* mice display multiple abnormalities in facial structures along with reduced ossification of the calvarial bones at E18.5 but not craniosynostosis [112]. The diversity of the RA-associated phenotypes indicate that the precise retinoic acid spatiotemporal regulation is crucial for normal cranial bone and suture formation. Interestingly comparable concentrations of retinoic acid have opposite effects on the mineralization of mesenchymal stem cells and more differentiated osteogenic populations such as MC3T3 preosteoblasts, with the former being induced and the latter being suppressed by RA [118-121]. Therefore, it is plausible that Erf, either through retinoic acid signalling or independently, could also affect the osteogenic pathway at various stages. Upon Erf deficiency the initial decreased MSC differentiation and osteoprogenitor expansion could lead to decreased ossification, while an accelerated differentiation of progenitors when they comprise the predominant suture cell population, could lead to depletion and premature ossification of the suture. Further studies would be necessary to explore the spatiotemporal function of Erf and its effect on RA concentration gradients in cranial bone and suture development. The absence of markers characterizing committed progenitor cells at various stages of osteogenic differentiation and the difficulties in isolation of particular populations for subsequent transcriptomic analysis, were some of the limiting factors to explore this question in our study.

Collectively, it appears that in the initial stages of the osteogenic pathway Erf downregulates *Cyp26b1*, thus increasing RA signalling and drives the subsequent commitment and differentiation of cranial suture mesenchymal stem/progenitor cells. Whether Erf has an inhibitory role at later stages of the osteogenic pathway either through retinoic acid or independently remains to be further studied (Figure 20).

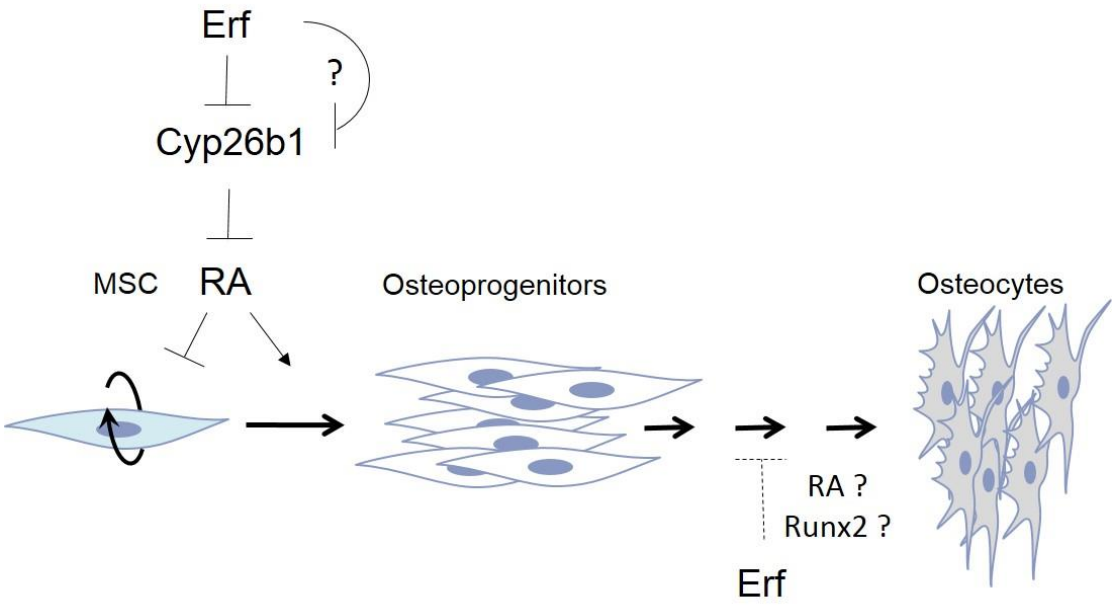

Figure 20: Mechanism of Erf effect in the osteogenic differentiation of cranial suture mesenchymal stem/progenitor cells. Erf promotes the differentiation of calvarial MSCs towards the osteogenic lineage through retinoic acid (RA) pathway regulation. Erf affects the level of retinoic acid possibly through the RA catabolizing enzyme Cyp26b1. Decreased levels of Erf leads to increased levels of Cyp26b1 which in turn decreases retinoic acid levels leading to reduced osteogenic differentiation and/or increased mesenchymal progenitor proliferation. Decreased levels of Erf earlier in development result in insufficient differentiation and bone formation. At a later stage when stem cells are diminishing, the insufficiency of osteoprogenitor cells (either due to decreased MSC commitment and/or due to accelerated differentiation of committed osteogenic precursors) leads to the premature closure of the cranial sutures. Dashed lines and question-marks indicate that further studies are needed in order to fully uncover the role of Erf and the other factors in the intramembranous ossification pathway.

4.4 Therapeutic outlook for Erf-associated craniosynostosis

Surgery is the only treatment currently available for craniosynostosis. Whether it involves an open cranial vault reconstruction procedure or a minimally invasive technique such as endoscopic craniectomy or distraction osteogenesis [24, 25], surgical intervention can be accompanied by complications like increased intraoperative blood loss, wound infection and fever [23]. Reoperation is also required in some cases. The usage of pharmacological compounds following surgery could potentially prevent recrudescence and ensure a better postoperative outcome.

ERF subcellular localization is dependent on its phosphorylation status that is in turn relied on Erk kinase activity [61, 66, 67]. Upon Erk1/2 activation, ERF is phosphorylated and exported from the nucleus via XPO1/CRM1 exportin. In this study, we utilized U0126, the inhibitor of MEK-ERK signaling, and the KPT330-

compound, the selective inhibitor of XPO1/CRM1, and studied their effects on the osteogenic differentiation of freshly isolated cranial suture cells. We observed that both molecules, when added at suboptimal concentrations that allow cell cycling, were able to increase the mineralization in differentiating $Erf^{LoxP/+}$ cells (Fig. 3). No effect was detected however in $Erf^{LoxP/-}$ cells, indicating possibly that sufficient Erf levels are necessary to elicit a response *in vitro*. Interestingly, additional studies performed in our laboratory showed that *in vivo* administration of the two inhibitors either locally through skull subcutaneous injections or systemically via intraperitoneal injections resulted in improvement of the craniofacial phenotype in Erf-craniosynostosis mice, thus opening the way for a pharmacological approach for the craniosynostosis treatment beyond the surgical intervention. Furthermore, since all-*trans* retinoic acid (RA) fully reversed the osteogenesis defect in Erf-insufficient cells (Fig. 19), exploring the potential therapeutic efficacy of RA administration in $Erf^{LoxP/-}$ mice would be an interesting next approach. However, since molecular signaling pathways such as the RAS-ERK1/2 and the retinoic acid (RA) pathway display often a time-, space- and dosage- dependent effect on craniofacial development, serious attention should be paid on the timing of any treatment involving pathway interference, the exact location and the drug quantities to obtain and secure a satisfactory result.

4.5 Conclusion & Future directions

In this work we provide evidence that Erf is required for the initial commitment of cranial suture MSCs towards the osteogenic lineage via retinoic acid (RA) pathway regulation, while at a later stage seems to be essential for the maintenance of committed proliferating progenitor cells undergoing differentiation. Upon Erf depletion, insufficient differentiation and a delayed ossification pattern is observed in $Erf^{LoxP/-}$ mice earlier in development, while at a later stage the limiting number of committed proliferating cells may finally drive the premature suture closure and the late-onset synostosis phenotype. Further studies are needed in order to define as far as possible the function of Erf in each particular differentiation step, from osteoprogenitors and pre-osteoblasts to osteoblasts and osteocytes, and to uncover the set of potential downstream targets, either within the RA pathway or independently, that may be involved in the regulation of these steps during intramembranous skull ossification. Space- and time- inducible Cre mouse lines would be a valuable tool in this effort [122-124]. Furthermore, since the mineralization of the extracellular matrix (ECM) is achieved to some extent through vesicles produced by osteoblasts [20], an additional study could include the potential effect of Erf on the formation and secretion of such matrix vesicles during bone formation. Another ERF-associated disorder, the Chitayat syndrome, includes also facial deformities along with bronchomalacia [59], indicating possibly that ERF, beyond its role in calvarial bones, could be involved in cartilage differentiation and chondrocyte ECM secretion in the bronchi, too.

Collectively, our data suggest that Erf regulates osteogenic lineage commitment via retinoic acid pathway modulation and shed light on the potential mechanisms through which the complicated phenotype of ERF-craniosynostosis (CRS-4) emerges. ERF, being a downstream effector of the RAS-ERK pathway and displaying a defined pattern of subcellular localization modulation, can act as point for intervention. Although a variety of different genes are implicated and there is still a long way to go for the full understanding of the disease pathogenesis, the results of our work hold promise for the future of CRS-4 and also perhaps of other craniosynostosis cases in which aberrant ERK1/2 signalling exists.

5. References

5. References

1. Morriss-Kay, G.M., and Wilkie, A.O. (2005). Growth of the normal skull vault and its alteration in craniosynostosis: insights from human genetics and experimental studies. J Anat *207*, 637-653.
2. Kaufman, M.H., and Bard, J.B.L. (1999). The anatomical basis of mouse development, (San Diego: Academic Press).
3. Lana-Elola, E., Rice, R., Grigoriadis, A.E., and Rice, D.P. (2007). Cell fate specification during calvarial bone and suture development. Dev Biol *311*, 335-346.
4. Opperman, L.A. (2000). Cranial sutures as intramembranous bone growth sites. Dev Dyn *219*, 472-485.
5. Sahar, D.E., Longaker, M.T., and Quarto, N. (2005). Sox9 neural crest determinant gene controls patterning and closure of the posterior frontal cranial suture. Dev Biol *280*, 344-361.
6. James, A.W., Xu, Y., Lee, J.K., Wang, R., and Longaker, M.T. (2009). Differential effects of TGF-beta1 and TGF-beta3 on chondrogenesis in posterofrontal cranial suture-derived mesenchymal cells in vitro. Plast Reconstr Surg *123*, 31-43.
7. Richtsmeier, J.T., and Flaherty, K. (2013). Hand in glove: brain and skull in development and dysmorphogenesis. Acta Neuropathol *125*, 469-489.
8. Jiang, X., Iseki, S., Maxson, R.E., Sucov, H.M., and Morriss-Kay, G.M. (2002). Tissue origins and interactions in the mammalian skull vault. Dev Biol *241*, 106-116.
9. Wilkie, A.O., and Morriss-Kay, G.M. (2001). Genetics of craniofacial development and malformation. Nat Rev Genet *2*, 458-468.
10. Yoshida, T., Vivatbutsiri, P., Morriss-Kay, G., Saga, Y., and Iseki, S. (2008). Cell lineage in mammalian craniofacial mesenchyme. Mech Dev *125*, 797-808.
11. Deckelbaum, R.A., Holmes, G., Zhao, Z., Tong, C., Basilico, C., and Loomis, C.A. (2012). Regulation of cranial morphogenesis and cell fate at the neural crest-mesoderm boundary by engrailed 1. Development *139*, 1346-1358.
12. Twigg, S.R., and Wilkie, A.O. (2015). A Genetic-Pathophysiological Framework for Craniosynostosis. Am J Hum Genet *97*, 359-377.
13. Vogiatzi, A., and Mavrothalassitis, G. (2019). Craniofacial, orofacial and dental disorders: the role of the RAS/ERK pathway. Expert Rev Mol Med *21*, e2.
14. Hermann, C.D., Richards, M.A., Chang, R., Olivares-Navarrete, R., Williams, J.K., Guldberg, R.E., Vidakovic, B., Schwartz, Z., and Boyan, B.D. (2013). Biphasic fusion of the murine posterior frontal suture. Plast Reconstr Surg *131*, 727-740.
15. Grova, M., Lo, D.D., Montoro, D., Hyun, J.S., Chung, M.T., Wan, D.C., and Longaker, M.T. (2012). Models of cranial suture biology. J Craniofac Surg *23*, 1954-1958.
16. Jin, S.W., Sim, K.B., and Kim, S.D. (2016). Development and Growth of the Normal Cranial Vault : An Embryologic Review. J Korean Neurosurg Soc *59*, 192-196.
17. Dixon, A.D., Hoyte, D.A.N., and Rönning, O. (1997). Fundamentals of craniofacial growth, (Boca Raton: CRC Press).

18. Tubbs, R.S., Bosmia, A.N., and Cohen-Gadol, A.A. (2012). The human calvaria: a review of embryology, anatomy, pathology, and molecular development. Childs Nerv Syst *28*, 23-31.
19. Mechiche Alami, S., Gangloff, S.C., Laurent-Maquin, D., Wang, Y., and Kerdjoudj, H. (2016). Concise Review: In Vitro Formation of Bone-Like Nodules Sheds Light on the Application of Stem Cells for Bone Regeneration. Stem Cells Transl Med *5*, 1587-1593.
20. Hasegawa, T. (2018). Ultrastructure and biological function of matrix vesicles in bone mineralization. Histochem Cell Biol *149*, 289-304.
21. Bottini, M., Mebarek, S., Anderson, K.L., Strzelecka-Kiliszek, A., Bozycki, L., Simao, A.M.S., Bolean, M., Ciancaglini, P., Pikula, J.B., Pikula, S., et al. (2018). Matrix vesicles from chondrocytes and osteoblasts: Their biogenesis, properties, functions and biomimetic models. Biochim Biophys Acta Gen Subj *1862*, 532-546.
22. Flaherty, K., Singh, N., and Richtsmeier, J.T. (2016). Understanding craniosynostosis as a growth disorder. Wiley Interdiscip Rev Dev Biol *5*, 429-459.
23. Kajdic, N., Spazzapan, P., and Velnar, T. (2018). Craniosynostosis - Recognition, clinical characteristics, and treatment. Bosn J Basic Med Sci *18*, 110-116.
24. Morris, L. (2016). Management of Craniosynostosis. Facial Plast Surg *32*, 123-132.
25. Mundinger, G.S., Rehim, S.A., Johnson, O., 3rd, Zhou, J., Tong, A., Wallner, C., and Dorafshar, A.H. (2016). Distraction Osteogenesis for Surgical Treatment of Craniosynostosis: A Systematic Review. Plast Reconstr Surg *138*, 657-669.
26. Mehta, V.A., Bettegowda, C., Jallo, G.I., and Ahn, E.S. (2010). The evolution of surgical management for craniosynostosis. Neurosurg Focus *29*, E5.
27. Czerwinski, M., Hopper, R.A., Gruss, J., and Fearon, J.A. (2010). Major morbidity and mortality rates in craniofacial surgery: an analysis of 8101 major procedures. Plast Reconstr Surg *126*, 181-186.
28. Wilkie, A.O., Slaney, S.F., Oldridge, M., Poole, M.D., Ashworth, G.J., Hockley, A.D., Hayward, R.D., David, D.J., Pulleyn, L.J., Rutland, P., et al. (1995). Apert syndrome results from localized mutations of FGFR2 and is allelic with Crouzon syndrome. Nat Genet *9*, 165-172.
29. Park, J., Park, O.J., Yoon, W.J., Kim, H.J., Choi, K.Y., Cho, T.J., and Ryoo, H.M. (2012). Functional characterization of a novel FGFR2 mutation, E731K, in craniosynostosis. J Cell Biochem *113*, 457-464.
30. Chen, L., Li, D., Li, C., Engel, A., and Deng, C.X. (2003). A Ser252Trp [corrected] substitution in mouse fibroblast growth factor receptor 2 (Fgfr2) results in craniosynostosis. Bone *33*, 169-178.
31. Chen, P., Zhang, L., Weng, T., Zhang, S., Sun, S., Chang, M., Li, Y., Zhang, B., and Zhang, L. (2014). A Ser252Trp mutation in fibroblast growth factor receptor 2 (FGFR2) mimicking human Apert syndrome reveals an essential role for FGF signaling in the regulation of endochondral bone formation. PLoS One *9*, e87311.
32. Shukla, V., Coumoul, X., Wang, R.H., Kim, H.S., and Deng, C.X. (2007). RNA interference and inhibition of MEK-ERK signaling prevent abnormal skeletal phenotypes in a mouse model of craniosynostosis. Nat Genet *39*, 1145-1150.
33. Lomri, A., Lemonnier, J., Hott, M., de Parseval, N., Lajeunie, E., Munnich, A., Renier, D., and Marie, P.J. (1998). Increased calvaria cell differentiation and

bone matrix formation induced by fibroblast growth factor receptor 2 mutations in Apert syndrome. J Clin Invest *101*, 1310-1317.

34. Lemonnier, J., Hay, E., Delannoy, P., Fromigue, O., Lomri, A., Modrowski, D., and Marie, P.J. (2001). Increased osteoblast apoptosis in apert craniosynostosis: role of protein kinase C and interleukin-1. Am J Pathol *158*, 1833-1842.
35. Yin, L., Du, X., Li, C., Xu, X., Chen, Z., Su, N., Zhao, L., Qi, H., Li, F., Xue, J., et al. (2008). A Pro253Arg mutation in fibroblast growth factor receptor 2 (Fgfr2) causes skeleton malformation mimicking human Apert syndrome by affecting both chondrogenesis and osteogenesis. Bone *42*, 631-643.
36. Wang, Y., Sun, M., Uhlhorn, V.L., Zhou, X., Peter, I., Martinez-Abadias, N., Hill, C.A., Percival, C.J., Richtsmeier, J.T., Huso, D.L., et al. (2010). Activation of p38 MAPK pathway in the skull abnormalities of Apert syndrome Fgfr2(+P253R) mice. BMC Dev Biol *10*, 22.
37. Muenke, M., Schell, U., Hehr, A., Robin, N.H., Losken, H.W., Schinzel, A., Pulleyn, L.J., Rutland, P., Reardon, W., Malcolm, S., et al. (1994). A common mutation in the fibroblast growth factor receptor 1 gene in Pfeiffer syndrome. Nat Genet *8*, 269-274.
38. Schell, U., Hehr, A., Feldman, G.J., Robin, N.H., Zackai, E.H., de Die-Smulders, C., Viskochil, D.H., Stewart, J.M., Wolff, G., Ohashi, H., et al. (1995). Mutations in FGFR1 and FGFR2 cause familial and sporadic Pfeiffer syndrome. Hum Mol Genet *4*, 323-328.
39. Cohen, M.M., Jr. (2009). Perspectives on craniosynostosis: sutural biology, some well-known syndromes, and some unusual syndromes. J Craniofac Surg *20 Suppl 1*, 646-651.
40. Moosa, S., and Wollnik, B. (2016). Altered FGF signalling in congenital craniofacial and skeletal disorders. Semin Cell Dev Biol *53*, 115-125.
41. Zhou, Y.X., Xu, X., Chen, L., Li, C., Brodie, S.G., and Deng, C.X. (2000). A Pro250Arg substitution in mouse Fgfr1 causes increased expression of Cbfa1 and premature fusion of calvarial sutures. Hum Mol Genet *9*, 2001-2008.
42. Purushothaman, R., Cox, T.C., Maga, A.M., and Cunningham, M.L. (2011). Facial suture synostosis of newborn Fgfr1(P250R/+) and Fgfr2(S252W/+) mouse models of Pfeiffer and Apert syndromes. Birth Defects Res A Clin Mol Teratol *91*, 603-609.
43. Rutland, P., Pulleyn, L.J., Reardon, W., Baraitser, M., Hayward, R., Jones, B., Malcolm, S., Winter, R.M., Oldridge, M., Slaney, S.F., et al. (1995). Identical mutations in the FGFR2 gene cause both Pfeiffer and Crouzon syndrome phenotypes. Nat Genet *9*, 173-176.
44. Reardon, W., Winter, R.M., Rutland, P., Pulleyn, L.J., Jones, B.M., and Malcolm, S. (1994). Mutations in the fibroblast growth factor receptor 2 gene cause Crouzon syndrome. Nat Genet *8*, 98-103.
45. Pfaff, M.J., Xue, K., Li, L., Horowitz, M.C., Steinbacher, D.M., and Eswarakumar, J.V.P. (2016). FGFR2c-mediated ERK-MAPK activity regulates coronal suture development. Dev Biol *415*, 242-250.
46. Liu, J., Kwon, T.G., Nam, H.K., and Hatch, N.E. (2013). Craniosynostosis-associated Fgfr2(C342Y) mutant bone marrow stromal cells exhibit cell autonomous abnormalities in osteoblast differentiation and bone formation. Biomed Res Int *2013*, 292506.
47. Mansukhani, A., Bellosta, P., Sahni, M., and Basilico, C. (2000). Signaling by fibroblast growth factors (FGF) and fibroblast growth factor receptor 2 (FGFR2)-activating mutations blocks mineralization and induces apoptosis in osteoblasts. J Cell Biol *149*, 1297-1308.

48. el Ghouzzi, V., Le Merrer, M., Perrin-Schmitt, F., Lajeunie, E., Benit, P., Renier, D., Bourgeois, P., Bolcato-Bellemin, A.L., Munnich, A., and Bonaventure, J. (1997). Mutations of the TWIST gene in the Saethre-Chotzen syndrome. Nat Genet *15*, 42-46.
49. Howard, T.D., Paznekas, W.A., Green, E.D., Chiang, L.C., Ma, N., Ortiz de Luna, R.I., Garcia Delgado, C., Gonzalez-Ramos, M., Kline, A.D., and Jabs, E.W. (1997). Mutations in TWIST, a basic helix-loop-helix transcription factor, in Saethre-Chotzen syndrome. Nat Genet *15*, 36-41.
50. Lonsdale, S., Yong, R., Khominsky, A., Mihailidis, S., Townsend, G., Ranjitkar, S., and Anderson, P.J. (2019). Craniofacial abnormalities in a murine model of Saethre-Chotzen Syndrome. Ann Anat *225*, 33-41.
51. Parsons, T.E., Weinberg, S.M., Khaksarfard, K., Howie, R.N., Elsalanty, M., Yu, J.C., and Cray, J.J., Jr. (2014). Craniofacial shape variation in Twist1+/- mutant mice. Anat Rec (Hoboken) *297*, 826-833.
52. Quarto, N., Senarath-Yapa, K., Renda, A., and Longaker, M.T. (2015). TWIST1 silencing enhances in vitro and in vivo osteogenic differentiation of human adipose-derived stem cells by triggering activation of BMP-ERK/FGF signaling and TAZ upregulation. Stem Cells *33*, 833-847.
53. Zhao, H., Feng, J., Ho, T.V., Grimes, W., Urata, M., and Chai, Y. (2015). The suture provides a niche for mesenchymal stem cells of craniofacial bones. Nat Cell Biol *17*, 386-396.
54. Behr, B., Longaker, M.T., and Quarto, N. (2011). Craniosynostosis of coronal suture in twist1 mice occurs through endochondral ossification recapitulating the physiological closure of posterior frontal suture. Front Physiol *2*, 37.
55. Twigg, S.R., Vorgia, E., McGowan, S.J., Peraki, I., Fenwick, A.L., Sharma, V.P., Allegra, M., Zaragkoulias, A., Sadighi Akha, E., Knight, S.J., et al. (2013). Reduced dosage of ERF causes complex craniosynostosis in humans and mice and links ERK1/2 signaling to regulation of osteogenesis. Nat Genet *45*, 308-313.
56. Glass, G.E., O'Hara, J., Canham, N., Cilliers, D., Dunaway, D., Fenwick, A.L., Jeelani, N.O., Johnson, D., Lester, T., Lord, H., et al. (2019). ERF-related craniosynostosis: The phenotypic and developmental profile of a new craniosynostosis syndrome. Am J Med Genet A *179*, 615-627.
57. Chaudhry, A., Sabatini, P., Han, L., Ray, P.N., Forrest, C., and Bowdin, S. (2015). Heterozygous mutations in ERF cause syndromic craniosynostosis with multiple suture involvement. Am J Med Genet A *167A*, 2544-2547.
58. Wilkie, A.O.M., Johnson, D., and Wall, S.A. (2017). Clinical genetics of craniosynostosis. Curr Opin Pediatr *29*, 622-628.
59. Balasubramanian, M., Lord, H., Levesque, S., Guturu, H., Thuriot, F., Sillon, G., Wenger, A.M., Sureka, D.L., Lester, T., Johnson, D.S., et al. (2017). Chitayat syndrome: hyperphalangism, characteristic facies, hallux valgus and bronchomalacia results from a recurrent c.266A>G p.(Tyr89Cys) variant in the ERF gene. J Med Genet *54*, 157-165.
60. Papadaki, C., Alexiou, M., Cecena, G., Verykokakis, M., Bilitou, A., Cross, J.C., Oshima, R.G., and Mavrothalassitis, G. (2007). Transcriptional repressor erf determines extraembryonic ectoderm differentiation. Mol Cell Biol *27*, 5201-5213.
61. Sgouras, D.N., Athanasiou, M.A., Beal, G.J., Jr., Fisher, R.J., Blair, D.G., and Mavrothalassitis, G.J. (1995). ERF: an ETS domain protein with strong transcriptional repressor activity, can suppress ets-associated tumorigenesis

and is regulated by phosphorylation during cell cycle and mitogenic stimulation. EMBO J *14*, 4781-4793.
62. Liu, D., Pavlopoulos, E., Modi, W., Moschonas, N., and Mavrothalassitis, G. (1997). ERF: genomic organization, chromosomal localization and promoter analysis of the human and mouse genes. Oncogene *14*, 1445-1451.
63. Hsing, M., Wang, Y., Rennie, P.S., Cox, M.E., and Cherkasov, A. (2020). ETS transcription factors as emerging drug targets in cancer. Med Res Rev *40*, 413-430.
64. Hollenhorst, P.C., McIntosh, L.P., and Graves, B.J. (2011). Genomic and biochemical insights into the specificity of ETS transcription factors. Annu Rev Biochem *80*, 437-471.
65. Polychronopoulos, S., Verykokakis, M., Yazicioglu, M.N., Sakarellos-Daitsiotis, M., Cobb, M.H., and Mavrothalassitis, G. (2006). The transcriptional ETS2 repressor factor associates with active and inactive Erks through distinct FXF motifs. J Biol Chem *281*, 25601-25611.
66. Le Gallic, L., Sgouras, D., Beal, G., Jr., and Mavrothalassitis, G. (1999). Transcriptional repressor ERF is a Ras/mitogen-activated protein kinase target that regulates cellular proliferation. Mol Cell Biol *19*, 4121-4133.
67. Le Gallic, L., Virgilio, L., Cohen, P., Biteau, B., and Mavrothalassitis, G. (2004). ERF nuclear shuttling, a continuous monitor of Erk activity that links it to cell cycle progression. Mol Cell Biol *24*, 1206-1218.
68. Verykokakis, M., Papadaki, C., Vorgia, E., Le Gallic, L., and Mavrothalassitis, G. (2007). The RAS-dependent ERF control of cell proliferation and differentiation is mediated by c-Myc repression. J Biol Chem *282*, 30285-30294.
69. Allegra, M., Zaragkoulias, A., Vorgia, E., Ioannou, M., Litos, G., Beug, H., and Mavrothalassitis, G. (2012). Semaphorin-7a reverses the ERF-induced inhibition of EMT in Ras-dependent mouse mammary epithelial cells. Mol Biol Cell *23*, 3873-3881.
70. Athanasiou, M., Blair, D.G., and Mavrothalassitis, G. (2003). ERF, an ETS-related transcriptional repressor, can induce erythroid differentiation. Anticancer Res *23*, 2143-2153.
71. Chou, Y.T., Lin, H.H., Lien, Y.C., Wang, Y.H., Hong, C.F., Kao, Y.R., Lin, S.C., Chang, Y.C., Lin, S.Y., Chen, S.J., et al. (2010). EGFR promotes lung tumorigenesis by activating miR-7 through a Ras/ERK/Myc pathway that targets the Ets2 transcriptional repressor ERF. Cancer Res *70*, 8822-8831.
72. Vorgia, E., Zaragkoulias, A., Peraki, I., and Mavrothalassitis, G. (2017). Suppression of Fgf2 by ETS2 repressor factor (ERF) is required for chorionic trophoblast differentiation. Mol Reprod Dev *84*, 286-295.
73. Peraki, I., Palis, J., and Mavrothalassitis, G. (2017). The Ets2 Repressor Factor (Erf) Is Required for Effective Primitive and Definitive Hematopoiesis. Mol Cell Biol *37*.
74. Mignone, J.L., Kukekov, V., Chiang, A.S., Steindler, D., and Enikolopov, G. (2004). Neural stem and progenitor cells in nestin-GFP transgenic mice. J Comp Neurol *469*, 311-324.
75. Xie, L., Zeng, X., Hu, J., and Chen, Q. (2015). Characterization of Nestin, a Selective Marker for Bone Marrow Derived Mesenchymal Stem Cells. Stem Cells Int *2015*, 762098.
76. Wiese, C., Rolletschek, A., Kania, G., Blyszczuk, P., Tarasov, K.V., Tarasova, Y., Wersto, R.P., Boheler, K.R., and Wobus, A.M. (2004). Nestin expression--a property of multi-lineage progenitor cells? Cell Mol Life Sci *61*, 2510-2522.

77. Muzumdar, M.D., Tasic, B., Miyamichi, K., Li, L., and Luo, L. (2007). A global double-fluorescent Cre reporter mouse. Genesis *45*, 593-605.
78. James, A.W., Theologis, A.A., Brugmann, S.A., Xu, Y., Carre, A.L., Leucht, P., Hamilton, K., Korach, K.S., and Longaker, M.T. (2009). Estrogen/estrogen receptor alpha signaling in mouse posterofrontal cranial suture fusion. PLoS One *4*, e7120.
79. James, A.W., Levi, B., Xu, Y., Carre, A.L., and Longaker, M.T. (2010). Retinoic acid enhances osteogenesis in cranial suture-derived mesenchymal cells: potential mechanisms of retinoid-induced craniosynostosis. Plast Reconstr Surg *125*, 1352-1361.
80. Xu, Y., Malladi, P., Chiou, M., and Longaker, M.T. (2007). Isolation and characterization of posterofrontal/sagittal suture mesenchymal cells in vitro. Plast Reconstr Surg *119*, 819-829.
81. Deng, M.J., Jin, Y., Shi, J.N., Lu, H.B., Liu, Y., He, D.W., Nie, X., and Smith, A.J. (2004). Multilineage differentiation of ectomesenchymal cells isolated from the first branchial arch. Tissue Eng *10*, 1597-1606.
82. Malaval, L., Gupta, A.K., and Aubin, J.E. (1995). Leukemia inhibitory factor inhibits osteogenic differentiation in rat calvaria cell cultures. Endocrinology *136*, 1411-1418.
83. Leyva-Leyva, M., Barrera, L., Lopez-Camarillo, C., Arriaga-Pizano, L., Orozco-Hoyuela, G., Carrillo-Casas, E.M., Calderon-Perez, J., Lopez-Diaz, A., Hernandez-Aguilar, F., Gonzalez-Ramirez, R., et al. (2013). Characterization of mesenchymal stem cell subpopulations from human amniotic membrane with dissimilar osteoblastic potential. Stem Cells Dev *22*, 1275-1287.
84. Russell, K.C., Phinney, D.G., Lacey, M.R., Barrilleaux, B.L., Meyertholen, K.E., and O'Connor, K.C. (2010). In vitro high-capacity assay to quantify the clonal heterogeneity in trilineage potential of mesenchymal stem cells reveals a complex hierarchy of lineage commitment. Stem Cells *28*, 788-798.
85. Xie, L., Zhang, N., Marsano, A., Vunjak-Novakovic, G., Zhang, Y., and Lopez, M.J. (2013). In vitro mesenchymal trilineage differentiation and extracellular matrix production by adipose and bone marrow derived adult equine multipotent stromal cells on a collagen scaffold. Stem Cell Rev Rep *9*, 858-872.
86. Gregory, C.A., Gunn, W.G., Peister, A., and Prockop, D.J. (2004). An Alizarin red-based assay of mineralization by adherent cells in culture: comparison with cetylpyridinium chloride extraction. Anal Biochem *329*, 77-84.
87. Nicoletti, I., Migliorati, G., Pagliacci, M.C., Grignani, F., and Riccardi, C. (1991). A rapid and simple method for measuring thymocyte apoptosis by propidium iodide staining and flow cytometry. J Immunol Methods *139*, 271-279.
88. Morgan, D.M. (1998). Tetrazolium (MTT) assay for cellular viability and activity. Methods Mol Biol *79*, 179-183.
89. Favata, M.F., Horiuchi, K.Y., Manos, E.J., Daulerio, A.J., Stradley, D.A., Feeser, W.S., Van Dyk, D.E., Pitts, W.J., Earl, R.A., Hobbs, F., et al. (1998). Identification of a novel inhibitor of mitogen-activated protein kinase kinase. J Biol Chem *273*, 18623-18632.
90. Etchin, J., Sanda, T., Mansour, M.R., Kentsis, A., Montero, J., Le, B.T., Christie, A.L., McCauley, D., Rodig, S.J., Kauffman, M., et al. (2013). KPT-330 inhibitor of CRM1 (XPO1)-mediated nuclear export has selective anti-leukaemic activity in preclinical models of T-cell acute lymphoblastic leukaemia and acute myeloid leukaemia. Br J Haematol *161*, 117-127.

91. Parikh, K., Cang, S., Sekhri, A., and Liu, D. (2014). Selective inhibitors of nuclear export (SINE)--a novel class of anti-cancer agents. J Hematol Oncol *7*, 78.
92. Dominici, M., Le Blanc, K., Mueller, I., Slaper-Cortenbach, I., Marini, F., Krause, D., Deans, R., Keating, A., Prockop, D., and Horwitz, E. (2006). Minimal criteria for defining multipotent mesenchymal stromal cells. The International Society for Cellular Therapy position statement. Cytotherapy *8*, 315-317.
93. Meirelles Lda, S., and Nardi, N.B. (2003). Murine marrow-derived mesenchymal stem cell: isolation, in vitro expansion, and characterization. Br J Haematol *123*, 702-711.
94. Zhu, H., Guo, Z.K., Jiang, X.X., Li, H., Wang, X.Y., Yao, H.Y., Zhang, Y., and Mao, N. (2010). A protocol for isolation and culture of mesenchymal stem cells from mouse compact bone. Nat Protoc *5*, 550-560.
95. Maruyama, T., Jeong, J., Sheu, T.J., and Hsu, W. (2016). Stem cells of the suture mesenchyme in craniofacial bone development, repair and regeneration. Nat Commun *7*, 10526.
96. Wilk, K., Yeh, S.A., Mortensen, L.J., Ghaffarigarakani, S., Lombardo, C.M., Bassir, S.H., Aldawood, Z.A., Lin, C.P., and Intini, G. (2017). Postnatal Calvarial Skeletal Stem Cells Expressing PRX1 Reside Exclusively in the Calvarial Sutures and Are Required for Bone Regeneration. Stem Cell Reports *8*, 933-946.
97. Anderson, P., Carrillo-Galvez, A.B., Garcia-Perez, A., Cobo, M., and Martin, F. (2013). CD105 (endoglin)-negative murine mesenchymal stromal cells define a new multipotent subpopulation with distinct differentiation and immunomodulatory capacities. PLoS One *8*, e76979.
98. da Silva Meirelles, L., Chagastelles, P.C., and Nardi, N.B. (2006). Mesenchymal stem cells reside in virtually all post-natal organs and tissues. J Cell Sci *119*, 2204-2213.
99. Kern, S., Eichler, H., Stoeve, J., Kluter, H., and Bieback, K. (2006). Comparative analysis of mesenchymal stem cells from bone marrow, umbilical cord blood, or adipose tissue. Stem Cells *24*, 1294-1301.
100. Holmes, G., Rothschild, G., Roy, U.B., Deng, C.X., Mansukhani, A., and Basilico, C. (2009). Early onset of craniosynostosis in an Apert mouse model reveals critical features of this pathology. Dev Biol *328*, 273-284.
101. Fragale, A., Tartaglia, M., Bernardini, S., Di Stasi, A.M., Di Rocco, C., Velardi, F., Teti, A., Battaglia, P.A., and Migliaccio, S. (1999). Decreased proliferation and altered differentiation in osteoblasts from genetically and clinically distinct craniosynostotic disorders. Am J Pathol *154*, 1465-1477.
102. Pricola, K.L., Kuhn, N.Z., Haleem-Smith, H., Song, Y., and Tuan, R.S. (2009). Interleukin-6 maintains bone marrow-derived mesenchymal stem cell stemness by an ERK1/2-dependent mechanism. J Cell Biochem *108*, 577-588.
103. Simann, M., Le Blanc, S., Schneider, V., Zehe, V., Ludemann, M., Schutze, N., Jakob, F., and Schilling, T. (2017). Canonical FGFs Prevent Osteogenic Lineage Commitment and Differentiation of Human Bone Marrow Stromal Cells Via ERK1/2 Signaling. J Cell Biochem *118*, 263-275.
104. Matsushita, T., Chan, Y.Y., Kawanami, A., Balmes, G., Landreth, G.E., and Murakami, S. (2009). Extracellular signal-regulated kinase 1 (ERK1) and ERK2 play essential roles in osteoblast differentiation and in supporting osteoclastogenesis. Mol Cell Biol *29*, 5843-5857.
105. Kyono, A., Avishai, N., Ouyang, Z., Landreth, G.E., and Murakami, S. (2012). FGF and ERK signaling coordinately regulate mineralization-related genes and play essential roles in osteocyte differentiation. J Bone Miner Metab *30*, 19-30.

106. Tsang, E.J., Wu, B., and Zuk, P. (2018). MAPK signaling has stage-dependent osteogenic effects on human adipose-derived stem cells in vitro. Connect Tissue Res *59*, 129-146.
107. Sumarsono, S.H., Wilson, T.J., Tymms, M.J., Venter, D.J., Corrick, C.M., Kola, R., Lahoud, M.H., Papas, T.S., Seth, A., and Kola, I. (1996). Down's syndrome-like skeletal abnormalities in Ets2 transgenic mice. Nature *379*, 534-537.
108. Greenwald, J.A., Mehrara, B.J., Spector, J.A., Warren, S.M., Fagenholz, P.J., Smith, L.E., Bouletreau, P.J., Crisera, F.E., Ueno, H., and Longaker, M.T. (2001). In vivo modulation of FGF biological activity alters cranial suture fate. Am J Pathol *158*, 441-452.
109. Iseki, S., Wilkie, A.O., and Morriss-Kay, G.M. (1999). Fgfr1 and Fgfr2 have distinct differentiation- and proliferation-related roles in the developing mouse skull vault. Development *126*, 5611-5620.
110. Li, S., Quarto, N., and Longaker, M.T. (2007). Dura mater-derived FGF-2 mediates mitogenic signaling in calvarial osteoblasts. Am J Physiol Cell Physiol *293*, C1834-1842.
111. Laue, K., Pogoda, H.M., Daniel, P.B., van Haeringen, A., Alanay, Y., von Ameln, S., Rachwalski, M., Morgan, T., Gray, M.J., Breuning, M.H., et al. (2011). Craniosynostosis and multiple skeletal anomalies in humans and zebrafish result from a defect in the localized degradation of retinoic acid. Am J Hum Genet *89*, 595-606.
112. Maclean, G., Dolle, P., and Petkovich, M. (2009). Genetic disruption of CYP26B1 severely affects development of neural crest derived head structures, but does not compromise hindbrain patterning. Dev Dyn *238*, 732-745.
113. Mercader, N., Leonardo, E., Piedra, M.E., Martinez, A.C., Ros, M.A., and Torres, M. (2000). Opposing RA and FGF signals control proximodistal vertebrate limb development through regulation of Meis genes. Development *127*, 3961-3970.
114. Probst, S., Kraemer, C., Demougin, P., Sheth, R., Martin, G.R., Shiratori, H., Hamada, H., Iber, D., Zeller, R., and Zuniga, A. (2011). SHH propagates distal limb bud development by enhancing CYP26B1-mediated retinoic acid clearance via AER-FGF signalling. Development *138*, 1913-1923.
115. Geelen, J.A. (1979). Hypervitaminosis A induced teratogenesis. CRC Crit Rev Toxicol *6*, 351-375.
116. Gardner, J.S., Guyard-Boileau, B., Alderman, B.W., Fernbach, S.K., Greene, C., and Mangione, E.J. (1998). Maternal exposure to prescription and non-prescription pharmaceuticals or drugs of abuse and risk of craniosynostosis. Int J Epidemiol *27*, 64-67.
117. Yip, J.E., Kokich, V.G., and Shepard, T.H. (1980). The effect of high doses of retinoic acid on prenatal craniofacial development in Macaca nemestrina. Teratology *21*, 29-38.
118. Weng, Z., Wang, C., Zhang, C., Xu, J., Chai, Y., Jia, Y., Han, P., and Wen, G. (2019). All-Trans Retinoic Acid Promotes Osteogenic Differentiation and Bone Consolidation in a Rat Distraction Osteogenesis Model. Calcif Tissue Int *104*, 320-330.
119. Cruz, A.C.C., Cardozo, F., Magini, R.S., and Simoes, C.M.O. (2019). Retinoic acid increases the effect of bone morphogenetic protein type 2 on osteogenic differentiation of human adipose-derived stem cells. J Appl Oral Sci *27*, e20180317.

120. Roa, L.A., Bloemen, M., Carels, C.E.L., Wagener, F., and Von den Hoff, J.W. (2019). Retinoic acid disrupts osteogenesis in pre-osteoblasts by down-regulating WNT signaling. Int J Biochem Cell Biol *116*, 105597.
121. Lind, T., Sundqvist, A., Hu, L., Pejler, G., Andersson, G., Jacobson, A., and Melhus, H. (2013). Vitamin a is a negative regulator of osteoblast mineralization. PLoS One *8*, e82388.
122. Feil, S., Valtcheva, N., and Feil, R. (2009). Inducible Cre mice. Methods Mol Biol *530*, 343-363.
123. Canalis, E., Parker, K., Feng, J.Q., and Zanotti, S. (2013). Osteoblast lineage-specific effects of notch activation in the skeleton. Endocrinology *154*, 623-634.
124. Maurel, D.B., Matsumoto, T., Vallejo, J.A., Johnson, M.L., Dallas, S.L., Kitase, Y., Brotto, M., Wacker, M.J., Harris, M.A., Harris, S.E., et al. (2019). Characterization of a novel murine Sost ER(T2) Cre model targeting osteocytes. Bone Res *7*, 6.

6. Publications

17/5/21 | 12:40 | 4/Color Fig: 1,2,3,4,5,6,7,8 | ArtID: 00149-21 | DOI:10.1128/MCB.00149-21 | CE: KGL-mab
Editor: Peter Tontonoz | Section: Research Article | Designation: T

AMERICAN SOCIETY FOR MICROBIOLOGY | Molecular and Cellular Biology®

RESEARCH ARTICLE

Erf Affects Commitment and Differentiation of Osteoprogenitor Cells in Cranial Sutures via the Retinoic Acid Pathway

AQ: au Angeliki Vogiatzi,[a] Ismini Baltsavia,[a] Emmanuel Dialynas,[b] Vasiliki Theodorou,[b] Yan Zhou,[c] Elena Deligianni,[b] Ioannis Iliopoulos,[a] Andrew O. M. Wilkie,[c] Stephen R. F. Twigg,[c] George Mavrothalassitis[a,b]

[a]Medical School, University of Crete, Heraklion, Crete, Greece
[b]IMBB, FORTH, Heraklion, Crete, Greece
[c]MRC Weatherall Institute of Molecular Medicine, University of Oxford, Oxford, United Kingdom

ABSTRACT ETS2 repressor factor (ERF) haploinsufficiency causes late-onset craniosynostosis (CRS) (OMIM entry 600775; CRS4) in humans, while in mice Erf insufficiency also leads to a similar multisuture synostosis phenotype preceded by mildly reduced calvarium ossification. However, neither the cell types affected nor the effects *per se* have been identified so far. Here, we establish an *ex vivo* system for the expansion of suture-derived mesenchymal stem and progenitor cells (sdMSCs) and analyze the role of Erf levels in their differentiation. Cellular data suggest that Erf insufficiency specifically decreases osteogenic differentiation of sdMSCs, resulting in the initially delayed mineralization of the calvarium. Transcriptome analysis indicates that Erf is required for efficient osteogenic lineage commitment of sdMSCs. Elevated retinoic acid catabolism due to increased levels of the cytochrome P450 superfamily member Cyp26b1 as a result of decreased Erf levels appears to be the underlying mechanism leading to defective differentiation. Exogenous addition of retinoic acid can rescue the osteogenic differentiation defect, suggesting that Erf affects cranial bone mineralization during skull development through retinoic acid gradient regulation.

KEYWORDS craniosynostosis, mesenchymal stem cells, Ets transcription factors, retinoic acid

Cranial sutures comprise the connective tissues between the bones of the skull and are considered to be major centers of bone growth during development (1, 2). Mesenchymal stem cells that reside in the suture mesenchyme commit and enter the intramembranous ossification pathway, giving rise to proliferating populations of osteoprogenitor and preosteoblast cells that eventually differentiate to osteoblasts at the edges of the developing bones (3, 4). The balance between the different cell types seems to be crucial for suture patency and consequently for the coordination of skull and brain development (5, 6). Craniosynostosis is a developmental disorder in which one or more of the cranial sutures close prematurely, leading to skull and facial deformities, along with complications that can affect vision, hearing, breathing, and learning ability. During the last 25 years, considerable effort has been put into unraveling the mechanisms that underlie craniosynostosis (7). However, the presence of multiple cell populations in sutures, the paucity of specific cellular markers, and difficulties in the identification and isolation of suture stem cells have hindered these efforts.

Genetic analysis has identified an increasing number of genes that, when mutated, cause craniosynostosis. Activating mutations in three members of the fibroblast growth factor receptor family (FGFR1, FGFR2, and FGFR3) and alterations in downstream signaling cascades such as the p38 MAPK, ERK1/2, PI3K/AKT, and PLCγ/PKC pathways has been commonly reported to be involved in syndromic cases (8–14). We previously reported that haploinsufficiency of the Ets domain transcriptional repressor factor ERF, a downstream target of ERKs that can regulate cellular proliferation and differentiation (15–18), causes premature suture

AQ: A

Citation Vogiatzi A, Baltsavia I, Dialynas E, Theodorou V, Zhou Y, Deligianni E, Iliopoulos I, Wilkie AOM, Twigg SRF, Mavrothalassitis G. 2021. Erf affects commitment and differentiation of osteoprogenitor cells in cranial sutures via the retinoic acid pathway. Mol Cell Biol 41:e00149-21. https://doi.org/10.1128/MCB.00149-21.

Address correspondence to George Mavrothalassitis, mavro@imbb.forth.gr.

Received 7 April 2021
Returned for modification 22 April 2021
Accepted 29 April 2021
Accepted manuscript posted online 10 May 2021
Published

17/5/21 | 12:40 | 4/Color Fig: 1,2,3,4,5,6,7,8 | ArtID: 00149-21 | DOI:10.1128/MCB.00149-21 | CE: KGL-mab

closure in humans (19, 20). This disorder, termed ERF-related craniosynostosis (CRS4; OMIM entry 61188) ranges widely in severity. Children affected by this disorder present synostosis after infancy more frequently compared to other craniosynostosis cases, and sometimes this is associated with an insidious onset of raised intracranial pressure, causing permanent visual impairment (19, 20). Although mice with the equivalent genotype (*Erf*$^{+/-}$) are phenotypically normal, by reducing the Erf dosage further to ~30% of the wild type by combining loss-of-function (*Erf*$^{-}$) and hypomorphic (*Erf*^{loxP}) alleles in *trans*, the resulting *Erf*-insufficient mice (*Erf*$^{loxP/-}$ mice) display facial dysmorphism with no other obvious skeletal defects beyond craniosynostosis and a mild reduction in the ossification of calvarial bones, closely recapitulating the human disease (20).

Retinoic acid (RA), acting as a morphogen, regulates developmental processes through concentration gradients in multiple systems. Neural crest cell induction, pharyngeal arch and trunk formation, and heart, eye, and limb development are among the biological events shown to be dependent on RA signaling (21–28). Calvarial bone formation also seems to be sensitive to retinoic acid concentration and action. Excessive amounts of RA have been shown to have teratogenic effects during pregnancy, causing multiple craniofacial abnormalities to embryos (29–31). Hypomorphic and null mutations in the gene coding for CYP26B1, the RA-catabolizing enzyme, lead to cranial bone hypoplasia and craniosynostosis in humans (32), while a significant decrease in retinol-binding protein 4 (RBP4), necessary for retinol transport, was detected in sutures from children with craniosynostosis in an independent study (33). In zebrafish, *cyp26b1* is shown to be expressed at the osteogenic fronts after suture formation and its partial loss results in craniosynostosis (32). Interestingly, *Cyp26b1*$^{-/-}$ mice display multiple abnormalities in facial structures, along with reduced ossification of the calvarial bones at E18.5, but not craniosynostosis (34). At the cellular level, the commitment of cranial bone mesenchymal progenitor cells along the osteogenic lineage in mice has been shown to be sensitive to balanced levels of retinoic acid and the epigenetic methyltransferase Ezh2 (35, 36). The diversity of the RA-associated phenotypes indicate that the precise retinoic acid spatiotemporal regulation is crucial for normal cranial bone and suture formation. Surprisingly, there is limited information on the factors that regulate RA signaling during calvarial development.

AQ: B

In the present study, by introducing modifications into previous suture cell isolation methods (37, 38), we developed a new approach to derive mesenchymal stem/progenitor cells from cranial sutures of Erf-competent (*Erf*$^{loxP/+}$) and Erf-insufficient (*Erf*$^{loxP/-}$) mice to evaluate their function. *Ex vivo* cellular differentiation studies of these suture-derived mesenchymal stem and progenitor cells (sdMSCs) show that decreased levels of *Erf* result in decreased osteogenic commitment and differentiation. Transcriptome analysis and correlation studies corroborate the cellular data and suggest that reduced retinoic acid signaling due to increased levels of the RA-catabolizing factor *Cyp26b1* may underlie the phenotype of Erf-insufficient cells. Exogenous addition of retinoic acid during sdMSC *in vitro* differentiation fully suppresses the osteogenic differentiation defect of Erf-insufficient cells without affecting the Erf-competent cell cultures. Our data indicate that Erf may affect cranial suture development via retinoic acid regulation, providing a link in the fibroblast growth factor (FGF)-RA control loop (39, 40).

RESULTS

LIF-selected long-term expanded suture derived cells possess *in vitro* characteristics of mesenchymal stem/progenitor cells. Cranial sutures constitute niches of highly heterogeneous cell populations related to bone growth (37). We thus focused our efforts on mesenchymal stem cell (MSC)-derived populations and, based on previous studies, established a new protocol utilizing leukemia inhibitory factor (LIF) for the selective expansion and maintenance of mesenchymal stem/progenitor cells from cranial sutures. Suture explants from postnatal day 5 (P5) mice and the resulting suture-derived cells were cultured in the presence of leukemia inhibitory factor, which is known for its role in sustaining the stem cell state while inhibiting differentiation (41, 42). Cultivation of suture-derived cells in the presence of LIF for a minimum of 8 population doublings (PDs) during a period of 50 to 60 days resulted in a population of cells that were plastic adherent, fibroblast-like in shape (Fig. 1A and B), and expressed increased levels of the MSC marker *Axin2* (43) and

F1

ID: gulrezaTime: 12:40I Path: //mumnasprod/home$/Mandar.Gawade$/SM-MCBJ210044

17/5/21 | 12:40 | 4/Color Fig: 1,2,3,4,5,6,7,8 | ArtID: 00149-21 | DOI:10.1128/MCB.00149-21 | CE: KGL-mab

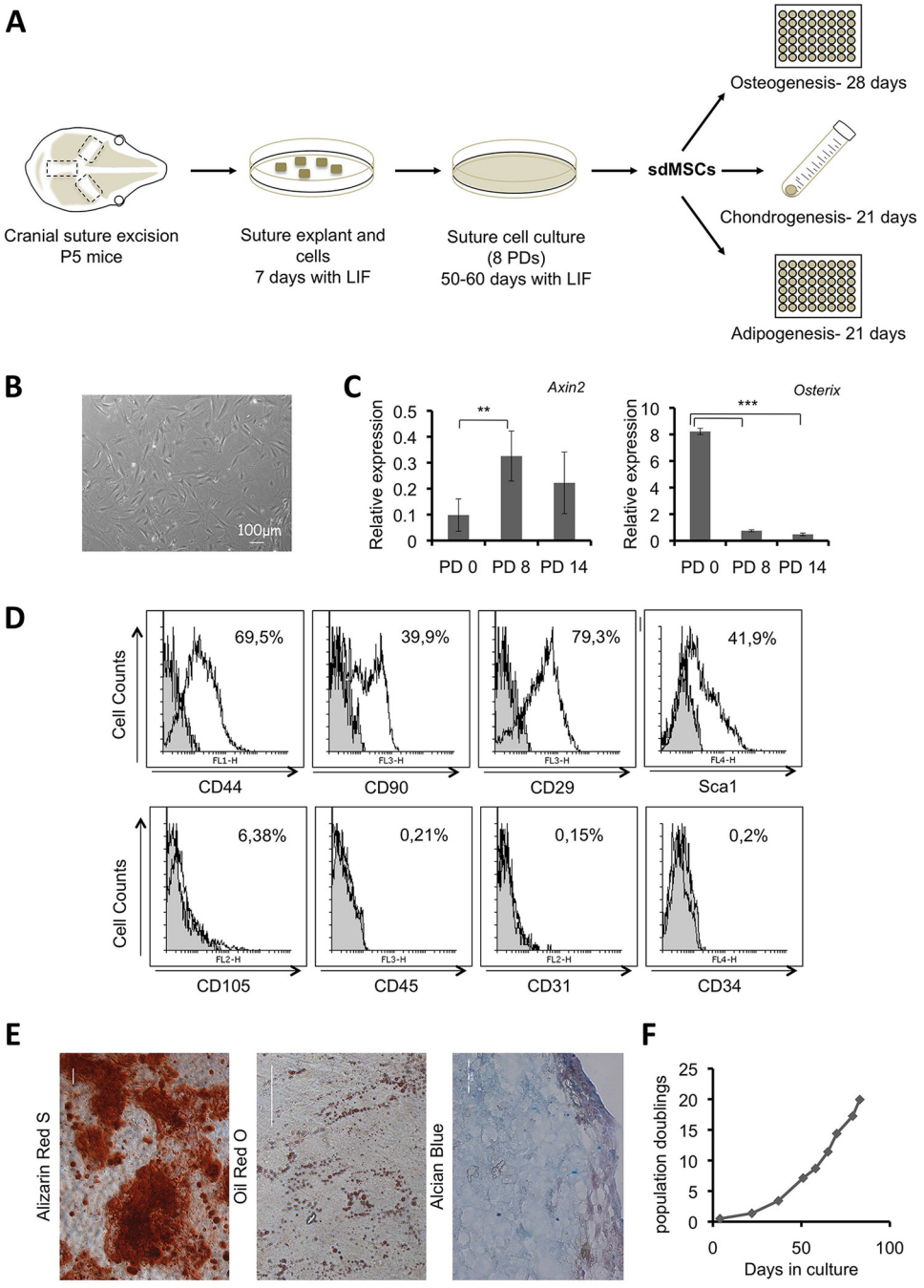

COLOR

FIG 1 Characterization of leukemia inhibitory factor (LIF)-selected suture-derived mesenchymal cells expanded in culture for 8 population doublings (PDs). (A) A schematic representation and timeline of the cell isolation, culture, and characterization process. (B) Phase-contrast image of suture-derived wild-type cells displaying a fibroblastoid morphology. (C) *Axin2* and *Osterix* mRNA levels normalized to *Gapdh* as determined by quantitative PCR (qPCR) in suture cells of the indicated population doubling (PD) level. Data were analyzed with one-way analysis of variance (ANOVA) followed by Dunnett's (two-sided) test to compare all groups against the control group (PD 0). *, $P < 0.05$; **, $P < 0.01$; ***, $P < 0.001$. (D) Flow cytometric analysis of cells for mesenchymal stem cell (MSC) markers (CD44, CD90, CD29, Sca1, and CD105) and hematopoietic/endothelial markers (CD45, CD34, and CD31). Filled histograms indicate the unlabeled cells used as negative controls. (E) Cells were induced to differentiate toward osteocytes, adipocytes, and chondrocytes, and were stained with alizarin red S, oil red O, and alcian blue/hematoxylin, respectively. Bars, 100 μm, 50 μm, and 20 μm, respectively. (F) Graph showing the population doublings over time in culture for LIF-expanded suture mesenchymal cells. Each measurement (point in graph) was performed at the end of each passage.

17/5/21 | 12:41 | 4/Color Fig: 1,2,3,4,5,6,7,8 | ArtID: 00149-21 | DOI:10.1128/MCB.00149-21 | CE: KGL-mab

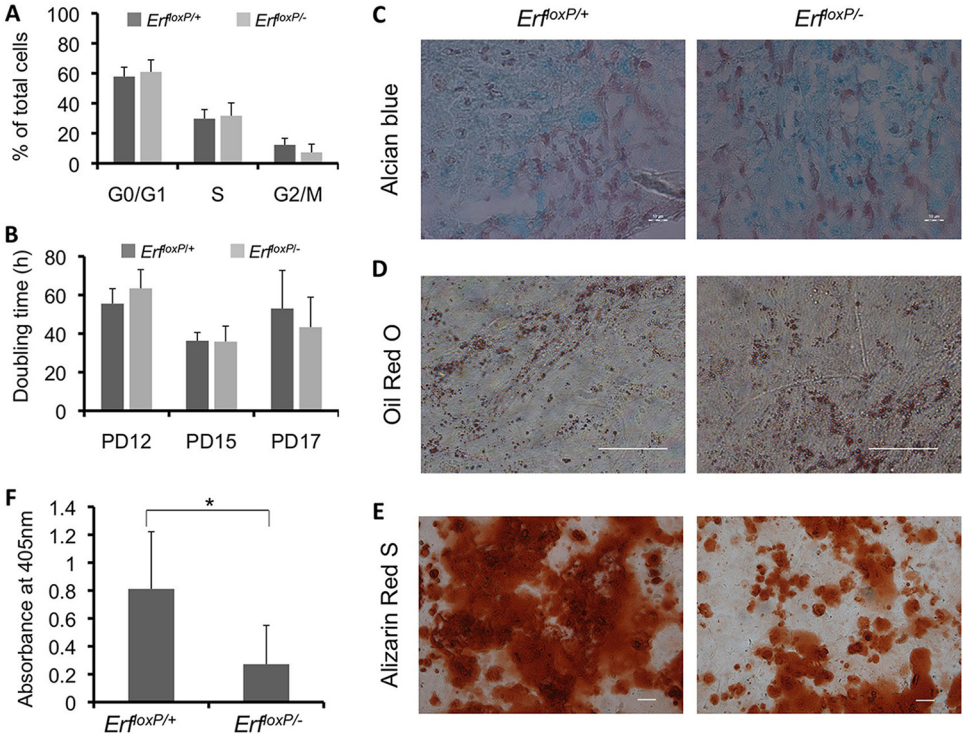

COLOR

FIG 2 Erf insufficiency compromises the ability of suture-derived mesenchymal stem and progenitor cells (sdMSCs) to mineralize. (A) Frequency in each of the cell cycle phases of cells growing in maintenance conditions as determined by propidium iodide staining and flow cytometry. (B) Doubling time in hours of $Erf^{loxP/+}$ and $Erf^{loxP/-}$ sdMSCs at the indicated population doubling (PD) levels. (C to E) sdMSCs were induced to differentiate along the chondrogenic lineage for 21 days (C), the adipogenic lineage for 21 days (D), and the osteogenic lineage for 28 days (E) and stained with alcian blue and hematoxylin, oil red O, and alizarin red S, respectively. Bars, 10 μm, 50 μm, and 100 μm, respectively. (F) Measurements of the alizarin red S dye extracted from the cells after 28 days of osteogenic differentiation. Three independent biological experiments were conducted, and the statistical analysis was performed using *an unpaired t* test with two-tailed distribution. *, $P < 0.05$.

AQ: C

reduced levels of the osteogenic differentiation marker *Sp7* compared to those in the initial population (Fig. 1C). The majority of these cells expressed the MSC-associated surface antigens CD44, CD90, CD29, and Sca1 (4, 44–46), while neither hematopoietic nor endothelial cell markers could be detected (Fig. 1D). This cell population growing in culture for more than 8 PDs could effectively undergo differentiation toward the chondrogenic, osteogenic, and adipogenic lineages (Fig. 1E), a hallmark of mesenchymal stem cells. These cells, which we label suture-derived mesenchymal stem/progenitor cells (sdMSCs), can be routinely maintained in culture for more than 20 PDs (Fig. 1F) and sustain their characteristics for at least 3 freeze-thaw cycles.

Utilizing this approach, we established sdMSCs from $Erf^{loxP/+}$ and $Erf^{loxP/-}$ P5 littermates, in at least 5 independent experiments, to study the effect of limited Erf levels on MSC growth and differentiation. At this time point, the mice have not yet developed the phenotype of synostosis.

Erf insufficiency compromises the commitment of suture mesenchymal stem/progenitor cells toward the osteogenic lineage. Although Erf is known to affect cellular proliferation (16, 47), cell cycle phase analysis of $Erf^{loxP/+}$ and $Erf^{loxP/-}$ sdMSCs showed no significant difference in the cell distribution profiles (Fig. 2A). There was also no difference in the cell doubling time throughout the life of the cultures (Fig. 2B), suggesting that Erf insufficiency does not affect sdMSC self-renewal rate. We then examined the impact of Erf levels on sdMSC differentiation. $Erf^{loxP/+}$ and $Erf^{loxP/-}$ cells showed comparable efficiency in *in vitro* chondrogenic and adipogenic commitment (Fig. 2C and D). However, $Erf^{loxP/-}$ cells displayed decreased ability to mineralize (Fig. 2E and F), implying an impairment in the osteogenic differentiation of these cells. The

F2

ID: gulrezaTime: 12:41I Path: //mumnasprod/home$/Mandar.Gawade$/SM-MCBJ210044

17/5/21 | 12:41 | 4/Color Fig: 1,2,3,4,5,6,7,8 | ArtID: 00149-21 | DOI:10.1128/MCB.00149-21 | CE: KGL-mab

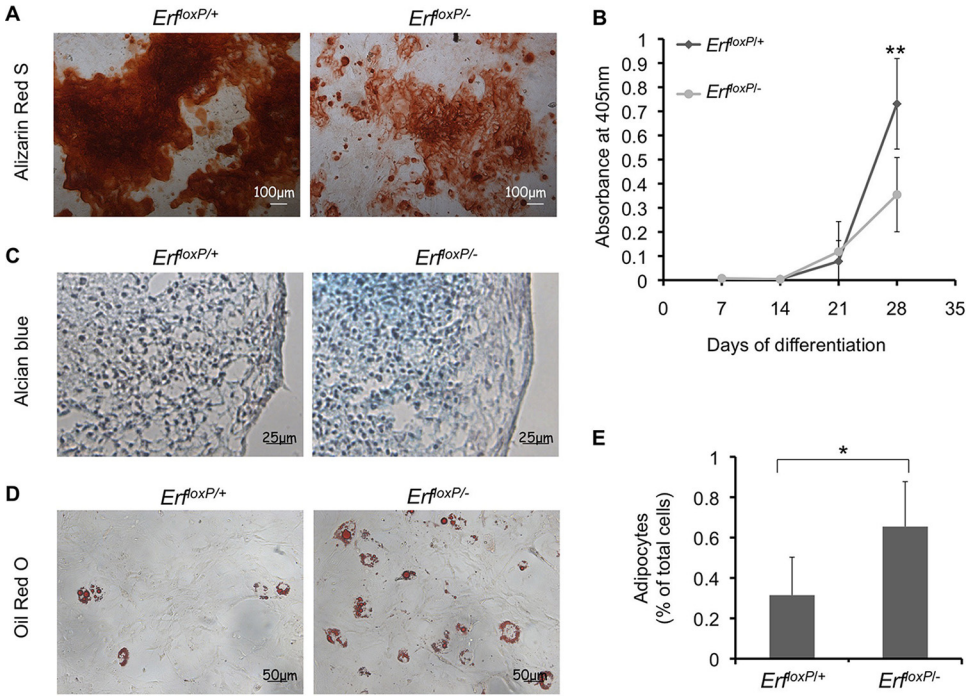

COLOR

FIG 3 Freshly isolated suture-derived Erf-insufficient cells display altered differentiation potential. (A) The initial heterogeneous population of cells was induced to differentiate along the osteogenic lineage for 28 days and stained with alizarin red S for calcium deposits. (B) Quantification of alizarin red S levels after extraction from culture wells at the indicated time points of differentiation. (C) Cells differentiating toward chondrocytes for 21 days, stained with alcian blue and hematoxylin. (D) Cells differentiating toward adipocytes for 7 days, stained with oil red O. (E) The total number of cells in adipocyte differentiation was determined by Hoechst 33342 staining of the nuclei. Statistical analysis was performed using a *t* test with two-tailed distribution. *, $P < 0.05$; **, $P < 0.01$.

reduced osteogenic differentiation was also apparent in the initial heterogeneous suture-derived cell population, in which $Erf^{loxP/-}$ cells displayed initially comparable but later decreased capacity to mineralize (Fig. 3A and B). Chondrogenic differentiation appeared unaffected, while the limited adipogenic differentiation was increased in $Erf^{loxP/-}$ cells (Fig. 3C to E), indicating the possible existence of a greater proportion of precursor populations among Erf-insufficient suture cells. These results indicate that the insufficiency of Erf reduces the osteogenic ability of suture-derived cells *in vitro*.

To gain further insight into the apparent differences in sdMSC osteogenic differentiation and to understand the possible role of Erf levels in this process, we analyzed transcriptome changes in suture-derived cells from $Erf^{loxP/+}$ and $Erf^{loxP/-}$ mice in 3 conditions. sdMSCs at PD8 in self-renewal or osteogenic differentiation medium for 24 h were used for early differentiation events, while the initial heterogeneous suture cell population growing in expansion medium, without LIF was used as a mixed differentiation state specimen (Fig. 4A). Consistent with a decrease rather than the elimination of *Erf* expression, a very limited number of genes were found to differ between the two genotypes. This was evident by the clustering of transcriptome samples according to culture conditions but not genotypes (Fig. 4B and Table 1). However, all 3 growth conditions produced distinct patterns that clustered together, assuring the consistency of the *ex vivo* cultures (Fig. 4C). The limited number of differentially expressed genes indicated a deficit of core matrisome genes in $Erf^{loxP/-}$ cells when tested against the GSEA database (48) (Fig. 5A and B and Table 1), supporting the hypothesis that Erf insufficiency leads to a defect in the osteogenic differentiation. This was consistent with the transcriptome differences of Erf-competent and Erf-insufficient cells upon osteogenic induction (see Table S1 in the supplemental material). $Erf^{loxP/-}$ cells exhibited considerably fewer genes associated with ossification and extracellular matrix organization than $Erf^{loxP/+}$ cells during induction of sdMSCs (Fig. 5C, L-O_minus and L-O_plus). Consistently, $Erf^{loxP/-}$ sdMSCs that

ID: gulrezaTime: 12:41I Path: //mumnasprod/home$/Mandar.Gawade$/SM-MCBJ210044

17/5/21 | 12:41 | 4/Color Fig: 1,2,3,4,5,6,7,8 | ArtID: 00149-21 | DOI:10.1128/MCB.00149-21 | CE: KGL-mab

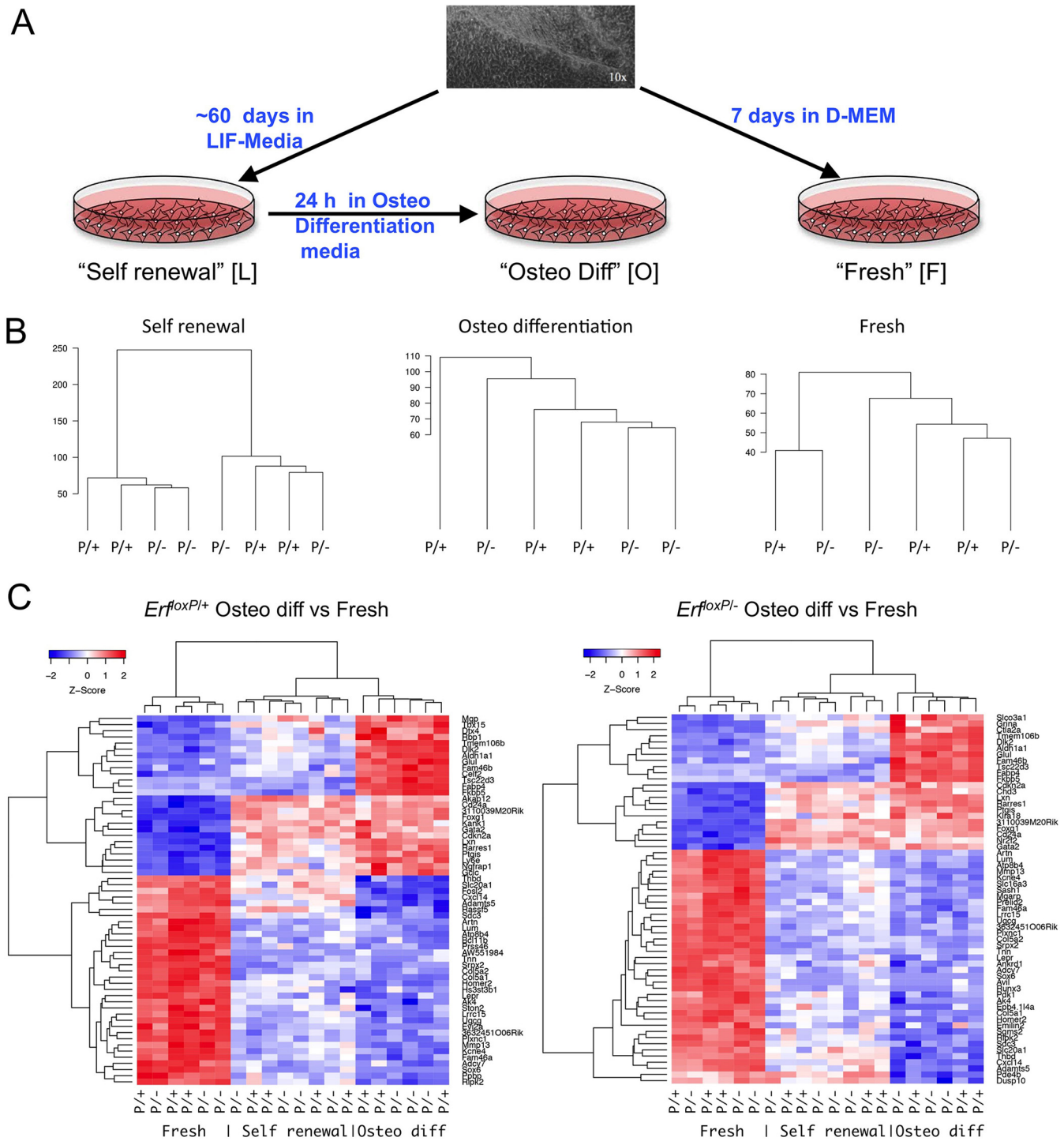

COLOR

FIG 4 Extensive transcriptional differences between growth conditions but not genotypes. (A) RNA was collected from suture-derived (top) freshly isolated suture cells cultured for 7 days (right, "fresh [F]"), sdMSCs cultured for 8 PDs in maintenance medium (left, "self-renewal [L]"), and sdMSCs of 8 PDs induced with osteogenic differentiation medium for 24 h (middle, "osteo diff [O]"). At least 3 or 4 mice were used per genotype for each of the above conditions tested per experiment, and at least 4 independent experiments were conducted. (B) Unsupervised clustering of gene expression experiment from Erf-competent $Erf^{loxp/+}$ (P/+) and Erf-insufficient $Erf^{loxp/-}$ (P/−) cells, indicating no genotype-specific associations. Self-renewal, sdMSCs in self renewal medium; osteo differentiation, sdMSCs 24 h in osteogenic differentiation medium; fresh cells, freshly isolated suture-derived cells. (C) Heatmaps based on the 60 most differentially expressed genes of the indicated comparison, showing a clear clustering between conditions but not between genotypes. P/+, Erf-competent ($Erf^{loxP/+}$) cells; P/−, Erf-insufficient ($Erf^{loxP/-}$) cells.

17/5/21 | 12:41 | 4/Color Fig: 1,2,3,4,5,6,7,8 | ArtID: 00149-21 | DOI:10.1128/MCB.00149-21 | CE: KGL-mab

TABLE 1 Differentially expressed genes between the two genotypes in each culture condition

Culture condition or genotype	Differentially expressed genes[a]
sdMSCs growing in	
Self-renewal (w/LIF)	
Upregulated in *Erf* $^{P/+}$	Add3, Amph, Epb4,1l4a, Erf, **Nell1**, Nts, Ostn, Slitrk6, **Tmod2**, Zfp729a
Upregulated in *Erf*$^{P/-}$	4930511M06Rik, **Cyp26b1**, **Fst**, Styk1
Osteogenic differentiation	
Upregulated in *Erf* $^{P/+}$	*Epb4.1l4a*, *Btbd2*, Cd34, ***Col14a1***, *Cthrc1*, Cygb, Cyp2c29, Cyp2c54, Cyp2d26, ***Emilin2***, Erf, *Esm1*, F5, **Gfra1**, **Gpx3**, H2afv, *Lrg1*, Mgst1, Nav1, **Rnpepl1**, Saa2, **Slc25a47**, Tmod2, Ttpa, Zfp738
Upregulated in *Erf*$^{P/-}$	Acta1, Actg2, Asb2, Atp2b4, Cnn1, **Cyp26b1**, Dmpk, Eng, F2r, **Fst**, Ldb3, **Lmod1**, Lrrc58, Mbp, Myh11, Pip4k2a, Plac8, Pnck, **Sh3bgr**, Tagln, Tbx18, Tnfaip2, Vwce
Freshly isolated suture-derived cells	
Upregulated in *Erf* $^{P/+}$	Arf1, AW551984, *Clec11a*, Dkk2, *Edil3*, Erf, *Gpc1*, *Igfbp5*, *Lum*, Lyz1, Med12l, Myof, *Ptn*, *Sema3a*, *Sema3e*, ***Serpinb1a***, Slc1a7, *Tgfbi*, Zcchc5
Upregulated in *Erf*$^{P/-}$	Ackr3, Ccl2, Ccl7, **Cyp26b1**, Dynap, F3, Fbxl19, Gsto1, Id4, **Irx1**, Lrrc32, Lrrk2, Ltbp2, **Lurap1l**, Mfap5, Ppap2b, Rgs16, Saal1, Serpinb2, Sfrp1, Siglecg, Stc1, Tm4sf1, **Twist2**

[a]Genes differing at least 1.5-fold with a false-discovery rate (FDR) of <0.05 are shown. Genes associated with the matrisome are shown in italics, and RA-related genes are bold.

either self-renewed or differentiated for 24 h required many more ossification-related changes to reach the differentiation state of the initial heterogeneous cell population than the *Erf*$^{loxP/+}$ cells (Fig. 5C, O-F_minus and O-F_plus).

We further examined the apparent contribution of *Erf* expression in the effective osteogenic differentiation, interrogating single cell RNA-sequencing data from mouse sutures available through the FaceBase Consortium (49, 50). Given the ubiquitous expression of *Erf* and its posttranscriptional regulation, we developed an approach to examine gene coexpression rather than cell cluster expression. We determined any expression correlation between the gene of interest and the rest of the cellular transcripts for each informative cell in the data and evaluated the known function of the correlated genes. *Erf* expression appeared to correlate with genes involved in ossification and extracellular matrix organization (Fig. 6A; see also Table S2 in the supplemental material). Compared to other suture ossification landmark genes subjected to the same correlation analysis, *Erf* clustered closely with *Sp7* in cells at E16.5 and with *Fgfr1*, *Runx2*, *Twist1*, and *Alpl* in cells at E18.5 and P10 (Fig. 6B and Table S2).

These data suggest that appropriate *Erf* expression level is required for proper differentiation of cranial suture cells toward the osteogenic pathway and are consistent with the decreased mineralization pattern observed previously *in vivo* (20), which could account for the late onset of Erf-related synostosis phenotype.

Erf insufficiency-induced osteogenic defect can be rescued by retinoic acid. In spite of the limited number of genes found to differ between Erf-competent and Erf-insufficient cells in all growth conditions, a group of genes associated with the retinoic acid (RA) pathway could be identified (Table 1). Characteristically, *Cyp26b1*, a gene coding for an RA-catabolizing enzyme known to affect suture development leading to craniosynostosis (32), was elevated upon Erf insufficiency in both proliferating and differentiating sdMSCs and in the initial heterogeneous suture cell population (Table 1 and Fig. 7A). *Cyp26b1* was drastically reduced upon normal sdMSC differentiation but remained in relatively high levels in Erf-insufficient cells (Fig. 7B), suggesting decreased levels of retinoic acid. Comparison of the genes differentially expressed during the differentiation of Erf-competent and Erf-insufficient sdMSCs with genes regulated by retinoic acid in mouse embryonic stem cells (mESCs) (51, 52) revealed a 4- to 5-order-of-magnitude higher significance for the Erf-competent (*Erf*$^{loxP/+}$) cell gene set (Fig. 7C; see also Tables S3 and S4 in the supplemental material). Analysis of these common genes (Table S4) through Metascape (53) indicated that indeed, in the case of Erf-competent (*Erf*$^{loxP/+}$) cells, they are associated with genes known to play a major role is suture development, such as *Runx*, *Twist*, and *BMP-Smad*. In contrast, in the case of Erf-insufficient (*Erf*$^{loxP/-}$) cells, they appear to associate with lymphoid and endothelial pathways (Fig. 7D). It would thus appear that Erf deficiency leads to a decreased retinoic acid response that affects suture development.

17/5/21 | 12:41 | 4/Color Fig: 1,2,3,4,5,6,7,8 | ArtID: 00149-21 | DOI:10.1128/MCB.00149-21 | CE: KGL-mab

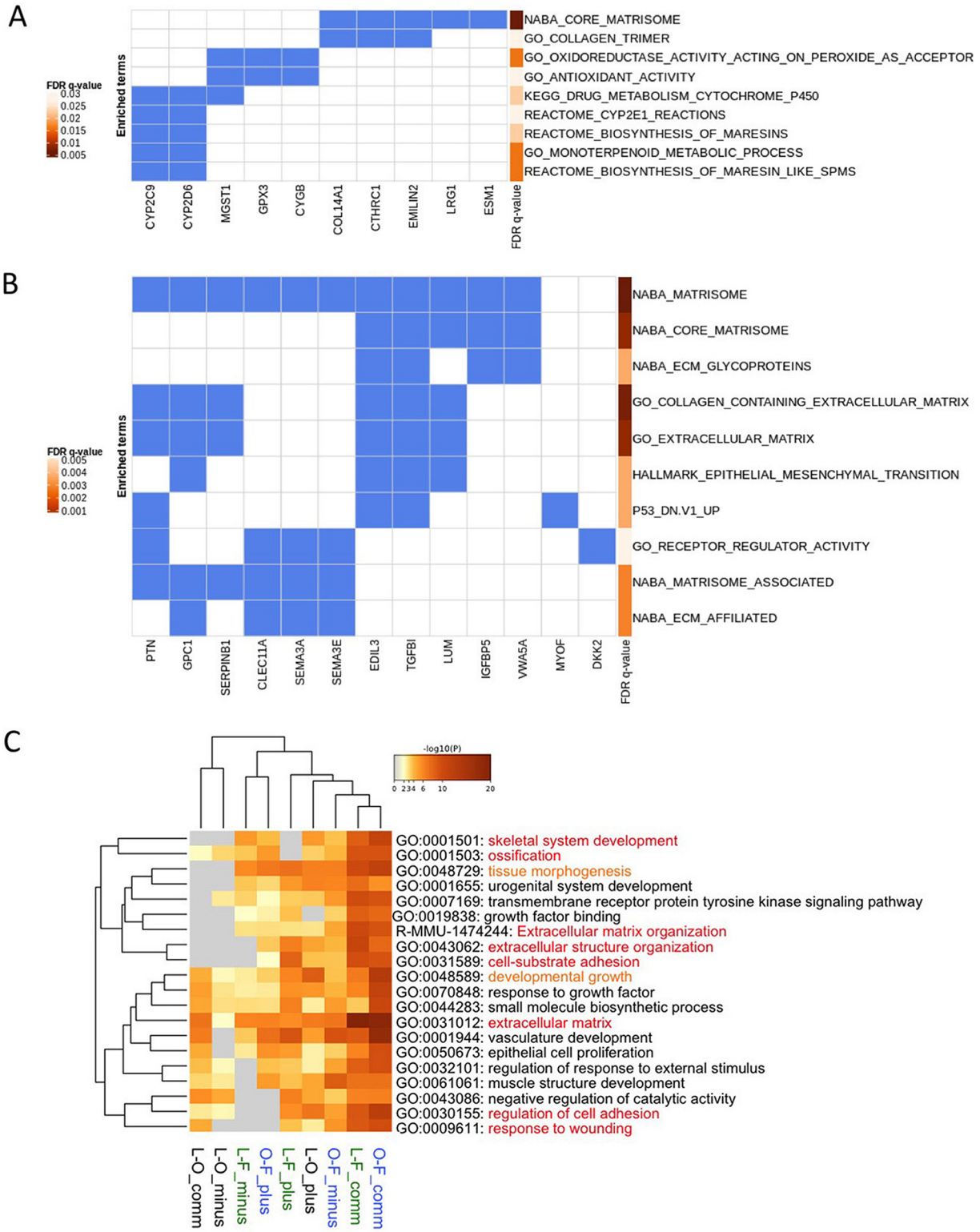

COLOR

FIG 5 Transcriptome analysis indicates a deficit of extracellular matrix- and ossification- related genes in Erf-insufficient cells. (A, B) The limited number of genes found to be significantly decreased in Erf-insufficient cells compared to Erf-competent cells (Table 1) were analyzed with the GSEA program and visualized with ComplexHeatmap in the R environment. The significance of the top 10 categories enriched in the query genes for the sdMSCs in osteogenic differentiation (A) and for the initial heterogeneous suture cell population (freshly isolated cells) (B) is shown. (C) Differentially expressed genes identified by transcriptome analysis (see Table S1 in the supplemental material) of sdMSCs (L), sdMSCs growing in osteogenic differentiation medium for 24 h ("O"), and freshly isolated suture cells ("F"), from Erf-competent ($Erf^{floxP/+}$; "plus") and Erf-insufficient ($Erf^{floxP/-}$; "minus") animals, were clustered, based on their ontology, with the Metascape program. L-O_comm, genes found to be differentially expressed during the 24-h induction of sdMSCs of both Erf-competent and Erf-insufficient cells; L-O_plus, genes found to be

(Continued on next page)

17/5/21 | 12:41 | 4/Color Fig: 1,2,3,4,5,6,7,8 | ArtID: 00149-21 | DOI:10.1128/MCB.00149-21 | CE: KGL-mab

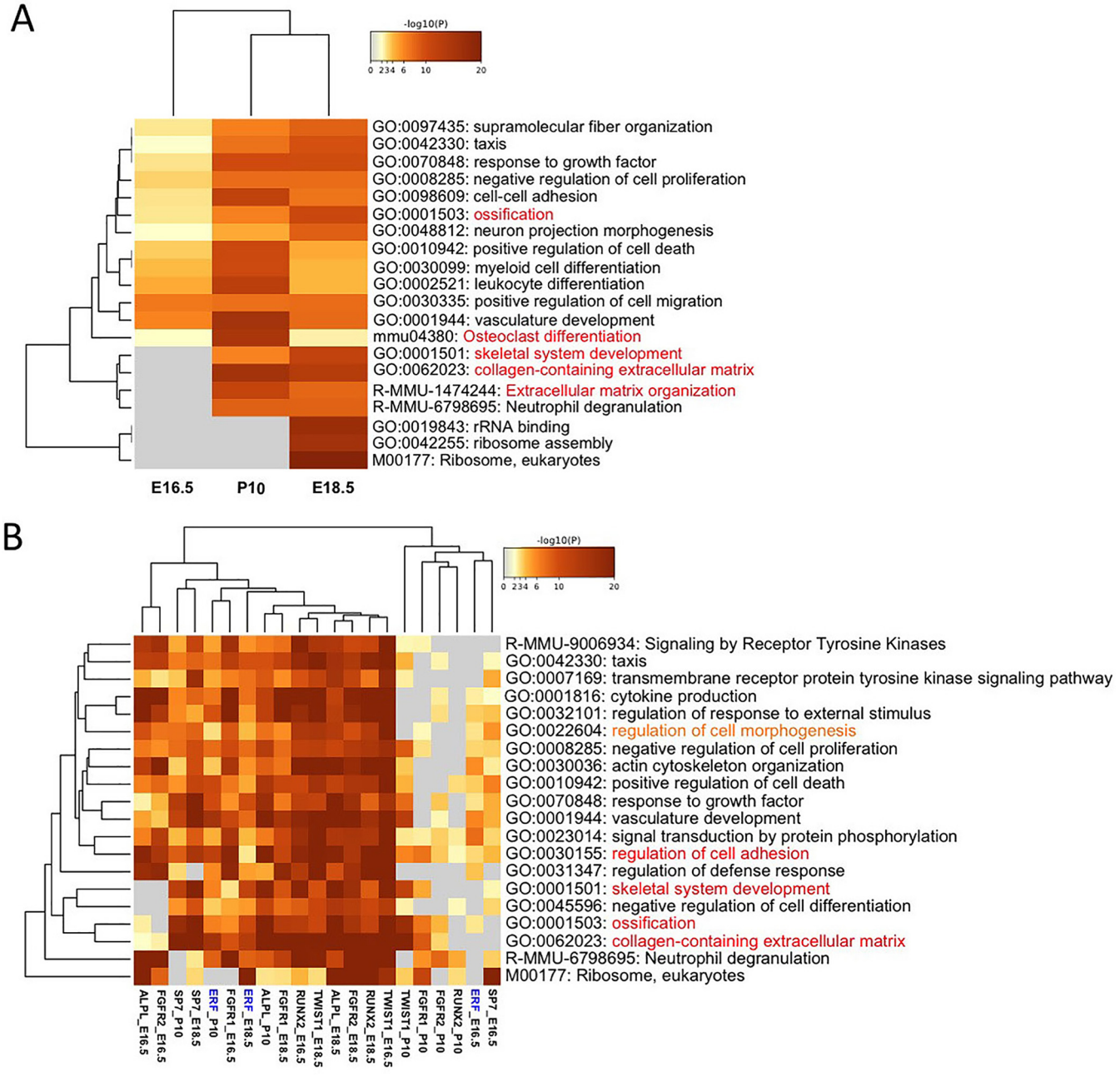

COLOR

FIG 6 *Erf* expression correlates with ossification- and extracellular matrix organization- related genes. (A) Genes found in mouse suture single-cell RNA sequencing experiments (see Table S2 in the supplemental material) to correlate with *Erf* expression were clustered based on their ontology with the Metascape program. P10, ~~small cytoplasmic~~ RNA sequencing (scRNA-seq) data from P10 animals; E16.5, scRNA-seq data from E16.5 embryos; E18.5, scRNA-seq data from E18.5 embryos. (B) As in panel A, but with the addition of data from genes correlated with *Alpl*, *Fgfr2*, *Runx2*, *Sp7*, and *Twist1* as markers for osteogenic differentiation stages. Red lettering indicates ossification-related and orange differentiation-related ontologies. Only the top 20 categories are shown.

Retinoic acid affects multiple developmental processes and pathways, and it has been suggested that its homeostasis is crucial for normal skeletogenesis (33, 54, 55). We thus evaluated the effect of RA on Erf-competent and Erf-insufficient sdMSCs. A characteristic feature of the differentiating suture-related $Erf^{loxP/-}$ sdMSCs is the higher

FIG 5 Legend (Continued)
differentially expressed during the 24-h induction only in the Erf-competent sdMSCs; L-O_minus, genes found to be differentially expressed during the 24-h induction only in the Erf-insufficient sdMSCs. "L-F" indicates genes found to be differentially expressed between sdMSCs and freshly isolated cells and "O-F" indicates differential expression between sdMSCs differentiating for 24 h and freshly isolated cells. Red lettering indicates ossification-related and orange lettering differentiation-related ontologies. Only the top 20 categories are shown. GO, gene ontology.

ID: gulrezaTime: 12:41I Path: //mumnasprod/home$/Mandar.Gawade$/SM-MCBJ210044

17/5/21 | 12:41 | 4/Color Fig: 1,2,3,4,5,6,7,8 | ArtID: 00149-21 | DOI:10.1128/MCB.00149-21 | CE: KGL-mab

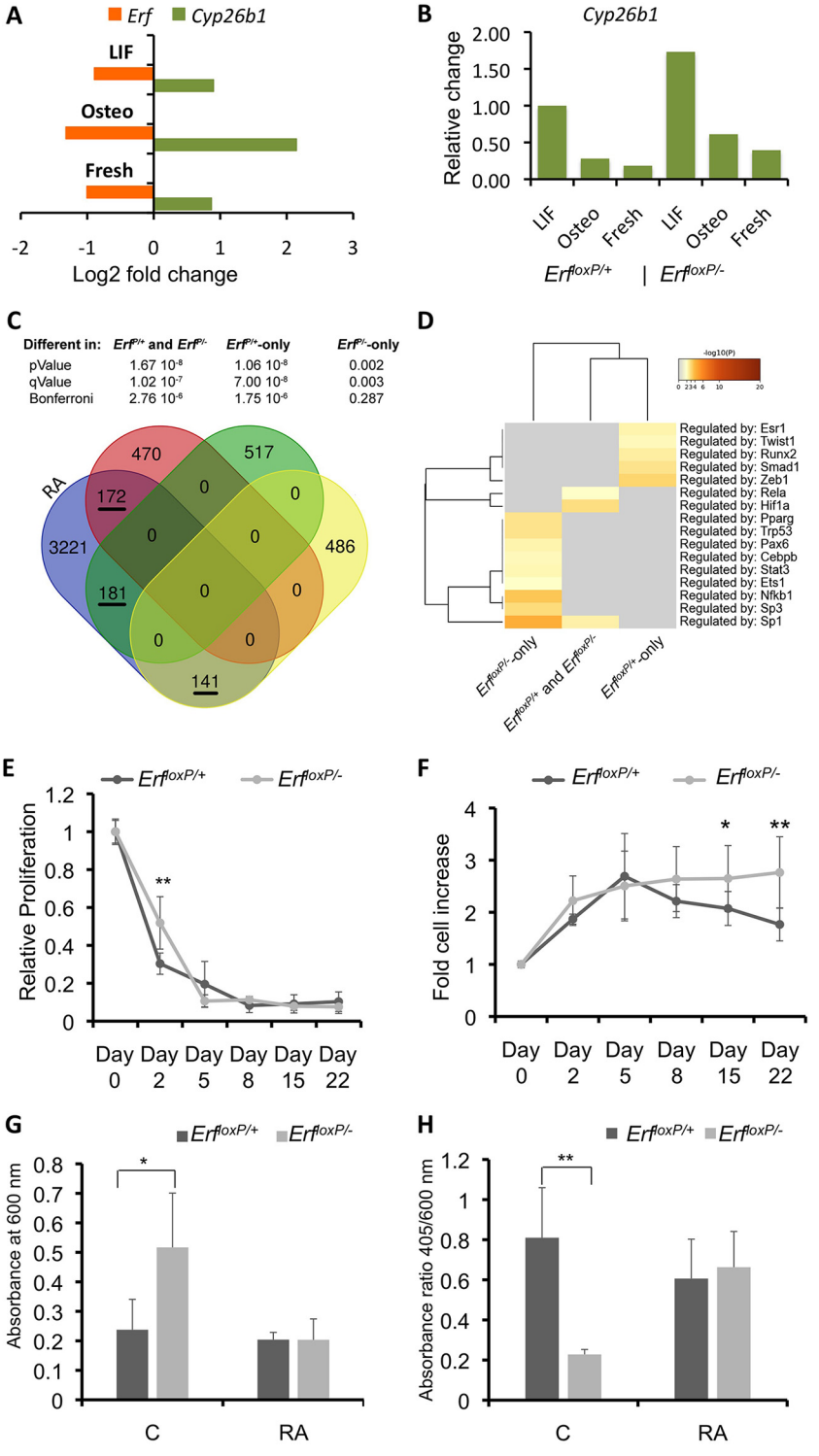

COLOR

FIG 7 Retinoic acid reverts the osteogenic deficiency of $Erf^{loxP/-}$ sdMSCs. (A) Fold change in the expression level of *Erf* and *Cyp26b1* between Erf-competent and Erf-deficient cells in self-renewing sdMSCs (LIF), differentiating sdMSCs (osteo) and freshly derived suture cells (fresh). (B) Relative expression level of *Cyp26b1* compared to Erf-competent ($Erf^{loxP/+}$) sdMSCs in proliferation medium (LIF). (C) Venn diagram showing genes differentially expressed during MSC differentiation for each genotype and genes found regulated in mouse embryonic stem cells (mESCs) after retinoic acid treatment. The table above indicates the significance of the enrichment in retinoic acid (RA)-related genes. The number of common genes in each comparison is underlined. (D) Analysis of genes associated with RA (underlined in panel C) via Metascape, in relation to other transcription factors. (E) Relative percentage of proliferating cells as estimated by BrdU incorporation during osteogenic

(Continued on next page)

17/5/21 | 12:41 | 4/Color Fig: 1,2,3,4,5,6,7,8 | ArtID: 00149-21 | DOI:10.1128/MCB.00149-21 | CE: KGL-mab

initial proliferation and final cell numbers (Fig. 7E and F), consistent with their decreased capacity to exit self-renewal and commit. Addition of retinoic acid at low concentrations does not appear to affect the growth/survival of Erf-competent sdMSCs (Fig. 7G). However, RA addition fully suppressed the increased cell numbers of the differentiating Erf-insufficient cells (Fig. 7G). More importantly, the decreased mineralization potential of $Erf^{loxP/-}$ cells was fully alleviated in the presence of RA without affecting the potential of the Erf-competent cells (Fig. 7H).

These data strongly suggest that Erf deficiency decreases retinoic acid levels leading to increased cellular proliferation and decreased osteogenic differentiation. Such changes could be the underlying cause of the late onset Erf-related craniosynostosis phenotype.

DISCUSSION

Syndromic craniosynostosis due to *ERF* haploinsufficiency presents some unique challenges and opportunities for disease understanding and management. In contrast to FGFR/MAPK-driven craniosynostosis syndromes, it has a late-onset phenotype, variable severity, and, in the mouse model, an initially decreased calvarial ossification. It would thus appear that Erf could mediate effects at multiple stages during suture development.

Understanding the formation of the cranial sutures is a challenging problem that is hampered by the multiple origins of the involved cells. We thus established a reliable and reproducible system to derive mesenchymal stem cells from murine cranial sutures and address the contribution of Erf levels in the process. Our cellular data indicate that although *Erf* elimination can affect multiple developmental processes, Erf insufficiency specifically attenuates osteogenic differentiation. This would be consistent with the role of Erk1/2 in sustaining the undifferentiated state of mesenchymal stem cells (56) and conforms with the absence of other major developmental defects in $Erf^{+/-}$ and $Erf^{loxP/-}$ mice (17, 18, 20). The transcriptional changes directly associated with Erf insufficiency were fairly limited, probably because the 50% reduction in *Erf* may not be sufficient to induce extensive quantitative changes that would evade our detection cutoff limits. However, the expression program during the differentiation of the sdMSCs was altered extensively as a result of the decreased Erf levels, suggesting a homeostatic effect or an effect on one or more morphogenetic factors.

One consistent effect of Erf insufficiency through all biological replicates and culture conditions was the elevated expression of *Cyp26b1*, a major retinoic acid catabolizing-enzyme, suggesting a possible decrease in retinoic acid levels affecting bone development (32–35, 54, 55, 57, 58). Consistently, addition of RA during differentiation of sdMSCs fully alleviated the Erf deficiency defect, with no apparent effect on Erf-competent cells, suggesting that *Erf*, through *Cyp26b1* regulation, affects retinoic acid levels, thus controlling the differentiation outcome. The inhibitory effect of Erf on *Cyp26b1* and the concomitant increase in retinoic acid levels would be consistent with the role of FGF, which has already been reported to activate *Cyp26b1* and downregulate RA availability (39, 40, 59). Given that Erf is inactivated via nuclear export as a result of Fgf signaling, the decreased Erf levels would resemble the increased Fgf signaling state.

It is unclear at this point if Erf regulates *Cyp26b1* directly or indirectly. Chromatin occupancy experiments in four independent mouse and human cellular systems, from our laboratory and others (20, 60–62), fail to identify any ERF binding site in the vicinity of *Cyp26b1*. The closest Erf

FIG 7 Legend (Continued)
differentiation of Erf-insufficient ($Erf^{loxP/-}$) and Erf-competent ($Erf^{loxP/+}$) sdMSCs. Data are derived from four independent biological experiments, each including two experimental replicates. (F) Relative cell number during the same experiment as in panel E. (G) Cell numbers, as evaluated by formazan absorbance after 28 days in osteogenic differentiation medium in the presence or absence ("C") of 0.5 μM all-*trans* retinoic acid (RA). (H) Calcification potential per cell as evaluated by the alizarin red S to formazan absorbance after 28 days of osteogenic differentiation in the presence or absence ("C") of 0.5 μM all-*trans* retinoic acid (RA). Data for panels A and B are derived from the RNA sequencing data set and analyzed as described in Materials and Methods. The values shown have a false-discovery rate (FDR) lower than 0.05. Data for panels G and H are from four experiments, and the statistical analysis was performed in all cases using an unpaired *t* test with two-tailed distribution. *, $P < 0.05$; **, $P < 0.01$; ***, $P < 0.001$.

17/5/21 | 12:41 | 4/Color Fig: 1,2,3,4,5,6,7,8 | ArtID: 00149-21 | DOI:10.1128/MCB.00149-21 | CE: KGL-mab

COLOR

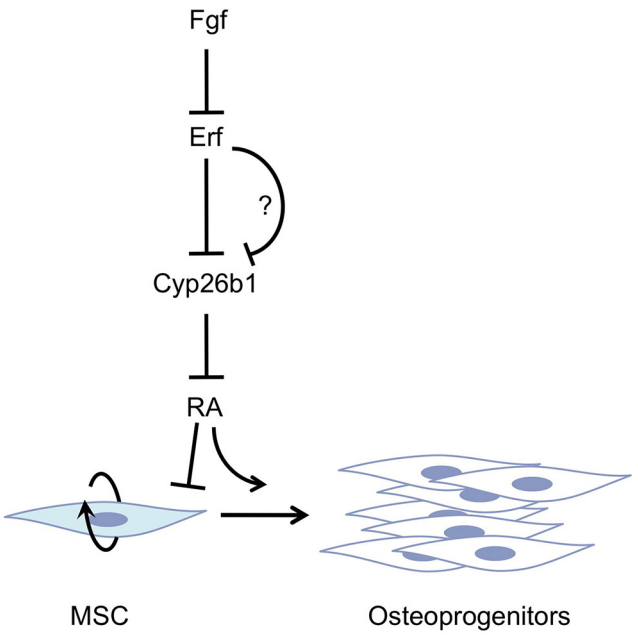

FIG 8 Mechanism of Erf effect in the osteogenic differentiation of cranial suture mesenchymal stem/progenitor cells. Erf, an FGF effector, affects the level of retinoic acid, possibly through the RA-catabolizing enzyme Cyp26b1. Decreased levels of Erf lead to increased levels of Cyp26b1, which in turn decrease retinoic acid levels, leading to reduced osteogenic differentiation and/or increased mesenchymal progenitor proliferation.

chromatin binding site appears to be 300 to 400 kb away in the proximity of the *Exoc6b* gene, rather than that of *Cyp26b1*. Neither reports of other Ets domain transcription factors directly affecting *Cyp26b1* transcription nor any confirmed functional Ets binding motifs in its regulatory regions have been found so far. Thus, Erf could affect its expression, either through a distal control element or indirectly by inhibiting a *Cyp26b1* activator (Fig. 8).

It is also conceivable that Erf levels affect MSC differentiation and homeostasis in synergy or in competition with other factors. We have previously shown a close proximity of Erf with Runx binding sites and a possible orchestrated regulation by the two factors (20). Erf could antagonize other Ets proteins, such as Ets1 and Ets2, that have been reported to affect skull shape and osteogenic differentiation (63, 64). Interestingly, genes differentially affected during Erf-competent and Erf-insufficient cell differentiation that harbor sites identified in Erf chromatin immunoprecipitation sequencing (ChIP-seq) experiments have these sites almost exclusively in putative regulatory regions and away from the transcription start site, where the repressive effect of Erf is more prominent (see Table S5 in the supplemental material). It would thus appear that Erf, in an orchestrated manner with other transcription factors, could regulate the homeostasis and kinetics of the process rather than being instructive.

The delayed ossification observed in MSC cultures may directly explain the early ossification defect observed in Erf-insufficient mice but may also be responsible for the craniosynostosis phenotype. Decreased MSC differentiation may lead to decreased populations of committed progenitor cells within the suture, which in turn fail to keep the suture open, resulting in craniosynostosis. Stem cell depletion (4), osteogenic differentiation-proliferation imbalance (6, 65, 66), and growth dynamics (67) have been previously proposed as potential mechanisms of synostosis. Indeed, there are several systems where *Erf* regulates differentiation. Chorionic trophoblast differentiation depends on *Erf* presence (17), *Erf* blocks the differentiation of Ras-deficient mESCs (62), and the rate of embryonic hematopoietic differentiation depends on *Erf* level (18). Whether Erf has additional roles, either positive or inhibitory ones, at later stages of the osteogenic differentiation pathway remains to be explored. Such an inhibitory

ID: gulrezaTime: 12:41I Path: //mumnasprod/home$/Mandar.Gawade$/SM-MCBJ210044

17/5/21 | 12:41 | 4/Color Fig: 1,2,3,4,5,6,7,8 | ArtID: 00149-21 | DOI:10.1128/MCB.00149-21 | CE: KGL-mab

effect in suture preosteoblast differentiation would be consistent with the reported function of Erk in late stages of the osteogenic pathway (68–70), as well as with the role of Runx2 in osteogenic differentiation and the antagonistic role of Erf (20), which could account for the craniosynostosis phenotype. Interestingly, comparable concentrations of retinoic acid have opposite effects on the mineralization of mesenchymal stem cells and more differentiated osteogenic populations such as MC3T3 preosteoblasts, with the former being induced and the latter being suppressed by RA (58, 71–75). Therefore, it is plausible that Erf, either through retinoic acid signaling or independently, could also affect the osteogenic pathway at later stages. Upon Erf deficiency, the initial decreased MSC differentiation and osteoprogenitor expansion could lead to decreased ossification, while an accelerated differentiation of progenitors when they comprise the predominant suture cell population could lead to depletion and premature ossification of the suture. Further studies would be necessary to explore the spatiotemporal function of Erf and its effect on RA concentration gradients in cranial bone and suture development.

In conclusion, our work provides evidence that Erf, an effector within the FGF/ERK pathway, affects suture formation and calvarial ossification through the regulation of retinoic acid levels.

MATERIALS AND METHODS

Mouse lines. Mice were bred and maintained in the animal facility of the Institute of Molecular Biology and Biotechnology (IMBB) in Greece. All experimental protocols were conducted with ethical guidelines and in compliance with the 3Rs. Protocols were approved by the bioethics committee of the IMBB and licensed from the General Directorate of Veterinary Services, Region Crete (permit numbers EL 91BIO-02 and EL91-BIOexp-02; project license no. 27289 to G. Mavrothalassitis). $Erf^{loxP/+}$ and $Erf^{loxP/-}$ littermates were obtained from crossing $Erf^{+/-}$ mice with $Erf^{loxP/loxP}$ mice, both of which have been reported in the literature (20).

Suture cell cultures and differentiation assays. Freshly isolated cranial suture cells were obtained as described previously (37, 58). Briefly, sagittal and coronal sutures containing approximately 0.5-mm bony margins were dissected from skulls of 5-day-old mice (P5). Following the removal of skin and dura mater, the suture explants were placed into 100-mm cell culture dishes, cut into tiny pieces, and cultured in the presence of Dulbecco's modified Eagle's medium (DMEM)-F12 medium (catalog no. 31330038; Gibco, Thermo Scientific) supplemented with 10% fetal bovine serum (FBS, catalog no. 10270106; Gibco, Thermo Scientific) and 100 U/ml penicillin/streptomycin (catalog no. 15140122; Gibco, Thermo Scientific) for 7 days. To obtain suture-derived long-term expanded mesenchymal stem/progenitor cells, suture explants were cultured into gelatinized dishes in the presence of KnockOut DMEM medium (catalog no. 10829018; Gibco, Thermo Scientific) supplemented with 12% FBS (catalog no. SV30160.03; HyClone, GE Healthcare), 2 mM L-glutamine (catalog no. 25030024; Gibco, Thermo Scientific), 1% nonessential amino acids (MEM-NEAA; catalog no. 11140050; Gibco, Thermo Scientific), 100 U/ml penicillin-streptomycin, 0.1 mM β-mercaptoethanol, and 0.3% vol/vol leukemia inhibitory factor (LIF; produced in our laboratory) for 7 days. Cells were then harvested and further cultured (without the explants) under the same conditions for a total of at least 8 population doublings (PDs) during a period of approximately 50 to 60 days (Fig. 1A). The cumulative population doubling level (CPD) was calculated as described in previous studies (76). At this stage, the cells were immunophenotypically evaluated by flow cytometric analysis and checked for osteogenic, chondrogenic, and adipogenic differentiation potential.

Osteogenic and chondrogenic differentiation was performed as described previously (77, 78). Osteogenesis was induced in 60 to 70% confluent cultures by the addition of DMEM (low glucose, catalog no. 21885025; Gibco, Thermo Scientific) supplemented with 10% FBS, 0.1 μM dexamethasone, 50 μM ascorbate-2-phosphate, and 10 mM β-glycerophosphate. In the experiments with retinoic acid, freshly prepared osteogenesis medium was supplemented with all-*trans* retinoic acid at a final concentration of 0.5 μM before every medium change. Adipogenesis was induced in postconfluence cultures by switching between adipogenic induction and adipogenic maintenance medium (79). One cycle of induction-maintenance was performed for freshly isolated suture cells and 3 cycles for LIF selection-subjected long-term expanded mesenchymal stem/progenitor cells. To assess the extent of differentiation, staining of cultures with oil red O (catalog no. O-9755; Sigma) and alcian blue (catalog no. A-5268; Sigma) was performed for the detection of adipocytes and cartilage, respectively. The evaluation of osteogenic differentiation was performed by alizarin red S (Sigma A-5533) staining of the cultures, followed by acetic acid extraction and quantification of the dye at 405 nm as already described (80).

Cell growth and viability studies. Cell doubling time was estimated at specific population doubling levels of the culture by using the already described logarithmic equation (81). The cell cycle phase study was performed in isolated nuclei by propidium iodide (PI) staining of cells in hypotonic solution (82), followed by flow cytometric analysis. Cells of population doubling level 20 (20 PDs) at 60 to 70% culture confluence were used in all cell cycle experiments. Data were analyzed using ModFitLT software. In order to evaluate the viability of cells during the osteogenic differentiation, an MTT [3-(4,5-dimethyl-2-thiazolyl)-2,5-diphenyl-2H-tetrazolium bromide] assay was conducted, and formazan absorbance was measured at 600 nm (83).

For *in vitro* proliferation assays, bromodeoxyuridine (BrdU; catalog no. B5002; Sigma) was added to the cell culture medium at a final concentration of 10 μM for 8 h, followed by fixation of the cells with 4%

ID: gulrezaTime: 12:41I Path: //mumnasprod/home$/Mandar.Gawade$/SM-MCBJ210044

17/5/21 | 12:41 | 4/Color Fig: 1,2,3,4,5,6,7,8 | ArtID: 00149-21 | DOI:10.1128/MCB.00149-21 | CE: KGL-mab

paraformaldehyde (PFA) solution. The detection of BrdU-positive cells was performed using the following antibodies and reagents: rat anti-BrdU antibody (catalog no. MCA2060GA; AbD Serotec) at a dilution of 1:800, biotin-conjugated anti-rat antibody (catalog no. B7139; Sigma) at 1:100, and fluorescein isothiocyanate (FITC)-conjugated streptavidin (catalog no. 405201; BioLegend) at 1:1,000. A TCS SP2 confocal microscope (Leica Microsystems) and an Operetta imaging system were used for signal visualization and analysis.

Flow cytometric analysis. LIF selection-subjected mesenchymal stem/progenitor cells of 8 PDs were harvested using 0.25% trypsin-EDTA solution (catalog no. 25200072; Gibco, Thermo Scientific) for 2 min at 37°C and stained with the following antibodies in 1% FBS-phosphate-buffered saline (PBS) solution for 30 min at 4°C: FITC-conjugated anti-CD44 (catalog no. 103006; BioLegend) at a dilution of 1:100, allophycocyanin (APC)-conjugated anti-Sca1 (catalog no. 108111; BioLegend) at 1:100, phycoerythrin (PE)-conjugated anti-CD105 (catalog no. 120407; BioLegend) at 1:200, PE/Cy5-conjugated anti-CD29 (catalog no. 102219; BioLegend) at 1:200, PE/Cy7-conjugated anti-CD90.2 (catalog no. 105325; BioLegend) at 1:600, PerCP/Cy5.5-conjugated anti-CD45 (catalog no. 103131; BioLegend) at 1:400, PE-conjugated anti-CD31 (catalog no. 553373; BD Pharmingen) at 1:200, and APC-conjugated anti-CD34 (catalog no. 119309; BioLegend) at 1:100. A Becton, Dickinson FACSCalibur flow cytometer was used in all experiments. The analysis was performed using Flowing Software version 2.5.1.

Quantitative PCR. Total RNA was extracted from cultured suture cells using TRI reagent (catalog no. T9424; Sigma) according to company's instructions. The mRNA was reverse transcribed using the SuperScript first-strand synthesis kit (catalog no. 11904-018), and 5 ng of the total synthesized cDNA was added in each real-time qPCR using 2× Brilliant III SYBR green quantitative PCR (qPCR) master mix (catalog no. 600882-51; Agilent) in an Applied Biosystems StepOne Plus real-time PCR machine. The expression levels of the following genes were detected using the following sets of primers: *Axin2* FW, 5′-AGCCTAAAGGTCTTATGTGG-3′, and RV, 5′-ATGGAATCGTCGGTCAGT-3′; *Osterix* (*Sp7*) FW, 5′-TCTGCTTGAGGAAGAAGCTC-3′, and RV, 5′-TCCATTGGTGC TTGAGAAGG-3′; and *Gapdh* FW, 5′-CCAGTATGACTCCACTCACG-3′, and RV, 5′-GACTCCACGACATACTCAGC-3′. The expression levels of the genes of interest were normalized to *Gapdh* expression levels for each particular sample.

RNA sequencing. Total RNA was isolated using the Qiagen RNeasy minikit. Each biological replicate was created by pooling suture-derived cells of at least three mice. Three or four independent biological replicates were conducted for the conditions tested. Next-generation sequencing (NGS) libraries were generated from 500 ng input total RNA with the Lexogen-QuantSeq 3′ mRNA-Seq library prep kit FWD
AQ: G for Illumina and run on an Illumina 500 instrument on 1 × 150 FlowCells.

Fastq files from Illumina BaseSpace were mapped to the mm10 genome (iGenomes UCSC/mm10) using hisat2 version 2.1.0 ("-score-min L 0,−0.5") (84). Gene counts were computed with htseq-count ("-s yes"; version 0.11.2) (85). Differential analysis was performed with edgeR version 3.24.3 (86, 87). Genes with a cpm of >2 in at least 3 samples were included in the analysis. Samples were normalized by trimmed mean of M-values (TMM). Sample grouping for the design matrix was performed by one combined factor, which took into account ERF status, (plus = ~~wild type~~ cells, minus = ~~ERF knockdown [KD]~~ cells) coupled to differentiation status (fresh = freshly harvested; LIF = long-term expanded; osteo = osteogenically induced), and also including batch
AQ: H effect correction [model.matrix(~0+ERFstatus.DIFFstatus+batch)]. Differential analyses were performed by likelihood ratio tests using the estimated negative binomial common dispersion.

Single-cell correlation analysis. Count matrices of ~~small cytoplasmic~~ RNA sequencing (scRNA-seq) data were first filtered following the quality assessment suggested by Harvard Chan Bioinformatics Core (https://hbctraining.github.io/scRNA-seq/lessons/04_SC_quality_control.html) and normalized following
AQ: I Seurat's default method (88). Features that were not detected in at least 2% of the cells were also eliminated to improve reliability of a possible correlation. Gene correlations with the false discovery rate at 0.05 significance were calculated using the "corr.test function" (89) in the R statistical environment (90). The Wilcoxon rank sum test, as implemented in the "wilcox.test" function from the *stats* package (90), was used to further evaluate differences in the distribution of the correlated gene in cells expressing the target gene or not. Enrichment analysis sets for *Mus musculus* were performed with the *gprofiler2* package (91), with a statistical domain size comprising genes that have at least one annotation and with the g:SCS multiple testing correction method. The whole workflow was implemented in R version 3.6.1 (5 July 2019). Clustering of correlated gene sets across different scRNA data sets and target genes was visualized with the Metascape web tool (53) and ComplexHeatmap (92). The analysis software and genelist files are deposited at https://github.com/mpaltsai/iRNA_project.

Statistical analysis. All experiments had a minimum of two biological replicates and two experimental replicates for each. At least 3 or 4 sibling mice were used to derive each biological sdMSC sample. Variation among experimental replicates was minimal. Equal numbers of experimental replicates were used for each biological replicate in each experiment. The data, unless otherwise stated, were analyzed using SPSS software. An unpaired (two-sided) *t* test was conducted for comparisons between two groups, and one-way analysis of variance (ANOVA) was performed for multiple comparisons, followed by a *post hoc* Dunnett's two-sided test according to the experimental requirements. Levels of significance were as follows: *, $P < 0.05$; **, $P < 0.01$; ***, $P < 0.001$.

Data availability. Sequencing data are deposited in the BioProject database under accession number
AQ: J PRJNA664970.

SUPPLEMENTAL MATERIAL

Supplemental material is available online only.

SUPPLEMENTAL FILE 1, XLSX file, 0.2 MB.

ID: gulrezaTime: 12:41I Path: //mumnasprod/home$/Mandar.Gawade$/SM-MCBJ210044

17/5/21 | 12:41 | 4/Color Fig: 1,2,3,4,5,6,7,8 | ArtID: 00149-21 | DOI:10.1128/MCB.00149-21 | CE: KGL-mab

ACKNOWLEDGMENTS

We are grateful to the IMBB Animal House and Gene Targeting Facility personnel for mouse breeding and maintenance and to the Genomics Facility personnel for high-throughput RNA sequencing.

This work was supported by IKY-SIEMENS grant AP2788 and GSRT Bioimaging-GR grant KA4937 to G.M. and by Onassis Foundation Fellowship GZM 008-1 to A.V. Work in Oxford was supported by Action Medical Research (GN2483; S.R.F.T.), the MRC through the WIMM Strategic Alliance (G0902418 and MC_UU_12025), the National Institute for Health Research, and Wellcome (investigator award 102731 to A.O.M.W. and project grant 093329 to A.O.M.W. and S.R.F.T.).

AQ: K

For the purpose of open access, the authors have applied a CC BY public copyright license to any author-accepted manuscript version arising from this submission.

We declare no conflicts of interest.

REFERENCES

1. Morriss-Kay GM, Wilkie AO. 2005. Growth of the normal skull vault and its alteration in craniosynostosis: insights from human genetics and experimental studies. J Anat 207:637–653. https://doi.org/10.1111/j.1469-7580.2005.00475.x.
2. Opperman LA. 2000. Cranial sutures as intramembranous bone growth sites. Dev Dyn 219:472–485. https://doi.org/10.1002/1097-0177(2000)9999:9999<::AID-DVDY1073>3.0.CO;2-F.
3. Debnath S, Yallowitz AR, McCormick J, Lalani S, Zhang T, Xu R, Li N, Liu Y, Yang YS, Eiseman M, Shim JH, Hameed M, Healey JH, Bostrom MP, Landau DA, Greenblatt MB. 2018. Discovery of a periosteal stem cell mediating intramembranous bone formation. Nature 562:133–139. https://doi.org/10.1038/s41586-018-0554-8.
4. Zhao H, Feng J, Ho TV, Grimes W, Urata M, Chai Y. 2015. The suture provides a niche for mesenchymal stem cells of craniofacial bones. Nat Cell Biol 17:386–396. https://doi.org/10.1038/ncb3139.
5. Lana-Elola E, Rice R, Grigoriadis AE, Rice DP. 2007. Cell fate specification during calvarial bone and suture development. Dev Biol 311:335–346. https://doi.org/10.1016/j.ydbio.2007.08.028.
6. Fragale A, Tartaglia M, Bernardini S, Di Stasi AM, Di Rocco C, Velardi F, Teti A, Battaglia PA, Migliaccio S. 1999. Decreased proliferation and altered differentiation in osteoblasts from genetically and clinically distinct craniosynostotic disorders. Am J Pathol 154:1465–1477. https://doi.org/10.1016/S0002-9440(10)65401-6.
7. Twigg SR, Wilkie AO. 2015. A genetic-pathophysiological framework for craniosynostosis. Am J Hum Genet 97:359–377. https://doi.org/10.1016/j.ajhg.2015.07.006.
8. Johnson D, Wilkie AO. 2011. Craniosynostosis. Eur J Hum Genet 19:369–376. https://doi.org/10.1038/ejhg.2010.235.
9. Yin L, Du X, Li C, Xu X, Chen Z, Su N, Zhao L, Qi H, Li F, Xue J, Yang J, Jin M, Deng C, Chen L. 2008. A Pro253Arg mutation in fibroblast growth factor receptor 2 (Fgfr2) causes skeleton malformation mimicking human Apert syndrome by affecting both chondrogenesis and osteogenesis. Bone 42:631–643. https://doi.org/10.1016/j.bone.2007.11.019.
10. Shukla V, Coumoul X, Wang RH, Kim HS, Deng CX. 2007. RNA interference and inhibition of MEK-ERK signaling prevent abnormal skeletal phenotypes in a mouse model of craniosynostosis. Nat Genet 39:1145–1150. https://doi.org/10.1038/ng2096.
11. Pfaff MJ, Xue K, Li L, Horowitz MC, Steinbacher DM, Eswarakumar JVP. 2016. FGFR2c-mediated ERK-MAPK activity regulates coronal suture development. Dev Biol 415:242–250. https://doi.org/10.1016/j.ydbio.2016.03.026.
12. Vogiatzi A, Mavrothalassitis G. 2019. Craniofacial, orofacial and dental disorders: the role of the RAS/ERK pathway. Expert Rev Mol Med 21:e2. https://doi.org/10.1017/erm.2019.2.
13. Miraoui H, Marie PJ. 2010. Fibroblast growth factor receptor signaling crosstalk in skeletogenesis. Sci Signal 3:re9. https://doi.org/10.1126/scisignal.3146re9.
14. Ornitz DM, Marie PJ. 2015. Fibroblast growth factor signaling in skeletal development and disease. Genes Dev 29:1463–1486. https://doi.org/10.1101/gad.266551.115.
15. Le Gallic L, Sgouras D, Beal G, Jr, Mavrothalassitis G. 1999. Transcriptional repressor ERF is a Ras/mitogen-activated protein kinase target that regulates cellular proliferation. Mol Cell Biol 19:4121–4133. https://doi.org/10.1128/mcb.19.6.4121.
16. Le Gallic L, Virgilio L, Cohen P, Biteau B, Mavrothalassitis G. 2004. ERF nuclear shuttling, a continuous monitor of Erk activity that links it to cell cycle progression. Mol Cell Biol 24:1206–1218. https://doi.org/10.1128/mcb.24.3.1206-1218.2004.
17. Papadaki C, Alexiou M, Cecena G, Verykokakis M, Bilitou A, Cross JC, Oshima RG, Mavrothalassitis G. 2007. Transcriptional repressor *Erf* determines extraembryonic ectoderm differentiation. Mol Cell Biol 27:5201–5213. https://doi.org/10.1128/MCB.02237-06.
18. Peraki I, Palis J, Mavrothalassitis G. 2017. The Ets2 repressor factor (Erf) is required for effective primitive and definitive hematopoiesis. Mol Cell Biol 37:e00183-17. https://doi.org/10.1128/MCB.00183-17.
19. Glass GE, O'Hara J, Canham N, Cilliers D, Dunaway D, Fenwick AL, Jeelani NO, Johnson D, Lester T, Lord H, Morton JEV, Nishikawa H, Noons P, Schwiebert K, Shipster C, Taylor-Beadling A, Twigg SRF, Vasudevan P, Wall SA, Wilkie AOM, Wilson LC. 2019. ERF-related craniosynostosis: the phenotypic and developmental profile of a new craniosynostosis syndrome. Am J Med Genet A 179:615–627. https://doi.org/10.1002/ajmg.a.61073.
20. Twigg SR, Vorgia E, McGowan SJ, Peraki I, Fenwick AL, Sharma VP, Allegra M, Zaragkoulias A, Sadighi Akha E, Knight SJ, Lord H, Lester T, Izatt L, Lampe AK, Mohammed SN, Stewart FJ, Verloes A, Wilson LC, Healy C, Sharpe PT, Hammond P, Hughes J, Taylor S, Johnson D, Wall SA, Mavrothalassitis G, Wilkie AO. 2013. Reduced dosage of ERF causes complex craniosynostosis in humans and mice and links ERK1/2 signaling to regulation of osteogenesis. Nat Genet 45:308–313. https://doi.org/10.1038/ng.2539.
21. Clagett-Dame M, DeLuca HF. 2002. The role of vitamin A in mammalian reproduction and embryonic development. Annu Rev Nutr 22:347–381. https://doi.org/10.1146/annurev.nutr.22.010402.102745E.
22. Duester G. 2008. Retinoic acid synthesis and signaling during early organogenesis. Cell 134:921–931. https://doi.org/10.1016/j.cell.2008.09.002.
23. Dersch H, Zile MH. 1993. Induction of normal cardiovascular development in the vitamin A-deprived quail embryo by natural retinoids. Dev Biol 160:424–433. https://doi.org/10.1006/dbio.1993.1318.
24. Dickman ED, Thaller C, Smith SM. 1997. Temporally-regulated retinoic acid depletion produces specific neural crest, ocular and nervous system defects. Development 124:3111–3121. https://doi.org/10.1242/dev.124.16.3111.
25. Lohnes D, Mark M, Mendelsohn C, Dolle P, Dierich A, Gorry P, Gansmuller A, Chambon P. 1994. Function of the retinoic acid receptors (RARs) during development (I). Craniofacial and skeletal abnormalities in RAR double mutants. Development 120:2723–2748. https://doi.org/10.1242/dev.120.10.2723.
26. Mendelsohn C, Lohnes D, Decimo D, Lufkin T, LeMeur M, Chambon P, Mark M. 1994. Function of the retinoic acid receptors (RARs) during development (II). Multiple abnormalities at various stages of organogenesis in RAR double mutants. Development 120:2749–2771. https://doi.org/10.1242/dev.120.10.2749.
27. Martinez-Morales PL, Diez del Corral R, Olivera-Martinez I, Quiroga AC, Das RM, Barbas JA, Storey KG, Morales AV. 2011. FGF and retinoic acid activity gradients control the timing of neural crest cell emigration in the trunk. J Cell Biol 194:489–503. https://doi.org/10.1083/jcb.201011077.
28. Sirbu IO, Zhao X, Duester G. 2008. Retinoic acid controls heart anteroposterior patterning by down-regulating Isl1 through the Fgf8 pathway. Dev Dyn 237:1627–1635. https://doi.org/10.1002/dvdy.21570.

ID: gulrezaTime: 12:41I Path: //mumnasprod/home$/Mandar.Gawade$/SM-MCBJ210044

17/5/21 | 12:41 | 4/Color Fig: 1,2,3,4,5,6,7,8 | ArtID: 00149-21 | DOI:10.1128/MCB.00149-21 | CE: KGL-mab

29. Geelen JA. 1979. Hypervitaminosis A induced teratogenesis. CRC Crit Rev Toxicol 6:351–375. https://doi.org/10.3109/10408447909043651.
30. Gardner JS, Guyard-Boileau B, Alderman BW, Fernbach SK, Greene C, Mangione EJ. 1998. Maternal exposure to prescription and non-prescription pharmaceuticals or drugs of abuse and risk of craniosynostosis. Int J Epidemiol 27:64–67. https://doi.org/10.1093/ije/27.1.64.
31. Yip JE, Kokich VG, Shepard TH. 1980. The effect of high doses of retinoic acid on prenatal craniofacial development in *Macaca nemestrina*. Teratology 21:29–38. https://doi.org/10.1002/tera.1420210105.
32. Laue K, Pogoda HM, Daniel PB, van Haeringen A, Alanay Y, von Ameln S, Rachwalski M, Morgan T, Gray MJ, Breuning MH, Sawyer GM, Sutherland-Smith AJ, Nikkels PG, Kubisch C, Bloch W, Wollnik B, Hammerschmidt M, Robertson SP. 2011. Craniosynostosis and multiple skeletal anomalies in humans and zebrafish result from a defect in the localized degradation of retinoic acid. Am J Hum Genet 89:595–606. https://doi.org/10.1016/j.ajhg.2011.09.015.
33. Leitch VD, Dwivedi PP, Anderson PJ, Powell BC. 2013. Retinol-binding protein 4 downregulation during osteogenesis and its localization to non-endocytic vesicles in human cranial suture mesenchymal cells suggest a novel tissue function. Histochem Cell Biol 139:75–87. https://doi.org/10.1007/s00418-012-1011-7.
34. Maclean G, Dolle P, Petkovich M. 2009. Genetic disruption of CYP26B1 severely affects development of neural crest derived head structures, but does not compromise hindbrain patterning. Dev Dyn 238:732–745. https://doi.org/10.1002/dvdy.21878.
35. Ferguson JW, Devarajan M, Atit RP. 2018. Stage-specific roles of Ezh2 and retinoic acid signaling ensure calvarial bone lineage commitment. Dev Biol 443:173–187. https://doi.org/10.1016/j.ydbio.2018.09.014.
36. Draut H, Liebenstein T, Begemann G. 2019. New insights into the control of cell fate choices and differentiation by retinoic acid in cranial, axial and caudal structures. Biomolecules 9:860. https://doi.org/10.3390/biom9120860.
37. Xu Y, Malladi P, Chiou M, Longaker MT. 2007. Isolation and characterization of posterofrontal/sagittal suture mesenchymal cells *in vitro*. Plast Reconstr Surg 119:819–829. https://doi.org/10.1097/01.prs.0000255540.91987.a0.
38. Aubin JE, Liu F, Malaval L, Gupta AK. 1995. Osteoblast and chondroblast differentiation. Bone 17:77S–83S. https://doi.org/10.1016/8756-3282(95)00183-E.
39. Mercader N, Leonardo E, Piedra ME, Martinez AC, Ros MA, Torres M. 2000. Opposing RA and FGF signals control proximodistal vertebrate limb development through regulation of Meis genes. Development 127:3961–3970. https://doi.org/10.1242/dev.127.18.3961.
40. Probst S, Kraemer C, Demougin P, Sheth R, Martin GR, Shiratori H, Hamada H, Iber D, Zeller R, Zuniga A. 2011. SHH propagates distal limb bud development by enhancing CYP26B1-mediated retinoic acid clearance via AER-FGF signalling. Development 138:1913–1923. https://doi.org/10.1242/dev.063966.
41. Deng MJ, Jin Y, Shi JN, Lu HB, Liu Y, He DW, Nie X, Smith AJ. 2004. Multilineage differentiation of ectomesenchymal cells isolated from the first branchial arch. Tissue Eng 10:1597–1606. https://doi.org/10.1089/ten.2004.10.1597.
42. Malaval L, Gupta AK, Aubin JE. 1995. Leukemia inhibitory factor inhibits osteogenic differentiation in rat calvaria cell cultures. Endocrinology 136:1411–1418. https://doi.org/10.1210/endo.136.4.7895651.
43. Maruyama T, Jeong J, Sheu TJ, Hsu W. 2016. Stem cells of the suture mesenchyme in craniofacial bone development, repair and regeneration. Nat Commun 7:10526. https://doi.org/10.1038/ncomms10526.
44. Dominici M, Le Blanc K, Mueller I, Slaper-Cortenbach I, Marini F, Krause D, Deans R, Keating A, Prockop D, Horwitz E. 2006. Minimal criteria for defining multipotent mesenchymal stromal cells. The International Society for Cellular Therapy position statement. Cytotherapy 8:315–317. https://doi.org/10.1080/14653240600855905.
45. da Silva Meirelles L, Nardi NB. 2003. Murine marrow-derived mesenchymal stem cell: isolation, *in vitro* expansion, and characterization. Br J Haematol 123:702–711. https://doi.org/10.1046/j.1365-2141.2003.04669.x.
46. Zhu H, Guo ZK, Jiang XX, Li H, Wang XY, Yao HY, Zhang Y, Mao N. 2010. A protocol for isolation and culture of mesenchymal stem cells from mouse compact bone. Nat Protoc 5:550–560. https://doi.org/10.1038/nprot.2009.238.
47. Verykokakis M, Papadaki C, Vorgia E, Le Gallic L, Mavrothalassitis G. 2007. The RAS-dependent ERF control of cell proliferation and differentiation is mediated by c-Myc repression. J Biol Chem 282:30285–30294. https://doi.org/10.1074/jbc.M704428200.
48. Subramanian A, Tamayo P, Mootha VK, Mukherjee S, Ebert BL, Gillette MA, Paulovich A, Pomeroy SL, Golub TR, Lander ES, Mesirov JP. 2005. Gene set enrichment analysis: a knowledge-based approach for interpreting genome-wide expression profiles. Proc Natl Acad Sci U S A 102:15545–15550. https://doi.org/10.1073/pnas.0506580102.
49. Brinkley JF, Fisher S, Harris MP, Holmes G, Hooper JE, Jabs EW, Jones KL, Kesselman C, Klein OD, Maas RL, Marazita ML, Selleri L, Spritz RA, van Bakel H, Visel A, Williams TJ, Wysocka J, FaceBase C, Chai Y, FaceBase Consortium. 2016. The FaceBase Consortium: a comprehensive resource for craniofacial researchers. Development 143:2677–2688. https://doi.org/10.1242/dev.135434.
50. Holmes G, Gonzalez-Reiche AS, Lu N, Zhou X, Rivera J, Kriti D, Sebra R, Williams AA, Donovan MJ, Potter SS, Pinto D, Zhang B, van Bakel H, Jabs EW. 2020. Integrated transcriptome and network analysis reveals spatiotemporal dynamics of calvarial suturogenesis. Cell Rep 32:107871. https://doi.org/10.1016/j.celrep.2020.107871.
51. Falker-Gieske C, Mott A, Franzenburg S, Tetens J. 2021. Multi-species transcriptome meta-analysis of the response to retinoic acid in vertebrates and comparative analysis of the effects of retinol and retinoic acid on gene expression in LMH cells. BMC Genomics 22:146. https://doi.org/10.1186/s12864-021-07451-2.
52. Terranova C, Narla ST, Lee YW, Bard J, Parikh A, Stachowiak EK, Tzanakakis ES, Buck MJ, Birkaya B, Stachowiak MK. 2015. Global developmental gene programming involves a nuclear form of fibroblast growth factor receptor-1 (FGFR1). PLoS One 10:e0123380. https://doi.org/10.1371/journal.pone.0123380.
53. Zhou Y, Zhou B, Pache L, Chang M, Khodabakhshi AH, Tanaseichuk O, Benner C, Chanda SK. 2019. Metascape provides a biologist-oriented resource for the analysis of systems-level datasets. Nat Commun 10:1523. https://doi.org/10.1038/s41467-019-09234-6.
54. Spoorendonk KM, Peterson-Maduro J, Renn J, Trowe T, Kranenbarg S, Winkler C, Schulte-Merker S. 2008. Retinoic acid and Cyp26b1 are critical regulators of osteogenesis in the axial skeleton. Development 135:3765–3774. https://doi.org/10.1242/dev.024034.
55. Roberts C. 2020. Regulating retinoic acid availability during development and regeneration: the role of the CYP26 enzymes. J Dev Biol 8:6. https://doi.org/10.3390/jdb8010006.
56. Pricola KL, Kuhn NZ, Haleem-Smith H, Song Y, Tuan RS. 2009. Interleukin-6 maintains bone marrow-derived mesenchymal stem cell stemness by an ERK1/2-dependent mechanism. J Cell Biochem 108:577–588. https://doi.org/10.1002/jcb.22289.
57. Song HM, Nacamuli RP, Xia W, Bari AS, Shi YY, Fang TD, Longaker MT. 2005. High-dose retinoic acid modulates rat calvarial osteoblast biology. J Cell Physiol 202:255–262. https://doi.org/10.1002/jcp.20115.
58. James AW, Levi B, Xu Y, Carre AL, Longaker MT. 2010. Retinoic acid enhances osteogenesis in cranial suture-derived mesenchymal cells: potential mechanisms of retinoid-induced craniosynostosis. Plast Reconstr Surg 125:1352–1361. https://doi.org/10.1097/PRS.0b013e3181d62980.
59. Gonzalez-Quevedo R, Lee Y, Poss KD, Wilkinson DG. 2010. Neuronal regulation of the spatial patterning of neurogenesis. Dev Cell 18:136–147. https://doi.org/10.1016/j.devcel.2009.11.010.
60. Bao X, Zhang X, Wang L, Wang Z, Huang J, Zhang Q, Ye Y, Liu Y, Chen D, Zuo Y, Liu Q, Xu P, Huang B, Fang J, Lao J, Feng X, Li Y, Kurita R, Nakamura Y, Yu W, Ju C, Huang C, Mohandas N, Li D, Zhao C, Xu X. 2021. Epigenetic inactivation of ERF reactivates gamma-globin expression in beta-thalassemia. Am J Hum Genet 108:709–721. https://doi.org/10.1016/j.ajhg.2021.03.005.
61. Bose R, Karthaus WR, Armenia J, Abida W, Iaquinta PJ, Zhang Z, Wongvipat J, Wasmuth EV, Shah N, Sullivan PS, Doran MG, Wang P, Patruno A, Zhao Y, Zheng D, Schultz N, Sawyers CL, International SU2C/PCF Prostate Cancer Dream Team. 2017. ERF mutations reveal a balance of ETS factors controlling prostate oncogenesis. Nature 546:671–675. https://doi.org/10.1038/nature22820.
62. Mayor-Ruiz C, Olbrich T, Drosten M, Lecona E, Vega-Sendino M, Ortega S, Dominguez O, Barbacid M, Ruiz S, Fernandez-Capetillo O. 2018. ERF deletion rescues RAS deficiency in mouse embryonic stem cells. Genes Dev 32:568–576. https://doi.org/10.1101/gad.310086.117.
63. Sumarsono SH, Wilson TJ, Tymms MJ, Venter DJ, Corrick CM, Kola R, Lahoud MH, Papas TS, Seth A, Kola I. 1996. Down's syndrome-like skeletal abnormalities in Ets2 transgenic mice. Nature 379:534–537. https://doi.org/10.1038/379534a0.
64. Vary CP, Li V, Raouf A, Kitching R, Kola I, Franceschi C, Venanzoni M, Seth A. 2000. Involvement of Ets transcription factors and targets in osteoblast differentiation and matrix mineralization. Exp Cell Res 257:213–222. https://doi.org/10.1006/excr.2000.4879.
65. Lomri A, Lemonnier J, Hott M, de Parseval N, Lajeunie E, Munnich A, Renier D, Marie PJ. 1998. Increased calvaria cell differentiation and bone matrix formation induced by fibroblast growth factor receptor 2 mutations in Apert syndrome. J Clin Invest 101:1310–1317.
66. Holmes G, Rothschild G, Roy UB, Deng CX, Mansukhani A, Basilico C. 2009. Early onset of craniosynostosis in an Apert mouse model reveals critical

ID: gulrezaTime: 12:41I Path: //mumnasprod/home$/Mandar.Gawade$/SM-MCBJ210044

17/5/21 | 12:41 | 4/Color Fig: 1,2,3,4,5,6,7,8 | ArtID: 00149-21 | DOI:10.1128/MCB.00149-21 | CE: KGL-mab

features of this pathology. Dev Biol 328:273–284. https://doi.org/10.1016/j.ydbio.2009.01.026.
67. Teng CS, Ting MC, Farmer DT, Brockop M, Maxson RE, Crump JG. 2018. Altered bone growth dynamics prefigure craniosynostosis in a zebrafish model of Saethre-Chotzen syndrome. Elife 7:e37024. https://doi.org/10.7554/eLife.37024.
68. Matsushita T, Chan YY, Kawanami A, Balmes G, Landreth GE, Murakami S. 2009. Extracellular signal-regulated kinase 1 (ERK1) and ERK2 play essential roles in osteoblast differentiation and in supporting osteoclastogenesis. Mol Cell Biol 29:5843–5857. https://doi.org/10.1128/MCB.01549-08.
69. Kyono A, Avishai N, Ouyang Z, Landreth GE, Murakami S. 2012. FGF and ERK signaling coordinately regulate mineralization-related genes and play essential roles in osteocyte differentiation. J Bone Miner Metab 30:19–30. https://doi.org/10.1007/s00774-011-0288-2.
70. Tsang EJ, Wu B, Zuk P. 2018. MAPK signaling has stage-dependent osteogenic effects on human adipose-derived stem cells *in vitro*. Connect Tissue Res 59:129–146. https://doi.org/10.1080/03008207.2017.1313248.
71. Weng Z, Wang C, Zhang C, Xu J, Chai Y, Jia Y, Han P, Wen G. 2019. All-trans retinoic acid promotes osteogenic differentiation and bone consolidation in a rat distraction osteogenesis model. Calcif Tissue Int 104:320–330. https://doi.org/10.1007/s00223-018-0501-6.
72. Cruz ACC, Cardozo F, Magini RS, Simoes CMO. 2019. Retinoic acid increases the effect of bone morphogenetic protein type 2 on osteogenic differentiation of human adipose-derived stem cells. J Appl Oral Sci 27:e20180317. https://doi.org/10.1590/1678-7757-2018-0317.
73. Roa LA, Bloemen M, Carels CEL, Wagener F, Von den Hoff JW. 2019. Retinoic acid disrupts osteogenesis in pre-osteoblasts by down-regulating WNT signaling. Int J Biochem Cell Biol 116:105597. https://doi.org/10.1016/j.biocel.2019.105597.
74. Bi W, Gu Z, Zheng Y, Zhang X, Guo J, Wu G. 2013. Heterodimeric BMP-2/7 antagonizes the inhibition of all-trans retinoic acid and promotes the osteoblastogenesis. PLoS One 8:e78198. https://doi.org/10.1371/journal.pone.0078198.
75. Lind T, Sundqvist A, Hu L, Pejler G, Andersson G, Jacobson A, Melhus H. 2013. Vitamin a is a negative regulator of osteoblast mineralization. PLoS One 8:e82388. https://doi.org/10.1371/journal.pone.0082388.
76. Cristofalo VJ, Allen RG, Pignolo RJ, Martin BG, Beck JC. 1998. Relationship between donor age and the replicative lifespan of human cells in culture: a reevaluation. Proc Natl Acad Sci U S A U S A 95:10614–10619. https://doi.org/10.1073/pnas.95.18.10614.
77. Sasaki M, Abe R, Fujita Y, Ando S, Inokuma D, Shimizu H. 2008. Mesenchymal stem cells are recruited into wounded skin and contribute to wound repair by transdifferentiation into multiple skin cell type. J Immunol 180:2581–2587. https://doi.org/10.4049/jimmunol.180.4.2581.
78. Kastrinaki MC, Andreakou I, Charbord P, Papadaki HA. 2008. Isolation of human bone marrow mesenchymal stem cells using different membrane markers: comparison of colony/cloning efficiency, differentiation potential, and molecular profile. Tissue Eng Part C Methods 14:333–339. https://doi.org/10.1089/ten.tec.2008.0173.
79. Russell KC, Phinney DG, Lacey MR, Barrilleaux BL, Meyertholen KE, O'Connor KC. 2010. In vitro high-capacity assay to quantify the clonal heterogeneity in trilineage potential of mesenchymal stem cells reveals a complex hierarchy of lineage commitment. Stem Cells 28:788–798. https://doi.org/10.1002/stem.312.
80. Gregory CA, Gunn WG, Peister A, Prockop DJ. 2004. An alizarin red-based assay of mineralization by adherent cells in culture: comparison with cetylpyridinium chloride extraction. Anal Biochem 329:77–84. https://doi.org/10.1016/j.ab.2004.02.002.
81. Gruber HE, Somayaji S, Riley F, Hoelscher GL, Norton HJ, Ingram J, Hanley EN, Jr. 2012. Human adipose-derived mesenchymal stem cells: serial passaging, doubling time and cell senescence. Biotech Histochem 87:303–311. https://doi.org/10.3109/10520295.2011.649785.
82. Nicoletti I, Migliorati G, Pagliacci MC, Grignani F, Riccardi C. 1991. A rapid and simple method for measuring thymocyte apoptosis by propidium iodide staining and flow cytometry. J Immunol Methods 139:271–279. https://doi.org/10.1016/0022-1759(91)90198-o.
83. Morgan DM. 1998. Tetrazolium (MTT) assay for cellular viability and activity. Methods Mol Biol 79:179–183. https://doi.org/10.1385/0-89603-448-8:179.
84. Kim D, Langmead B, Salzberg SL. 2015. HISAT: a fast spliced aligner with low memory requirements. Nat Methods 12:357–360. https://doi.org/10.1038/nmeth.3317.
85. Anders S, Pyl PT, Huber W. 2015. HTSeq—a Python framework to work with high-throughput sequencing data. Bioinformatics 31:166–169. https://doi.org/10.1093/bioinformatics/btu638.
86. Robinson MD, McCarthy DJ, Smyth GK. 2010. edgeR: a Bioconductor package for differential expression analysis of digital gene expression data. Bioinformatics 26:139–140. https://doi.org/10.1093/bioinformatics/btp616.
87. McCarthy DJ, Chen Y, Smyth GK. 2012. Differential expression analysis of multifactor RNA-Seq experiments with respect to biological variation. Nucleic Acids Res 40:4288–4297. https://doi.org/10.1093/nar/gks042.
88. Stuart T, Butler A, Hoffman P, Hafemeister C, Papalexi E, Mauck WM, 3rd, Hao Y, Stoeckius M, Smibert P, Satija R. 2019. Comprehensive integration of single-cell data. Cell 177:1888–1902.e1821. https://doi.org/10.1016/j.cell.2019.05.031.
89. Revelle W. 2019. psych: procedures for psychological, psychometric, and personality research. Northwestern University, Evanston, IL.
90. R Core Team. 2019. R: a language and environment for statistical computing. R Foundation for Statistical Computing, Vienna, Austria.
91. Raudvere U, Kolberg L, Kuzmin I, Arak T, Adler P, Peterson H, Vilo J. 2019. g:Profiler: a web server for functional enrichment analysis and conversions of gene lists (2019 update). Nucleic Acids Res 47:W191–W198. https://doi.org/10.1093/nar/gkz369.
92. Gu Z, Eils R, Schlesner M. 2016. Complex heatmaps reveal patterns and correlations in multidimensional genomic data. Bioinformatics 32:2847–2849. https://doi.org/10.1093/bioinformatics/btw313.

ID: **gulreza**Time: 12:41I Path: //mumnasprod/home$/Mandar.Gawade$/SM-MCBJ210044

AUTHOR QUERIES

Below are queries from the copy editor indicating specific areas of concern. Please respond in-line in the main text above, either by marking a change or indicating "ok."

1

AQau—Please make certain that all authors' names are spelled correctly, and confirm the givennames and surnames are identified properly by the colors (this is important for how the names are indexed).
■= Given-Name, ■= Surname

AQau—An ORCID ID was provided for at least one author during submission. Please click the name associated with the ORCID ID icon () in the byline to verify that the link is working and that it links to the correct author.

AQabbr—Please check any added introductions of abbreviations and correct them if necessary.

AQfund— The table below includes funding information that you provided on the submission form when you submitted the manuscript. This funding information will not appear in the article, but it will be provided to CrossRef and made publicly available. Please check it carefully for accuracy and mark any necessary corrections. If you would like statements acknowledging financial support to be published in the article itself, please make sure that they appear in the Acknowledgments section. Statements in Acknowledgments will have no bearing on funding data deposited with CrossRef and vice versa.

Funder	Grant(s)	Author(s)	Funder ID
Alexander S. Onassis Public Benefit Foundation (Onassis Foundation)	GZM 088-1	Angeliki Vogiatzi	https://doi.org/10.13039/501100005302
General Secretariat for Research and Technology (GSRT)	KA4937	George Mavrothalassitis	https://doi.org/10.13039/501100003448
State Scholarships Foundation (IKY)	AP2788	George Mavrothalassitis, Angeliki Vogiatzi	https://doi.org/10.13039/501100003447
Wellcome	093329	Stephen R. F. Twigg, Andrew O. M. Wilkie	https://doi.org/10.13039/100004440
Wellcome	102731	Andrew O. M. Wilkie	https://doi.org/10.13039/100004440

AQA—Are the changes of "ets domain" to "Ets domain" ok/correct? Please verify, or edit further if necessary (e.g., if this should be "ETS domain").

AUTHOR QUERIES

Below are queries from the copy editor indicating specific areas of concern. Please respond in-line in the main text above, either by marking a change or indicating "ok."

AQB—Note that per ASM style, gene designations are italicized and protein designations are in roman text. Please check throughout that these designations are styled as desired, i.e., that protein names are not italicized and gene names are.

AQC—Please verify edits per ASM style/for clarity to the figure legends, or edit further if necessary. In particular, in the Fig. 7 legend, is the location of "(E)" correct?

AQD—Note that Table 1 was rotated and edited per ASM style/for clarity. Please verify edits, or edit further if necessary for accuracy. In particular, in the row labels, are the changes of "Up" to "Upregulated" ok/correct?

AQE—In the sentence beginning "However, all 3 growth conditions. . .," is "assuring" (confirming) correct/as meant, or should this be changed to "ensuring" (guaranteeing)?

AQF—In the sentence beginning "The limited number of differentially expressed. . .," is "supporting the hypothesis that" ok/correct? Please verify, or edit further if necessary.

AQG—In the sentence beginning "Next-generation sequencing (NGS) libraries. . .," is "1 × 150" ok, or does it need a unit (e.g., "1 × 150-bp")?

AQH—Please verify that "knockdown" is the correct spelled-out introduction for "KD," or edit further if necessary.

AQI—In the sentence beginning "Count matrices of small cytoplasmic RNA. . .," is the change of "analyzed filtered" to "filtered" correct/as meant? Please verify, or edit further if necessary.

AQJ—Per ASM style, accession numbers for newly submitted sequences were moved to a separate paragraph at the end of the text. Please check the new paragraph and verify the database. ASM policy requires that new nt/protein/microarray data be available to the public upon online posting of the article, so please verify all links to records (particularly for new sequences) and that each number retrieves the full record of the data (not just the

AUTHOR QUERIES

Below are queries from the copy editor indicating specific areas of concern. Please respond in-line in the main text above, either by marking a change or indicating "ok."

3

home page). If the link takes you to an empty record, instruct the production staff to remove the link. If a new accession number is not linked in the proof or a link is broken, provide production staff with the specific URL for the record. If the accession numbers for new data are not publicly accessible by the proof stage, publication of your article may be delayed; please contact the ASM production staff immediately with the expected release date.

AQK—Please verify edits per ASM style to the Acknowledgments, or edit further if necessary.

Expert Reviews in Molecular Medicine

cambridge.org/erm

Craniofacial, orofacial and dental disorders: the role of the RAS/ERK pathway

Angeliki Vogiatzi[1] and George Mavrothalassitis[1,2]

[1]School of Medicine, University of Crete, Crete, Greece and [2]IMBB, FORTH, Heraklion, Crete 71003, Greece

Review

Cite this article: Vogiatzi A, Mavrothalassitis G (2019). Craniofacial, orofacial and dental disorders: the role of the RAS/ERK pathway. *Expert Reviews in Molecular Medicine* **21**, e2, 1–13. https://doi.org/10.1017/erm.2019.2

Received: 7 September 2018
Revised: 31 January 2019
Accepted: 8 February 2019

Keywords:
Craniofacial disorders; dental abnormalities; ERK signalling pathway; head development; orofacial abnormalities

Corresponding author:
George Mavrothalassitis
E-mail: mavro@imbb.forth.gr

Deviations from the precisely coordinated programme of human head development can lead to craniofacial and orofacial malformations often including a variety of dental abnormalities too. Although the aetiology is still unknown in many cases, during the last decades different intracellular signalling pathways have been genetically linked to specific disorders. Among these pathways, the RAS/extracellular signal-regulated kinase (ERK) signalling cascade is the focus of this review since it encompasses a large group of genes that when mutated cause some of the most common and severe developmental anomalies in humans. We present the components of the RAS/ERK pathway implicated in craniofacial and orodental disorders through a series of human and animal studies. We attempt to unravel the specific molecular targets downstream of ERK that act on particular cell types and regulate key steps in the associated developmental processes. Finally we point to ambiguities in our current knowledge that need to be clarified before RAS/ERK-targeting therapeutic approaches can be implemented.

Introduction

From the moment life begins from a single fertilised egg all the way until the formation of structures, organs and the development of the foetus, signalling molecules and cascades play crucial roles in the orchestration and the entire generation of the new organism. Studies on a variety of model organisms have increased our understanding of how different signalling pathways can control developmental processes and how dysregulation of these pathways can lead to abnormal phenotypes and pathological conditions (Refs 1, 2). In terms of head development, structures are formed and integrated through a complex sequence of cross-talk events between different germ layers and tissues involving activation of molecular signalling cascades at distinct locations and stages. Hedgehog, Wnt, TGF and FGF signalling have been shown to regulate the patterning of craniofacial and orodental structures in the developing embryo (Ref. 3). The extracellular signal-regulated kinase (ERK) pathway is considered to have a central role in mediating a panoply of extracellular signals from the plasma membrane to the nucleus of the cell, thus controlling cellular response to particular stimuli during head formation. In this well-studied pathway, extracellular signals, such as growth factors, bind to receptor tyrosine kinase proteins (RTKs), which upon dimerisation and cross-phosphorylation on tyrosine residues interact with adaptor proteins such as the GRB2 (Refs 4, 5). This interaction leads to the recruitment of guanine nucleotide exchange factors (GEFs) like SOS to the plasma membrane of the cell and the subsequent conformational change of RAS proteins towards their active GTP-bound form (Refs 6, 7). This event promotes the activation of RAF kinases, which in turn phosphorylate MEK kinases resulting finally in ERK1/2 (MAPK3/1) activation and the subsequent regulation of a variety of intracellular targets.

Although RAS/ERK signalling cascade has been extensively studied in the context of tumourigenesis, it also plays a major role in craniofacial and orodental development. Mutations in the components of this particular pathway can lead to some of the most common skull and face disorders in humans. In addition to RASopathies that are well studied and reviewed elsewhere (Refs 8, 9), a variety of craniosynostosis cases as well as orofacial abnormalities, such as cleft lip and palate, spring from dysregulation of the RAS/ERK pathway activation. This review focuses on all these cases and is divided into three main sections representing the corresponding areas of research: (1) orofacial development with respect to palate and mandibular formation, (2) craniofacial development with respect to calvarial bone and suture formation and (3) dental development including studies of enamel, dentine and cementum generation. It also analyses human disorders that are not so widely known yet they have severe phenotypes and are linked to the RAS/ERK cascade too. Although a plethora of human developmental abnormalities are associated with mutations on *RTKs*, for example, Muenke syndrome, osteoglophonic dysplasia, we concentrate on cases that have been suggested to be specifically mediated by the ERK pathway. An overview of the downstream molecular mechanisms affecting specific cell types and developmental stages that are implicated in the pathophysiology of these disorders is also provided in this review.

RAS/ERK pathway in orofacial malformations

Orofacial development

In mammals, the nasal cavity and the oral cavity of the face are separated by palate, a tissue that contains an anterior bony part, the hard palate, and a posterior mainly muscular part,

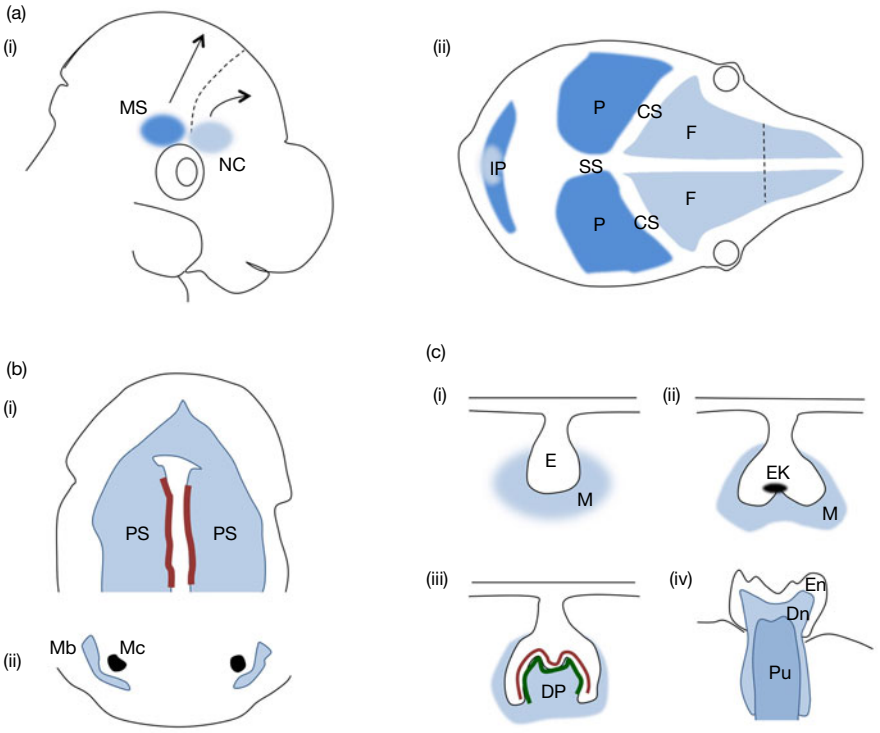

Fig. 1. Mouse embryonic craniofacial and orodental development. The scheme summarises main events of mouse craniofacial, orofacial and dental development described in the review. (a) Developmental origin of calvarial bones. (I) Populations of mesoderm-derived mesenchymal cells (shown in dark blue) and neural crest-derived mesenchymal cells (shown in light blue) accumulate at the supraorbital regulatory centre at E10.5, from which they migrate to the sites of the future parietal and frontal bones, respectively, shown in (II). MS, mesoderm-derived mesenchymal cells; NC, neural crest-derived mesenchymal cells; F, frontal bone; P, parietal bone; IP, interparietal bone; CS, coronal suture; SS, sagittal suture. (b) Development of the oral cavity and jaw. (I) Oral view of secondary palate at E14.5. Palatal shelves consisting of neural crest-derived mesenchymal cells are depicted in light blue. Epithelial cells that will constitute the MEE (medial edge epithelium) are shown in dark red. (II) Mandibular bone is formed by differentiating neural crest-derived mesenchymal cells (light blue) in proximity to Meckel's cartilage depicted in black. PS, palatal shelf; Mb, mandibular bone; Mc, Meckel's cartilage. (c) Tooth development from (I) bud through (II) cap and (III) bell stage until (IV) eruption. Neural crest-derived structures are indicated by blue colour. At the bell stage, ameloblasts and odontoblasts are shown in red and green, respectively. E, epithelium; M, mesenchyme; EK, enamel knot; DP, dental papilla; En, enamel; Dn, dentine; Pu, pulp.

the soft palate. During embryonic development, the hard palate derives from the primary and secondary palate, while the soft palate originates exclusively from the secondary palate.

In mice, the primary palate and the upper lip are formed when the medial nasal prominences start to fuse with the maxillary prominences on embryonic day 11.5 (E11.5). At the same time, outgrowths of the maxillary prominences form the secondary palatal shelves that upon fusion with each other will finally give rise to the secondary palate on E14.5–E15.5 (Refs 10, 11). Each palatal shelf consists of neural crest-derived mesenchymal cells surrounded by epithelial cells. As the two shelves approach to each other and fuse, the epithelial cells previously located at the edge of each shelf lie at the midline of the secondary palate constituting the medial edge epithelium (MEE). By E15.5 MEE cells have disappeared from the midline either through apoptosis, migration or epithelial-to-mesenchymal transition and a continuous mesenchymal palate tissue is formed (Refs 12, 13). In addition to the mechanisms mentioned above, a recent study revealed that cell intercalation drives the convergence of the MEE cells to the midline, followed by displacement and cell extrusion events that lead to the removal of the epithelial cells from the palatal mesenchyme (Ref. 14). Finally the fusion between primary and secondary palate takes place resulting in the creation of a complete mouth roof by E17. Sonic hedgehog (Shh), Fgf10 and Fgf7 seem to have crucial roles in the palatal shelf development and patterning, while TGF-β3 signalling through Smads and p38 MAPK pathway seems to be important for normal palatal fusion (Ref. 15). However, less is known about the role of Ras/Erk pathway in these processes. Studies on Erk activation pattern reveal the presence of phosphorylated Erk1/2 from E12.5 to E14.5 in the palatal shelves in both epithelial and mesenchymal cells as well as in the muscles of the tongue on E14.5 (Refs 16, 17).

The lower jaw, the mandible, is formed by the mandibular prominences. The mandibular bone develops from neural crest-derived mesenchymal cells in proximity to a cartilaginous structure called Meckel's cartilage. Figure 1 summarises key steps of mouse craniofacial and orodental development. The largest part of the mandibular bone is created through the intramembranous ossification process. On E12.5 phosphorylated Erk1/2 is detected in the chondrocytes of Meckel's cartilage and on E13.5 in the osteogenic fronts of the mandibular bone (Ref. 16). However, by E14.5 studies report that the presence of active Erk1/2 is restricted only to the undifferentiated mesenchymal cells of the jaw, while the perichondrium of Meckel's cartilage displays also an amount of phosphorylated kinase that is detected specifically on the side of the tongue (Ref. 17). These data indicate the existence of a defined spatiotemporal pattern of ERK1/2 activation during orofacial development.

Human orofacial disorders and associated animal studies

Mutations in members of the RAS/ERK signalling pathway have been identified as a cause of certain human orofacial disorders, while ERK signalling appears to also mediate the effects of mutations in factors that were previously not connected directly to the ERK kinase. Orofacial clefts constitute the most common facial disorder with an occurrence rate of about 1–700 births and among them cleft lip and cleft palate appear to be the malformations most often observed among individuals. Genomic studies on cleft patients indicate the presence of *ERK1* (*MAPK3*) duplication as the sole gene alteration observed in some cases (Ref. 18), while individuals that carry loss-of-function mutations in *SPROUTY2* (*SPRY2*) gene coding for an inhibitor of the RAS/ERK pathway display also cleft palate (Ref. 19). Of note, *Sprouty2*$^{-/-}$ (for the MGI nomenclature of the genetically modified mouse strains reviewed herein, see Box 1) mice exhibit the cleft phenotype with a prevalence of 22% (Ref. 20). Human craniofrontonasal syndrome (CFNS) is caused by mutations in *EPHRINB1* gene, and studies on *EphrinB1*$^{+/-}$ mice with a CFNS-like phenotype including frontonasal dysplasia, abnormalities of thoracic skeleton and cleft palate reveal that elevated Erk signalling provokes the increase in cellular proliferation observed in the affected palates (Ref. 21).

Surprisingly, similar phenotypes are also derived by mutations that result in the overall decrease of ERK signalling. Haploinsufficiency of ERK2 has been shown to be the cause of the facial phenotype in patients with 1Mb microdeletion of the distal 22q11.2 locus encompassing *ERK2* (*MAPK1*) gene (Ref. 22). The

BOX 1. MGI nomenclature of reviewed mouse strains

Sprouty2$^{-/-}$	*Spry2*^{tm1Ayos}/*Spry2*^{tm1Ayos}
EphrinB1$^{+/-}$	*Efnb1*^{tm1Sor}/*Efnb1*$^{+}$
Wnt1-Cre;Erk2$^{LoxP/LoxP}$	*H2afv*$^{Tg(Wnt1cre)11Rth}$/0; *Mapk1*^{tm1Gela}/*Mapk1*^{tm1Gela}
Osr2-Cre;Erk2$^{LoxP/LoxP}$	*Osr2*$^{tm2(cre)Jian}$/*Osr2*$^{+}$; *Mapk1*^{tm1Gela}/*Mapk1*^{tm1Gela}
Col2a1-Cre;Shp2$^{LoxP/LoxP}$	*Tg(Col2a1-cre/ERT2)1Dic/0; Ptpn11*^{tm1Gsf}/*Ptpn11*^{tm1Gsf}
Wnt1-Cre;Srf$^{LoxP/LoxP}$	*H2afv*$^{Tg(Wnt1-cre)11Rth}$/0; *Srf*^{tm1Rmn}/*Srf*^{tm1Rmn}
Fgfr2$^{S252W/+}$	*Fgfr2*^{tm2Cxd}/*Fgfr2*$^{+}$
Fgfr2c$^{C342Y/+}$	*Fgfr2*^{tm4Lni}/*Fgfr2*$^{+}$
Fgfr2c$^{-/-}$	*Fgfr2*^{tm2Lni}/*Fgfr2*^{tm2Lni}
Erf$^{loxP/-}$	*Erf*^{tm1Gmav}/*Erf*^{tm2Gmav}
Wnt1-Cre;Shp2^{Q79R}	*H2afv*$^{Tg(Wnt1-cre)11Rth}$/0; *Tg (CAG-cat,-Ptpn11*Q97R)1Rbns/0*
Raf1$^{L613V/+}$	*Raf1*$^{tm1.1Bgn}$/*Raf1*$^{+}$
Ptpn11$^{D61G/+}$	*Ptpn11*^{tm1Bgn}/*Ptpn11*$^{+}$
Ptpn11$^{Y279C/+}$	*Ptpn11*$^{tm4.2Bgn}$/*Ptpn11*$^{+}$
Braf$^{Q241R/+}$	*Braf*^{tm1Tumg}/*Braf*$^{+}$
Mlk3$^{-/-}$	*Map3k11*^{tm1Rjd}/*Map3k11*^{tm1Rjd}
Hras$^{G12V/+}$	*Hras*^{tm1Jaf}/*Hras*$^{+}$
Rsk2$^{-/Y}$	*Rps6ka3*$^{tm1.1Kry}$ /*Y*

deleted region is different from the common DiGeorge syndrome region which includes many genes, yet *ERK2* is located outside this area. These patients display a craniofacial phenotype similar to those observed in DiGeorge cases and exhibit among others mandibular hypoplasia, bifid uvula as well as cardiac anomalies. Moreover, there is evidence supporting the hypothesis that ERK2 inadequacy accounts for the pathologic phenotype in the case of Pierre–Robin syndrome, in which individuals display micrognathia (short mandible), incorrect tongue position and cleft palate (Ref. 16).

Mice in which the *Erk2* gene has been eliminated in neural crest-derived cells under the control of Wnt1-Cre transgene – *Wnt1-Cre;Erk2*$^{LoxP/LoxP}$ mice – display complete cleft palate, hypoplasia of maxilla and mandible as well as tongue malformations including microglossia and incorrect tongue position (Refs 16, 22). These phenotypic characteristics present remarkable overlap with the human phenotypes observed in patients with the 1Mb 22q11.2 microdeletion and Pierre–Robin syndrome. Detailed analysis of the orofacial defects in *Wnt1-Cre;Erk2*$^{LoxP/LoxP}$ mice revealed that the cleft palate is not a primary but rather a secondary disease trait since isolated palatal shelves are able to fuse normally in ex vivo cultures. In support of this finding, *Osr2-Cre;Erk2*$^{LoxP/LoxP}$ mice in which *Erk2* is deleted specifically in E12.5 palatal shelves but not in the tongue or mandible do not exhibit the cleft phenotype (Ref. 16). The tongue malformation seems to be also a secondary defect in *Wnt1-Cre;Erk2*$^{LoxP/LoxP}$ mice since the excision of the mandible restores the normal phenotype. Interestingly, however, the elimination of Erk2 seems to primarily affect the formation of the lower jaw in these animals. Diminished condyle size and decreased osteogenic differentiation of the mandibular bone were observed in mutant mice, indicating the significance of Erk signalling in mandibular development. Consistent with the previous findings, conditional deletion of *Ptpn11* gene that codes for Shp2, a tyrosine phosphatase required for the activation of the Ras/Erk cascade, results in severe malformation of the mandibular condyle in *Col2a1-Cre;Shp2*$^{LoxP/LoxP}$ mice (Ref. 23). Taken together, both activating and suppressive alterations in the ERK pathway seem to lead to similar phenotypes in the affected individuals implying that possibly orofacial development is sensitive to the exact location, the timing or even the activation level of this particular signalling cascade.

Molecular mechanisms

Although the amount of information on the downstream targets of the RAS/ERK cascade involved in the pathogenesis of orofacial malformations is limited, there are some studies that shed light on the possible molecular mechanisms underlying specific phenotypic outcomes. In mandibular formation, Erks seem to act at least in part through the serum response factor (Srf), a downstream target of MAPKs, since *Wnt1-Cre;Srf*$^{LoxP/LoxP}$ mice exhibit the same mandibular phenotype as the one observed in the case of *Wnt1-Cre;Erk2*$^{LoxP/LoxP}$ mice (Ref. 22). A study on palatal mesenchymal cells isolated from E13.5 embryos revealed that Srf regulates the expression of genes particularly involved in cytoskeletal organisation via MRTF (myocardin-related transcription factors) recruitment depending on differential response to extracellular signals, thus playing a crucial role in the migration and proliferation of orofacial neural crest cells (Ref. 24). In another model organism, zebrafish, the migration of neural crest-derived mesenchymal cells is shown to be dependent on Gata6 phosphorylation by Erks (Ref. 25), indicating the importance of Erk signalling and its downstream target, Gata6, in craniofacial development.

In mandibular condyles, Shp2 via Erk1/2 phosphorylation is proposed to induce the expression of the intraflagellar transport complexes (Ref. 23). These complexes are necessary for the formation of the primary cilia and the differentiation of chondrocytes. Consequently, Shp2 via Erk signalling positively regulates condyle formation in the jaw.

One of the cellular mechanisms underlying the emergence of cleft palate is the inability of MEE cells to stop proliferation and enter apoptosis. In the EGF-induced cleft palate model, increased levels of phosphorylated Erk1/2 were detected in the nuclei of MEE cells in palate organ cultures treated with EGF, while non-treated palatal cells displayed cytoplasmic kinase activity (Ref. 26). Activated nuclear Erk1/2 was proposed to be responsible for the sustained DNA replication and proliferation of MEE cells, since the addition of U0126, inhibitor of MEK1/2, was shown to stop proliferation and restore normal palatal fusion. However, no downstream targets have been identified in this particular cleft palate model so far.

RAS/ERK pathway in craniofacial malformations

Craniofacial development

Although the facial skeleton is derived primarily by neural crest mesenchymal stem cells, the bones of the cranial vault originate from two sources: both neural crest- and mesoderm-derived mesenchymal cells. More specifically, the frontal bones and the squamous temporal bones come from the cranial neural crest cells, while the parietal bones and the occipital one come primarily from mesoderm-derived mesenchymal stem cells (Refs 27, 28). In mice, at around E10 mesenchymal cells of neural crest and mesoderm origin complete their migration towards the first and second branchial arches and the positions of the future skull bones (Ref. 29). In the case of the parietal and frontal bones, groups of mesoderm- and neural crest-derived cells accumulate initially in a place above the embryonic eye called the supraorbital regulatory centre at E10.5 (Fig. 1), from which they migrate to the

sites of the future parietal and frontal bones, respectively, between E11.5 and E13.5 (Refs 30, 31). Proliferation and condensation take place, while from E13.5 and on, the expression of osteogenic markers is evident leading to the formation of a calcified extracellular matrix between E15.5 and E17.5. At the same time, the formation of cranial sutures is completed. Sutures comprise the fibrous tissues existing between the bones of the skull and have crucial role in the maintenance of the coordinated growth between calvarial bones and the brain. Non-committed mesenchymal stem cells are found to be located in the middle of the sutures (Ref. 32), often expressing the markers *Twist1* and *Gli1*. More differentiated cells are found to populate the region surrounding the osteogenic fronts. Although the suture between the frontal bones – interfrontal suture – and the one between the parietal bones – sagittal suture – are mainly populated by neural crest-derived mesenchymal cells, the sutures between parietal and frontal bones – coronal sutures – contain exclusively mesoderm-derived mesenchymal cells (Ref. 33). The flat bones of the skull – the parietal and frontal bones – along with the majority of the facial bones are formed through the intramembranous ossification process, thus the sutures have generally been characterised as intramembranous bone growth sites (Ref. 34). Yet there are studies in rodents revealing that the posterior part of the interfrontal suture fuses through a cartilaginous template, thereby displaying endochondral ossification ability (Refs 35, 36).

WNT signalling through β-catenin, TCF and TWIST1, and BMP signalling through MSX2 and FGF signalling through the RAS/ERK cascade (reviewed in (Ref. 37)) seem to have important roles in the regulation of craniofacial development. These roles are constantly being uncovered and studied particularly due to the variety of human craniofacial syndromes that arise upon mutations in components of these pathways.

Human craniofacial disorders and associated animal studies

Craniosynostosis

Craniosynostosis is the condition in which one or more of the cranial sutures ossify prematurely resulting in abnormal head shapes, facial deformities and vision, hearing defects or even mental impairment. Craniosynostosis cases have an occurrence rate of about one in 2500 births and can be divided into non-syndromic and syndromic cases according to the presence of additional phenotypic traits beyond the fused sutures. In the case of Apert craniosynostosis syndrome, gain-of-function mutations in *FGFR2* account for the majority of incidences (Ref. 38). Increased ERK1/2 signalling has been shown to mediate the appearance of the abnormal phenotypes in a significant amount of studies on Apert syndrome mouse models such as the $Fgfr2^{P253R/+}$ mice displaying craniosynostosis, cranial base abnormalities and defects in the growth plates of long bones (Ref. 39), and the $Fgfr2^{S252W/+}$ mice that exhibit craniosynostosis, hypertelorism and midface hypoplasia (Ref. 40), having significant overlap with the human Apert features. The administration of MEK/ERK inhibitors starting on embryonic day 13 (E13) alleviates or, in some cases, even completely inhibits the premature fusion of the cranial sutures in $Fgfr2^{S252W/+}$ animals (Ref. 41). Further studies on mice carrying the same mutations show however that increased p38 MAPK signalling in neurocranial tissues is also observed along with the increase in the phosphorylation level of Erk1/2 (Ref. 42), indicating that possibly additional pathways play roles in the development of skull phenotype in Apert syndrome. A different group of mutations in *FGFR2* cause Crouzon syndrome in humans (Ref. 43). Chick embryos infected with a virus expressing the Crouzon-related FGFR2-Cys278Phe mutant develop craniofacial malformations and exhibit decreased levels of phosphorylated Erk1/2 in frontonasal prominences, possibly due to increased expression of the Sprouty inhibitors via negative feedback mechanisms (Ref. 44). Mice carrying the Crouzon gain-of-function mutation Cys342Tyr, $Fgfr2c^{C342Y/+}$ mice, display severe coronal synostosis along with elevated levels of phosphorylated Erk1/2 in coronal sutures from E18.5 to postnatal day 1 (P1) (Ref. 45). Interestingly, although $Fgfr2c^{-/-}$ mice exhibit decreased mineralisation of the calvarial bones and lower levels of phosphorylated Erk1/2, they also develop the craniosynostosis phenotype, which features the complexity of the role of the ERK pathway in cranial suture formation and maintenance.

Loss-of-function mutations in a variety of negative regulators of the RAS/ERK cascade, such as SPRY1, SPRY4, RASAL2 and ARAP3, have also been associated with a particular number of midline non-syndromic craniosynostosis cases (Ref. 46), yet the causative role of these mutations in the development of the disease is not well defined so far. However, the strongest link between ERK1/2 signalling and cranial suture development was established when loss-of-function mutations in Ets2 repressor factor (ERF), a downstream target of ERKs, were shown to be the cause for ERF-complex craniosynostosis disorder (Refs 47, 48) as well as for some non-syndromic cases of premature suture fusion in humans (Ref. 49). Unpublished data of our laboratory reveal that Erk1/2 inhibition starting on postnatal day 5 (P5) is able to prevent the premature suture ossification observed in $Erf^{loxP/-}$ mice having about 30% of functional Erf protein, indicating that cranial suture closure can possibly be sensitive to subtle changes in ERK signalling mediated by ERF.

RASopathies

Germ-line mutations in components of the RAS cascade lead to a group of developmental disorders called RASopathies which often present overlapping characteristics such as craniofacial malformations, skin and skeletal abnormalities, heart defects and an increased cancer risk. Noonan syndrome is caused by gain-of-function mutations in *PTPN11* – coding for SHP2 – in about half of the syndrome cases, while mutations in *SOS1*, *KRAS* and *RAF1* have also been reported to lead to a Noonan phenotype in humans (Ref. 50). Mouse models that recapitulate many characteristics of Noonan syndrome patients have been constructed through the years. However, the features they display often depend on the genetic background of the animals and attention should be paid during experimentation and phenotypic evaluation (Ref. 9). Increased levels of phosphorylated Erk1/2 are detected in the frontal bones of *Wnt1-Cre*;$Shp2^{Q79R}$ mice displaying growth retardation and craniofacial abnormalities (Ref. 51) as well as in hearts of $Raf1^{L613V/+}$ mice that exhibit short stature, craniofacial dysmorphia and cardiac hypertrophy (Ref. 52). In this latter case, MEK/ERK inhibition leads to the restoration of the normal cardiac and facial phenotypes starting the treatment either at 4 weeks of age or on postnatal day 0 (P0), respectively (Ref. 52). Additionally, in $Ptpn11^{D61G/+}$ Noonan mice, elevated Erk1/2 activation is shown to be responsible for the decrease in the levels of insulin-like growth factor 1 (Igf-1), thus promoting the growth retardation evident in both mouse and human patients (Ref. 53). In the above studies, animals of mixed 129/SV × C57BL/6 background were utilised. Finally, in zebrafish, the expression of the Noonan-associated KRAS-Asn116Ser mutant results in heart developmental defects reminiscent of those observed in human patients, while knock-down of the normal *kras* gene causes craniofacial and heart malformations as well (Ref. 54).

Although gain-of-function mutations in *PTPN11* lead to Noonan syndrome, loss-of-function mutations in the same gene account for the diseased phenotype in the majority of incidences with LEOPARD syndrome (Lentigines, Electrocardiographic conduction abnormalities, Ocular hypertelorism, Pulmonic stenosis, Abnormal genitalia, Retardation of growth and sensorineural

Deafness). In *ptpn11a−/−;ptpn11b−/−* zebrafish embryos, craniofacial defects are evident by day 4 postfertilisation (4dpf) accompanied by decreased Erk1/2 phosphorylation levels at 5dpf (Ref. 55). In heart lysates of $Ptpn11^{Y279C/+}$ LEOPARD mice, decreased Shp2 and Erk1/2 activity is detected along with elevated Akt and mTOR activation (Ref. 56). However, a downregulation in the activity of Erk kinases cannot be commonly confirmed by different studies so far. Conflicts regarding the changes in Erk1/2 signalling exist also in the case of cardio-facio-cutaneous (CFC) syndrome, which is caused by gain-of-function mutations in *BRAF*, *MEK1/2* and *KRAS*. Although the majority of mutations lead to increased kinase activity, there are three particular modifications in BRAF (E501G, G469V and D638E) that result in a decline in its action (Ref. 57). Mice carrying the $Braf^{Q241R}$ allele, corresponding to the CFC human mutation Q257R, display craniofacial, heart and lymphatic defects and are embryonic/neonatal lethal (Ref. 58). Increased phosphorylation of Erk1/2 is detected in the hearts of these mice accompanied by elevated levels of *Etv1*, *Etv4* and *Etv5* expression. Administration of the MEK inhibitor PD0325901 from E10.5 to E18.5 although rescuing lethality, is unable to restore the normal craniofacial morphology. In zebrafish embryos, the continuous application of the same inhibitor at low doses for the first 5 days of development is able to alleviate the CFC-like phenotypes caused by the expression of the human $BRAF^{Q257R}$ allele (Ref. 59). Collectively, although the majority of RASopathies involve an upregulation of ERK1/2 signalling, suppressive mutations leading to pathway downregulation result in similar phenotypes, suggesting that further studies are required in order to discriminate between primary and secondary phenotypic traits and specify the structures, the developmental stage and the dosage of ERK1/2 action for proper craniofacial formation.

Rare craniofacial syndromes

In addition to the craniosynostosis and RASopathies cases, there are some rare craniofacial conditions that seem to arise by changes in the ERK1/2 pathway. Faciogenital dysplasia or Aarskog–Scott syndrome is an X-linked disease caused by loss-of-function mutations in *FGD1* encoding a GEF protein (Ref. 60). In vitro studies on human mesenchymal stem cells as well as on human cell lines showed that FGD1 along with CDC42 activate MLK3 (mixed lineage kinase 3) which in turn leads to ERK1/2 phosphorylation and subsequent RUNX2 activation (Ref. 61). $Mlk3^{-/-}$ mice exhibit defective skeletal mineralisation, reminiscent of the bone phenotype of patients, while they also display reduced Erk1/2 phosphorylation levels in calvarial osteoblasts undergoing osteogenic differentiation.

A distinct mutation in ERF, Tyr89Cys, was recently found to be the cause of Chitayat syndrome, a rare condition in which individuals display facial malformations along with bronchomalacia and hyperphalangism, without however any sign of premature cranial suture fusion (Ref. 62). Current studies aim to decipher the result of this mutation on ERF protein functionality and investigate the role of this particular effector of ERK pathway in the regulation of craniofacial development.

Kabuki syndrome is another disorder affecting craniofacial, mental and heart development and it is usually caused by loss-of-function mutations in *KMT2D* and *KDM6A* genes coding for two chromatin regulators, lysine-specific methyltransferase 2D and lysine-specific demethylase 6A, respectively (Refs 63, 64). Recently, two novel alterations were reported to lead to Kabuki syndrome, one in RAP1A and one in RAP1B, both belonging to the RAS family of small GTPases (Ref. 65). MEK/ERK signalling is shown to mediate the diseased condition since inhibition of this particular cascade at the one- to four-cell stage embryo restores normal phenotype in zebrafish models, despite however the fact that RAP1 is reported to have contradictory effects on the activation of the pathway in ex vivo and in vivo studies (Refs 65–67). All in all, further research is needed in order to clarify the role of the RAS/ERK cascade in these rare syndromes. A list including known human craniofacial disorders that are caused by mutations in the components of the RAS/ERK signalling cascade is provided in Table 1.

Molecular mechanisms

Although a great number of animal models for craniofacial disorders have been generated and phenotypically well characterised during the last decades, the knowledge of the precise molecular mechanisms downstream of the affected signalling pathways is still limited. In the case of craniosynostosis disorders, both the complexity in the origin of the calvarial cells and the heterogeneity of cellular populations make the discovery of the implicated targets even more difficult. In a study on calvarial pre-osteoblasts, Fgf2 was shown to activate Erk1/2 via Frs2, leading to an increase in the transcriptional activity of Msx2 and Runx2 (Ref. 91). According to this study, Msx2 and Runx2 bind then to the promoter of the *Pc1* (*Enpp1*) gene coding for the generator of pyrophosphate (PPi) which is further hydrolysed by alkaline phosphatase (TNAP) towards inorganic phosphate. Upon aberrant FGFR-ERK1/2 signalling, increased expression of PC1 is considered to drive the accumulation of PPi levels, leading to the formation of calcium pyrophosphate dehydrate crystals instead of hydroxyapatite crystals and the subsequent calcification of soft tissues (Refs 92, 93). Consistent with this hypothesis, $Tnap^{-/-};Pc1^{-/-}$ double knock-out mice display normal mineralisation of the calvarial bones (Ref. 94).

In a study on MC3T3 murine calvarial cell line, stimulation of ERK1/2 by FGF2 was shown to increase the expression of activator protein 1 (AP1), which subsequently induces the expression of osteopontin and the onset of osteogenic differentiation (Ref. 95). Apart from that, in C3H10T1/2 murine mesenchymal cell line and in human primary adipose-derived mesenchymal stem cells (hASCs), TAZ (transcriptional coactivator with PDZ-binding motif) is found to play a central role downstream of ERK1/2 signalling cascade (Refs 96, 97). More specifically, in hASCs, suppression of TWIST1 is shown to activate both BMP and FGF/ERK pathways which lead to an increase in the osteogenic differentiation of these cells mediated by TAZ upregulation (Ref. 97). These data suggest that ERK1/2 signalling could potentially mediate some of the effects of TWIST1 loss-of-function mutations in the case of Saethre–Chotzen craniosynostosis syndrome by controlling TAZ activity. Furthermore, in an independent study on calvarial explants isolated from E15 mouse embryos, FGF2 is shown to drive *Twist* upregulation in suture mesenchymal cells (Ref. 98). In turn Twist suppresses Fgfr signalling and subsequent osteoblast differentiation, indicating that feedback mechanisms and complex integration of molecular pathways such as those of FGF and TWIST can regulate calvarial suture formation and maintenance.

In opposition to the studies showing that RAS/ERK cascade has a positive effect on the osteogenic differentiation of calvarial cells, there are reports indicating that increased ERK1/2 signalling may have an overall inhibitory act upon calvarial osteoblast mineralisation. In primary osteoblasts isolated from calvarial bones, addition of FGF1 is shown to drive SHP2-FRS2-GRB2 complex formation, resulting in the activation of ERK1/2 signalling followed by an increase in the proliferation of cells and a decrease in their mineralisation ability (Ref. 99). Furthermore in the same study, OB1 osteoblastic cell lines modified to express the Crouzon-related C342Y-FGFR2 mutant or the Apert-related S252W-FGFR2 mutant display diminished calcification upon in

Table 1. Human cranio-oro-dento-facial disorders associated with alterations of the RAS/ERK signalling cascade

Human disorders	Mutated gene(s)	Comment	References
Apert syndrome	*FGFR2*	gain-of-function	(Refs 38, 41, 68)
Crouzon syndrome	*FGFR2*	gain-of-function	(Refs 43, 45)
Pfeiffer syndrome	*FGFR1, FGFR2*	gain-of-function	(Refs 69–71)
Beare Stevenson cutis gyrata	*FGFR2*	gain-of-function	(Refs 72, 73)
Bent bone dysplasia	*FGFR2*	loss-of-function	(Ref. 74)
ERF-associated craniosynostosis	*ERF*	loss-of-function	(Ref. 47)
Midline non-syndromic craniosynostosis	*SPRY1, SPRY4, RASAL2, ARAP3*[c]	loss-of-function	(Ref. 46)
Noonan syndrome	*PTPN11, SOS1, KRAS, RAF1, RIT1, BRAF, NRAS, MEK*	gain-of-function	(Refs 50, 75–77)
LEOPARD syndrome	*PTPN11*	loss-of-function	(Ref. 78)
	BRAF, RAF1	gain-of-function	(Refs 79, 80)
Cardio-facio-cutaneous syndrome	*BRAF, MEK1, 2, KRAS*	gain-of-function	(Refs 57, 81, 82)
Costello syndrome	*HRAS*	gain-of-function	(Ref. 83)
Neurofibromatosis type 1	*NF1*	loss-of-function	(Ref. 84)
Legius syndrome	*SPRED1*	loss-of-function	(Ref. 85)
CM-AVM[a]	*RASA1*	loss-of-function	(Ref. 86)
HGF[b]	*SOS1*	gain-of-function	(Ref. 87)
Aarskog–Scott syndrome	*FGD1*	loss-of-function	(Ref. 60)
Kabuki syndrome	*RAP1A, RAP1B*	loss-of-function	(Ref. 65)
Chitayat syndrome	*ERF*	uncharacterised	(Ref. 62)
Coffin–Lowry syndrome	*RSK2*	loss-of-function	(Refs 88, 89)
Cleft lip/palate	*ERK1 (MAPK3)*	duplication	(Ref. 18)
	ERK2 (MAPK1)	deletion	(Ref. 22)
	SPRY2	loss-of-function	(Ref. 19)
Class III malocclusion	*DUSP6*	loss-of-function	(Ref. 90)

[a]Capillary malformation–arteriovenous malformation.
[b]Hereditary gingival fibromatosis.
[c]The causative role of the mutations is still not well defined.

vitro osteogenic differentiation conditions. In bone marrow mesenchymal cells derived from the Crouzon mouse model $Fgfr2^{C342Y/+}$, increased early-stage osteogenic differentiation is evident upon in vitro induction conditions, followed however by decreased late-stage mineralisation in comparison to that of wild-type cells (Ref. 100). Last but not least, in an independent study, administration of a virus carrying a dominant negative form of *Ras* gene into the skull of newborn mice accelerated calvarial calcification, while administration of a virus carrying a constitutively active form of Mek1 repressed it, indicating an inhibitory effect of Erk pathway on matrix mineralisation (Ref. 101). However, until now there are no reports regarding downstream molecular effectors that could account for these phenotypes. Unpublished data of our laboratory indicate that cranial suture cells isolated from $Erf^{loxP/-}$ craniosynostotic mice display diminished mineralisation upon in vitro osteogenic conditions, featuring ERF as an effector that could potentially account for the inhibitory act of ERK cascade on matrix calcification. All in all, although a great number of studies have been conducted in animal models and a group of potential downstream targets have already been explored, there is still a long way to go for a full understanding of how RAS/ERK pathway and its effectors act on primitive as well as on differentiating cells during the different steps of craniofacial construction and development. Thus, similar to orofacial disorders, alterations in the spatiotemporal pattern of ERK1/2 activation or even in the strength of signalling appear to affect the overall phenotypic outcome.

RAS/ERK pathway in dental malformations

Dental development

Four types of teeth are commonly observed in mammals: incisors, canines, premolars and molars. Rodents however, lack canines and display an empty space between the incisor and the molar instead, called diastema. In mice, one incisor and three molars are observed in each side of the jaw. Interactions between neural crest-derived mesenchymal cells and epithelial cells take place during tooth development (Refs 102). Initially, at the site of the future tooth, the oral epithelium becomes thicker and finally buds towards the underlying mesenchymal tissue. This is called 'the bud stage'. Condensation of mesenchymal cells takes place around the bud, followed by a sequence of morphogenetic processes during the cap and bell stages of tooth development. At the cap stage, a small group of epithelial cells aggregate and form the primary enamel knot which serves as a signalling centre required for the development of tooth cusps (Fig. 1). In mouse embryos the formation of the enamel knot is observed at around E14.5 and a wide range of signalling molecules are found to be expressed such as Bmp2, 4, 7, Shh, Fgf4 and Spry2 (Refs 103, 104). At the end of the cap stage, apoptosis becomes evident among the cells of the enamel knot and finally at the late bell stage, the knot does not exist anymore. Ameloblasts and odontoblasts are driven into terminal differentiation at this stage too. Ameloblasts are the epithelial cells that produce the enamel of teeth, while odontoblasts originate from neural crest-derived

mesenchymal cells and form the dentine matrix of teeth. Neural crest mesenchymal cells differentiate and form the dentin pulp and cementum too. Tooth eruption comes in the end. During dental development, Erk1/2 is shown to be active in the tooth germ on E13.5 in both epithelial and mesenchymal cells (Ref. 17). Studies on molar teeth isolated from mice reveal the presence of phosphorylated Erk1/2 at the dental epithelium and cervical loop on E15.5 and E16.5 (Ref. 105), while on E18.5 and later on postnatal day 2 (P2), phosphorylated Mek1/2 and Erk1/2 are highly expressed in ameloblasts and odontoblasts in mandibular molars and incisors (Refs 105, 106).

Human dental abnormalities and associated animal studies

A variety of dental malformations are often observed in individuals with orofacial and craniofacial disorders associated with the RAS/ERK pathway. In patients displaying cleft lip and/or cleft palate, deformities in crown and root are usually observed along with hypodontia or supernumerary teeth. Enamel hypoplasia is another feature in some cases (Ref. 107). Individuals with RASopathies usually present dental characteristics such as missing teeth, often observed in LEOPARD and neurofibromatosis type 1 syndrome, and malocclusion with anterior open bite and posterior crossbite in Noonan, Costello and CFC syndromes. All these phenotypic traits are already reviewed in detail (Ref. 108). The mineralisation of enamel is severely affected in Costello syndrome patients (Refs 109, 110). In the mouse model of Costello syndrome, $Hras^{G12V}$ mice, diminished enamel mineralisation is detected along with increased levels of phosphorylated Erk1/2 protein in the incisor (Ref. 110). Ameloblasts exhibit higher growth rate than normal controls and their cell polarity is destroyed. Inhibition of Mek1/2 in 12-week-old mice results in the restoration of the normal phenotype in ameloblasts while inhibition of PI3K is not able to completely reverse the pathologic condition, indicating the role of Ras/Erk signalling in the ameloblast phenotypic outcome in Costello syndrome. On the contrary, CFC patients do not have any defects in enamel mineralisation; however, malocclusion and dental crowding are often observed (Ref. 111). Among the syndromic craniosynostosis cases, individuals with Apert syndrome display also enamel defects as well as missing or supernumerary teeth. Furthermore, increased growth rate of isolated dental pulp and enamel organ epithelia cells from Apert patients is observed in this case (Ref. 112). Finally, individuals carrying the missense substitution of serine residue 182 by phenylalanine on DUSP6 exhibit Class III malocclusion (Ref. 90), a situation in which incorrect alignment of teeth happens, mainly due to maxilla and/or mandible growth defects.

Another link between dental development and the RAS/ERK signalling pathway is provided by studies on mutant mice that lack expression of some inhibitory molecules of the RAS cascade. $Sprouty2^{-/-}$ mice display supernumerary teeth in the mandible, while $Sprouty4^{-/-}$ mice share also the same defect, yet this abnormal phenotype is observed in both the upper and the lower jaw (Ref. 113). Finally in the same study mice that lack Rsk2, an ERK1/2 substrate, mutations of which are associated with Coffin–Lowry syndrome in humans exhibit supernumerary teeth either in the upper or in the lower jaw with a prevalence of 14%.

Molecular mechanisms

Studies on ex vivo cultures of ameloblasts, odontoblasts and stem cells from either dental pulp or periodontal ligament have improved the understanding of mechanisms by which the RAS/ERK signalling cascade might act on the differentiation and growth of these particular dental cell types. In ameloblasts isolated from rat mandible incisors, Erk1/2 activation results in significant increase in *Amelogenin* mRNA expression (Ref. 114). Amelogenin is an extracellular matrix protein involved in enamel mineralisation. Consequently, according to that particular study, Erk signalling is considered to have a positive effect on ameloblast differentiation. On the contrary, however, ameloblasts isolated from Costello syndrome mouse models (CS mice) display significantly increased levels of phosphorylated Erk1/2 along with diminished enamel mineralisation (Ref. 110), indicating that further studies are needed in order to decipher the role of RAS/ERK pathway in the differentiation of this specific cell type and the formation of enamel.

In primary cultures of murine pulp cells, exposure to Ffg2 is shown to have a dual effect on the differentiation towards odontoblasts, with early and short exposure to enhance while long-term exposure to inhibit odontoblastic differentiation (Ref. 115). In any case, the effect of Fgf2 is shown to be mediated by Erk1/2 signalling since the addition of U0126, inhibitor of Mek1/2, is able to restore the normal phenotype (Ref. 116). Further study on the stimulatory mechanism in the case of the short-term exposure reveals that Erk1/2 signalling along with Bmp signalling induces the expression of dentin matrix acidic phosphoprotein 1 (Dmp1) and dentin sialophosphoprotein (Dspp) – both required for proper dentin mineralisation – thus enhancing odontoblastic differentiation (Ref. 117). Dentin phosphoprotein (Dpp) is the proteolytic product of Dspp. In dental pulp mesenchymal stem cells, Dpp is shown to interact with integrins and drive focal adhesion kinase phosphorylation which subsequently activates Erk1/2 kinases (Ref. 118). This event leads to the activation of Elk1, an Ets-domain transcription factor, and the induction of genes facilitating odontogenic differentiation such as *Dmp1*. The stimulatory effect of Erk1/2 signalling on the differentiation of dental pulp stem cells towards odontoblasts is confirmed by further studies on human cultures upon binding of extracellular calcium and strodium to the calcium-sensing receptor in stem cells (Ref. 119).

Another study on human adult dental pulp mesenchymal stem cells reveals that upon EphrinB binding to the EphB receptor, Erk1/2 signalling is activated leading to a block in the migration of dental pulp stem cells in ex vivo cultures (Ref. 120). The reduction in migratory ability is rescued after treatment with specific Mek1/2 inhibitors indicating the importance of Erk in adult pulp stem cell mobilisation.

Finally, in ex vivo cultures of periodontal ligament stem cells isolated from humans and dogs, elevated extracellular calcium levels are observed to drive phosphorylation of Erk1/2 kinases and the subsequent increase in the expression of cementum-associated proteins, such as cementum protein 1 (CEMP1) and protein tyrosine phosphatase-like, member A/cementum attachment protein (PTPLA/CAP) (Ref. 121). As a result, the periodontal ligament stem cells are induced to acquire a cementoblastic phenotype. All in all, during the last decades the isolation and the successful cultivation of dental stem cells from a variety of sources, such as the dental pulp, mandibular bone and the periodontal ligament in studies as those described above, have provided a deeper understanding of the mechanisms underlying dental development and disease. Figure 2 collectively depicts the downstream molecular players of the ERK cascade that regulate dental, craniofacial and orofacial formation analysed in this review.

Is it a matter of neural crest cells?

It is known that the majority of facial structures and a considerable number of cranial bones and sutures are derived from mesenchymal stem cells of neural crest origin. Descendants of neural crest cells contribute to both craniofacial and orofacial development as well as tooth formation. But would it be wise to conclude a neural crest cell-autonomous effect of ERK1/2 signalling in the

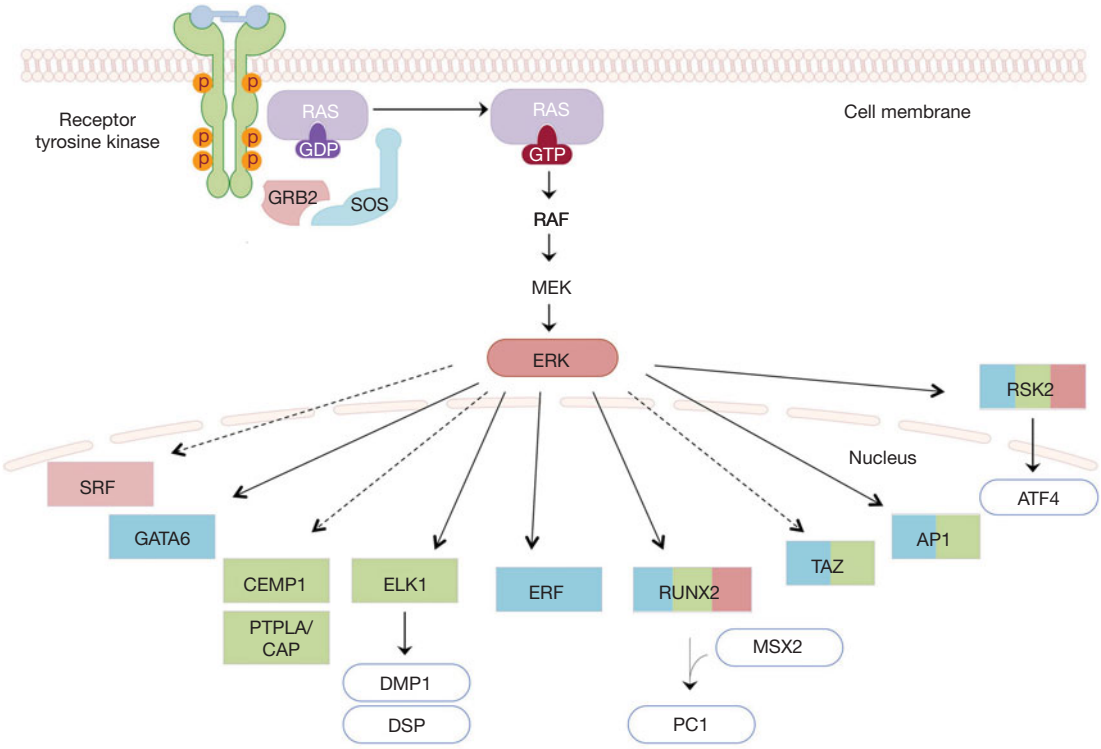

Fig. 2. Molecular targets of the RAS/ERK cascade in craniofacial and orodental development. A collective illustration of the effectors of the ERK kinase found to play crucial roles during craniofacial, orofacial and dental development is given by colour-coded boxes (blue for craniofacial, red for orofacial and green for dental development). RUNX2 and RSK2 are implicated in all three aspects of head development. In addition to their role in craniofacial development, TAZ and AP1 are found to have an effect in tooth formation (Refs 122, 123). FGF1, FGF2 and EphrinB are among the ligands that activate the RTKs, as described in the text. Dashed arrows indicate targets that are activated by ERK, yet no direct phosphorylation is reported so far. In the case of SRF, ERK phosphorylates ternary complex factors (TCFs) which in turn activate SRF (Refs 24, 124, 125). Common arrows are used in cases in which the corresponding effectors are known substrates of ERK1/2.

development of head structures? On the one hand, there is strong evidence that the Erk1/2 pathway regulates neural crest cell migration and differentiation, with the majority of the respective publications already described in this review including studies performed on crest-specific *Wnt1-Cre* mice that recapitulate a number of the human phenotypes (Refs 16, 22). A set of studies report the role of this cascade in neural crest induction and proliferation too, being however less clear about a direct or indirect mode of Erk function on this particular cell type, as recently reviewed (Ref. 126). On the other hand, however, during development, neural crest cells interact extensively with neighbouring paraxial mesoderm cells and these interactions have been shown to guide the movements of neural crest cells (Refs 127–129), resulting finally in the creation of well-defined head structures originating from the one of the two sources either the neural crest- or the mesoderm-derived progenitors. Furthermore, the branchial arch ectoderm, the endoderm and the paraxial mesoderm as well have been shown to play crucial roles in the determination of neural crest cell fate, providing signalling molecules that control the patterning of craniofacial structures. During mandibular formation, the oral ectoderm is the source of FGF and BMP signals that in turn regulate the expression of a variety of transcription factors in neural crest mesenchymal cells thus determining the polarity along the proximal–distal axis (Refs 130–132). Regarding tooth formation, the proximal domain of the mandibular ectoderm that produces FGF8 specifies the neural crest mesenchyme to form molars, while the distal domain which produces BMP4 instructs the neural crest mesenchyme to form incisors (Refs 133–135). Consequently, signals arising from paraxial mesodermal populations, the endoderm and ectoderm could guide and potentially affect the location, the final size and the fate of the neural crest populations. Therefore, we should not exclude the possibility that in some craniofacial disorders and even in some cases of neurocristopathies, particular malformations could spring from a primary defect in mesoderm-derived mesenchymal populations or even in the endodermal and ectodermal layers. The study of particular pathways in certain cell types in combination with cell tracing techniques would possibly provide answers to these questions.

Concluding remarks

RAS/ERK signalling has a major role in craniofacial and orodental development as evidenced by the plethora of human disorders triggered by mutations in the components of this particular pathway. Animal models and ex vivo studies have already revealed structures, cell types and stages of Erk1/2 action during development (summarised in Table 2); however, the precise molecular and cellular mechanisms are still under investigation. A number of features increase the difficulty in understanding the mechanisms underlying the pathophysiology of these disorders. First, there are cases in which a single mutation in one component of the pathway results in different phenotypic outcomes and consequently, in different syndromes in the affected individuals. For example, the E433K substitution in SOS1 that was initially discovered to lead to Noonan syndrome is also reported in patients with CFC syndrome and reversely, the K499E substitution in BRAF, although previously being reported only in CFC cases, is currently also found in patients with Noonan (Ref. 136).

Furthermore, different mutations in a single component often cause syndromes with features that are distinct, yet overlap in some cases. Noonan syndrome is caused by gain-of-function mutations in *PTPN11* (Ref. 75), while loss-of-function mutations in the same gene lead to LEOPARD syndrome (Ref. 78) which shares common craniofacial features with Noonan. Heterozygous inactivating mutations in *ERF* cause complex

Table 2. Overview of head developmental processes regulated by RAS/ERK pathway activity

Developmental system	Process	Ref(s)
Orofacial development	Mandibular bone formation	(Refs 16, 22)
	Mandibular condyle formation	(Ref. 23)
	Palatal fusion	(Refs 24, 26)
Craniofacial development	Neural crest cell migration	(Refs 24, 25)
	Myogenic differentiation	(Refs 137, 138)
	Calvarial bone mineralisation	(Refs 91, 95, 99, 101)
Dental development	Enamel mineralisation	(Refs 109, 110, 114)
	Odontoblast differentiation	(Refs 115–119)
	Cementoblast differentiation	(Ref. 121)
	Dental pulp stem cell migration	(Ref. 120)

craniosynostosis in humans along with facial malformations (Ref. 47), while novel still uncharacterised mutations in the same gene cause craniofacial abnormalities without any evidence for craniosynostosis in the case of the newly discovered Chitayat syndrome (Ref. 62).

The administration of MEK/ERK inhibitors is efficiently used for the restoration of the normal phenotype in some animal models of RASopathies and craniosynostosis disorders, indicating the importance of rebalancing RAS/ERK signalling for normal development. A variety of compounds that inhibit different components of the RAS/ERK cascade have reached clinical trials for the treatment of specific types of cancer, such as PD184352 (MEK1/2 inhibitor) and Ulixertinib (ERK1/2 inhibitor), while others have already gained approval, as is the case of Trametinib, inhibitor of MEK1/2, for BRAF-mutant melanoma (Ref. 139). The experience in drug discovery obtained through years of research on this molecular pathway holds promise for a potential therapeutic application in craniofacial disorders (Ref. 140). However, since similar phenotypes are sometimes derived from either activating or overall suppressive mutations for this cascade, as observed for instance in some cases of orofacial clefts and RASopathies, further research is needed in order to gain an insight into the precise structures, developmental stages and molecular targets that are specifically involved each time. Variations in signal initiation and intensity can also lead to altered transcriptional outputs (Ref. 141). Additionally, cross-talks between ERK and other signalling pathways such as TGF-β/BMP (Refs 142, 143) and WNT pathway (Ref. 144) taking place during head formation increase the complexity surrounding the developmental outcome of particular modifications. Consequently, current studies aim to shed light on the accurate networks of players that regulate these processes downstream of the RAS/ERK cascade.

The greatest difficulty in understanding these mechanisms springs from the fact that calvarial and brain development, facial development as well as oral, jaw and dental formation are tightly connected and affected by each other. This could be the underlying reason for the opposing results observed for many of the involved factors and Erk activity *per se*. It is important to establish the exact cell that is affected by the specific genetic changes and the cell-autonomous or intercellular mechanisms causing the defects. Dental, oral and craniofacial manifestations often co-occur and attention should be also paid to the precise phenotypic characterisation of disease animal models. Although they recapitulate many disease features, in some cases they either display additional traits or miss some others, while particular phenotypes depend on the genetic background (Ref. 9). The need to separate primary from secondary effects of each mutation and study the specific phenotypes in isolated cell- or organ-culture systems is inevitable. In this direction, the isolation of specific populations of mesenchymal stem cells that give rise to craniofacial and dental structures is currently being explored with promising results (Refs 145–148). Organoid cultures have already been established for modelling microcephaly, Crown's and Alagille syndrome in addition to cancer and infectious diseases (Ref. 149) and could potentially serve as a useful tool for studying tooth development as well (Ref. 150). On the whole, stem cell-based technologies have a lot to offer in unravelling the precise molecular background of craniofacial and dental defects. Without this information, the extensive pipeline of RTK/RAS/ERK pathway-targeting drugs for cancer and other pathologies will be very difficult to be extrapolated to these genetic, early-onset developmental disorders.

Author ORCIDs. George Mavrothalassitis, 0000-0001-6214-3179

Acknowledgments. We apologise to researchers whose work was not cited because of space limitations or was cited indirectly through other publications. We would like to thank professor Andrew OM Wilkie for helpful comments and suggestions on the manuscript.

Financial support. This work was supported by an IKY-SIEMENS #AP2788 and a GSRT #KA4937 grant to GM and an Onassis Foundation Fellowship #GZM 008-1 to AV.

Conflict of interest. None.

References

1. **New HV, Howes G and Smith JC** (1991) Inductive interactions in early embryonic development. *Current Opinion in Genetics & Development* **1**, 196–203.
2. **Van Otterloo E, Williams T and Artinger KB** (2016) The old and new face of craniofacial research: how animal models inform human craniofacial genetic and clinical data. *Developmental Biology* **415**, 171–187.
3. **Neben CL and Merrill AE** (2015) Signaling pathways in craniofacial development: insights from rare skeletal disorders. *Current Topics in Developmental Biology* **115**, 493–542.
4. **Schlessinger J** (2000) Cell signaling by receptor tyrosine kinases. *Cell* **103**, 211–225.
5. **Pawson T** (2002) Regulation and targets of receptor tyrosine kinases. *European Journal of Cancer* **38**(Suppl 5), S3–10.
6. **Marshall CJ** (1996) Ras effectors. *Current Opinion in Cell Biology* **8**, 197–204.
7. **Quilliam LA, Khosravi-Far R, Huff SY and Der CJ** (1995) Guanine nucleotide exchange factors: activators of the Ras superfamily of proteins. *Bioessays* **17**, 395–404.
8. **Denayer E, de Ravel T and Legius E** (2008) Clinical and molecular aspects of RAS related disorders. *Journal of Medical Genetics* **45**, 695–703.
9. **Hernandez-Porras I and Guerra C** (2017) Modeling RASopathies with genetically modified mouse models. *Methods in Molecular Biology* **1487**, 379–408.
10. **Bush JO and Jiang R** (2012) Palatogenesis: morphogenetic and molecular mechanisms of secondary palate development. *Development* **139**, 231–243.
11. **Lan Y, Xu J and Jiang R** (2015) Cellular and molecular mechanisms of palatogenesis. *Current Topics in Developmental Biology* **115**, 59–84.
12. **Dudas M, Li WY, Kim J, Yang A and Kaartinen V** (2007) Palatal fusion – where do the midline cells go? A review on cleft palate, a major human birth defect. *Acta Histochemica* **109**, 1–14.

13. **Jalali A, Zhu X, Liu C and Nawshad A** (2012) Induction of palate epithelial mesenchymal transition by transforming growth factor beta3 signaling. *Development Growth & Differentiation* **54**, 633–648.
14. **Kim S, Lewis AE, Singh V, Ma X, Adelstein R and Bush JO** (2015) Convergence and extrusion are required for normal fusion of the mammalian secondary palate. *PLoS Biology* **13**, e1002122.
15. **Li C, Lan Y and Jiang R** (2017) Molecular and cellular mechanisms of palate development. *Journal of Dental Research* **96**, 1184–1191.
16. **Parada C, Han D, Grimaldi A, Sarrion P, Park SS, Pelikan R, Sanchez-Lara PA and Chai Y** (2015) Disruption of the ERK/MAPK pathway in neural crest cells as a potential cause of Pierre Robin sequence. *Development* **142**, 3734–3745.
17. **Cho KW, Cho SW, Lee JM, Lee MJ, Gang HS and Jung HS** (2008) Expression of phosphorylated forms of ERK, MEK, PTEN and PI3K in mouse oral development. *Gene Expression Patterns: GEP* **8**, 284–290.
18. **Conte F, Oti M, Dixon J, Carels CE, Rubini M and Zhou H** (2016) Systematic analysis of copy number variants of a large cohort of orofacial cleft patients identifies candidate genes for orofacial clefts. *Human Genetics* **135**, 41–59.
19. **Vieira AR, Avila JR, Daack-Hirsch S, Dragan E, Felix TM, Rahimov F, Harrington J, Schultz RR, Watanabe Y, Johnson M, Fang J, O'Brien SE, Orioli IM, Castilla EE, Fitzpatrick DR, Jiang R, Marazita ML and Murray JC** (2005) Medical sequencing of candidate genes for nonsyndromic cleft lip and palate. *PLoS Genetics* **1**, e64.
20. **Matsumura K, Taketomi T, Yoshizaki K, Arai S, Sanui T, Yoshiga D, Yoshimura A and Nakamura S** (2011) Sprouty2 controls proliferation of palate mesenchymal cells via fibroblast growth factor signaling. *Biochemical and Biophysical Research Communications* **404**, 1076–1082.
21. **Bush JO and Soriano P** (2010) Ephrin-B1 forward signaling regulates craniofacial morphogenesis by controlling cell proliferation across Eph-ephrin boundaries. *Genes & Development* **24**, 2068–2080.
22. **Newbern J, Zhong J, Wickramasinghe RS, Li X, Wu Y, Samuels I, Cherosky N, Karlo JC, O'Loughlin B, Wikenheiser J, Gargesha M, Doughman YQ, Charron J, Ginty DD, Watanabe M, Saitta SC, Snider WD and Landreth GE** (2008) Mouse and human phenotypes indicate a critical conserved role for ERK2 signaling in neural crest development. *Proceedings of the National Academy of Sciences of the USA* **105**, 17115–17120.
23. **Kamiya N, Shen J, Noda K, Kitami M, Feng GS, Chen D and Komatsu Y** (2015) SHP2-Deficiency in chondrocytes deforms orofacial cartilage and ciliogenesis in mice. *Journal of Bone and Mineral Research* **30**, 2028–2032.
24. **Vasudevan HN and Soriano P** (2014) SRF regulates craniofacial development through selective recruitment of MRTF cofactors by PDGF signaling. *Developmental Cell* **31**, 332–344.
25. **Kelly ML, Astsaturov A, Rhodes J and Chernoff J** (2014) A Pak1/Erk signaling module acts through Gata6 to regulate cardiovascular development in zebrafish. *Developmental Cell* **29**, 350–359.
26. **Yamamoto T, Cui XM and Shuler CF** (2003) Role of ERK1/2 signaling during EGF-induced inhibition of palatal fusion. *Developmental Biology* **260**, 512–521.
27. **Morriss-Kay GM and Wilkie AO** (2005) Growth of the normal skull vault and its alteration in craniosynostosis: insights from human genetics and experimental studies. *Journal of Anatomy* **207**, 637–653.
28. **Richtsmeier JT and Flaherty K** (2013) Hand in glove: brain and skull in development and dysmorphogenesis. *Acta Neuropathologica* **125**, 469–489.
29. **Yoshida T, Vivatbutsiri P, Morriss-Kay G, Saga Y and Iseki S** (2008) Cell lineage in mammalian craniofacial mesenchyme. *Mechanisms of Development* **125**, 797–808.
30. **Twigg SR and Wilkie AO** (2015) A genetic-pathophysiological framework for craniosynostosis. *American Journal of Human Genetics* **97**, 359–377.
31. **Deckelbaum RA, Holmes G, Zhao Z, Tong C, Basilico C and Loomis CA** (2012) Regulation of cranial morphogenesis and cell fate at the neural crest-mesoderm boundary by engrailed 1. *Development* **139**, 1346–1358.
32. **Lana-Elola E, Rice R, Grigoriadis AE and Rice DP** (2007) Cell fate specification during calvarial bone and suture development. *Developmental Biology* **311**, 335–346.
33. **Jiang X, Iseki S, Maxson RE, Sucov HM and Morriss-Kay GM** (2002) Tissue origins and interactions in the mammalian skull vault. *Developmental Biology* **241**, 106–116.
34. **Opperman LA** (2000) Cranial sutures as intramembranous bone growth sites. *Developmental Dynamics* **219**, 472–485.
35. **Sahar DE, Longaker MT and Quarto N** (2005) Sox9 neural crest determinant gene controls patterning and closure of the posterior frontal cranial suture. *Developmental Biology* **280**, 344–361.
36. **James AW, Xu Y, Lee JK, Wang R and Longaker MT** (2009) Differential effects of TGF-beta1 and TGF-beta3 on chondrogenesis in posterofrontal cranial suture-derived mesenchymal cells in vitro. *Plastic and Reconstructive Surgery* **123**, 31–43.
37. **Katsianou MA, Adamopoulos C, Vastardis H and Basdra EK** (2016) Signaling mechanisms implicated in cranial sutures pathophysiology: craniosynostosis. *Bba Clinical* **6**, 165–176.
38. **Wilkie AO, Slaney SF, Oldridge M, Poole MD, Ashworth GJ, Hockley AD, Hayward RD, David DJ, Pulleyn LJ, Rutland P, Malcolm S, Winter RM and Reardon W** (1995) Apert syndrome results from localized mutations of FGFR2 and is allelic with Crouzon syndrome. *Nature Genetics* **9**, 165–172.
39. **Yin L, Du X, Li C, Xu X, Chen Z, Su N, Zhao L, Qi H, Li F, Xue J, Yang J, Jin M, Deng C and Chen L** (2008) A Pro253Arg mutation in fibroblast growth factor receptor 2 (Fgfr2) causes skeleton malformation mimicking human Apert syndrome by affecting both chondrogenesis and osteogenesis. *Bone* **42**, 631–643.
40. **Chen L, Li D, Li C, Engel A and Deng CX** (2003) A Ser252Trp [corrected] substitution in mouse fibroblast growth factor receptor 2 (Fgfr2) results in craniosynostosis. *Bone* **33**, 169–178.
41. **Shukla V, Coumoul X, Wang RH, Kim HS and Deng CX** (2007) RNA interference and inhibition of MEK-ERK signaling prevent abnormal skeletal phenotypes in a mouse model of craniosynostosis. *Nature Genetics* **39**, 1145–1150.
42. **Wang Y, Sun M, Uhlhorn VL, Zhou X, Peter I, Martinez-Abadias N, Hill CA, Percival CJ, Richtsmeier JT, Huso DL and Jabs EW** (2010) Activation of p38 MAPK pathway in the skull abnormalities of Apert syndrome Fgfr2(+P253R) mice. *BMC Developmental Biology* **10**, 22.
43. **Reardon W, Winter RM, Rutland P, Pulleyn LJ, Jones BM and Malcolm S** (1994) Mutations in the fibroblast growth factor receptor 2 gene cause Crouzon syndrome. *Nature Genetics* **8**, 98–103.
44. **Li X, Young NM, Tropp S, Hu D, Xu Y, Hallgrimsson B and Marcucio RS** (2013) Quantification of shape and cell polarity reveals a novel mechanism underlying malformations resulting from related FGF mutations during facial morphogenesis. *Human Molecular Genetics* **22**, 5160–5172.
45. **Pfaff MJ, Xue K, Li L, Horowitz MC, Steinbacher DM and Eswarakumar JVP** (2016) FGFR2c-mediated ERK-MAPK activity regulates coronal suture development. *Developmental Biology* **415**, 242–250.
46. **Timberlake AT, Furey CG, Choi J, Nelson-Williams C, Loring E, Galm A, Kahle KT, Steinbacher DM, Larysz D, Persing JA and Lifton RP** (2017) De novo mutations in inhibitors of Wnt, BMP, and Ras/ERK signaling pathways in non-syndromic midline craniosynostosis. *Proceedings of the National Academy of Sciences of the USA* **114**, E7341–E7E47.
47. **Twigg SR, Vorgia E, McGowan SJ, Peraki I, Fenwick AL, Sharma VP, Allegra M, Zaragkoulias A, Sadighi Akha E, Knight SJ, Lord H, Lester T, Izatt L, Lampe AK, Mohammed SN, Stewart FJ, Verloes A, Wilson LC, Healy C, Sharpe PT, Hammond P, Hughes J, Taylor S, Johnson D, Wall SA, Mavrothalassitis G and Wilkie AO** (2013) Reduced dosage of ERF causes complex craniosynostosis in humans and mice and links ERK1/2 signaling to regulation of osteogenesis. *Nature Genetics* **45**, 308–313.
48. **Chaudhry A, Sabatini P, Han L, Ray PN, Forrest C and Bowdin S** (2015) Heterozygous mutations in ERF cause syndromic craniosynostosis with multiple suture involvement. *American Journal of Medical Genetics. Part A* **167A**, 2544–2547.
49. **Clarke CM, Fok VT, Gustafson JA, Smyth MD, Timms AE, Frazar CD, Smith JD, Birgfeld CB, Lee A, Ellenbogen RG, Gruss JS, Hopper RA and Cunningham ML** (2018) Single suture craniosynostosis: identification of rare variants in genes associated with syndromic forms. *American Journal of Medical Genetics. Part A* **176**, 290–300.
50. **Bezniakow N, Gos M and Obersztyn E** (2014) The RASopathies as an example of RAS/MAPK pathway disturbances – clinical presentation and molecular pathogenesis of selected syndromes. *Developmental Period Medicine* **18**, 285–296.
51. **Nakamura T, Gulick J, Pratt R and Robbins J** (2009) Noonan syndrome is associated with enhanced pERK activity, the repression of which can prevent craniofacial malformations. *Proceedings of the National Academy of Sciences of the USA* **106**, 15436–15441.

52. **Wu X, Simpson J, Hong JH, Kim KH, Thavarajah NK, Backx PH, Neel BG and Araki T** (2011) MEK-ERK pathway modulation ameliorates disease phenotypes in a mouse model of Noonan syndrome associated with the Raf1(L613V) mutation. *Journal of Clinical Investigation* **121**, 1009–1025.
53. **De Rocca Serra-Nedelec A, Edouard T, Treguer K, Tajan M, Araki T, Dance M, Mus M, Montagner A, Tauber M, Salles JP, Valet P, Neel BG, Raynal P and Yart A** (2012) Noonan syndrome-causing SHP2 mutants inhibit insulin-like growth factor 1 release via growth hormone-induced ERK hyperactivation, which contributes to short stature. *Proceedings of the National Academy of Sciences of the USA* **109**, 4257–4262.
54. **Razzaque MA, Komoike Y, Nishizawa T, Inai K, Furutani M, Higashinakagawa T and Matsuoka R** (2012) characterization of a novel KRAS mutation identified in Noonan syndrome. *American Journal of Medical Genetics. Part A* **158A**, 524–532.
55. **Bonetti M, Rodriguez-Martinez V, Paardekooper Overman J, Overvoorde J, van Eekelen M, Jopling C and Hertog J** (2014) Distinct and overlapping functions of ptpn11 genes in Zebrafish development. *PLoS ONE* **9**, e94884.
56. **Marin TM, Keith K, Davies B, Conner DA, Guha P, Kalaitzidis D, Wu X, Lauriol J, Wang B, Bauer M, Bronson R, Franchini KG, Neel BG and Kontaridis MI** (2011) Rapamycin reverses hypertrophic cardiomyopathy in a mouse model of LEOPARD syndrome-associated PTPN11 mutation. *Journal of Clinical Investigation* **121**, 1026–1043.
57. **Rodriguez-Viciana P and Rauen KA** (2008) Biochemical characterization of novel germline BRAF and MEK mutations in cardio-facio-cutaneous syndrome. *Methods in Enzymology* **438**, 277–289.
58. **Inoue S, Moriya M, Watanabe Y, Miyagawa-Tomita S, Niihori T, Oba D, Ono M, Kure S, Ogura T, Matsubara Y and Aoki Y** (2014) New BRAF knockin mice provide a pathogenetic mechanism of developmental defects and a therapeutic approach in cardio-facio-cutaneous syndrome. *Human Molecular Genetics* **23**, 6553–6566.
59. **Anastasaki C, Rauen KA and Patton EE** (2012) Continual low-level MEK inhibition ameliorates cardio-facio-cutaneous phenotypes in zebrafish. *Disease Models & Mechanisms* **5**, 546–552.
60. **Pasteris NG, Cadle A, Logie LJ, Porteous ME, Schwartz CE, Stevenson RE, Glover TW, Wilroy RS and Gorski JL** (1994) Isolation and characterization of the faciogenital dysplasia (aarskog-scott syndrome) gene: a putative Rho/Rac guanine nucleotide exchange factor. *Cell* **79**, 669–678.
61. **Zou W, Greenblatt MB, Shim JH, Kant S, Zhai B, Lotinun S, Brady N, Hu DZ, Gygi SP, Baron R, Davis RJ, Jones D and Glimcher LH** (2011) MLK3 regulates bone development downstream of the faciogenital dysplasia protein FGD1 in mice. *Journal of Clinical Investigation* **121**, 4383–4392.
62. **Balasubramanian M, Lord H, Levesque S, Guturu H, Thuriot F, Sillon G, Wenger AM, Sureka DL, Lester T, Johnson DS, Bowen J, Calhoun AR, Viskochil DH, Bejerano G, Bernstein JA and Chitayat D** (2017) Chitayat syndrome: hyperphalangism, characteristic facies, hallux valgus and bronchomalacia results from a recurrent c.266A > G p.(Tyr89Cys) variant in the ERF gene. *Journal of Medical Genetics* **54**, 157–165.
63. **Ng SB, Bigham AW, Buckingham KJ, Hannibal MC, McMillin MJ, Gildersleeve HI, Beck AE, Tabor HK, Cooper GM, Mefford HC, Lee C, Turner EH, Smith JD, Rieder MJ, Yoshiura K, Matsumoto N, Ohta T, Niikawa N, Nickerson DA, Bamshad MJ and Shendure J** (2010) Exome sequencing identifies MLL2 mutations as a cause of Kabuki syndrome. *Nature Genetics* **42**, 790–793.
64. **Lederer D, Grisart B, Digilio MC, Benoit V, Crespin M, Ghariani SC, Maystadt I, Dallapiccola B and Verellen-Dumoulin C** (2012) Deletion of KDM6A, a histone demethylase interacting with MLL2, in three patients with Kabuki syndrome. *American Journal of Human Genetics* **90**, 119–124.
65. **Bogershausen N, Tsai IC, Pohl E, Kiper PO, Beleggia F, Percin EF, Keupp K, Matchan A, Milz E, Alanay Y, Kayserili H, Liu Y, Banka S, Kranz A, Zenker M, Wieczorek D, Elcioglu N, Prontera P, Lyonnet S, Meitinger T, Stewart AF, Donnai D, Strom TM, Boduroglu K, Yigit G, Li Y, Katsanis N and Wollnik B** (2015) RAP1-mediated MEK/ERK pathway defects in Kabuki syndrome. *Journal of Clinical Investigation* **125**, 3585–3599.
66. **York RD, Yao H, Dillon T, Ellig CL, Eckert SP, McCleskey EW and Stork PJ** (1998) Rap1 mediates sustained MAP kinase activation induced by nerve growth factor. *Nature* **392**, 622–626.
67. **Hu CD, Kariya K, Kotani G, Shirouzu M, Yokoyama S and Kataoka T** (1997) Coassociation of Rap1A and Ha-Ras with Raf-1 N-terminal region interferes with ras-dependent activation of Raf-1. *Journal of Biological Chemistry* **272**, 11702–5.
68. **Park J, Park OJ, Yoon WJ, Kim HJ, Choi KY, Cho TJ and Ryoo HM** (2012) Functional characterization of a novel FGFR2 mutation, E731 K, in craniosynostosis. *Journal of Cellular Biochemistry* **113**, 457–464.
69. **Muenke M, Schell U, Hehr A, Robin NH, Losken HW, Schinzel A, Pulleyn LJ, Rutland P, Reardon W, Malcolm S and Winter RM** (1994) A common mutation in the fibroblast growth factor receptor 1 gene in Pfeiffer syndrome. *Nature Genetics* **8**, 269–274.
70. **Schell U, Hehr A, Feldman GJ, Robin NH, Zackai EH, de Die-Smulders C, Viskochil DH, Stewart JM, Wolff G, Ohashi H, Price RA, Cohen Jr MM and Muenke M** (1995) Mutations in FGFR1 and FGFR2 cause familial and sporadic Pfeiffer syndrome. *Human Molecular Genetics* **4**, 323–328.
71. **Rutland P, Pulleyn LJ, Reardon W, Baraitser M, Hayward R, Jones B, Malcolm S, Winter RM, Oldridge M, Slaney SF, Poole MD and Wilkie AOM** (1995) Identical mutations in the FGFR2 gene cause both Pfeiffer and Crouzon syndrome phenotypes. *Nature Genetics* **9**, 173–176.
72. **Przylepa KA, Paznekas W, Zhang M, Golabi M, Bias W, Bamshad MJ, Carey JC, Hall BD, Stevenson R, Orlow S, Cohen Jr MM and Jabs EW** (1996) Fibroblast growth factor receptor 2 mutations in Beare-Stevenson cutis gyrata syndrome. *Nature Genetics* **13**, 492–494.
73. **Wang Y, Zhou X, Oberoi K, Phelps R, Couwenhoven R, Sun M, Rezza A, Holmes G, Percival CJ, Friedenthal J, Krejci P, Richtsmeier JT, Huso DL, Rendl M and Jabs EW** (2012) P38 inhibition ameliorates skin and skull abnormalities in Fgfr2 Beare-Stevenson mice. *Journal of Clinical Investigation* **122**, 2153–2164.
74. **Merrill AE, Sarukhanov A, Krejci P, Idoni B, Camacho N, Estrada KD, Lyons KM, Deixler H, Robinson H, Chitayat D, Curry CJ, Lachman RS, Wilcox WR and Krakow D** (2012) Bent bone dysplasia-FGFR2 type, a distinct skeletal disorder, has deficient canonical FGF signaling. *American Journal of Human Genetics* **90**, 550–557.
75. **Tartaglia M, Mehler EL, Goldberg R, Zampino G, Brunner HG, Kremer H, van der Burgt I, Crosby AH, Ion A, Jeffery S, Kalidas K, Patton MA, Kucherlapati RS and Gelb BD** (2001) Mutations in PTPN11, encoding the protein tyrosine phosphatase SHP-2, cause Noonan syndrome. *Nature Genetics* **29**, 465–468.
76. **Moncini S, Bonati MT, Morella I, Ferrari L, Brambilla R and Riva P** (2015) Differential allelic expression of SOS1 and hyperexpression of the activating SOS1 c.755C variant in a Noonan syndrome family. *European Journal of Human Genetics* **23**, 1531–1537.
77. **Aoki Y, Niihori T, Banjo T, Okamoto N, Mizuno S, Kurosawa K, Ogata T, Takada F, Yano M, Ando T, Hoshika T, Barnett C, Ohashi H, Kawame H, Hasegawa T, Okutani T, Nagashima T, Hasegawa S, Funayama R, Nakayama K, Inoue S, Watanabe Y, Ogura T and Matsubara Y** (2013) Gain-of-function mutations in RIT1 cause Noonan syndrome, a RAS/MAPK pathway syndrome. *American Journal of Human Genetics* **93**, 173–180.
78. **Digilio MC, Conti E, Sarkozy A, Mingarelli R, Dottorini T, Marino B, Pizzuti A and Dallapiccola B** (2002) Grouping of multiple-lentigines/LEOPARD and Noonan syndromes on the PTPN11 gene. *American Journal of Human Genetics* **71**, 389–394.
79. **Pandit B, Sarkozy A, Pennacchio LA, Carta C, Oishi K, Martinelli S, Pogna EA, Schackwitz W, Ustaszewska A, Landstrom A, Bos JM, Ommen SR, Esposito G, Lepri F, Faul C, Mundel P, Lopez Siguero JP, Tenconi R, Selicorni A, Rossi C, Mazzanti L, Torrente I, Marino B, Digilio MC, Zampino G, Ackerman MJ, Dallapiccola B, Tartaglia M and Gelb BD** (2007) Gain-of-function RAF1 mutations cause Noonan and LEOPARD syndromes with hypertrophic cardiomyopathy. *Nature Genetics* **39**, 1007–1012.
80. **Sarkozy A, Carta C, Moretti S, Zampino G, Digilio MC, Pantaleoni F, Scioletti AP, Esposito G, Cordeddu V, Lepri F, Petrangeli V, Dentici ML, Mancini GM, Selicorni A, Rossi C, Mazzanti L, Marino B, Ferrero GB, Silengo MC, Memo L, Stanzial F, Faravelli F, Stuppia L, Puxeddu E, Gelb BD, Dallapiccola B and Tartaglia M** (2009) Germline BRAF mutations in Noonan, LEOPARD, and cardiofaciocutaneous syndromes: molecular diversity and associated phenotypic spectrum. *Human Mutation* **30**, 695–702.
81. **Narumi Y, Aoki Y, Niihori T, Neri G, Cave H, Verloes A, Nava C, Kavamura MI, Okamoto N, Kurosawa K, Hennekam RC, Wilson LC,**

Gillessen-Kaesbach G, Wieczorek D, Lapunzina P, Ohashi H, Makita Y, Kondo I, Tsuchiya S, Ito E, Sameshima K, Kato K, Kure S and Matsubara Y (2007) Molecular and clinical characterization of cardio-facio-cutaneous (CFC) syndrome: overlapping clinical manifestations with Costello syndrome. *American Journal of Medical Genetics. Part A* **143A**, 799–807.

82. **Niihori T, Aoki Y, Narumi Y, Neri G, Cave H, Verloes A, Okamoto N, Hennekam RC, Gillessen-Kaesbach G, Wieczorek D, Kavamura MI, Kurosawa K, Ohashi H, Wilson L, Heron D, Bonneau D, Corona G, Kaname T, Naritomi K, Baumann C, Matsumoto N, Kato K, Kure S and Matsubara Y** (2006) Germline KRAS and BRAF mutations in cardio-facio-cutaneous syndrome. *Nature Genetics* **38**, 294–296.
83. **Aoki Y, Niihori T, Kawame H, Kurosawa K, Ohashi H, Tanaka Y, Filocamo M, Kato K, Suzuki Y, Kure S and Matsubara Y** (2005) Germline mutations in HRAS proto-oncogene cause Costello syndrome. *Nature Genetics* **37**, 1038–1040.
84. **Wallace MR, Marchuk DA, Andersen LB, Letcher R, Odeh HM, Saulino AM, Fountain JW, Brereton A, Nicholson J, Mitchell AL, Brownstein BH and Collins FS** (1990) Type 1 neurofibromatosis gene: identification of a large transcript disrupted in three NF1 patients. *Science* **249**, 181–186.
85. **Brems H, Chmara M, Sahbatou M, Denayer E, Taniguchi K, Kato R, Somers R, Messiaen L, De Schepper S, Fryns JP, Cools J, Marynen P, Thomas G, Yoshimura A and Legius E** (2007) Germline loss-of-function mutations in SPRED1 cause a neurofibromatosis 1-like phenotype. *Nature Genetics* **39**, 1120–1126.
86. **Eerola I, Boon LM, Mulliken JB, Burrows PE, Dompmartin A, Watanabe S, Vanwijck R and Vikkula M** (2003) Capillary malformation-arteriovenous malformation, a new clinical and genetic disorder caused by RASA1 mutations. *American Journal of Human Genetics* **73**, 1240–1249.
87. **Hart TC, Zhang Y, Gorry MC, Hart PS, Cooper M, Marazita ML, Marks JM, Cortelli JR and Pallos D** (2002) A mutation in the SOS1 gene causes hereditary gingival fibromatosis type 1. *American Journal of Human Genetics* **70**, 943–954.
88. **Temtamy SA, Miller JD, Dorst JP, Hussels-Maumenee I, Salinas C, Lacassie Y and Kenyon KR** (1975) The Coffin-Lowry syndrome: a simply inherited trait comprising mental retardation, faciodigital anomalies and skeletal involvement. *Birth Defects Original Article Series* **11**, 133–152.
89. **Trivier E, De Cesare D, Jacquot S, Pannetier S, Zackai E, Young I, Mandel JL, Sassone-Corsi P and Hanauer A** (1996) Mutations in the kinase Rsk-2 associated with Coffin-Lowry syndrome. *Nature* **384**, 567–570.
90. **Nikopensius T, Saag M, Jagomagi T, Annilo T, Kals M, Kivistik PA, Milani L and Metspalu A** (2013) A missense mutation in DUSP6 is associated with class III malocclusion. *Journal of Dental Research* **92**, 893–898.
91. **Li Y, Liu J, Hudson M, Kim S and Hatch NE** (2010) FGF2 promotes Msx2 stimulated PC-1 expression via Frs2/MAPK signaling. *Journal of Cellular Biochemistry* **111**, 1346–1358.
92. **Thouverey C, Bechkoff G, Pikula S and Buchet R** (2009) Inorganic pyrophosphate as a regulator of hydroxyapatite or calcium pyrophosphate dihydrate mineral deposition by matrix vesicles. *Osteoarthritis and Cartilage/OARS, Osteoarthritis Research Society* **17**, 64–72.
93. **Terkeltaub RA** (2001) Inorganic pyrophosphate generation and disposition in pathophysiology. *American Journal of Physiology. Cell Physiology* **281**, C1–C11.
94. **Hessle L, Johnson KA, Anderson HC, Narisawa S, Sali A, Goding JW, Terkeltaub R and Millan JL** (2002) Tissue-nonspecific alkaline phosphatase and plasma cell membrane glycoprotein-1 are central antagonistic regulators of bone mineralization. *Proceedings of the National Academy of Sciences of the USA* **99**, 9445–9449.
95. **Kim HJ, Lee MH, Park HS, Park MH, Lee SW, Kim SY, Choi JY, Shin HI and Ryoo HM** (2003) Erk pathway and activator protein 1 play crucial roles in FGF2-stimulated premature cranial suture closure. *Developmental Dynamics* **227**, 335–346.
96. **Byun MR, Kim AR, Hwang JH, Kim KM, Hwang ES and Hong JH** (2014) FGF2 stimulates osteogenic differentiation through ERK induced TAZ expression. *Bone* **58**, 72–80.
97. **Quarto N, Senarath-Yapa K, Renda A and Longaker MT** (2015) TWIST1 silencing enhances in vitro and in vivo osteogenic differentiation of human adipose-derived stem cells by triggering activation of BMP-ERK/FGF signaling and TAZ upregulation. *Stem Cells* **33**, 833–847.
98. **Rice DP, Aberg T, Chan Y, Tang Z, Kettunen PJ, Pakarinen L, Maxson RE and Thesleff I** (2000) Integration of FGF and TWIST in calvarial bone and suture development. *Development* **127**, 1845–1855.
99. **Mansukhani A, Bellosta P, Sahni M and Basilico C** (2000) Signaling by fibroblast growth factors (FGF) and fibroblast growth factor receptor 2 (FGFR2)-activating mutations blocks mineralization and induces apoptosis in osteoblasts. *Journal of Cell Biology* **149**, 1297–1308.
100. **Liu J, Kwon TG, Nam HK and Hatch NE** (2013) Craniosynostosis-associated Fgfr2(C342Y) mutant bone marrow stromal cells exhibit cell autonomous abnormalities in osteoblast differentiation and bone formation. *Biomed Research International* **2013**, 292506.
101. **Kono SJ, Oshima Y, Hoshi K, Bonewald LF, Oda H, Nakamura K, Kawaguchi H and Tanaka S** (2007) Erk pathways negatively regulate matrix mineralization. *Bone* **40**, 68–74.
102. **Thesleff I** (2003) Epithelial-mesenchymal signalling regulating tooth morphogenesis. *Journal of Cell Science* **116**, 1647–1648.
103. **Thesleff I and Sharpe P** (1997) Signalling networks regulating dental development. *Mechanisms of Development* **67**, 111–123.
104. **Klein OD, Minowada G, Peterkova R, Kangas A, Yu BD, Lesot H, Peterka M, Jernvall J and Martin GR** (2006) Sprouty genes control diastema tooth development via bidirectional antagonism of epithelial-mesenchymal FGF signaling. *Developmental Cell* **11**, 181–190.
105. **Cho KW, Cai J, Kim HY, Hosoya A, Ohshima H, Choi KY and Jung HS** (2009) ERK activation is involved in tooth development via FGF10 signaling. *Journal of Experimental Zoology. Part B, Molecular and Developmental Evolution* **312**, 901–911.
106. **Lee MJ, Cai J, Kwak SW, Cho SW, Harada H and Jung HS** (2009) MAPK mediates Hsp25 signaling in incisor development. *Histochemistry and Cell Biology* **131**, 593–603.
107. **Akram A, McKnight MM, Bellardie H, Beale V and Evans RD** (2015) Craniofacial malformations and the orthodontist. *British Dental Journal* **218**, 129–141.
108. **Cao H, Alrejaye N, Klein OD, Goodwin AF and Oberoi S** (2017) A review of craniofacial and dental findings of the RASopathies. *Orthodontics & Craniofacial Research* **20**(Suppl 1), 32–38.
109. **Goodwin AF, Oberoi S, Landan M, Charles C, Massie JC, Fairley C, Rauen KA and Klein OD** (2014) Craniofacial and dental development in Costello syndrome. *American Journal of Medical Genetics. Part A* **164A**, 1425–1430.
110. **Goodwin AF, Tidyman WE, Jheon AH, Sharir A, Zheng X, Charles C, Fagin JA, McMahon M, Diekwisch TG, Ganss B, Rauen KA and Klein OD** (2014) Abnormal Ras signaling in Costello syndrome (CS) negatively regulates enamel formation. *Human Molecular Genetics* **23**, 682–692.
111. **Goodwin AF, Oberoi S, Landan M, Charles C, Groth J, Martinez A, Fairley C, Weiss LA, Tidyman WE, Klein OD and Rauen KA** (2013) Craniofacial and dental development in cardio-facio-cutaneous syndrome: the importance of Ras signaling homeostasis. *Clinical Genetics* **83**, 539–544.
112. **Lu C, Huguley S, Cui C, Cabaniss LB, Waite PD, Sarver DM, Mamaeva OA and MacDougall M** (2016) Effects of FGFR signaling on cell proliferation and differentiation of Apert dental cells. *Cells Tissues Organs* **201**, 26–37.
113. **Marangoni P, Charles C, Tafforeau P, Laugel-Haushalter V, Joo A, Bloch-Zupan A, Klein OD and Viriot L** (2015) Phenotypic and evolutionary implications of modulating the ERK-MAPK cascade using the dentition as a model. *Scientific Reports* **5**, 11658.
114. **Abe K, Miyoshi K, Muto T, Ruspita I, Horiguchi T, Nagata T and Noma T** (2007) Establishment and characterization of rat dental epithelial derived ameloblast-lineage clones. *Journal of Bioscience and Bioengineering* **103**, 479–485.
115. **Sagomonyants K and Mina M** (2014) Stage-specific effects of fibroblast growth factor 2 on the differentiation of dental pulp cells. *Cells Tissues Organs* **199**, 311–328.
116. **Sagomonyants K, Kalajzic I, Maye P and Mina M** (2017) FGF signaling prevents the terminal differentiation of odontoblasts. *Journal of Dental Research* **96**, 663–670.
117. **Sagomonyants K, Kalajzic I, Maye P and Mina M** (2015) Enhanced dentinogenesis of pulp progenitors by early exposure to FGF2. *Journal of Dental Research* **94**, 1582–1590.
118. **Eapen A, Ramachandran A and George A** (2012) Dentin phosphoprotein (DPP) activates integrin-mediated anchorage-dependent signals in

undifferentiated mesenchymal cells. *Journal of Biological Chemistry* **287**, 5211–5224.
119. **Mizumachi H, Yoshida S, Tomokiyo A, Hasegawa D, Hamano S, Yuda A, Sugii H, Serita S, Mitarai H, Koori K, Wada N and Maeda H** (2017) Calcium-sensing receptor-ERK signaling promotes odontoblastic differentiation of human dental pulp cells. *Bone* **101**, 191–201.
120. **Stokowski A, Shi S, Sun T, Bartold PM, Koblar SA and Gronthos S** (2007) Ephb/ephrin-B interaction mediates adult stem cell attachment, spreading, and migration: implications for dental tissue repair. *Stem Cells* **25**, 156–164.
121. **Paula-Silva FW, Ghosh A, Arzate H, Kapila S, da Silva LA and Kapila YL** (2010) Calcium hydroxide promotes cementogenesis and induces cementoblastic differentiation of mesenchymal periodontal ligament cells in a CEMP1- and ERK-dependent manner. *Calcified Tissue International* **87**, 144–157.
122. **Wang J and Martin JF** (2017) Hippo pathway: an emerging regulator of craniofacial and dental development. *Journal of Dental Research* **96**, 1229–1237.
123. **Matsushita K, Motani R, Sakuta T, Yamaguchi N, Koga T, Matsuo K, Nagaoka S, Abeyama K, Maruyama I and Torii M** (2000) The role of vascular endothelial growth factor in human dental pulp cells: induction of chemotaxis, proliferation, and differentiation and activation of the AP-1-dependent signaling pathway. *Journal of Dental Research* **79**, 1596–1603.
124. **Esnault C, Gualdrini F, Horswell S, Kelly G, Stewart A, East P, Matthews N and Treisman R** (2017) ERK-Induced Activation of TCF family of SRF cofactors initiates a chromatin modification cascade associated with transcription. *Molecular Cell* **65**, 1081–1095, e5.
125. **Buchwalter G, Gross C and Wasylyk B** (2004) Ets ternary complex transcription factors. *Gene* **324**, 1–14.
126. **Dinsmore CJ and Soriano P** (2018) MAPK and PI3K signaling: at the crossroads of neural crest development. *Developmental Biology*. https://doi.org/10.1016/j.ydbio.2018.02.003
127. **Vitelli F, Morishima M, Taddei I, Lindsay EA and Baldini A** (2002) Tbx1 mutation causes multiple cardiovascular defects and disrupts neural crest and cranial nerve migratory pathways. *Human Molecular Genetics* **11**, 915–922.
128. **Trainor P and Krumlauf R** (2000) Plasticity in mouse neural crest cells reveals a new patterning role for cranial mesoderm. *Nature Cell Biology* **2**, 96–102.
129. **Noden DM and Trainor PA** (2005) Relations and interactions between cranial mesoderm and neural crest populations. *Journal of Anatomy* **207**, 575–601.
130. **Trumpp A, Depew MJ, Rubenstein JL, Bishop JM and Martin GR** (1999) Cre-mediated gene inactivation demonstrates that FGF8 is required for cell survival and patterning of the first branchial arch. *Genes & Development* **13**, 3136–3148.
131. **Tucker AS, Yamada G, Grigoriou M, Pachnis V and Sharpe PT** (1999) Fgf-8 determines rostral-caudal polarity in the first branchial arch. *Development* **126**, 51–61.
132. **Liu W, Selever J, Murali D, Sun X, Brugger SM, Ma L, Schwartz RJ, Maxson R, Furuta Y and Martin JF** (2005) Threshold-specific requirements for Bmp4 in mandibular development. *Developmental Biology* **283**, 282–293.
133. **Tucker AS, Matthews KL and Sharpe PT** (1998) Transformation of tooth type induced by inhibition of BMP signaling. *Science* **282**, 1136–1138.
134. **Tucker AS and Sharpe PT** (1999) Molecular genetics of tooth morphogenesis and patterning: the right shape in the right place. *Journal of Dental Research* **78**, 826–834.
135. **Chai Y and Maxson Jr RE**. (2006) Recent advances in craniofacial morphogenesis. *Developmental Dynamics* **235**, 2353–2375.
136. **Nystrom AM, Ekvall S, Berglund E, Bjorkqvist M, Braathen G, Duchen K, Enell H, Holmberg E, Holmlund U, Olsson-Engman M, Anneren G and Bondeson ML** (2008) Noonan and cardio-facio-cutaneous syndromes: two clinically and genetically overlapping disorders. *Journal of Medical Genetics* **45**, 500–506.
137. **Michailovici I, Harrington HA, Azogui HH, Yahalom-Ronen Y, Plotnikov A, Ching S, Stumpf MP, Klein OD, Seger R and Tzahor E** (2014) Nuclear to cytoplasmic shuttling of ERK promotes differentiation of muscle stem/progenitor cells. *Development* **141**, 2611–2620.
138. **Michailovici I, Eigler T and Tzahor E** (2015) Craniofacial muscle development. *Current Topics in Developmental Biology* **115**, 3–30.
139. **Garcia-Gomez R, Bustelo XR and Crespo P** (2018) Protein-protein interactions: emerging oncotargets in the RAS-ERK pathway. *Trends in Cancer* **4**, 616–633.
140. **Wilkie AO** (2007) Cancer drugs to treat birth defects. *Nature Genetics* **39**, 1057–1059.
141. **Patel AL and Shvartsman SY** (2018) Outstanding questions in developmental ERK signaling. *Development* **145**. https://doi.org/10.1242/dev.143818
142. **Guo X and Wang XF** (2009) Signaling cross-talk between TGF-beta/BMP and other pathways. *Cell Research* **19**, 71–88.
143. **Rahman MS, Akhtar N, Jamil HM, Banik RS and Asaduzzaman SM** (2015) TGF-beta/BMP signaling and other molecular events: regulation of osteoblastogenesis and bone formation. *Bone Research* **3**, 15005.
144. **Cervenka I, Wolf J, Masek J, Krejci P, Wilcox WR, Kozubik A, Schulte G, Gutkind JS and Bryja V** (2011) Mitogen-activated protein kinases promote WNT/beta-catenin signaling via phosphorylation of LRP6. *Molecular and Cellular Biology* **31**, 179–189.
145. **Mao JJ and Prockop DJ** (2012) Stem cells in the face: tooth regeneration and beyond. *Cell Stem Cell* **11**, 291–301.
146. **Zhao H, Feng J, Ho TV, Grimes W, Urata M and Chai Y** (2015) The suture provides a niche for mesenchymal stem cells of craniofacial bones. *Nature Cell Biology* **17**, 386–396.
147. **Xu Y, Malladi P, Chiou M and Longaker MT** (2007) Isolation and characterization of posterofrontal/sagittal suture mesenchymal cells in vitro. *Plastic and Reconstructive Surgery* **119**, 819–829.
148. **Maruyama T, Jeong J, Sheu TJ and Hsu W** (2016) Stem cells of the suture mesenchyme in craniofacial bone development, repair and regeneration. *Nature Communications* **7**, 10526.
149. **Dutta D, Heo I and Clevers H** (2017) Disease modeling in stem cell-derived 3D organoid systems. *Trends in Molecular Medicine* **23**, 393–410.
150. **Athanassiou-Papaefthymiou M, Papagerakis P and Papagerakis S** (2015) Isolation and characterization of human adult epithelial stem cells from the periodontal ligament. *Journal of Dental Research* **94**, 1591–1600.